Modeling a Bender Element Test using Abaqus Finite Element Program

by

Sean Johnson

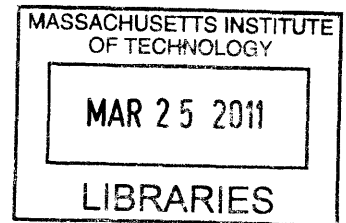B.S. Civil Engineering
Florida State University (2008)

Submitted to the Department of Civil and Environmental Engineering in Partial
Fulfillment of the Requirements for the Degree of

Master of Science in Civil and Environmental Engineering
At the
Massachusetts Institute of Technology

February, 2011

©2011 Massachusetts Institute of Technology
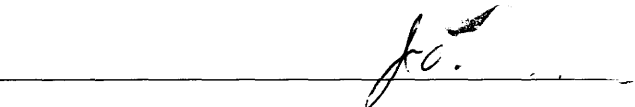All rights reserved.

Author_____
Department of Civil and Environmental Engineering
January 14, 2011

Certified by_____
John T Germaine
Senior Research Associate of Civil and Environmental Engineering
Thesis Supervisor

Accepted by_____
Heidi Nepf
Chair, Departmental Committee for Graduate Students

Modeling a Bender Element Test using Abaqus Finite Element Program

by

Sean Johnson

Submitted to Department of Civil and Environmental Engineering

On January 14, 2011 in Partial Fulfillment of the

Requirements for the Degree of

Master of Science in Civil and Environmental Engineering

ABSTRACT

Finite Element Methods hold promise for modeling the behavior of an unsaturated soil specimen subjected to bender element agitation. The immediate objective of this research project is to reproduce a bender element test using Abaqus Finite Element Software assuming elastic and isotropic conditions. Extensive compressions were made of bender element testing of unsaturated Ticino Sand specimens uniaxially compressed and the Abaqus Finite Element Method program simulation. The research determined that the mesh resolution of a numerical analysis are optimal at a resolution of a twentieth of the shear wavelength and the integration time step has a negligible effect on the observed wave velocity. Moreover, it is possible to reproduce an uniaxially stressed bender element experiments of unsaturated Ticino sand in an Abaqus Finite Element Method program with relatively minimal error of the body wave velocity measurements if the source receiver distance is beyond two shear wavelengths and the reflected signals from the boundaries are suppressed.

Thesis Supervisor: John T. Germaine

Title: Senior Research Associate of Civil and Environmental Engineering

Acknowledgments

Table of Contents

List of Tables

List of Figures

13

1. Introduction

The small strain shear modulus is a fundamental geotechnical engineering property of soil and is an essential parameter used in the geophysical sciences and geotechnical engineering. The small strain shear modulus can be measured using the bender element technique documented by (Arulnathan et al. 1998; Viggiani, 1997). The bender element method converts the observed shear wave propagation velocity measured by an oscilloscope into the small strain shear modulus. The calculation for the small strain shear modulus is the product of the mass density and the square of the shear wave velocity.

The bender element technique is presented by the geotechnical literature an attractive method for measuring the small strain modulus because it is considered to be a quick and non-destructive procedure. However, there exist ambiguities translating the oscilloscope data into the direct velocity of the shear wave. It is known that interference of the apparatus boundary will affect the observed received oscilloscope signal. Moreover, the superposition of the compression wave and the shear will interfere with the received oscilloscope signal. For these reasons, the bender element test was reproduced into Abaqus Finite Element Program for investigation.

Models created in the Abaqus finite element programs can support an isotropic elastic medium subjected to body wave propagation. The body wave propagation is measured by recording the displacement of nodal position with respect to its lateral and vertical components. The strain aspect of the wave propagation can be measured by recording the displacement of two nodes spaced at a finite distance. Moreover, body wave propagation can be determined in Abaqus by recording variations of the stress state at a node.

It is known that an infinite elastic medium can sustain only two kinds of waves: the compression or P-wave and the shear or S-wave. Collectively, these waves are called body waves. The P-wave and the S-wave represent two distinct forms of body motion and two different propagation velocities. The S-wave propagates with shear strains orthogonal to the direction of propagation and the compression wave propagates with compressive strains in the direction of the propagation.

Numerous bender element tests were done on unsaturated Ticino Sand with an associated density, stress state at OCR=1. The bender element tests were then represented in two dimensional plane strain space using Abaqus. The boundary conditions of the model were assumed from the known geometry of the test specimen; the mass density was directly measured; the Poisson's ratio was assumed to be 0.3. The bender element signal was represented as a fixed nodal displacement. Recordings were made of the displacement and strain field output of the nodes located down the centerline of the source. It is intended that the Abaqus numerical analysis produces a good fit with the observed oscilloscope data captured by the actual bender element test.

This Thesis investigates modeling a bender element test into Abaqus Finite Element Program. The introduction and conclusion are the first and last chapters respectively.

The second chapter provides background into wave propagation theory. The chapter provides basic derivations for equations used in the bender element method. In addition, there is a narrative of the important issues that are fundamental tied to bender element testing of soils. This includes a discussion of recent testing of unsaturated Ticino Sand in a triaxial apparatus.

The third chapter gives insight into building a bender element test in Abaqus.

The fourth chapter investigates the issues of mesh resolution and integration time steps of the bender element testing. The appropriate mesh size resolution of the specimen required to accurately capture body wave propagation is determined. In addition, investigations were done to examine the effect of altering the time step duration in the model.

The fifth chapter discusses six models made in Abaqus. The important issues discussed are the recorded pulse velocities, the source receiver distance, and different methods of modeling the source and receiver signals in Abaqus.

The sixth chapter makes direct comparisons of bender element test on unsaturated Ticino Sand to models made in Abaqus.

2. Background

2.1. Definitions of Elementary Terms and Harmonic Motion

Wave propagation is governed by the elementary laws of classical mechanics. These laws are the conservation of mass and momentum and Hooke's law. (Mei, 2006) Moreover, Newton's second law, stating that the force of an infinitesimal point is equal to the product of mass and acceleration and the third law which states that a force on an infinitesimal point will cause an equal and opposite force is used extensively in wave dynamics. The use of these concepts produces the foundation for investigations of wave propagation.

For the purposes of inquiry, consider a simple one dimension harmonic example. Harmonic motion is equivalent to sinusoid motion or the motion that can be described using a sine function such that (Richart, 1970)

$$z = A * \sin(\omega t - m) \tag{1}$$

Here it is shown that the one dimensional space value, in this case z, is a function of time and three undefined variables, A, ω, and m. It is possible to graph this function in length range and time domain. Ignoring the variables ω and m it is obvious that the variable A is a multiple of the output z. In fact, it is a product of A and it dictates the magnitude of z; this is referred to as the amplitude of wave. In spatial range, the amplitude is in units of length.

In trying to understand the other components of this equations consider the variable ω. Here the variable ω is being used as a multiple of t. It is easy to see that the ω determines the rate of oscillation of the sine wave. In fact, this variable has a liner affect on the sine wave such that doubling the ω will double the rate of oscillation. This particular result will be documented later when this function is differentiated causing a multiplication with the amplitude. ω is referred to as the Frequency given in units of radians/time.

There are two types of frequency. The first type of frequency is an absolute value of the inverse of time in units of 1/time and known as a "Hertz"; it is units of cycles/s. The second type of frequency is referred to as angular or circular frequency, which is simply the frequency in radial values; it is in units of radians/s.

The absolute frequency in units of inverse time is:

$$f = \omega/(2\pi) \tag{2}$$

Where ω is the angular frequency.

It is possible to know the time of oscillation from the absolute frequency, which will henceforth be called simply the frequency, by taking the inverse of the frequency. This value is called the Period or Period of harmonic motion and it is defined as:

$$T = \frac{1}{f} = f^{-1} \tag{3}$$

If angular frequency is in units of radians per second then the equation becomes

$$T = \frac{2\pi}{\omega} \tag{4}$$

The last undefined term is the value m. Here m subtracts from the product of the frequency and the time. If plotted in Cartesian coordinates it is obvious that variations in m will cause the wave to shift with respect to time. Appropriately, this value is referred to as the Phase Shift.

2.1.1. Definitions of Wavelength, Phase Velocity, Group Velocity, Mode, Wave Number, and Degrees of Freedom.

The velocity of any object can be expressed as the first derivative with respect to time of its displacement. This is applicable to harmonic motion. Taking the first derivative of equation (1) we get:

$$\frac{dz}{dt} = \omega * A * \cos(\omega t - m) \tag{5}$$

This function gives the velocity of 1-D harmonic motion. The label 'velocity' will be refined later when the distinction between phase velocity and group velocity is made but just accept for now that the this equation describes velocity. Like the circular frequency this value is in units of radians per second. The conversion from radians to units of length is possible through a division of 2π.

From this formulation it is evident that if the time variable is substituted for the period then it is possible to arrive at a wavelength that describes the geometry of the wave in units of length or radians.

Therefore, it can be said that:

$$Wavelength = \lambda = \frac{dz}{dt} * T \tag{6}$$

The wave number is the reciprocal of the wavelength. Thus, the wavelength to wave number relationship is analogous to period and frequency relationship.

$$Wavenumber = k = \lambda^{-1} \tag{7}$$

Alternatively the Wavenumber can be expressed:

$$k = \frac{f}{Velocity} \tag{8}$$

This is in units of length inverse.

The velocity of harmonic motion considered assumes that there is one wave traveling through the medium at a constant amplitude, frequency, and phase shift. However, consider a system where many waves with different parameters are imposed on a single medium. Suppose that the motion of many waves in this medium is better described by another metric rather than the periodic time.

20

A method to determine the velocity of the superposition of many waves is referred to as the group velocity. A velocity measurement that uses the period as a reference is called phase velocity.
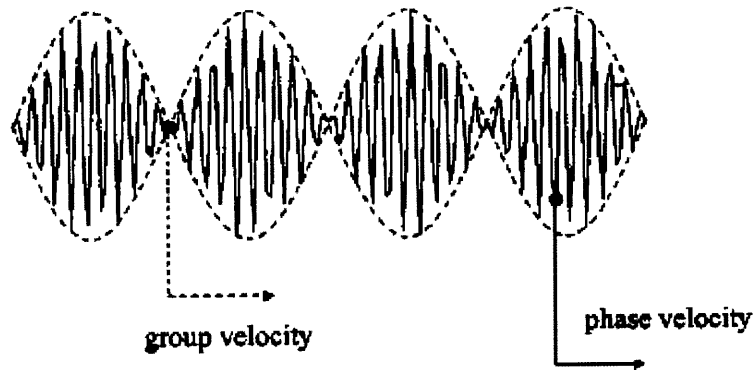
Figure 2.1: Graphical Representation of Group and Phase Velocity. From (Kausel 2005)

The phase velocity is the velocity of one phase of wave traveling through space. This is equivalent to the velocity of the phase during one frequency. The phase velocity can be expressed

$$Phase\ Velocity = \frac{\lambda}{T} \qquad (9)$$

Alternatively,

$$Phase\ Velocity = \frac{f}{k} \qquad (10)$$

The group velocity is the velocity of the envelope of amplitudes from the superposition of waves. This value is also referred to as the modulation velocity or envelope velocity of the wave. A general equation exists to solve group velocity if the waveform is localized in time and space

$$Group\ Velocity = \frac{\partial f}{\partial k} \qquad (11)$$

Harmonic motion may have an infinite number of frequencies of vibration. If the total length of a continuous model is finite and has boundary conditions imposed then the number frequencies remain infinite. (Kausel Manolis, 2000) However, the mathematics of harmonic motion states

21

that frequencies must adhere to the boundary conditions. The harmonic motion that conforms to the boundary conditions has a mode. The mode is defined as a solution that describes constant harmonic motion under a boundary condition. The number of the mode is directly a function of the period of wave.

For a given modal number the period of the wave will remain constant for all points in the length and the motion will oscillate at a constant frequency. The mode can be thought of as a series of possible solutions for the model.
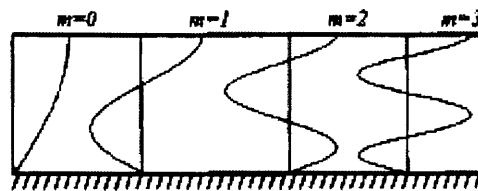
Figure 2.2: Solution of Modal Values for a Fix-Free Boundary Condition. From (Kausel Manolis, 2000)

2.2. Introduction of Formulas and Relationships that Govern Wave Propagation

It is required to adopt our vocabulary to construct equations that will provide a basis for explorations into numerical analysis. The equations that will be provided are extensively documented in soil dynamics literature. The following sections will derive the Compression and Shear Wave equation and give a general introduction to the classical wave equation. There is comparable evaluation for the coupled wave.

2.2.1. Brief Derivation of the Compression Wave Equation

Consider an elastic isotropic rod with a cross sectional area A an Young's Modulus E and a unit weight γ. It is necessary to assume the following:

22

1. The rod remains uniform with respect to area, modulus, and unit weight for all points in the domain x

2. The stress applied is uniform or constant on the area A.

3. The cross section remains plane during motion.

A representation of the elastic rod is provided in Figure 2.3. Consider a differential length delta x along the rod. From a free body diagram it be shown that the stresses are oriented such that at a distance x the stress is σ_x and that at a distance of the differential boundary x+dx the stress is $(\sigma_x + \frac{\partial \sigma_x}{\partial x} * dx)$ where the change is stress is governed by a partial differential with respect to the length.
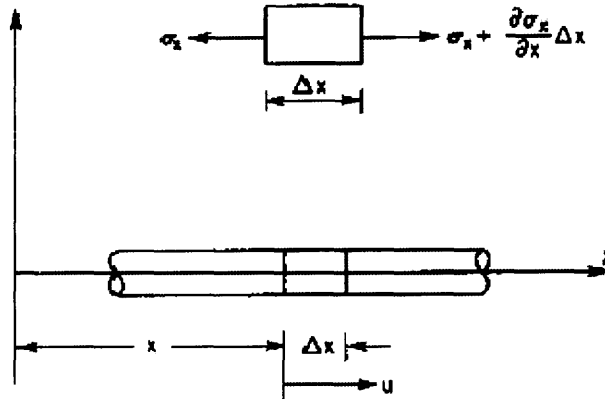
Figure 2.3: An Infinite Rod Subject to an Pulsation Axial Stress. $\Delta x = dx$ From (Prakash, 1983)

A simple application of Newton's third law yields the following result.

$$\Sigma Fx = -\sigma_x + (\sigma_x + \frac{\partial \sigma_x}{\partial x} * dx)$$

(12)

If there is some acceleration in the differential element then the summation of forces in the x direction will not equal zero because:

$$\Sigma Fx = m * \frac{d^2 u}{dt^2} \text{ in the x direction}$$

(13)

23

And the element is not massless. The mass can be defined in terms of its unit weight and geometry.

$$m = A * \frac{\gamma}{g} * dx$$

(14)

The scalar force is equal to the product of stress and area.

$$F = \sigma * A$$

(15)

An application of Newton's second law will produce the following equation.

$$A * \frac{\gamma}{g} * dx * \frac{d^2u}{dt^2} = -\sigma x * A + A * (\sigma x + \frac{\partial \sigma x}{\partial x} * dx)$$

(16)

The differential d^2u must not be confused with dx. The former describes the derivative of the displacement of an element and the latter describes the space of the free body diagram.

The equation is equivalent to:

$$\frac{d^2u}{dt^2} * \frac{\gamma}{g} = \frac{\partial \sigma x}{\partial x}$$

(17)

From linear elasticity, Hooke's law the stress of an element is equal to the strain multiplied by the Young's Modulus. Strain is defined as displacement divided by the original length.

$$Strain = \varepsilon = \frac{du}{dx}$$

(18)

Thus, in our element the following relationship is true.

$$\sigma x = E * \frac{\partial u}{\partial x}$$

(19)

The partial differential is equal to the different because the strain equation is a single variable differential.

24

Therefore, taking the first partial derivative with respect to length yields.

$$\frac{\partial \sigma x}{\partial x} = E * \frac{\partial^2 u}{\partial x^2} \tag{20}$$

Substituting the original equation with the first partial derivative of stress produces.

$$E \frac{\partial^2 u}{\partial x^2} = \frac{\gamma}{g} \frac{\partial^2 u}{\partial t^2} \tag{21}$$

Mass density is equal to the unit weight divided by the acceleration of gravity

$$\frac{\gamma}{g} = \rho \tag{22}$$

Substitution yields:

$$E \frac{\partial^2 u}{\partial x^2} = \rho \frac{\partial^2 u}{\partial t^2} \tag{23}$$

Rearranging the terms:

$$\frac{E}{\rho} = \frac{\partial^2 u}{\partial t^2} * \left(\frac{\partial^2 u}{\partial x^2}\right)^{-1} \tag{24}$$

Reduction of terms:

$$\frac{E}{\rho} = \frac{dx^2}{dt^2} = Vp^2 \tag{25}$$

Therefore

$$Vp = \sqrt{\frac{E}{\rho}} \tag{26}$$

Vp is defined as the velocity of the wave traveling a distance over the differential element length with respect to a differential quantity in time. The wave is a 1-Dimensional wave and it is traveling in the same direction as the strains produced by the wave. Thus, a compression and

tensile effect is present through strain equation. This velocity is equal to the P-wave; it is labeled the compression wave or dilatational wave in literature.

2.2.2. Brief Derivation of the Shear Wave Equation

The derivation of the shear wave equation will be conducted in a similar manor to that of the compression wave equation. However, instead of the rod imparted by a in-plane stress, such as used to derive the p-wave equation, consider the application of a torque on a elastic isotropic rod with the same assumptions used in the previous section..

The derivation will examine the influence of torque or torsion on this rod and will reduce a section of it a differential length as shown in Figure 2.4. The application of a torsion force will produce an angle of displacement θ in the rod measured relative to a zero point.
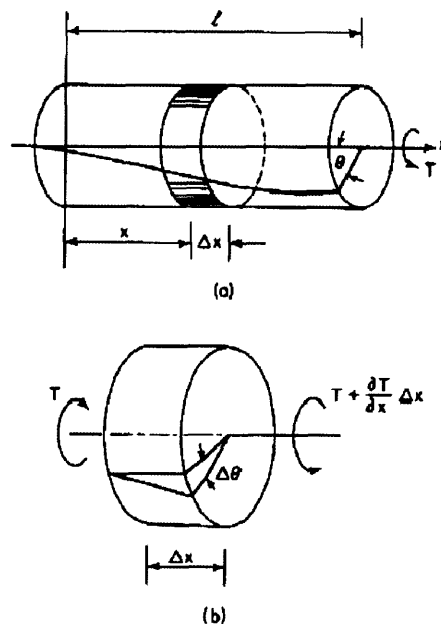
Figure 2.4: An Infinite Rod Subject to a Torisonal Stress. $\Delta x = \partial x$ From (Prakash, 1983)

An equation for the Torsion in the rod (Prakash, 1983)

$$T = G * Ip * \frac{\partial \theta}{\partial x} \tag{27}$$

26

Where G is the shear modulus, known also as the rigidity, in units of [$\frac{F}{L^2}$]. Ip is the moment of inertia of the rod which is uniform and constant with respect to x and it has units of [L^4]. Θ can be expressed as degrees or radians it is irrelevant to the scope of this problem.

Over the differential length dx the sum of the torsion can be expressed.

$$\Sigma T = -\,T + (T + \frac{\partial T}{\partial x} * dx) \tag{28}$$

Applying Newton's second law to the element dx gives an equation for the summation of torques. (Richart, 1970)

$$\Sigma T = \rho * Ip * dx * \frac{\partial^2 \theta}{\partial t^2} \tag{29}$$

Thus

$$\rho * Ip * dx * \frac{\partial^2 \theta}{\partial t^2} = -\,T + (T + \frac{\partial T}{\partial x} * dx) \tag{30}$$

Simplified,

$$\frac{\partial^2 \theta}{\partial t^2} * \rho * Ip = \frac{\partial T}{\partial x} \tag{31}$$

Performing a substitution for the definition of torsion T yields.

Or

$$\frac{\partial^2 \theta}{\partial t^2} * \rho * Ip = \frac{\partial}{\partial x}(G * Ip * \frac{\partial \theta}{\partial x}) \tag{32}$$

27

$$\frac{G}{\rho} = \frac{\partial^2 \theta}{\partial t^2} * \left(\frac{\partial^2 \theta}{\partial x^2}\right)^{-1}$$

(33)

Or

$$\frac{G}{\rho} = \frac{\partial x^2}{\partial t^2} = Vs^2$$

(34)

Thus

$$Vs = \sqrt{\frac{G}{\rho}}$$

(35)

Vs is defined as the velocity of the wave traveling a distance over the differential element length with respect to a differential quantity in time. The wave propagates orthogonal to the torsion strains produced by the wave. Thus, a shear effect is present. This velocity is equal to the S-wave; it is labeled the shear, transverse, secondary or distortional wave in literature.

2.3. Brief Discussion of the Classical Wave Equation

The classical one dimensional wave equation takes the form. (Mei, 2006)

$$c^2 \frac{\partial^2 u}{\partial x^2} = \frac{\partial^2 u}{\partial t^2}$$

(36)

The solution to this classical wave equation is obtained through calculus and given. (Mei, 2006)

$$u(x,t) = f(x - ct) + g(x + ct)$$

(37)

f(x,t) and g(x,t) are arbitrary functions of x and t. (Mei, 2006) where c is the constant velocity. In this solution the $F(\xi)$ represents the wave traveling in the positive x dimension. Conversely, $G(\xi)$ represents the wave traveling in the negative x direction. (Mei, 2006)

28

The previous examinations of an elastic isotropic rod conform to the classical wave equation as given.

For P-Wave vibration

$$\frac{E}{\rho}\frac{\partial^2 u}{\partial x^2} = \frac{\partial^2 u}{\partial t^2}$$

(38)

For S-wave vibration

$$\frac{G}{\rho}\frac{\partial^2 \theta}{\partial x^2} = \frac{\partial^2 \theta}{\partial t^2}$$

(39)

Where both $\frac{G}{\rho}$ and $\frac{E}{\rho}$ represents the velocity component c as proven prior to this section. It is expected that a general solution can be found for the P-wave and S-wave vibration models using the classical wave equation.

Ignoring negative propagation, the derivations for the P-Wave model are given.

$\frac{\partial u}{\partial x} = f'(x - ct)$ and $\frac{\partial u}{\partial t} = -c * f'(x - ct)$

$\frac{\partial^2 u}{\partial x^2} = f''(x - ct)$ and $\frac{\partial^2 u}{\partial t^2} = c^2 * f'(x - ct)$

And the S-wave derivations are given.

$\frac{\partial \theta}{\partial x} = f'(x - ct)$ and $\frac{\partial \theta}{\partial t} = -c * f'(x - ct)$

$\frac{\partial^2 \theta}{\partial x^2} = f''(x - ct)$ and $\frac{\partial^2 \theta}{\partial t^2} = c^2 * f'(x - ct)$

Unfortunately, it is impossible to proceed further. Information regarding the boundary conditions of both P and S wave formulations is required to so for the unknown function f. However, future sections will return to these derivations to make analytical solutions.

2.4. Stress Waves in Elastic Isotropic Medium

A stress wave is a disturbance in a medium that is mathematically explained through classical mechanics. (Prakash, 1983). When a source, cause, or disturbance creates a particle motion then a wave is produced. The motion of particles entails the production of strains. The strains created by the propagation of the wave do not produce mass motion because the strains are oriented around a reference point in the medium. In a body element, such as examined here in Figure 2.5, two types of waves are produced (1) shear and (2) compression. A mathematical framework given through Newtonian mechanics explains this phenomena.

A wavefront is a surface connecting all points of equal phase at a point in time. (Van Der Hilst, 2004). Consequently, at a wavefront all particles move in phase. The surface geometry of the wavefront is orthogonal to the direction vector of the wave spread. (Van Der Hilst, 2004).

2.5. Derivation of Stress Waves in Elastic Isotropic Infinite Medium

Consider an infinite, homogenous isotropic, elastic medium. Elementary mechanics states an applied stress will create a strain. In this medium, a stress applied at an arbitrary point within the body will not disturb the whole body instantly. Instead a stress gradient or differential will immerge. Consequently a strain differential will appear in the element. Strain is a function of stress and the Young's Modulus remains constant in all points in the element. The perturbation will radiate outward from the source according to wave dynamics. This radial spread will cause the strains to spread as a function of space and time. (Prakash, 1983)

30
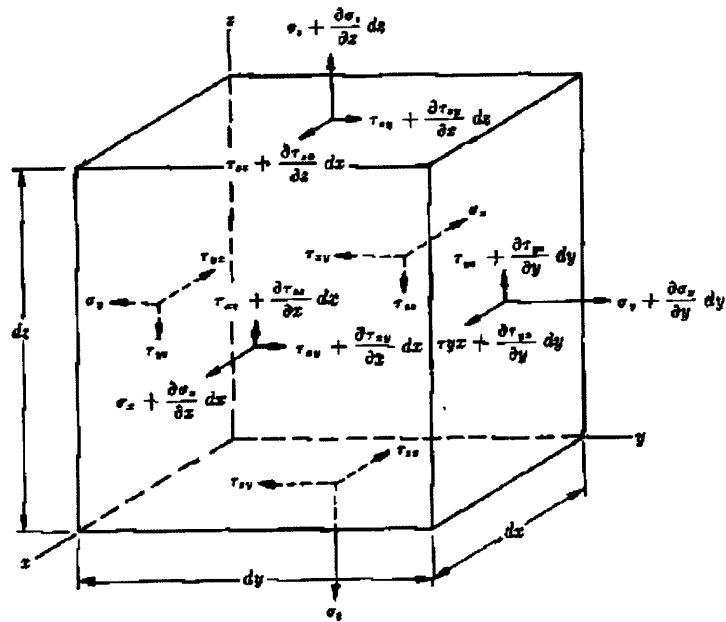
Figure 2.5: An Isotropic Elastic Element From an Infinite Medium. From (Wu, 1970)

In tensor form the stresses are given. (Wu, 1970)

$$\begin{bmatrix} \sigma x & \tau xy & \tau xx \\ \tau xy & \sigma y & \tau yz \\ \tau zx & \tau yz & \sigma z \end{bmatrix} \tag{40}$$

And the principle stresses are given. (Wu, 1970)

$$\begin{bmatrix} \sigma x & 0 & 0 \\ 0 & \sigma y & 0 \\ 0 & 0 & \sigma z \end{bmatrix} \tag{41}$$

31

The stresses on each face of the element are orthogonal vectors (Prakash, 1983) (Richart, 1970). Assuming the element is in equilibrium the sum of the forces in the z direction can be given.

$$\Sigma Fz = \left(\sigma z + \frac{\partial \sigma z}{\partial z} * dz\right) dxdy - (\sigma z)dxdy + \left(\tau zx + \frac{\partial \tau zx}{\partial x} * dx\right) dydz - (\tau zx)dydz$$
$$+ \left(\tau zy + \frac{\partial \tau zy}{\partial y} * dy\right) dxdz - (\tau zy)dxdz \tag{42}$$

If there is some dynamic action

$$\Sigma Fz = \rho \frac{\partial^2 u}{\partial t^2} dxdydz \tag{43}$$

Such that the mass of the element is

$$m = \rho \, dxdydz \tag{44}$$

And its acceleration in scalar form is

$$a = \frac{\partial^2 u}{\partial t^2} \tag{45}$$

Applying Newton's second law produces the following equation.

$$\left(\sigma z + \frac{\partial \sigma z}{\partial z} * dz\right) dxdy - (\sigma z)dxdy + \left(\tau zx + \frac{\partial \tau zx}{\partial x} * dx\right) dydz - (\tau zx)dydz$$
$$+ \left(\tau zy + \frac{\partial \tau zy}{\partial y} * dy\right) dxdz - (\tau zy)dxdz = \rho \frac{\partial^2 u}{\partial t^2} dxdydz \tag{46}$$

Simplified

$$\left(\frac{\partial \sigma z}{\partial z} + \frac{\partial \tau zx}{\partial x} + \frac{\partial \tau zy}{\partial y}\right) dxdydz = \rho \frac{\partial^2 u}{\partial t^2} dxdydz \tag{47}$$

Or

$$\left(\frac{\partial \sigma z}{\partial z} + \frac{\partial \tau zx}{\partial x} + \frac{\partial \tau zy}{\partial y}\right) = \rho \frac{\partial^2 u}{\partial t^2} \tag{48}$$

$$\nabla \cdot (\sigma z + \tau zx + \tau zy) = \rho \frac{\partial^2 u}{\partial t^2} \tag{49}$$

32

Consequently the same formulations and methodology can be used to prove the following relationships for the remaining two dimensions. (Richart, 1970)

$$\left(\frac{\partial \sigma x}{\partial x} + \frac{\partial \tau xy}{\partial y} + \frac{\partial \tau xz}{\partial z}\right) = \rho \frac{\partial^2 v}{\partial t^2} \tag{50}$$

$$\left(\frac{\partial \sigma y}{\partial y} + \frac{\partial \tau yx}{\partial x} + \frac{\partial \tau yz}{\partial z}\right) = \rho \frac{\partial^2 w}{\partial t^2} \tag{51}$$

Here u is the displacement in the z-axis; v is the displacement in the x axis; w is the displacement in the y axis.

Suppose that there is only shear force acting on the element. Notice that the equation is one dimensional through the axis z.

$$\nabla(\tau zx + \tau zy) = \rho \frac{\partial^2 u}{\partial t^2} \tag{52}$$

This is a two dimensional differential equation with terms ∂y and ∂x. It is possible to convert this two dimensional problem into a one dimensional space by creating a new coordinate axis s such that
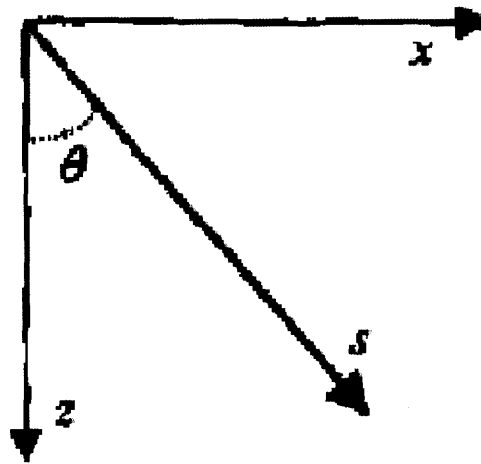
Figure 2.6: Reference system definition sketch. From (Kausel Manolis, 2000)

$$s = x\sin\theta + z\cos\theta \tag{53}$$

Assuming that θ is the angle between the z axis and the constructed spatial dimension. (Kausel Manolis, 2000)

Recalling the equation for strain provided in equation 13 and substituting strain for stress the equation becomes a scalar equation. (Kausel Manolis, 2000)

$$\nabla^2(u) = (\frac{\rho}{G})^2 \frac{\partial^2 u}{\partial t^2} \tag{54}$$

Or

$$\nabla^2(u) = \frac{1}{Vs} \frac{\partial^2 u}{\partial t^2} \tag{55}$$

Equivalently

$$\frac{\partial^2 u}{\partial x^2} = \frac{1}{Vs} \frac{\partial^2 u}{\partial t^2} \tag{56}$$

Which is the familiar one dimensional wave equation. The solution to this equation is.

$$u(x,t) = f(x - ct) + g(x + ct) \tag{57}$$

If there is a body force on the element then this reduction is incorrect because $\sigma z \neq 0$. The purpose of its derivation was to show how manipulations to the formulation of the problem can produce a return to the classic 1-D wave equation and solution.

Returning to the assumption that is there a body force present and must be accounted for then the problem becomes slightly more complicated. However, its exploration will help the reader, and the author, understand the mathematics behind stress wave propagation.

In an elastic medium the following relationships for stress in scalar space are true.

$$\sigma x = \lambda(\varepsilon x + \varepsilon y + \varepsilon z) + 2 * G\varepsilon x \tag{58}$$

$$\sigma y = \lambda(\varepsilon x + \varepsilon y + \varepsilon z) + 2 * G\varepsilon y \tag{59}$$

$$\sigma z = \lambda(\varepsilon x + \varepsilon y + \varepsilon z) + 2 * G\varepsilon z \tag{60}$$

34

And

$$\tau xy = \tau yx = G\gamma xy \tag{61}$$

$$\tau yz = \tau zy = G\gamma yz \tag{62}$$

$$\tau yz = \tau zy = G\gamma yz \tag{63}$$

$$\tau zx = \tau xz = G\gamma zx \tag{64}$$

In the above equations the values λ and G are Lamè's constants. Moreover, the value G is the shear modulus. The term γ is the shear strain of the isotropic elastic medium. The shear modulus is assumed to remain constant in the element.

The Lame Constant, λ, and the Shear Modulus completely define the elastic behavior of an isotopic solid. The Lame Constant λ, can be expressed.

$$\lambda = \frac{\eta E}{(1 + \eta)(1 - 2\eta)} \tag{65}$$

The equation follows from a synthesis of all the premises given in one derivation. (Richart, 1970).

$$\rho \frac{\partial^2 u}{\partial t^2} = (\lambda + G)\frac{\partial}{\partial z}(\varepsilon x + \varepsilon y + \varepsilon z) + G\left(\frac{\partial^2 u}{\partial z^2} + \frac{\partial^2 u}{\partial x^2} + \frac{\partial^2 u}{\partial y^2}\right) \tag{66}$$

Equivalently

$$\rho \frac{\partial^2 u}{\partial t^2} = (\lambda + G)\frac{\partial}{\partial z}(\varepsilon x + \varepsilon y + \varepsilon z) + G\nabla^2 u \tag{67}$$

And the following applies for motion in the x and y dimensions. (Richart, 1970).

$$\rho \frac{\partial^2 v}{\partial t^2} = (\lambda + G)\frac{\partial}{\partial x}(\varepsilon x + \varepsilon y + \varepsilon z) + G\nabla^2 v \tag{68}$$

$$\rho \frac{\partial^2 w}{\partial t^2} = (\lambda + G) \frac{\partial}{\partial y} (\varepsilon x + \varepsilon y + \varepsilon z) + G \nabla^2 w \tag{69}$$

There are two possible methods to solve the last three equations. The first method solves the differential equation in irrotational propagation and second assumes rotational propagation. (Richart, 1970). The first solution requires differentiation with respect to x, y, and z and taking the sum of each expression, in particular the strains. (Prakash, 1983)

Using the first method to solve the differential equation. The operation produces (Prakash, 1983)

$$\rho \frac{\partial^2 (\varepsilon x + \varepsilon y + \varepsilon z)}{\partial t^2} = (\lambda + 2G) \nabla^2 (\varepsilon x + \varepsilon y + \varepsilon z) \tag{70}$$

Or

$$\rho \frac{\partial^2 (\varepsilon x + \varepsilon y + \varepsilon z)}{\partial t^2} = (\lambda + 2G) \nabla^2 (\varepsilon x + \varepsilon y + \varepsilon z) \tag{71}$$

$$\frac{\partial^2 (\varepsilon x + \varepsilon y + \varepsilon z)}{\partial t^2} = Vc^2 \nabla^2 (\varepsilon x + \varepsilon y + \varepsilon z) \tag{72}$$

This equation takes the form of the classical wave equation.

Therefore

$$Vc = \sqrt{\frac{(\lambda + 2G)}{\rho}} \tag{73}$$

Using the definition of Lamè's constant λ the following is true.

$$Vc = \sqrt{\frac{E(1 - \eta)}{\rho(1 + \eta)(1 - 2\eta)}} = \sqrt{\frac{E_b}{\rho}} \tag{74}$$

36

The variable E_b is defined as the bulk modulus of the element. The variable η is the Poisson's Ratio, a familiar term in civil engineering, which is the ratio of body's radial strains to the axial strains.

In an infinite medium the appropriate modulus is the Bulk Modulus for the P-wave velocity The Young's modulus is the appropriate modulus in an elastic rod subjected to an uniaxial and uniform stress state and allowed to deform laterally. The constrained modulus is the appropriate modulus in an elastic rod subjected to an uniaxial and uniform stress state and not allowed to deform laterally.

The second solution to the differential equation assumes a rotational wave propagation mechanism. Suppose we differentiate the equation that describes motion in the x axis with respect to y and we differentiate the equation that describes motion in the y axis with respect to x. This operation yields the following solution. (Prakash, 1983)

$$\rho \frac{\partial^2}{\partial t^2} \left(\frac{\partial w}{\partial x} - \frac{\partial v}{\partial y} \right) = G\nabla^2 \left(\frac{\partial w}{\partial x} - \frac{\partial v}{\partial y} \right) \tag{75}$$

This equation can be expressed in terms of rotation such that the following relationship is true. The term ωz can be defined as the rotation of the element orientated around the z-axis. (Richart, 1970)

$$\left(\frac{\partial w}{\partial x} - \frac{\partial v}{\partial y} \right) = \omega z \tag{76}$$

Therefore

$$\rho \frac{\partial^2}{\partial t^2} \omega z = G\Delta\omega z \tag{77}$$

Or

$$\rho \frac{\partial^2}{\partial t^2} \omega z = Vs^2 \Delta \omega z \tag{78}$$

Such that

$$Vs = \sqrt{\frac{G}{\rho}} \tag{79}$$

A substitution computation can be made such that the compression wave velocity and the shear wave velocity are combined and expressed as a ratio.

$$\frac{Vc}{Vs} = \sqrt{\frac{(2 - 2\eta)}{(1 - 2\eta)}} \tag{80}$$

These equations are essential to continue with the exploration into the numerical analysis of a shear wave propagation. It is essential to remember that these solutions and derivations are only applicable in mediums that are isotropic and elastic.

2.6. Boundary Conditions in Body Wave Propagation in an Elastic Isotropic Medium

In this investigation only two possible boundary states will be considered. The first is an infinitely rigid and infinitely thin boundary and the second is the free boundary. The occurrence of layering of multiple elastic mediums has been discussed at length, notably by (Prakash, 1983) (Richart, 1970) (Kausel Manolis, 2000) (Kausel 2005) . The reader should be encourage to read the mechanics of elastic layering because it is an interesting phenomenon in the sources cited but an analysis will be excluded here because layering is beyond the scope of this chapter. Moreover, it is not pertinent to the experimental research.

When a wave strikes a boundary or discontinuity, reflection, and refraction of the wave will occur. (Wu, 1970) The science of optics, in particular Snell's law, is applicable to wave propagation in soils. (Wu, 1970). Furthermore, the assumption of elasticity detailed in pervious sections is valid in soils because seismic waves are low magnitude. (Wu, 1970)

2.6.1. Free Boundary P-wave Reflection

Consider a free boundary shown in Figure 2.7 with an incident P-wave striking a free boundary producing a reflected shear wave and a compression wave.
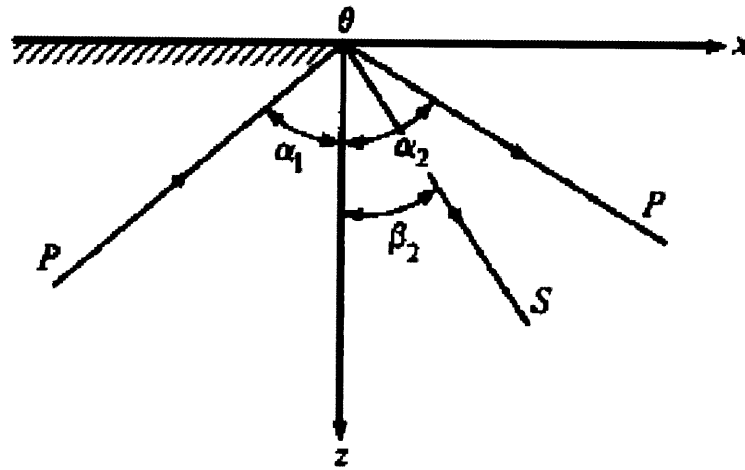
Figure 2.7: P-wave reflecting a free boundary. From (Wu, 1970)

The P wave has the following form such that S_1 is the displacement in the direction of wave propagation.

$$S_1 = A_1 \sin[B_1(c_1 t + r)] = A_1 \sin[B_1(c_1 t + x\cos\alpha_1 + z\sin\alpha_1)]$$

(81)

Such that A and B are constants, r is the distance along the direction of the wave, and c_1 is the velocity of the incidence wave.

The displacements u and w, corresponding to the x and z directions respectively, of the initial wave are

$$u_1 = s_1 \cos\alpha_1 \ and \ w_1 = s_1 \sin\alpha_1$$

(82)

At the free boundary the following conditions are true. (Wu, 1970)

$$\sigma_z = 0 \ and \ \tau_{zx} = 0 \ at \ z = 0$$

(83)

Therefore

$$\left(\frac{\partial u}{\partial z} + \frac{\partial w}{\partial x}\right) = 0 \tag{84}$$

$$\lambda(\varepsilon x + \varepsilon y + \varepsilon z) + 2 * G\varepsilon z = 0 \tag{85}$$

Where u is the displacement of the wave with respect to the x axis and z is the displacement with respect to the y axis. (Wu, 1970).

And the reflected compression and shear wave are respectively. (Wu, 1970).

$$s_p = A_2 \sin[B_2(c_1 t + \psi_2 + x\cos\alpha_2 + z\sin\alpha_2)] \tag{86}$$

$$s_v = A_3 \sin[B_2(c_2 t + \psi_3 + x\cos\beta_2 + z\sin\beta_2)] \tag{87}$$

Such that ψ denotes the phase changes of the wave upon reflection, and c_2 is the velocity of the reflected shear wave. The displacements in the x and z directions due to the reflected compression and shear waves are given:

$$u_2 = s_p \cos\alpha_2 \ and \ w_2 = s_p \sin\alpha_2 \tag{88}$$

$$u_3 = s_v \cos\beta_2 \ and \ w_3 = s_v \sin\beta_2 \tag{89}$$

Suppose that a compression wave is reflected. To satisfy the initial boundary conditions stated it is necessary that (Wu, 1970).

$$\alpha_1 = \alpha_2 \ and \ \psi_2 = 0, \tag{90}$$

A general form of the equation can be made.

$$\frac{\sin\alpha_2}{\sin\beta_2} = \frac{c_1}{c_2} = \frac{Vp}{Vs} \tag{91}$$

Where $\alpha 1$ is the incident compression wave angle and β_2 is the reflected shear wave angle. The compression wave is reflected at the angle of incidence and the shear wave is reflected at an angle β_2.

The amplitudes coefficients A_1, A_2, A_3 are of importance when analyzing the displacement magnitudes of the reflections. Kolsky made a derivation of the Amplitudes; the value of the amplitude coefficients are functions of the angle of incidence α_1 the angle of reflection β_2 and the Lamè constants of the material. (Kolsky 1958) A fundamental property of Kolsky's derivation is that the energy of the reflected waves is equal to the incidence wave. Accordingly, at normal incidence, $\alpha_1 = 0$, there is no reflected shear wave and $A_3 = 0$ and $A_1 = A_2$. There is a phase change of π on reflection of the boundary. This condition applies for an incidence angle of 90 degrees such that there is no reflected shear wave.

Kolsky asserts the amplitude of the reflected shear wave reaches a maximum at an angle of incidence of about 48 degrees. At this point the amplitude of the reflected shear wave approaches the amplitude of the incidence wave. (Kolsky 1958) The amplitude of the reflected compression wave reaches a minimum at an angle of incidence of about 65 degrees. The amplitude of the reflected compression wave is near 40 percent of the incidence wave. (Kolsky 1958)

2.6.2. Free Boundary S-wave Reflection
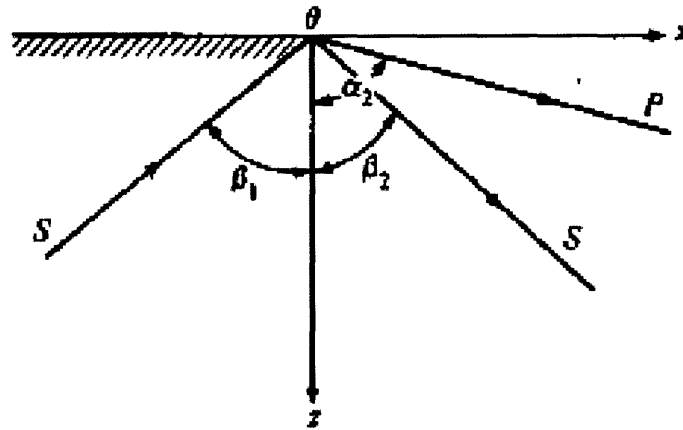
Figure 2.8: S-wave reflecting a free boundary. From (Wu, 1970)

Using an equivalent derivation it is true that $\beta_1 = \beta_2$. The formulation to arrive at this conclusion is identical to the one used to prove $\alpha_1 = \alpha_2$. The boundary conditions must be satisfied for both the P-Wave reflection and the S-wave reflection. The angles can be stated mathematically as

$$\frac{sin\alpha_2}{sin\beta_1} = \frac{Vp}{Vs} \tag{92}$$

Where β_1 is the incident shear wave angle and $\alpha2$ is the reflected P-Wave angle.

2.6.3. Rigid Boundary P-wave Reflection

When a incidence wave strikes an elastic boundary two waves are reflected as shown in Figure 2.9. (Wu, 1970). The boundary is assumed to be infinitely thin and rigid. Two reflection waves produced.
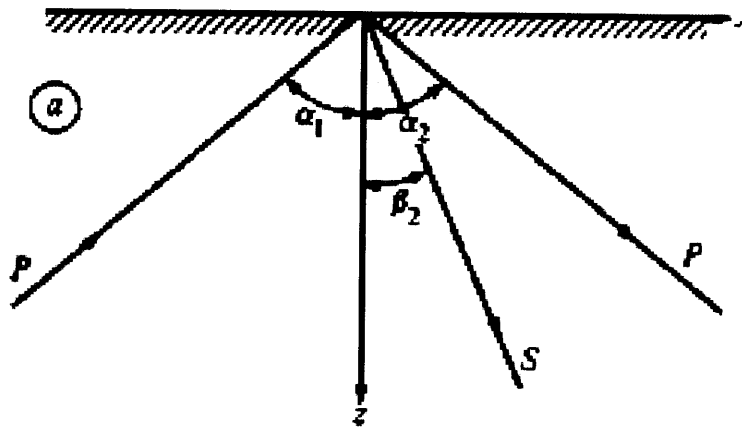
Figure 2.9: P-wave reflecting an infinitely rigid boundary. From (Wu, 1970)

The relationship of the angles to the velocities of the reflection is (Richart, 1970)

$$\alpha_1 = \alpha_2$$

$$\frac{sin\alpha_1}{Vp_{incidence}} = \frac{sin\alpha_2}{Vp_{reflection}} = \frac{sin\beta_1}{Vs_{reflection}} \tag{93}$$

2.6.4. Rigid Boundary P-wave Reflection

Consider a shear incidence wave as shown in Figure 2.10.
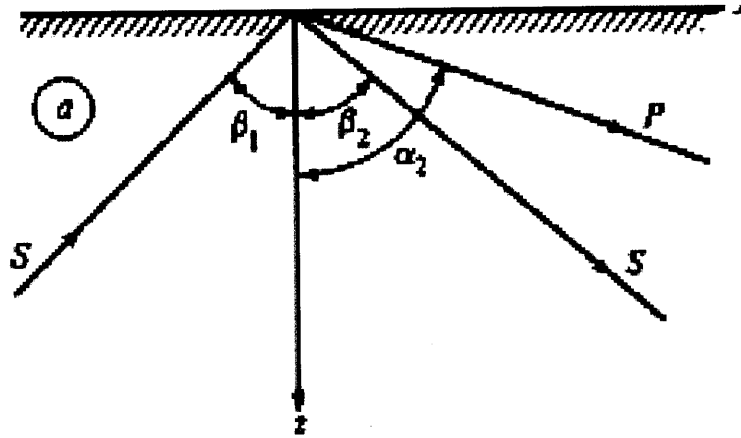
Figure 2.10: S-wave reflecting an infinitely rigid boundary. From (Wu, 1970)

Furthermore the equations are true for a shear incidence wave, (Richart, 1970)

$$\beta_1 = \beta_2$$

$$\frac{sin\beta_1}{Vs_{incidence}} = \frac{sin\beta_2}{Vs_{reflection}} = \frac{sin\alpha_2}{Vp_{reflection}} \tag{94}$$

These derivations are reiterations of Snell's Law.

2.7. Numerical and Analytic Methods

The subject of wave propagation has received an abundance of attention in the sciences. Numerous articles exist exploring the subject from many perspectives and aimed at many different audiences in academia. Basics assumptions, such as homogeneity, isotropy, elasticity, and non dispersitivity pore structure variability dimensional limitations fluid structure interaction are deconstructed and manipulated. The result from this inquiry is a fantastic wealth of mathematical solutions, models, and brilliant solutions for all sorts of boundary conditions! The purpose of this section is not to summarize the countless advances made but rather to provide a

very basic overview of an analytic solutions of body wave propagation. In all solutions provided in this review isotropy, elasticity, and homogeneity is assumed.

Returning to the formulation provided for 1-D stress waves. Recall that the spatial dimension w refers to the Y axis.

$$\left(\frac{\partial \sigma y}{\partial y} + \frac{\partial \tau yx}{\partial x} + \frac{\partial \tau yz}{\partial z}\right) = \rho \frac{\partial^2 w}{\partial t^2} \tag{95}$$

This formulation can be expressed alternatively using the elementary definitions of axial and shear strain.

$$\left(\frac{\partial^2 w}{\partial y^2} E + G\left(\frac{\partial^2 w}{\partial x^2} + \frac{\partial^2 w}{\partial z^2}\right)\right) = \rho \frac{\partial^2 w}{\partial t^2} \tag{96}$$

Suppose we perform the following operation

$$\frac{\partial^2 w}{\partial t^2} = \frac{1}{\rho}\left(\frac{\partial^2 w}{\partial y^2} E + G\left(\frac{\partial^2 w}{\partial x^2} + \frac{\partial^2 w}{\partial z^2}\right)\right) \tag{97}$$

Assume that there is no body load and Shear Forces are the only type transmitting through the element. If this assumption holds then the following equation must be true

$$\frac{\partial^2 w}{\partial t^2} = \frac{G}{\rho}\left(\left(\frac{\partial^2 w}{\partial x^2} + \frac{\partial^2 w}{\partial z^2}\right)\right) \tag{98}$$

Which is equal to

$$\frac{1}{Vs^2}\frac{\partial^2 w}{\partial t^2} = \left(\left(\frac{\partial^2 w}{\partial x^2} + \frac{\partial^2 w}{\partial z^2}\right)\right) \tag{99}$$

And then applying a Fourier Transform such that space and time are transformed into wavenumber and frequency. A Fourier transform is useful because it can take any harmonic signal in time and space and represent it mathematically as the summation of an infinite number sine and cosine waves.

$$U(k, \omega) = \int_{-\infty}^{\infty} \int_{-\infty}^{\infty} U(x, t) e^{-(\omega t - kx)} \, dx \, dt \qquad (100)$$

Capitalized W represents the transformed solution in wavenumber domain and frequency range to the displacement of the differential equation w.

After the transform is conducted the following differential equation is true. (Kausel 2005)

$$\frac{\partial^2 W}{\partial z^2} = \left[-k^2 + \frac{\omega^2}{Vs} \right] * W \qquad (101)$$

The solution to this differential equation takes the form

$$W = C_1 e^{-i\beta\theta} + C_2 e^{i\beta\theta} \qquad (102)$$

$$\beta = \sqrt{-k^2 + \frac{\omega^2}{Vs}} \qquad (103)$$

2.7.1. Near Field Affect

The near field affect is the phenomena where wave fronts generated by a point source in a three dimensional elastic space attenuate at variable rates and propagate at different velocities. This condition arises from the coupling behavior of wave fronts emanating spherically from the source. Analytical solutions exist for the near field using Stokes's fundamental solution and a Green displacement vector field (Arulnathan et al. 1998).

In an elastic infinite medium a harmonic source emanates wave fronts that are either dilatational or longitudinal. The near field affect generates shear wave motion due to compression wave interference. The error from the near field affect can be reduced by increasing the frequency of the input signal and increasing the distance from the source to the receiver element. In the latter

case, the separation distance is expressed as a ratio of the tip to tip distance and the wavelength of the source, or $\frac{L_{tip\ to\ tip}}{\lambda}$. Theoretical work has proven that the near field affect will cause significant errors in travel time measurements when $\frac{L_{tip\ to\ tip}}{\lambda} > 1$. A ratio between 2 and 10 is recommended and a value of 3.33 or greater is suggested to minimize the error in the output single. The near field cannot be totally eliminated by increasing the distance of separation or increasing the input frequency.

2.8. Bender Element Instrumentation

2.8.1. Piezoelectricity

Piezoelectricity is a material property that relates mechanical deformation to an electric potential. In a piezoelectric material deformations are possible through the application of an electric current. Conversely, a piezoelectric material will produce a voltage if it is mechanically deformed. (Deniz, 2008). The voltage output is a function of the polarization direction of the crystalline structure. (Lee and Sanatmarina, 2005).
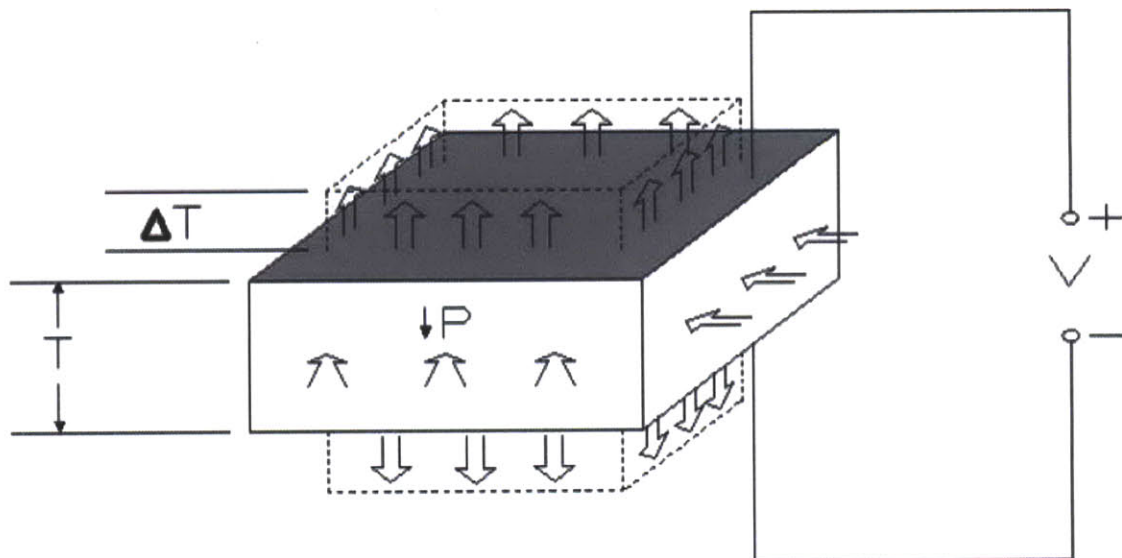
Figure 2.11: A Piezoelectric Element deforming laterally to an applied potential. From (Deniz, 2008)

48

2.8.2. Bender Element Composition

Bender elements are tiny plates composed of piezoelectric ceramics (Deniz, 2008). These plates behave as electro-mechanic transducers converting electrical energy to or from mechanical energy.

A bender element consists of two piezoelectric plates divided by a metal shim at the center. When an electrical current is applied to either of the piezoelectric surfaces an elongation or contraction effect is produced depending on the polarization. The surfaces are not free to expand or contract independently. The net product of this action is a bending deflection of the entire element.

Referring to Figure 2.12 (a) piezoelectric ceramic plate subject to expansion will experience tension and the ceramic plate contracting will undergo compression. This results in an mechanical defection in the bender element similar to a cantilever beam subjected to vertical displacement.
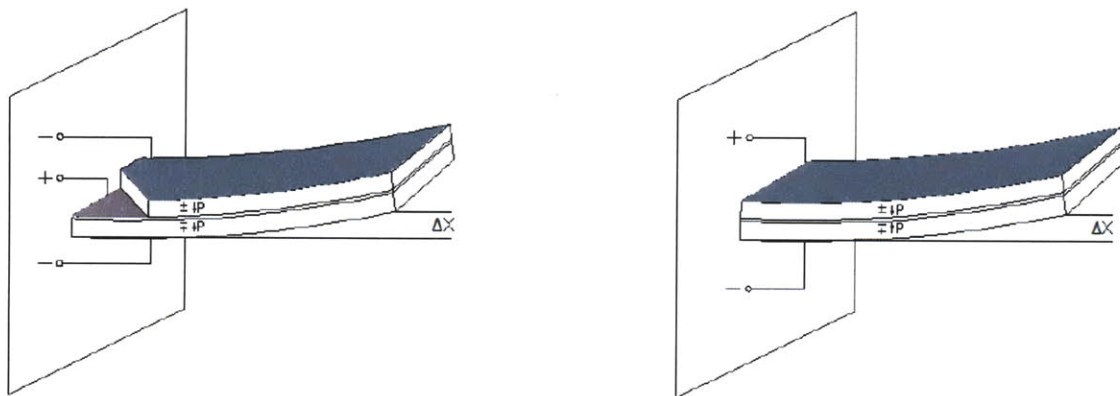
Figure 2.12: (a) a parallel connection bender element. (b) a series connection bender element. From (Deniz, 2008)

2.8.3. Bender Element Configurations

It is possible to manufacture bender elements with piezoelectric ceramic plates that have an identical polarity configuration such that both plates will behave identically to an applied voltage or an opposite polarity such that the plates will have an opposite reaction. The former is referred to as a Parallel connection bender element, also known as a Y-Poled bender element, and is provided in Figure 2.12(a). The later is referred to as a Series connection bender element, also known as a X-Poled bender element, and a Figure is provided in 2.13(b).

2.8.4. Mathematics of Bender Element Configurations

It is possible to determine deflection and voltage output of a parallel connection bender element and a series connection bender element by utilizing known mathematical relationships of deflection to geometry and material properties. (Leong et al. 2005)

For a parallel connection bender element then the following relationships are true.

$$V = \frac{3FLg_{31}}{4WT} \tag{104}$$

$$X = \frac{3VL^2d_{31}}{T^2} \tag{105}$$

Here d_{31} and g_{31} are the piezoelectric constants for the bender element ceramic material. g_{31} is in units of $[\frac{V*L}{F}]$ and d_{31} is in units of $[\frac{L}{V}]$. L is the cantilever length of the bender element. W represents the width and T is the thickness of the bender element. V is the voltage, F is the force.

The a series connection bender element.

$$V = \frac{3FLg_{31}}{2T^2} \tag{106}$$

$$X = \frac{3VL^2 d_{31}}{2T^2}$$

(107)
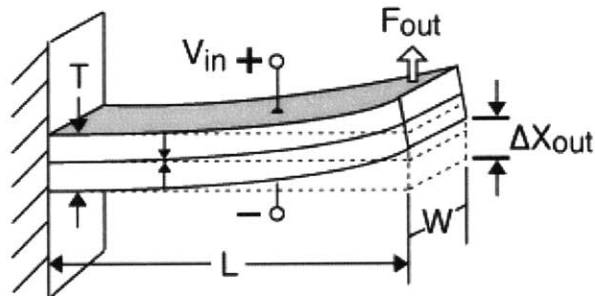
Figure 2.12c: A representative series bender element produce both deflection and force. Note Δx = x in the equations above. From (Piezosystems 2010)

The equations for series and parallel configured bender elements are expressed in terms of voltage proportional to force. The second form of equation is voltage proportional to deflection expressed as x. An applied voltage can produce a force F_b that does not have a deflection component or the applied voltage can produce a deflection X_f that exerts no force. A linear relationship can be expressed that relates the force exerted to the deflection produced. A diagram of this relationship is provided in 2.12d.
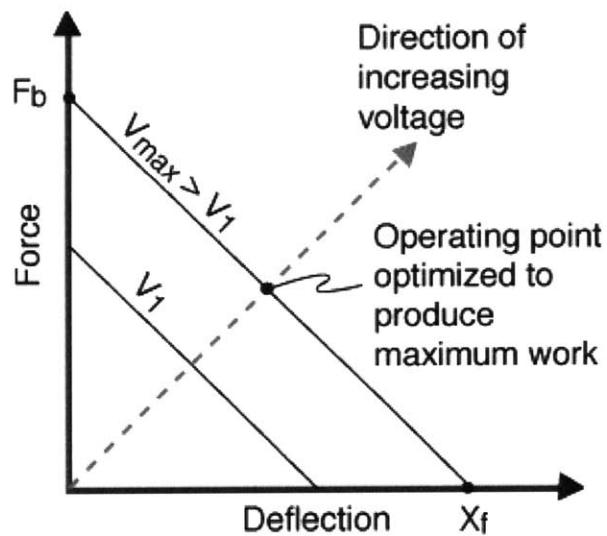
Figure 2.12d: Relationship of force to deflection in a bender element. From (Piezosystems 2010)

2.9. Methods of Interpreting Bender Element Tests

It has been established that body waves for an elastic medium are composed of both compression and shear waves. An accurate bender element test should correctly provide an input or source signal and an output or receiver signal in amplitude, usually in space, range and time domain. However directly processing the input and output signals into P and S wave velocity measurements is not a seamless step. It requires an interpretation of the output signal using travel time methods. Moreover interpretation of the input signal can be represented as a free deflection or a blocked force scalar with the corresponding equations in provided in (101), (102), (103), and (104).

2.9.1. Methodology of Determining Travel Time for a Bender Element Test

The travel time of a wave with a constant velocity can be defined as the time elapsed for the wave to travel between two arbitrary points in space. For bender element testing, there are three accepted methods of determining traveling time in geotechnical literature. They are (1) first arrival method, (2) peak to peak, and (3) cross correlation method. Currently, ambiguity exists for researchers and academics regarding exactly what method is standard or optimal.

2.9.2. First Time Arrival Method

The first time of arrival method asserts that the travel time between two points in space may be taken as the difference of first direct arrivals at the two points (Arulnathan et al. 1998). This computation is achieved through taking the difference between the instantaneous point in time the source signal is sent and the instantaneous start of the major arrival of the receiver signal. The major arrival is a subjective determination of the significant wavefront. In a bender element test this would translate as the time between the start of the voltage pulse input and the beginning of the first arrival signal. The initial weak portion of the received signal should be discarded in this method for both P and S wave velocity measurements. A weak initial arrival in S-wave testing indicates the presence of the near field affect (Kumar and Madhusudhan 2010). Ambiguities exist in this method because there is no objective criteria to determine the location

52

of the first signal (Arulnathan et al. 1998). An illustration of this method is provided in Figure 2.15

2.9.3. Peak Time Arrival Method

Travel time of a sinusoidal wave may be taken as the time between any two characteristic points of the source and receiver wave while ignoring initial weak portions of the received single (Kumar and Madhusudhan 2010). The most common points taken for this method are the peaks of the source and receiver wave. Other facets of the geometry could theoretically be used and the method is not exclusive to the peaks of the signals. A graphical representation, tpp, of the method is provided in Figure 2.13.
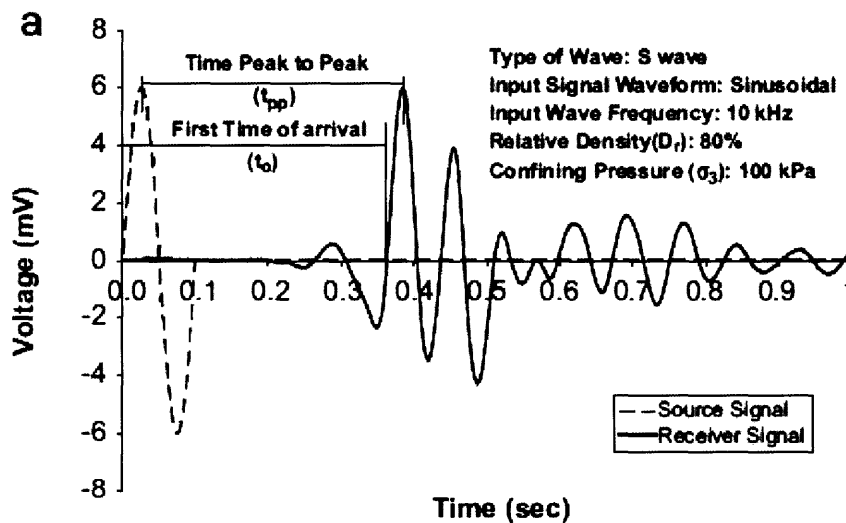
Figure 2.13: A graphical representation of an source and receiver signal. (a) Illustration demonstrating First Time of Arrival method to (b) Illustration demonstrating Peak to Peak method tp. From (Arulnathan et al. 1998).

2.9.4. Cross Correlation Method

Unlike the previous two methods, the cross correlation method is an analytic operation. The cross correlation method asserts that the travel time between two points in space may be

calculated as a time shift that creates the peak cross correlation between signals recorded between the aforementioned two points (Viggiani and Atkinson. 1995). This method assumes that source and receiver signals are true plane wave fronts and that any reflected or refracted waves are negligible (Arulnathan et al. 1998).

The cross-correlation function is a measure of the degree of correlation of the receiver and source signals, represented as X(T) and Y(T) respectively, imposed against a time shift τ. This method transforms two signals, of known space and time, into signals of space and frequency using a Fast Fourier Transform and then uses computational methods to determine the mathematical optimal correlation between the two signals.

The analytical representation of the cross correlation is provided.

$$CC_{xy}(t) = \lim_{\tau \to \infty} \int_{\tau} X(T)Y(T+t)dt \tag{108}$$

To solve this integral using non-intensive mathematics the standard procedure is to transform both the source and receiver signal into frequency domain using a Fast Fourier Transform, represented as FFT.

$$L_x(f) = FFT[X(t)] \tag{109}$$

$$L_y(f) = FFT[Y(t)] \tag{110}$$

Here Lx and Ly are the frequency domain representations of the receiver and source signal respectively. The cross power spectrum of the frequency is the product of the complex conjugate of the source signal in frequency domain and the receiver signal in frequency domain. Alternatively this can be represented as

$$GGxy = L_y^*(f)L_x(f) \tag{111}$$

$$L_y^*(f) = complex\ conjugate\ L_y(f)$$

The cross correlation of the source and receiver signals can now be taken.

54

$$IFFT(GGxy) = CCxy \tag{112}$$

Here IFFT represents the inverse Fast Fourier Transform; its calculation produces signal in space and time domain. The travel time of the sine pulse can now be taken as the time value that corresponds to the maximum amplitude of the cross correlation. The maximum $CCxy$ extracted from this calculation is used to normalize the range of $CCxy$ values. Accordingly, the cross correlation travel time occurs where $\frac{CCxy}{CCxymax} = 1$. A graphical representation is provided in Figure 2.14.
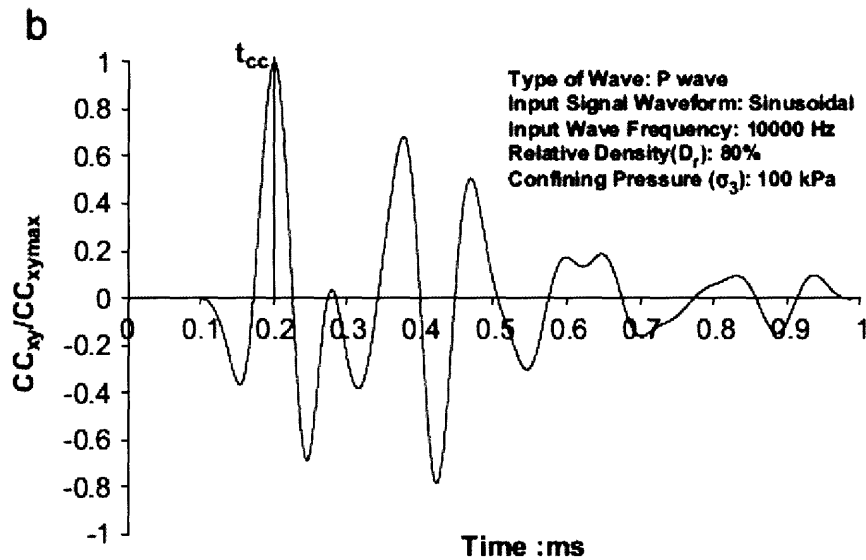
Figure 2.14: Typical output for a cross correlation function from a bender element measurement. Notice tcc is the maximum normalized value in the function. From (Arulnathan et al. 1998).

2.10. Development of empirical relationships in field conditions that incorporate void ratio and stress state into shear wave velocity measurements

The necessity to adopt wave propagation theory into a Geotechnical framework has lead to many engineers formulating wave propagation in terms of stress state, over consolidation ratio, and void ratio. Both sands and clays are considered in this framework and empirical relationships have been developed to assess sand and clay wave propagation. In both coarse grained soil and fine grained soil, knowledge of shear wave propagation velocity in shear testing

55

leads to information about the engineering properties of the soil, in particular, the shear modulus and anisotropy, the void ratio and the stress state. Examinations of wave propagation documented for sands (Fioravante et al. 2001) and clayey soils (Shibuya et al. 1997) , (Joviĉić et al. 1998) have tried to structure these relationships to a reliable framework.

Under isotropic conditions, the relationship between the shear modulus and the velocity of shear waves is:

$$Gmax = \rho * Vs^2 \tag{113}$$

The maximum observed Shear Modulus of the soil medium is $Gmax$. The mass density of the soil medium is ρ . If the soil is dry then the mass density is the dry density of the soil specimen "$\rho(d)$". If the soil is saturated then ρ is the saturation density "$\rho(sat)$". (2008. Qiu. et al.) Shear wave velocity is Vs.

Models provided for sand and clay assume that equation (110) is valid. It lacks the rigor to explain the physics behind wave propagation in all orientations because soil deposits rarely have isotropic behavior in field conditions. The shear modulus recorded in one direction of propagation may not equal the modulus for other directions of propagation. Typically, the anisotropy is divided between the horizontal and vertical directions; this is termed cross anisotropy if the cross-anisotropy is formed by 1-D deposition (Fioravante 2001). The equation relating the velocity of wave motion to the square root of the shear modulus divided by mass density is the foundation for further derivation of a wave propagation soil model. The implications of this equation are:

1. The total mass density of the soil is proportional to the shear modulus. In highly compacted soil the calculated shear modulus should be greater than a loose deposit of the same soil assuming constant anisotropy if the shear velocity is constant.
2. Accordingly, the void ratio and the specific volume of the soil should be inversely proportional to the wave velocity. The void ratio reduces with the application of a one dimensional stress according to 1-D consolidation.
3. The experimental shear wave velocity depends on the soil anisotropy.

56

Further exploration of the shear modulus shows that there is a relationship between the shear modulus and the Young's Modulus with the addition of the Poisson's ratio given by equation (111). Where the Young's modulus of the soil medium is E and the Poisson's ratio of the soil medium is η

$$G = \frac{E}{2(1 + \eta)} \tag{114}$$

Shibuya (1978) constructs an empirical interpretation that states that the shear modulus of a soil under isotropic consolidation can be expressed:

$$Gmax = C * OCR^k * f(e) * \sigma'c^n * \sigma r^{(1-n)} \tag{115}$$

C is an empirical constant of soil medium. The overconsolidation ratio, OCR, is the ratio describing the stress history of the soil. An arbitrary void ratio function is f(e). The current effective confining stress is σ'c. A reference stress, typically used as the atmospheric pressure, utilized to make independent of units, or more correctly, to give $Gmax$ in units of choice. Independent exponents are k and n.

The void ratio of a soil is a function of the current stress state according to consolidation theory. According to this framework the void ratio function $f(e)$ is a function of the current void ratio e at the confining stress. $f(e)$ is not an analytically derived function but an empirical equation taken from the interpreted shear wave velocity.

Alterations to this framework are possible to produce a better function in engineering practice. Experimentation of wave propagation in soil concludes that the affect of the OCR has a negligible effect on Gmax if the void ratio function is taken into account. (Shibuya 1998), Moreover, the out of plane stress normal to shear wave propagation is independent of Gmax (Shibuya 1998).

Shibuya (1998) simplifies his original empirical equation to:

$$Gmax = Svh * f(e) * \sigma'v^{nv} * \sigma'h^{nh} * \sigma r^{(1-nv-nh)} \tag{116}$$

Svh is material constant derived from the soil structure and σ'v, σ'h are the effective vertical

and horizontal effective stresses, respectively. While nv ,nh are independent exponents.

In conditions where the exponent of the vertical stress is equivalent to the exponent of the

horizontal stress the equation is simplified (Shibuya 1998).

$$nv = nh \tag{117}$$

This condition applies to conventional down-hole seismic surveys on level ground or in

laboratory tests using vertically cut specimens. Under these conditions the effects of the two

principal stresses on Gmax are equal:

$$Gmax = A * f(e) * \sigma'v^{2nv} * \sigma r^{(1-2nv)} \tag{118}$$

$$A = Svh * K0^{nv} \tag{119}$$

The K0 value is defined as the coefficient of earth pressure at rest.

Jovičić (1998) conducted an investigation of anisotropy of Kaolin clay with bender elements.

The same basic principle of shear wave propagation used in Shibuya's construction is used in

Jovičić's examination, however, in a slightly altered framework. Jovičić inserts the atmospheric

stress as the reference stress rather than an arbitrary reference stress, which Shibuya assumes.

Jovičić's model for reconstituted Kaolin assumes an empirical relation provided.

$$Gmax = S * OCR^k * f(e) * p^m * pa^{(1-n)} \tag{120}$$

Such that:

η: (=q/p')

Here p' and q are the Cambridge stress space values.

$$p' = \frac{1}{3} * (\sigma'v + 2\sigma'r,) \; q = \sigma'v - \sigma'r \tag{121}$$

58

The term pa is the atmospheric pressure. S is defined as the coefficient relating to the soil fabric and n is an independent exponent.

Jovičić's equation for clays constructs the shear modulus as a function of both the confining stress (Cambridge "p") and the shear stress (Cambridge "q"), which are defined above. This is a better method of determining the shear modulus than other equations that depend solely on the one dimensional isotropic confining stress. The shear modulus cannot depend only on the confining stress because the application of a shear stress component will produce some degree of work in the specimen. (Jovičić 1998)

An obvious observation is the empirical equations are remarkably similar. According to Kaolin clay equation the current stress state is expressed in terms of the Cambridge definition of p' and atmospheric stress and Shibuya's equation uses a reference stress and an isotropic confining stress. Both use empirical constants as multiplication operators, C and S. It is clear that these equations are simply manipulations of the same concept. The shear modulus, which is measured through bender elements, is directly a function of the void ratio, stress state, fabric, and the over consolidation ratio.

As demonstrated, these equations are empirical relations that approximate the shear modulus to engineering parameters. However, the over consolidation ratio is of negligible value if the void ratio is accounted (1998 Shibuya). The shear wave velocity can be directly substituted in place of the shear modulus. A direct relationship of the shear wave velocity to the stress and volumetric state can be formed. Fioravante's examination of piezoelectric transducers in triaxial testing of sandy soils uses a simplified mathematical construction (Fioranvante 2001).

$$ Vs = Cs[f(e)\psi(\sigma')]^{0.5} $$

Cs is a material constant. A generalized void ratio function, f(e), is used. Fioravante uses f(e) = e^(2d) in his formulation but additional proposed equations exist. A normalized effective stress function is defined as

$$ \psi(\sigma') = (\frac{\sigma'a}{pa})^{2na} + (\frac{\sigma'b}{pa})^{2nb} + (\frac{\sigma'c}{pa})^{2nc} \tag{122} $$

Here $\sigma'a$, $\sigma'b$, and $\sigma'c$ are the principle stresses in three dimensional space. Pa is atmospheric pressure. Fioravante (2001) manipulates his initial equation of shear wave velocity in sands to write a general equation for the shear modulus as a function of void ratio and stress state.

$$Gmax = \rho * Cs^2 (f(e)\psi(\sigma'))^{0.5}$$

(123)

2.10.1. Expression for the Young's Modulus of Normally Consolidated and Over Consolidated Resedimented Boston Blue Clay

Santagata et al. stated that the Young's modulus, excluding creeping effects, at a given OCR in NC and OC RBBC is correlated to the differences in the pre-shear void ratio. The initial void ratio has a direct relationship with the stress state. Accordingly, the Young's modulus can be expressed as a function of the initial mean effective stress state. It was found that the expression fits well all the data obtained for RBBC with OCR 1-8.

$$EuMAX = A * OCR^k * p'mc^n$$

(124)

Alternatively, initial Young's modulus can be expressed by both e and $\sigma'vc$, taking an equation of the form:

$$EuMAX = A * OCR^k * p'mc^n$$

(125)

This equation is better suited for predictive purposes because in situ mean effective stress and OCR are more easily determined than void ratio. Equations (124) and (125) are invalided if large aging effects occur on the soil.

2.10.2. Matrix Formuation of wave propagation

60

In an infinite medium the velocity of compression or dilatational wave is a function of the Bulk Modulus rather than the Young's Modulus. A mathematical derivation proving this fact is provided in section "2.5. Derivation of Stress Waves in Elastic Isotropic Infinite Medium". In a stress state such that only axial strains exist in a three dimensional specimen, the bulk modulus is equal to the constrained modulus.

The shear modulus and constrained modulus are simply the ratios of applied stress and strain. There are six independent dimensions of stress and strain, specifically, the three principle stress directions and the three principle shear stress directions. (Fioravante 2001). A matrix can be constructed that uses all the principle components to express stress as a product of modulus and strain. The six independent dimension of normal and shear stress are listed in the matrix columns. The matrix function is attached:

$$
\begin{bmatrix} \sigma_x \\ \sigma_y \\ \sigma_z \\ \tau_{zx} \\ \tau_{zy} \\ \tau_{xy} \end{bmatrix} = \begin{bmatrix} M_H & M_H - 2G_{HH} & C_{13} & 0 & 0 & 0 \\ M_H - 2G_{HH} & M_H & C_{13} & 0 & 0 & 0 \\ C_{13} & C_{13} & M_V & 0 & 0 & 0 \\ 0 & 0 & 0 & G_{VH} & 0 & 0 \\ 0 & 0 & 0 & 0 & G_{VH} & 0 \\ 0 & 0 & 0 & 0 & 0 & G_{HH} \end{bmatrix} \begin{bmatrix} \varepsilon_x \\ \varepsilon_y \\ \varepsilon_z \\ \gamma_{zx} \\ \gamma_{zy} \\ \gamma_{xy} \end{bmatrix} \quad [5]
$$

Four of the five constants can be determined from seismic body wave velocities along the two principal stress directions (i.e., axial ≡ vertical and radial ≡ horizontal) as follows:

- $M_H = \rho V_{P,H}^2$: horizontal constrained modulus, gathered from horizontal P_H-waves.
- $M_V = \rho V_{P,V}^2$: vertical constrained modulus, from P_V-waves vertically propagated.
- $G_{VH} = \rho V_{S,VH}^2$: shear modulus in a plane including the axis of symmetry, obtained from S_{VH}-wave vertically propagated with soil particles vibrating in horizontal direction.
- $G_{HH} = \rho V_{S,HH}^2$: shear modulus in the plane of isotropy, from S_{HH}-wave, horizontally propagated with soil particles vibrating in the horizontal plane.

Figure 2.15: Fioranvante's matrix construction. From (Fioravante 2001).

Using this model Fioranvante (2001) evaluated five independent constants, assuming a soil deposit characterized by a vertical axis of symmetry and cross anisotropy. This framework of anisotropy provides a sound basis to approach a wave propagation problem because it accounts for anisotropy using the principle stress components by analyzing each spatial dimension individually.

Fioranvante (2001) and Jovičić (1998) use a triaxial cell to control the stress induced anisotropy. Triaxial cells have a direct advantage over other shear testing apparatuses because of the greater control over the stress state of the soil. Triaxial cells can provide an isotropic stress state and an anisotropic stress state, with the radial stress value having a different value than the axial stress. Moreover, the triaxial cell gives better control and measurement over the pore pressures than other shear devices such as DSS. Bender element investigations use a triaxial cell configuration with bender elements grafted to the specimen membrane to produce shear waves. Jovičić (1998) uses a similar configuration.

2.11. Anisotropy and Isotropy

By definition, isotropy is a unique condition where uniformity of elastic properties is present in all orientations. Anisotropy is the negation of this condition, discontinuity with respect to orientation and direction. In soils, an isotropic state has uniformity, in all spatial directions, with respect to a defined engineering property. Stress isotropy is a state of stress where a soil element is under equal stress in all dimensions. An anisotropic stress state is a state of stress where there is inequality between the principle stresses.

The behavior of soils to wave agitation requires further exploration into soil anisotropy. Fioravante assumes that soil anisotropic behavior can be expressed as the sum of two components (Fioravante 2001).

1. Inherit anisotropy: Anisotropy resulting from the fabric and inherit structure of the soil forming from the depositional process, bonding/aging affects, and age morphology.

2. Stress induced anisotropy: Anisotropy resulting from the current stress conditions imparted on the soil.

2.11.1. Inherit Anisotropy

Soil deposits are frequently formed in approximately horizontal layers. Submerged layers are subjected to a one dimensional load from the overburden. Under virgin compression the coefficient of earth pressure at rest is less than one. This causes an anisotropic stress state. The mode of deposition of the soil produces a preferred orientation of packing. The deformation characteristics of the layered soil have anisotropic behavior. According to Ladd, nearly all natural deposits have anisotropic packing. The depositional process is the mechanism for the one-dimensional stress history in soils, therefore, the inherit anisotropy could account for all or the majority of the strain anisotropy (Ladd 1977).

2.11.2. Literature Discussion of Anisotropy

In clays created from slurry Jovičić (1998) adds an additional mode of anisotropy strain anisotropy. Strain induced anisotropy is the anisotropic behavior resulting from earlier plastic strains in the soil not resulting from the depositional process but resulting from compression of a slurry. Jovičić defines inherent anisotropy as the state of anisotropy of the soil in the in situ condition and the strain induced anisotropy as the anisotropy resulting from strains observed in a reconstituted specimen where the inherent bonding of the soil is negligible .

Fioranvante (2001) assumes that cross anisotropy can be expressed as a ratio of the horizontal wave velocity to the vertical wave velocity. In an isotropic stress state, the wave propagation ratio is expressed:

$$\text{Inherent Anisotropy} = \frac{V_{S,HH}}{V_{S,VH}} \tag{126}$$

Vs is observed shear velocity, the first subscript indicates the type of wave (shear), the second subscript indicates the wave direction, and the third subscript indicates the wave polarization.

Therefore, assuming constant density throughout the specimen, the equation can be rewritten as:

$$\text{Inherent Anisotropy} = \sqrt{\frac{G_H}{G_V}} \tag{127}$$

Moreover, if the void ratio function is assumed to be uniform throughout the specimen and the specimen is sheared so that radial strains do not develop then K0 can be expressed: (Fioravante 2001).

$$f(\frac{V_{S,HH}}{V_{S,VH}})^n = \frac{\sigma'_r}{\sigma'_a} = K_0 \tag{128}$$

$$n = na + nr = empirical\ exponents$$

2.12. Bender Element Testing for Shear Wave Propagation in Drained Ticino Sand Specimens

Two triaxial tests were conducted on Ticino Sand specimens reconstituted by pluvial deposition and at nearly the same initial void ratio (0.86 and 0.90). The specimens were compressed under isotropic effective stresses at intervals of (20,25,50,100 kPa). Wave velocity measurements were taken at the end of each step after a ten minute rest period. The results are attached:
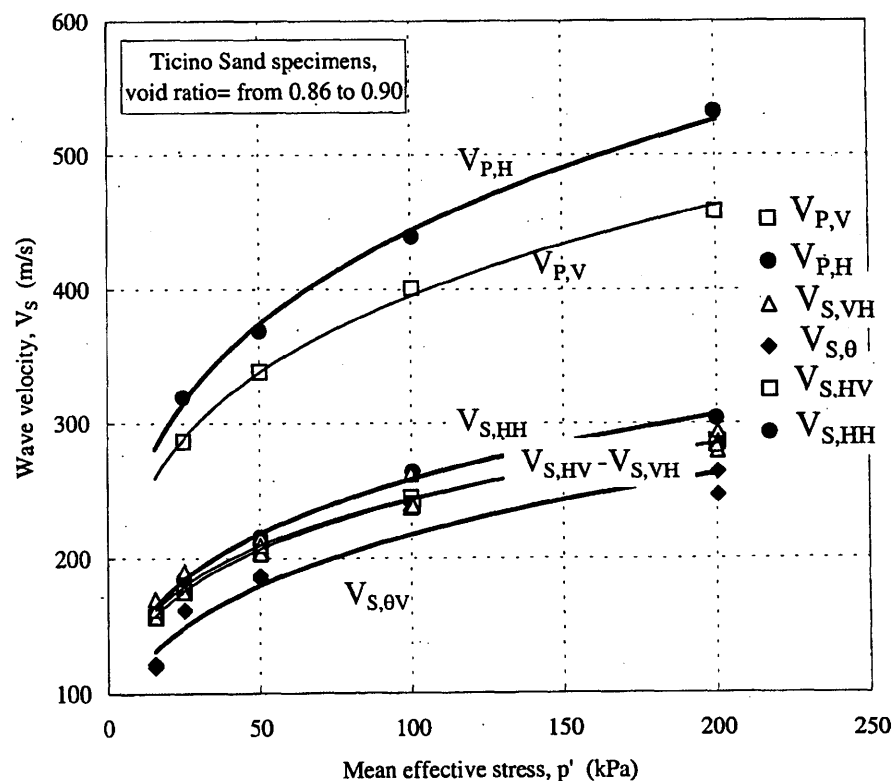
Figure 2.16: Effects of mean effective stress on the P and S wave velocities. From (Fioravante 2001).

Fioravante (2001) conducted two wave velocity measurements: compression (P) and shear (S) in different directions and polarizations in the shear case. The shear component was measured at oblique orientations (neither horizontal nor vertical) represented by theta. The capital letter V refers to propagation velocity, the first subscript indicates the type of wave (shear

or compression), the second subscript indicates the wave direction, and the third subscript indicates the wave polarization.

These results lead to two conclusions about drained Ticino Sand subject to wave propagation testing. The shear wave velocities in the horizontal and vertical directions are equivalent provided either the polarization or direction of the shear wave is within the principle direction in the vertical plane. Secondly, the inherit anisotropy of the Ticino Sand dictates that the shear waves having both direction and polarization in the horizontal plane move faster than the vertical.

Fioranvante (2001) applied anisotropic stress conditions in other triaxial tests of the specimens to investigate stress induced anisotropy. The anisotropic stress conditions were tuned such that the cell pressure was held constant at 300kPa while the axial stress varied from 200 to 750kPa. The experimental results are graphed in Figure 2.17.
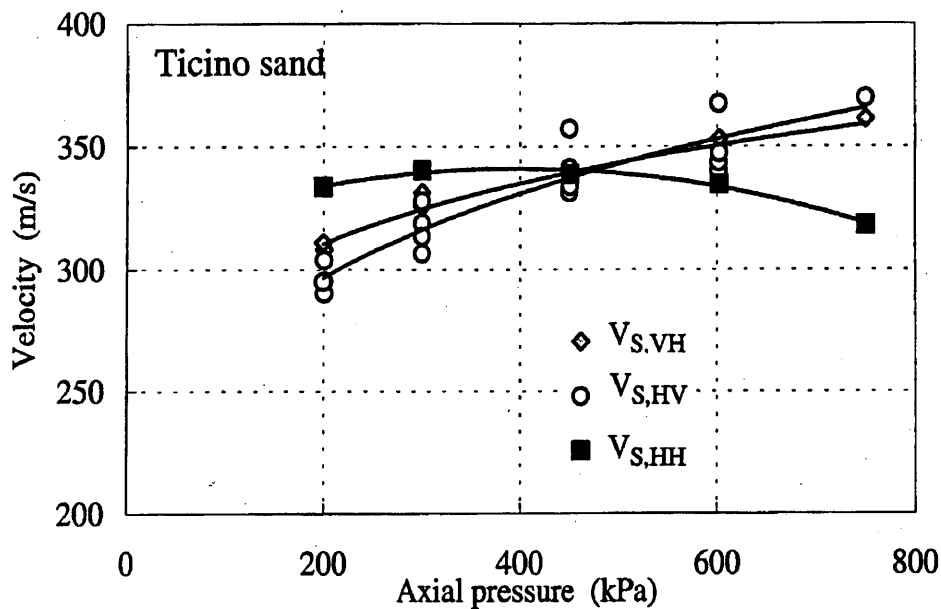
Figure 2.17: Effects of the axial pressure on horizontal and vertical S-waves propagated in a loose Ticino Sand triaxial specimen under a constant radial stress of 300 kPa. From (Fioravante 2001).

Two trends of wave velocity are present in the three shear wave tests. The shear wave velocity increases with the application of axial stress, as predicted by the empirical equations

66

when either a polarization component or a velocity directional component is in the direction of stress application. The velocity of the shear wave, $V_{S,HH}$ having components of polarization and directional velocity that are out of plane with the application of axial stress shows little to zero variation as the axial stress increases. This result supports Jovičić's assertion for clays that the anisotropy of the stress state influences the small strain shear modulus acting in the direction of wave propagation and the direction of particle motion, but that variations in the out of plane stresses, in this case $V_{S,HH}$, did not. (1998. Jovičić et al.)

2.13. Bender Element Testing for Shear Wave Propagation in Natural London Clay

Jovičić (1998) conducted bender element tests to understand the anisotropic behavior of clay. This testing attempted to investigate the inherent anisotropy of intact London Clay specimens. Natural London Clay specimens were gathered at controlled depths and subjected to an isotropic effective stress state with the intention to reproduce the in situ stress conditions. The large overconsolidation ratio of the London Clay minimized the development of strains from the applied isotropic stress. There was a difficultly preparing high quality specimens because of the presence of fissures within the clay and the amount of test specimens were minimized. The specimens had isotropic effective stresses applied that were equal to in situ. As a consequence of soil overconsolidation, the application of the isotropic stresses produces small strains.
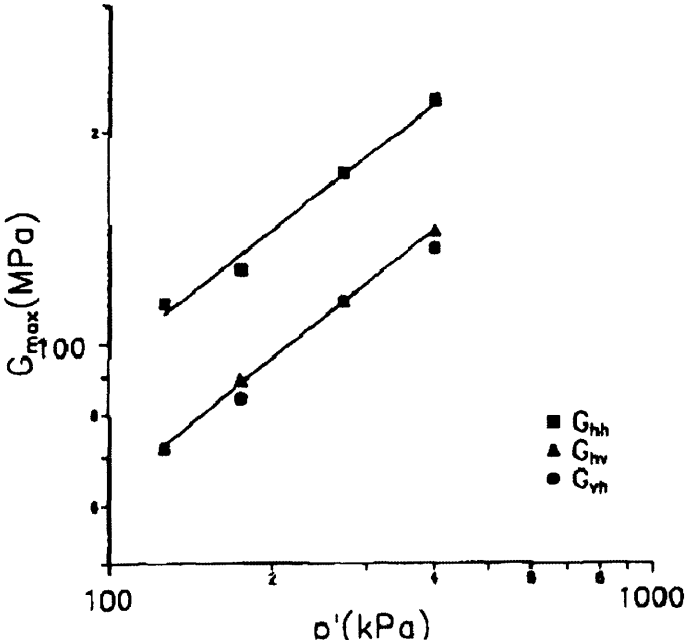
Figure 2.18: Bender Element Tests on Oriented Specimens of Intact London Clay

The tests conclude that natural intact London clay has inherent cross anisotropy. The relationship of confining stress to the shear modulus has a well defined linear log behavior for both the horizontal and the vertical directions, which have an equal first derivative.

3. Explanation of Abaqus Finite Element Model

3.1 Introduction

This section will establish procedures used to construct valid models for Finite Element Analysis. Abaqus is a commercial finite element analysis software program. It is advertised as a finite element method or FEM capable of solving problems ranging from relatively simple linear analyses to nonlinear simulations which include heat transfer, mass diffusion, thermal management of electrical components (coupled thermal-electrical analyses), acoustics, soil mechanics (coupled pore fluid-stress analyses), and piezoelectric analysis. Accordingly, it can compute dynamic wave propagation problems.

The finite element method, otherwise known is finite element analysis, is a numerical method used to find solutions to partial differential equations (PDE) and integration operations. The analysis can be done by suppressing the differential operator by assuming steady state or solving ordinary differential equations through standard mathematical algorithms.

A finite element simulation constructs a model by dividing the actual geometry of a structure using a collection of finite elements. A finite element corresponds to a discretized portion of the model geometry. The finite elements are joined by nodes. The aggregate collection of the nodes in the model geometry is the mesh.

The objective of the finite element analysis in this research is to arrive at an accurate approximation to bender element testing done in consolidometer or triaxial environments. Through the analysis it is necessary that the FEM method be able to simulate experimental bender element testing. The analysis depends on the initial conditions or boundary conditions of the model. In our experiments the boundary conditions include confining stress state, material compositions and geotechnical engineering properties, geometry, and bender element orientation.

The procedure Abaqus follows when solving a model is divided into three intervals. The intervals are input, computation, and output.

3.2. Essential Abaqus Intervals

3.2.1 Input Interval

The input interval can be completed either through the Abaqus Graphical User Interface, indentified as Abaqus CAE, or by writing a script using Python programming language. Abaqus CAE automatically writes an input file based on the information provided in the graphical user interface. Alternatively, an input file can be written directly by using a standard text program to code commands in Python using syntax and keywords defined in the Abaqus library.
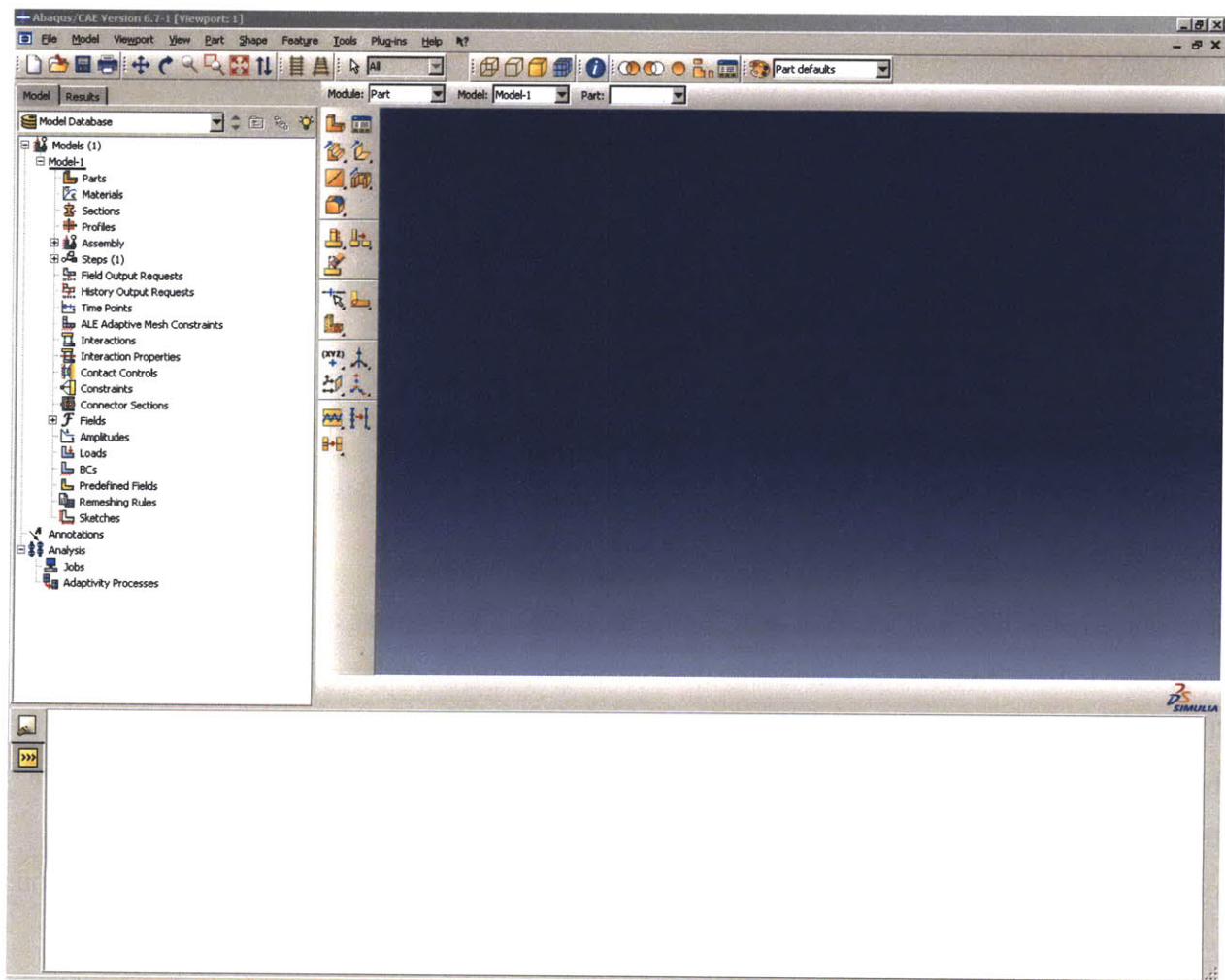
Figure 3.1: Abaqus CAE

3.2.2. Computation Interval

The computation interval processes the input file into Abaqus' default solver. This procedure is the most computationally demanding interval of the analysis. The solver transforms the input file into a coherent finite element analysis matrix framework using methods established by finite element analysis. The time of computation is dependant on the number of elements, the complexity of the mesh parameters, the number of time steps, the number of dimensions required for analysis, and the requirements of the field output.

3.2.3. Output Interval

The output interval is the graphical solution of the computation interval. Its purpose is the provide a graphical tabulation of the PDE solutions defined by the input and computation intervals. The output of a model can be refined by defining parameters in the field output request located in the input interval. A field output request defines the quantities and nodes to be solved. The information contained in the output file depends entirely on the field output request. It follows that a given output file can be very large, in terms of byte, and contain a considerable amount of information. Conversely, the field output is comparatively small if the field output is restricted only to include a smaller amount of nodes or output variables.

3.3. Building an Example Model

Over the course of the research several models using Abaqus were developed. The example model corresponds to a representation of the variety of models examined. This section illustrates the development process using a single example.

3.3.1. Defining the Geometry

All finite element models require a geometry to discretize into elements and nodes for finite element analysis. The geometry of a model can contain multiple parts that interact through defined interactions or a single part acting as a singular unit. The input geometry is defined using spatial dimensions, Length $[L^1]$, Area $[L^2]$, and Volume$[L^3]$.

In the Abaqus CAE or graphical user interface, the geometry is defined through the part module. In the part module, the physical geometry of a model built through the sketch command. In the sketch command it is possible to construct many shapes and possible geometries. The geometry is restricted to Euclidian definitions.

Consider a simple geometry, a cylinder, or a rod, in units of $[L^3]$. Suppose the diameter, H, of the cylinder is x_1 and the length, or height, is y_1. Assume it is necessary to represent this geometry into a two dimensional plane strain model. It follows that it is required to reduce this volumetric geometry to two dimensions. A good two dimensional representation of the cylinder is a plane bisecting it through the centroid. The cross section of cylinder through its centroid is a rectangle with a cross sectional area $[L^2]$, decomposed with dimensions Length $[L^1]$ and Width $[L^1]$. Accordingly, at this plane the width of the cross section is equivalent to the diameter. It is of note that the plane strain model is not the optimal setting for an axisymmetric rod; the loading asymmetric nature of the loading require plane strain conditions.
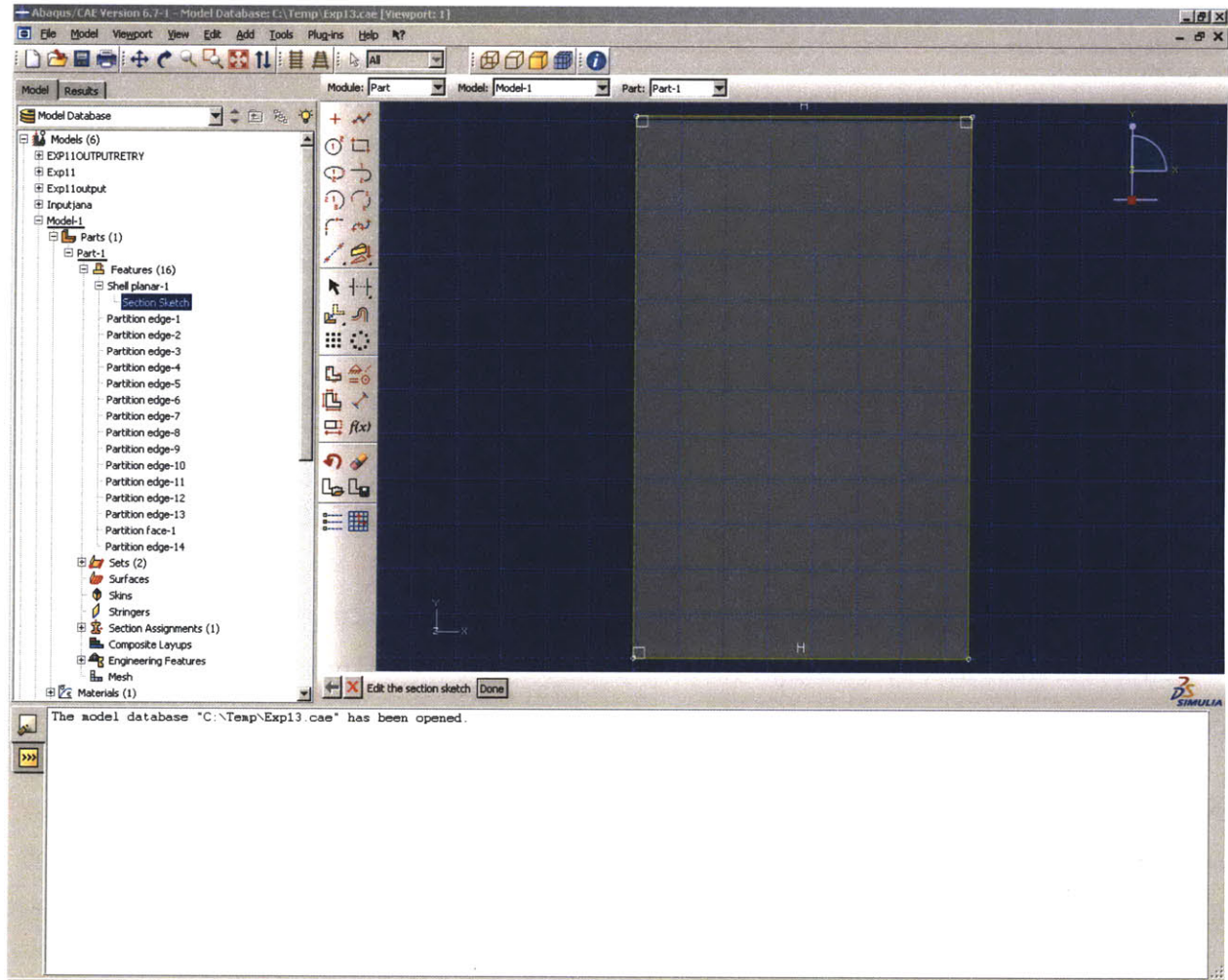
Figure 3.2: Sketching the geometry through the Part Module

3.3.2. Defining the Material Properties

The material definition of the geometry will govern how it will react to external and internal loading and displacement. It is essential to accurately know the material parameters of a geometry for quality analysis. Suppose that our wave propagation model experiences only elastic deformation, which is an essential assumption according to chapter two. Therefore, no plastic deformation will occur; it is correct to define the yield strength as infinity or a value that is sufficiently large such that the no elements will reach that strain level.

Consider the examination of a cube subjected to principle and shear stresses submerged in an infinite isotropic elastic space. According to the equations that govern wave propagation in that environment the material variables that determine the velocity of the compressional and shear wavefront are mass density, Poisson's ratio, and Young's modulus. The shear, bulk, and constrained modulus can be determined from the aforementioned values.

Standard measurements can lead to accurate values of the mass density and Poisson's ratio of soil. The Young's modulus can be determined through referring to the engineering properties of the soil or through estimation using the analytic equations developed in the background chapter.

The model will be restricted to assume that it has a mass density of 2000 kg/m and a Poisson ratio of 0.3. The shear wave front is assumed to be 100 m/s. Using the following relationships it is possible to determine the small strain shear modulus of the material.

$$G_{max} = V_s^2 * \rho_m$$

(129)

And

$$G_{max} = \frac{E}{2(1 + \eta)}$$

(130)

Therefore through substitution to find the Young's Modulus,

$$E = 2(1 + \eta) * V_s^2 * \rho_m$$

(131)

74

The Bulk Modulus, E_b, is defined as

$$E_b = \frac{E}{3(1 - 2\eta)}$$

The Constrained Modulus, C, is the ratio of axial stress to axial strain for confined compression. The Constrained Modulus takes the form.

$$C = \frac{E(1 - \eta)}{(1 + \eta)(1 - 2\eta)}$$

The Young's modulus is in units of $[\frac{F}{L^2}]$. This information is adequate to define the material properties. The material is isotropic and elastic

Young's Modulus, E	Calculated	52 MPa
Shear Modulus, G_{max}	Calculated	16 MPa
Shear Phase Velocity, V_s	Input	100 m/s
Possion's Ratio, η	Input	0.3
Mass Density, ρ_m	Input	2000 kg/m
Bulk Modulus, E_b	Calculated	43.3 MPa
Constrained Modulus, C	Calculated	38.6 MPa

Table 3.1. Material Properties
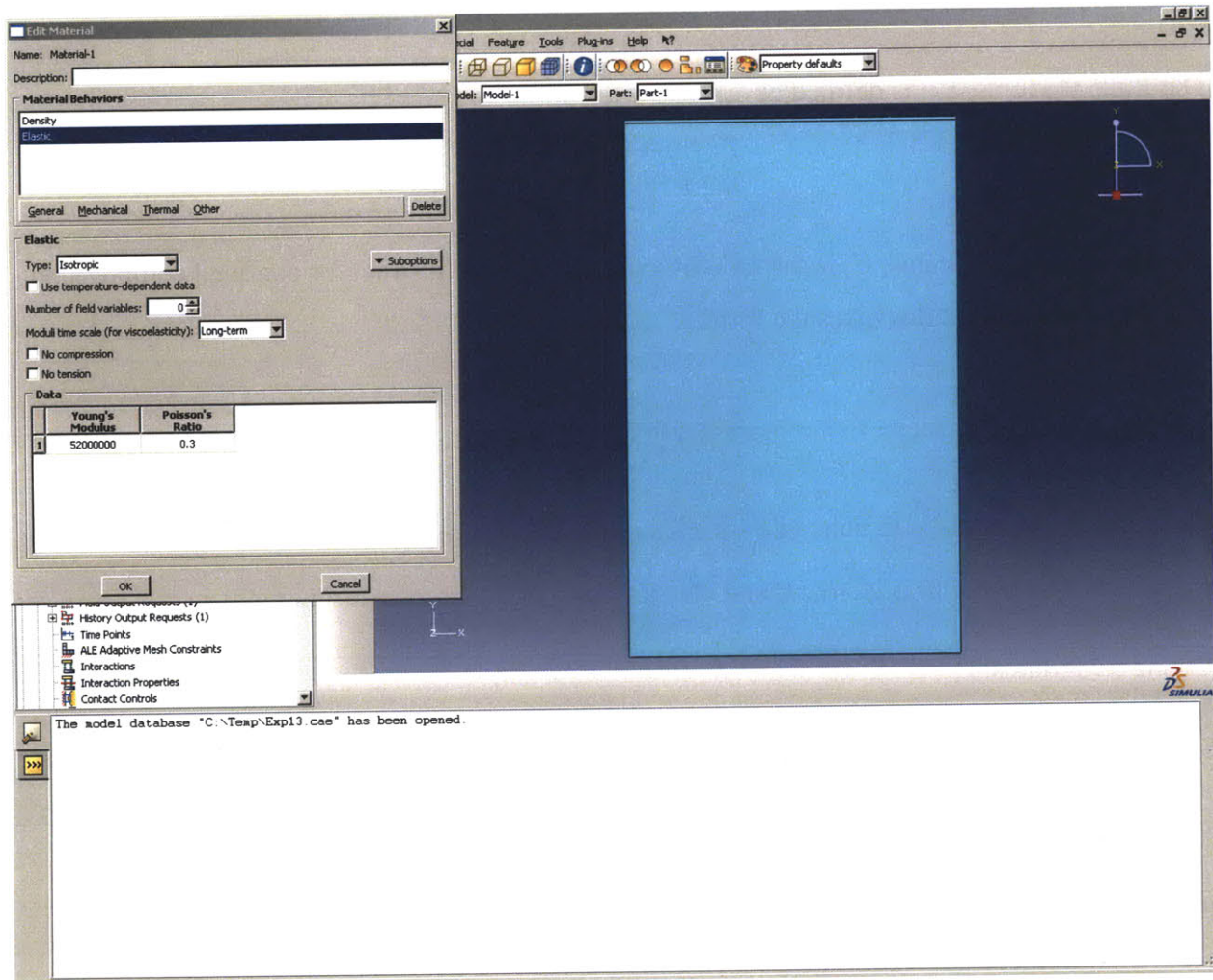
Figure 3.3: Defining the Material Properties of the Geometry.

3.3.3. Defining the Boundary Conditions

The boundary conditions specify the constraints of nodes or a collection of nodes with respect to displacement, force, moment, or mechanical thermal properties. In Abaqus it is possible to select the time increments that the boundary condition is applied or removed.

In the two dimensional plane strain model consider only force, moment, and displacement will be considered as viable boundary constraints. The location and orientation of the boundary conditions depends entirely on the desired output information of the model. Along the edge of

the model a rigid boundary is suitable to stimulate rigid surface interaction and a free boundary is suitable to simulate a free surface. Moreover, infinite surfaces can be simulated using dampers.

A rigid boundary can be simulated by assigning a time independent deformation boundary condition along the nodes that form the edge or geometric limit of the model. A rigid boundary will behave as a material with an infinite stiffness unable to deform. The direction of the displacement vector can be limited to include or omit a given dimension. In two dimensional space it is possible to restrict lateral displacement at a node of the boundary condition by setting $Displacement_x = 0$ or vertical displacement $Displacement_y = 0$. The deformation boundary condition can be applied at the beginning of the analysis $or\ t = 0s$ through $t = t_{end}, the\ domain\ of\ analysis.$

The displacement boundary condition can be labeled in conventional civil engineering terminology. If rigidity in a single dimension is required then the constraint takes the form of a "roller." If the rigidity extends to two dimensions then it is "pinned."

Suppose that the upper and lower bounding surfaces are assumed to be constrained by horizontal rollers In addition these surfaces are restrained laterally, or pinned, at the, corner nodes for the purpose of preventing rigid body motion. It is necessary to define a $Displacement_y = 0$ boundary condition along nodes that compose this boundary and $Displacement_y = Displacement_x = 0$ at the corner nodes.
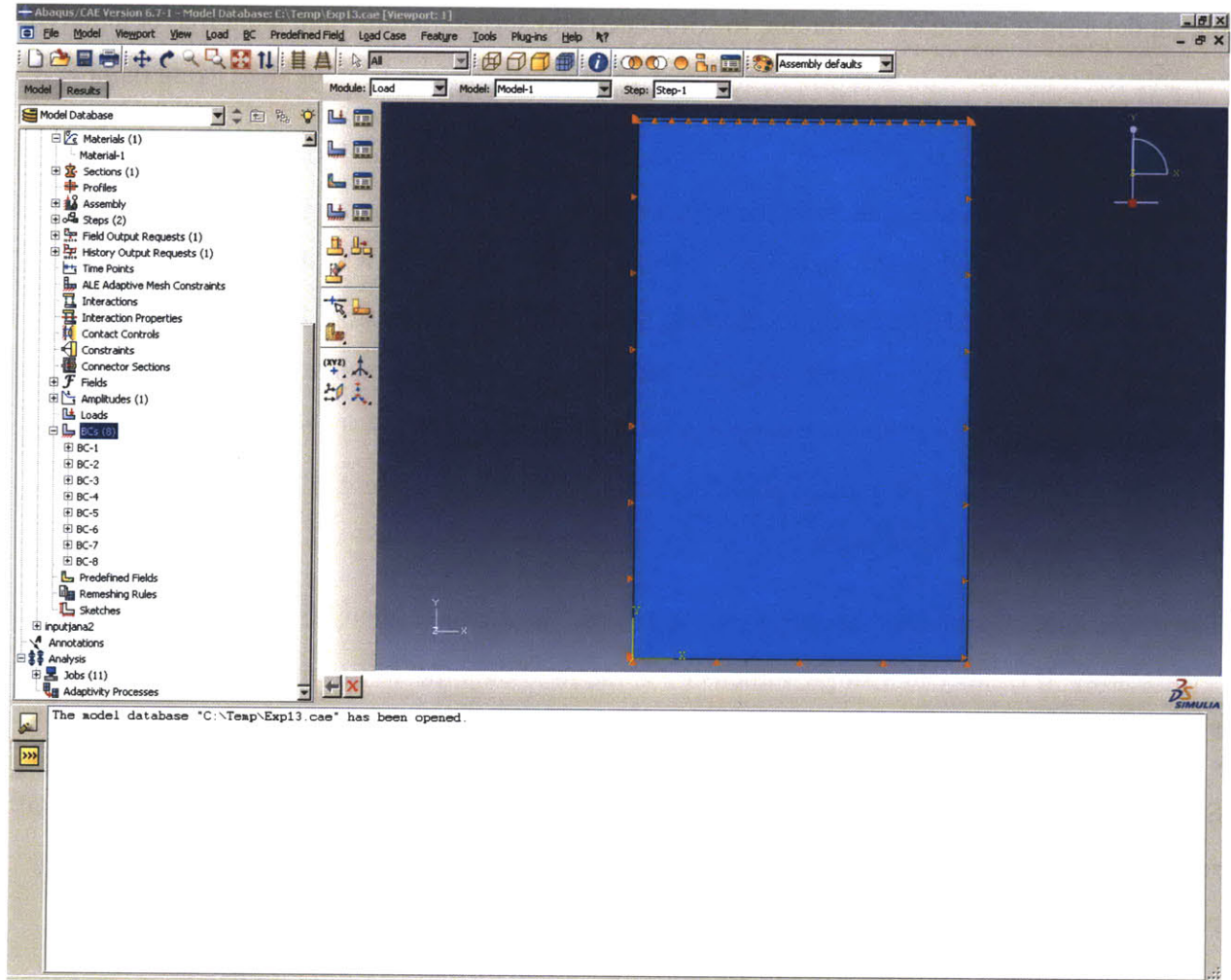
Figure 3.4: Defining the Displacement Boundary Conditions

3.3.4. An Infinite Boundary Condition at Lateral Boundary.

Suppose it is required to simulate an infinite surface along the x direction. At these nodes it is necessary to introduce dampers that can effectively simulate an infinite boundary condition. The domain of an infinite boundary is infinity and can be truncated by substitution with dashpots. Since the lateral boundary is infinite the equivalent spring stiffness is equal to zero. However, the damper coefficient will not equal zero but rather a scalar that corresponds to the reaction of the nodal displacement resulting from the wave propagation.

Polarization is the direction of particle motion with respect to a defined location of the wave front in a two dimensional wave propagation problem. In a finite element analysis polarization translates to a scalar nodal displacement in the vertical or the horizontal direction. The damped boundary requires a damper coefficient that corresponds to particle motion in the lateral and vertical directions, or dashpots oriented parallel to the x and y axis.
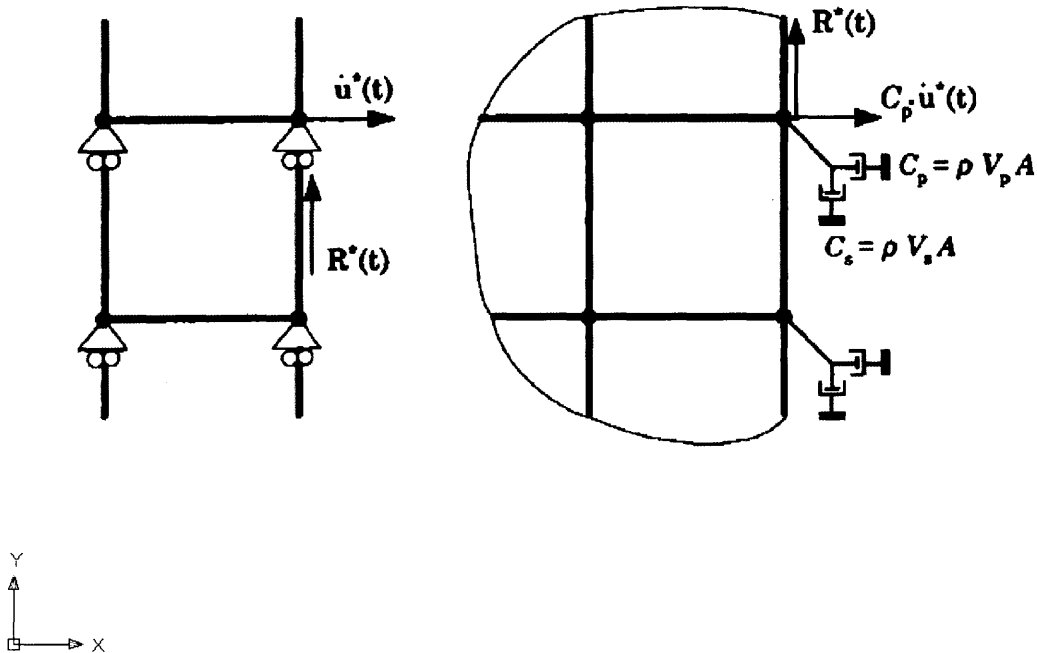
Figure 3.5: Damped Boundaries from (Assimaki 2004)

Figure 3.5 illustrates a mesh attached to shear and compression dampers along the lateral boundary constrained in the y axis and limited to deformation in the x. Body waves propagate at a velocity $\dot{u}^*(t)$ directionally at $\hat{x}$, and $\dot{R}^*(t)$ corresponds to the reaction stress at an unit vector $\hat{y}$. Dampers are applied to the boundaries represented by C_p and C_s. The shear damper is oriented along the y-axis, which corresponds to the shear wave front polarization. The compression damper is orient along the x-axis which corresponds to the compression wave front polarization.

Assuming body wave propagation numerical analysis two damper values are required for both the shear and compression wave fronts. A compression wave front will be polarized in the same direction as the velocity vector. A shear wave front will be polarized orthogonal to the velocity vector. It is necessary to align the dampers such that the orientation corresponds to the polarization of the wave front.

The dampers represent fictitious forces applied at the lateral boundary to simulate an infinite continuum of elements (Assimaki 2004).

The damper coefficient of the force is equal to the following relationships. This is an approximate fix to the problem and as presented applies to the horizontal propagation only. It is assumed effective in different degrees depending on the nodal accelerations.

P-Wave damper

$$C_p = \rho_m V_p A \tag{132}$$

S-Wave damper

$$C_s = \rho_m V_s A \tag{133}$$

The area of required for the damped coefficient is equal to the product of the vertical node spacing and the plane strain thickness. The plane strain thickness is a model assumption defined through the section module. The default value for the plane strain thickness is 1. At the corner boundaries where the area is equal the product of the vertical node spacing and the plane strain thickness. The mass density and shear and compression wave velocity are required quantities for this solution. (Assimaki 2004)

The equations for the damper coefficients only apply to linear numerical analysis. If the numerical analysis is not linear the material stiffness and damped are adjusted to the instantaneous levels of strain induced by the propagation at every time step of the time domain solution (Assimaki 2004). The resulting material response from the applied dampers no longer represent an infinite boundary condition and the material response to the dashpots will differ from a linear analysis.

80

3.3.5. An Infinite Boundary Condition at Lateral Boundary Applied in Abaqus.

A damped boundary condition intended to represent an infinite boundary can be done in Abaqus using the Interaction Model. The interaction model governs the behavior of a model's relationship among its geometric parts and the physical boundaries. Springs and dashpots are added through the Special feature tab in the scroll bar in the Interaction model. This is shown in Figure 3.6
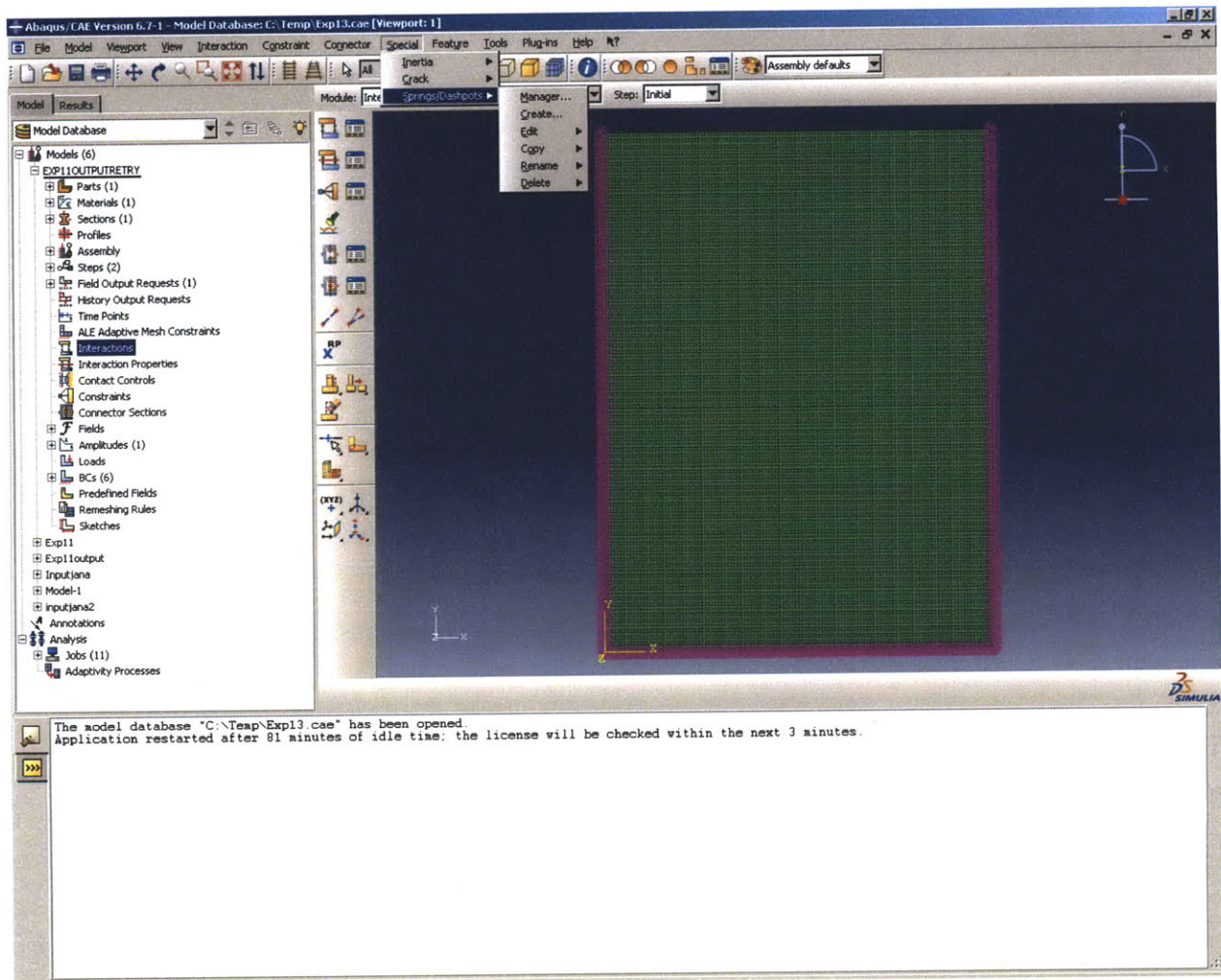
Figure 3.6:. Defining the Dashpots along the Lateral and Bottom Boundaries.

Abaqus requires a nodal selection to locate the placement of the dashpots. It is possible to define a series or collection of nodes to apply dashpots or a singular node. The node selection is not limited to the boundaries and dashpots can be applied to interior nodes.
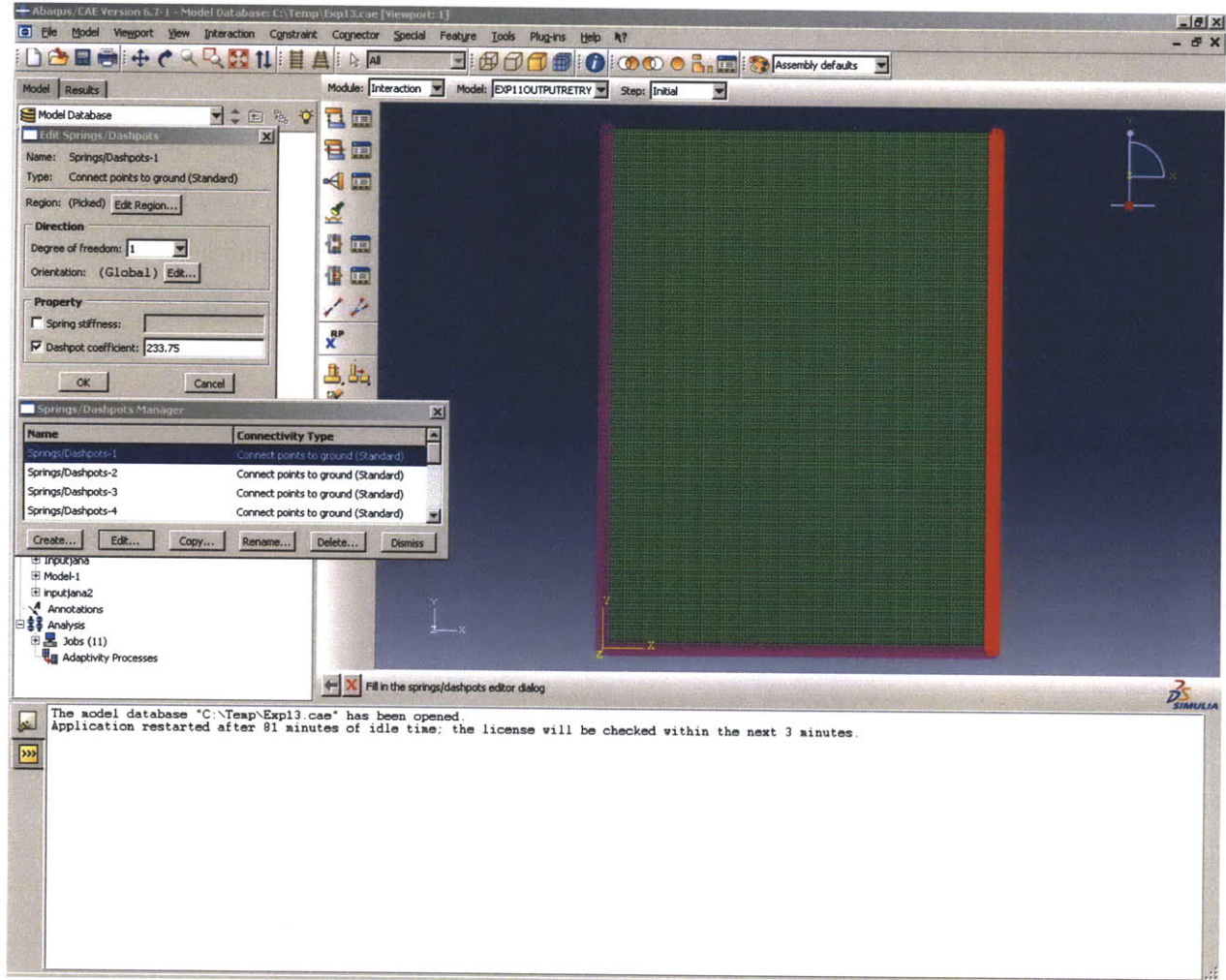
Figure 3.7:. Selecting the Node Set to Apply the Dashpots.

The calculation of the dashpot coefficient is required to apply the interaction. Continuing with the example, suppose that material properties remain constant such that

$$Vc = Vs * \sqrt{\frac{(2 - 2\eta)}{(1 - 2\eta)}} = 100\frac{m}{s} * \sqrt{\frac{(2 - .6)}{(1 - .6)}} = 187\frac{m}{s}$$

Therefore,

Mass Density, ρ_m	Input	2000 kg/m
Shear Modulus, G_{max}	Calculated	16 Mpa
Shear Phase Wave Velocity, V_s	Input	100 m/s
Compression Phase Wave Velocity, V_p	Calculated	187 m/s
Nodal Area	Calculated	0.000625m * 1m

Table 3.2 Damped Boundary Parameters

The dashpot coefficient for the shear wave at the lateral boundaries excluding corner nodes are

$$C_s = \rho_m V_s A = 2000 \frac{kg}{m^3} * 100 \frac{m}{s} * 0.000625 m^2 = 125 \frac{kg}{s}$$

The dashpot coefficient for the compression wave at the lateral boundaries excluding corner nodes are

$$C_p = \rho_m V_s A = 2000 \frac{kg}{m^3} * 173.2 \frac{m}{s} * 0.000625 m^2 = 233.75 \frac{kg}{s}$$

At the corner nodes the dashpot coefficient for the shear wave are,

$$C_s = \rho_m V_s A = 2000 \frac{kg}{m^3} * 100 \frac{m}{s} * \frac{0.000625}{2} m^2 = 62.5 \frac{kg}{s}$$

And the compression wave

$$C_p = \rho_m V_s A = 2000 \frac{kg}{m^3} * 173.2 \frac{m}{s} * \frac{0.000625}{2} m^2 = 116.875 \frac{kg}{s}$$

The implementation of the dashpot interaction will be able to simulate an infinite boundary along the surfaces or node regions selection. The dashpots will suppress the reflection and refraction of

both shear and compression wave front at the selected nodes. This method is a numerical approximation of wave propagation theory and should be used with care if it is unknown if the numerical analysis is linear.

3.3.6. Loading Conditions in Abaqus

Harmonic Motion can be represented in Abaqus by means of two methods. The first is to impart a harmonic force at a specific node using a sinusoidal wave function. The second is to prescribe a fixed displacement at a node using a sinusoidal wave function. Since displacements are fundamentally related to forces in numerical dynamic analysis both approaches will facilitate wave propagation.

The arrangement of forces or displacements can represent different conditions. A single point force or a displacement at a specific node represents a point source. A coupling of forces or displacements represents an applied moment. Researchers such as Arutnathan, Boulanger, and Riemer state that an applied moment gives a more accurate representation of piezocremaic behavior than point displacements or forces (Arulanthan 1998). However, academics such as Jovicic and Coop used fixed displacements (Jovičić 1998). Currently, a standard procedure is needed to model bender elements in numerical analysis.

In the background, an elastic isotropic element was subjected to shear and principle stresses to create equations for wave propagation. That derivation assumed force applications not moment applications. Green's analytic solutions for harmonic motion in soil assumed a single harmonic source. The equations derived are the basis for what is intended to be examined in numerical analysis. It would be reasonable to retain a point source to represent a single application of force or displacement to keep the relevance of the derivations. This example will use a single point source for the input wave.

A harmonic source can be added in Abaqus using a tabular input in the Load module. The amplitude definition must be given in the Load module. This definition can be given in the form of a loading function or a constant scalar. The amplitude definition can be adopted for defined displacements.

The sinusoidal amplitude is defined through a domain and range tabulation. The domain in the tabular input is the time required in the analysis. The range of the tabular input is the magnitude of the force or displacement. The time steps have a shorter duration than the tabulated input. The amplitude behaves as a step function over the domain. A graphical representation of this process is given in Figure 3.8.
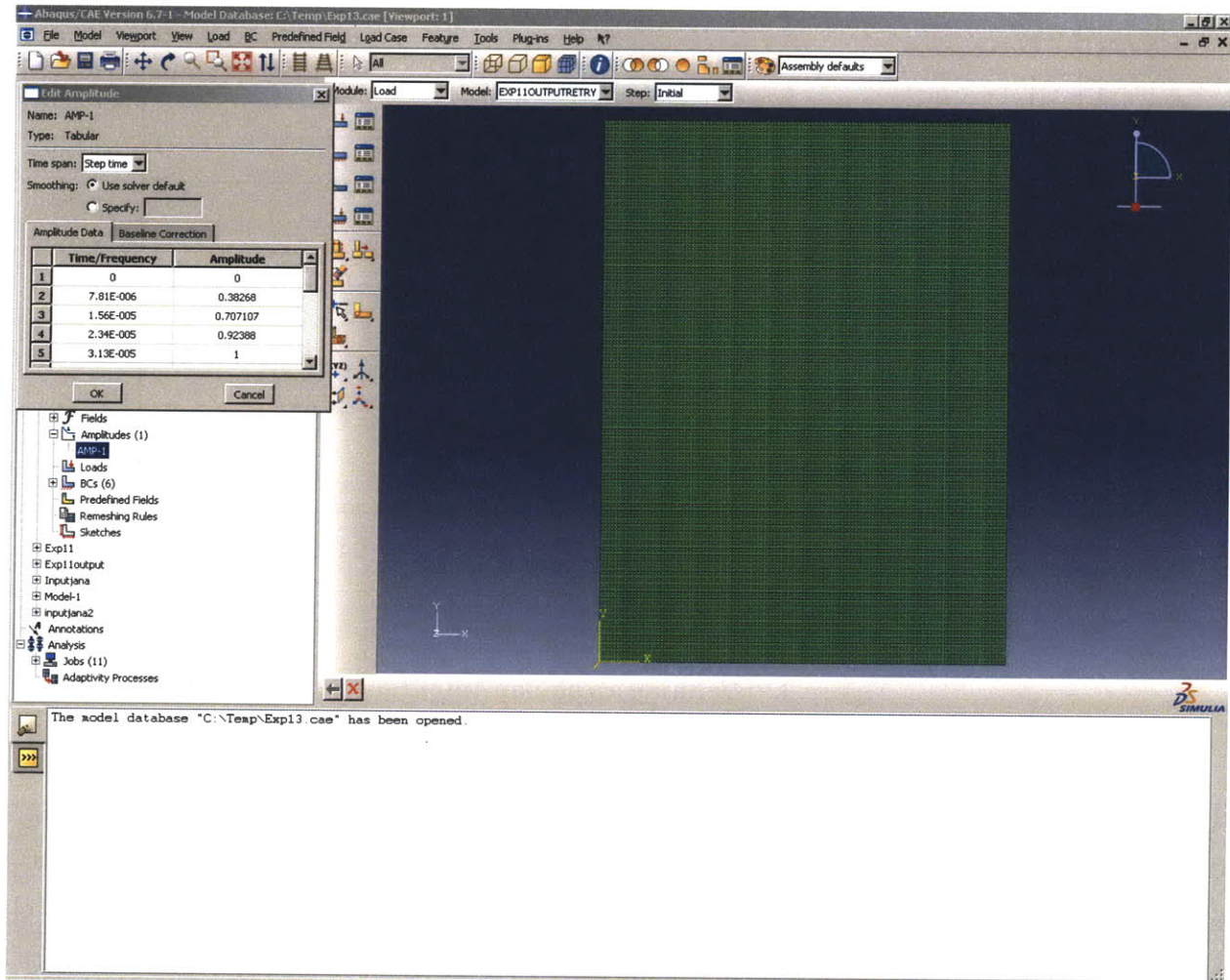
Figure 3.8: Defining a Tabular Amplitude.

The tabulation of these values produced the following amplitude curve for a frequency of 8kHz.
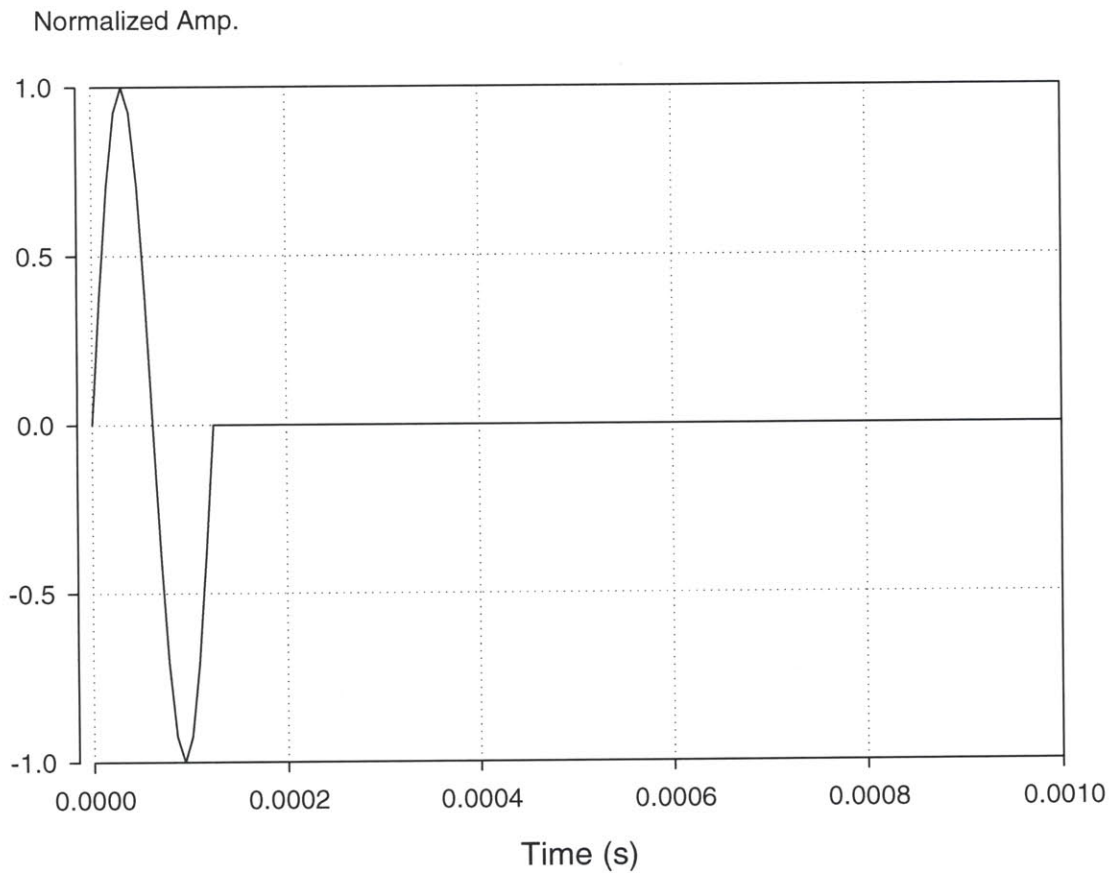
Figure 3.9: Defining a Tabular Amplitude.

The Loading module can impose a load on a singular node or a series of nodes in defined directions. According to Piezosystems the free deflection of a bender element is 270μm and the block force is 0.15N. Suppose in this model the input single pulse is simulated through a prescribed displacement at a single node and the external forces applied are zero. This would be done through the Loading module but as an applied boundary condition. This is shown in Figure 3.10. Take care to notice that the amplitude is set to the defined amplitude function.
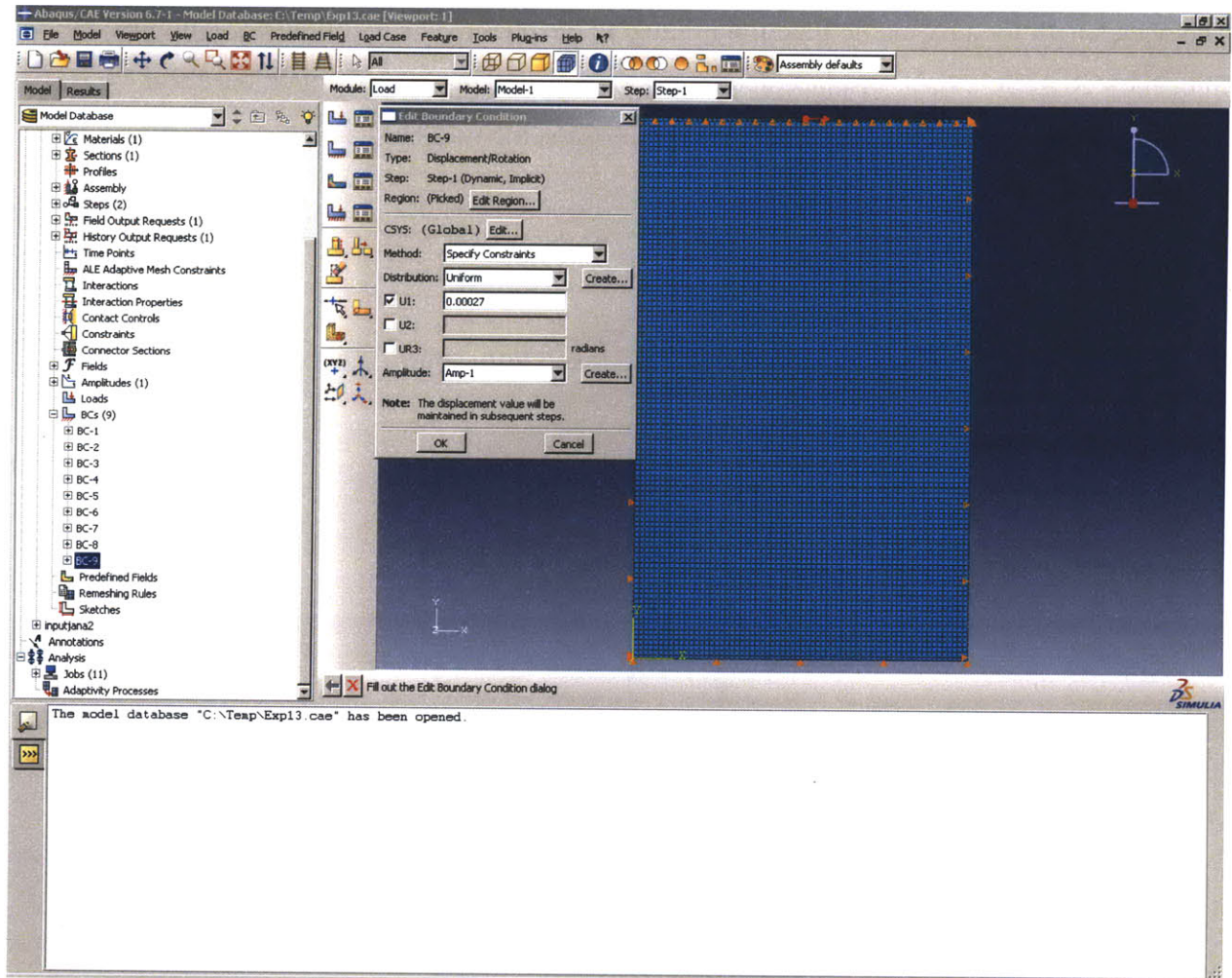
Figure **3.10: Defining a Deflection.**

The applied deflection will serve as the source or input of the body waves. The output of the displacement node should follow a sinusoidal curve defined through the amplitude with maximum amplitude of 270μm. This will be confirmed in the output file.

3.3.7. Mesh Size and Integration Time Steps.

According to Ju and Ni, who wrote extensively on using numerical analysis to model Rayleigh damping parameters, a mesh spacing of the input wave length of the harmonic motion divided by six is adequate for dynamic analysis (Ju 2007). However, study has concluded that a mesh size of wavelength divided by twenty is necessary. The example model assumes nodal spacing of the input wavelength divided by twenty is appropriate.

The wavelength for a harmonic function is equal to the phase velocity of the wave divided by frequency. Since it is shear displacement that is of most interest to the output, the shear wavelength will be taken in terms of the shear phase velocity. The shear phase velocity is assumed to be $100\frac{m}{s}$ for the example.

Therefore,

$$Mesh\ Size = \frac{Lambda(S)}{20} = 0.000625m$$

For the P-Wave

$$\frac{Lambda(P)}{Mesh\ Size} = 37.4$$

(134)
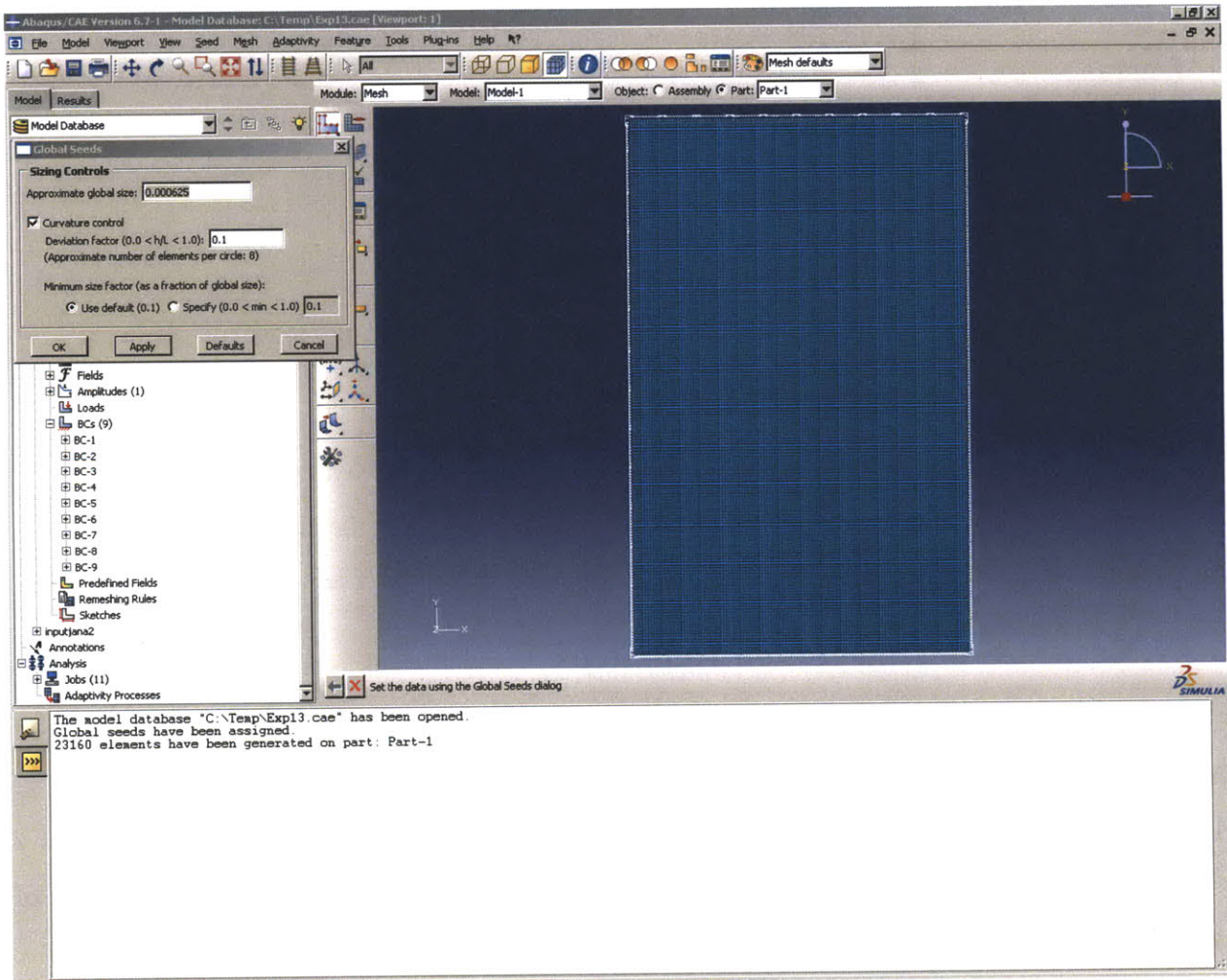
Figure 3.11: Defining a mesh size.

The elements are defined as a Plane Strain mesh with the option for reduced integration disabled. While deselecting reduced integration decreases computation time it may compromise results. The Abaqus default options for the mesh remain unchanged.
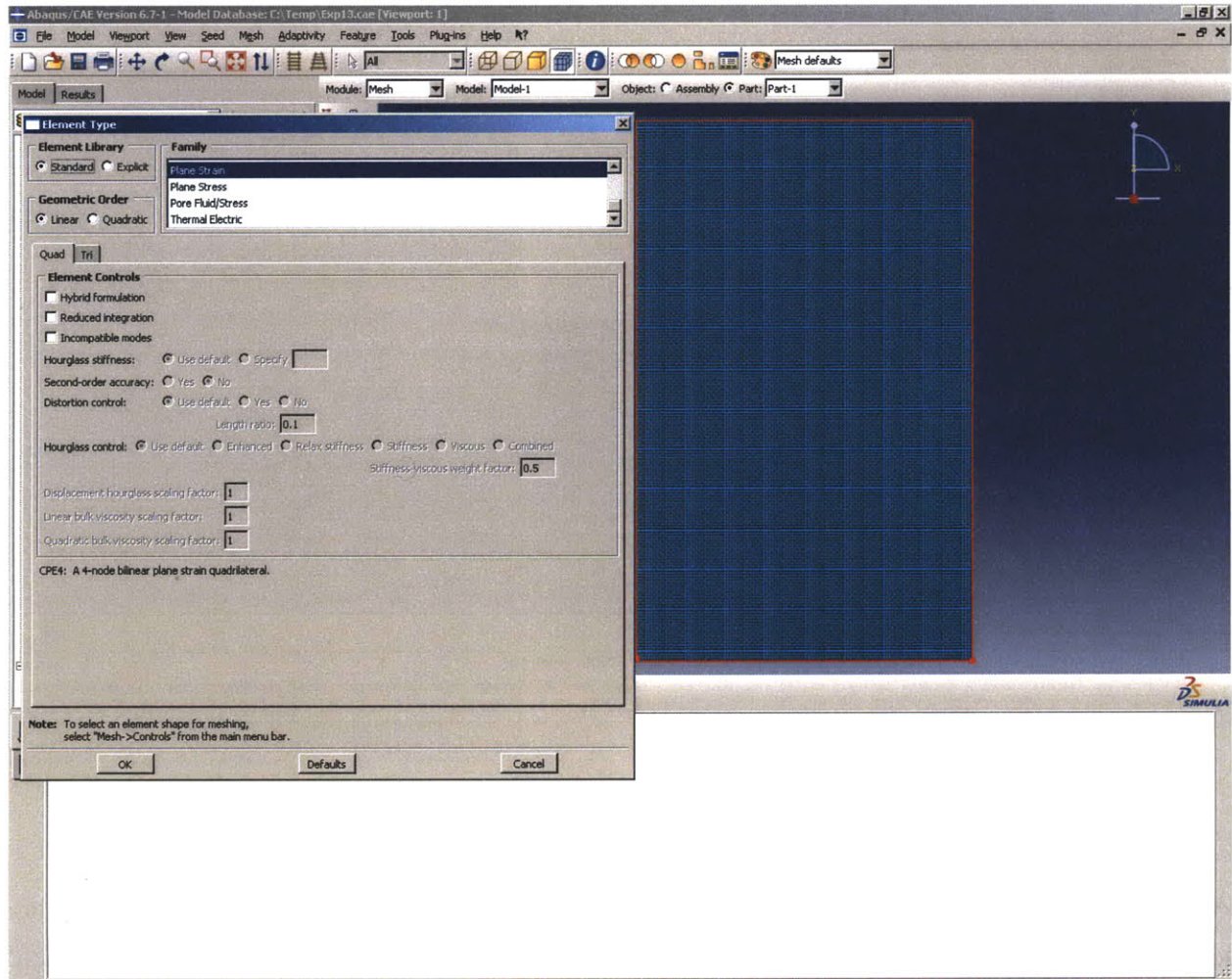
Figure 3.12: Defining the Element Type

Next it is necessary to define the time steps and analysis type in the Step module. The Step module divides tasks in the analysis through defined steps. A step is a command that instruct Abaqus how the analysis will be conducted, what time interval the domain will be, and the time scale of the integration time steps. The type of analysis for the example is dynamic and will be using implicit integration.
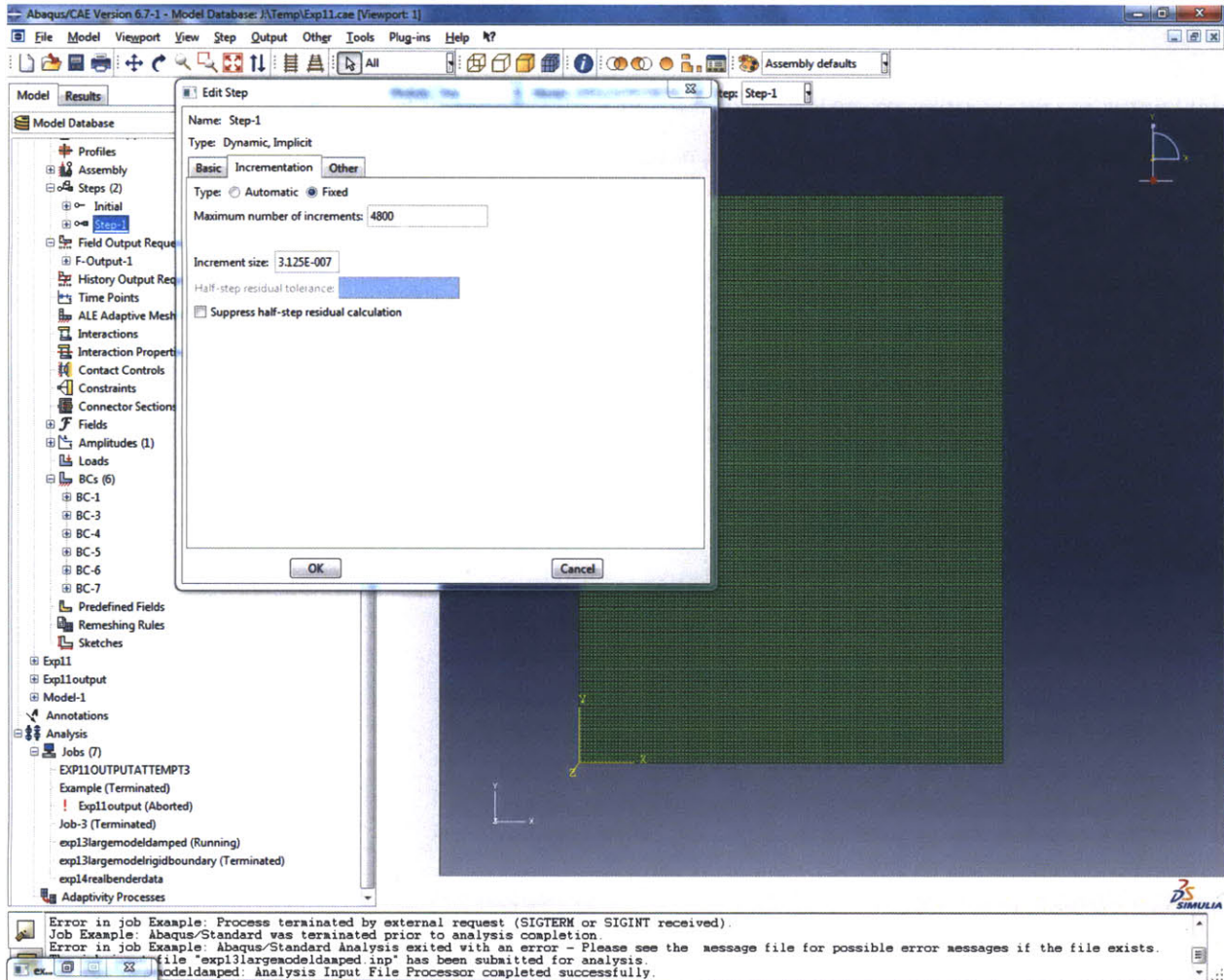
Figure 3.13: Defining the Step

According to Ju and Ni, the accuracy of the numerical analysis results is determined through the length of the integration time (Ju 2007). There are methods to determine the appropriate integration time step. One method is to divide the input signal period by a scalar and use it as the integration time (Ju 2007). Investigations show that the integration time step must be small enough that a compressional or shear wave front does not pass through one element length during a time increment. Moreover, the integration time step must be small enough to capture the linear displacement behavior of the node. Investigations show that dividing the integration time step by the travel time a P-wave or S-wave to pass through one element length should be sufficiently small. The numerical analysis would be flawed if the P-wave travels more than one

element during one time step. In this example, the integration time will equal the one twentieth the time it takes a shear wave to travel through one element.

$$\frac{Time\ required\ for\ shear\ wvae\ front\ to\ pass\ through\ one\ element}{20} = \frac{Vertical\ Nodal\ Spacing}{Shear\ Wave\ Velocity} * \frac{1}{20}$$

$$= \frac{0.000625m}{100\frac{m}{s}} * \frac{1}{20} = 3.125 * 10^{-7}s$$

The domain is the total time required for analysis. It can be expressed as the product of the time step increment and the number of time steps selected.

$$Domain = Integration\ Time * n_{number\ of\ time\ steps} \tag{135}$$

The domain of interest, for dynamic analysis is the time required for the input signal to arrive at the output node. The output node is the location of interest at the arrival. A bender element experiment modeled in Abaqus places the output node at the location of the receiver bender element. A model with distance x_1 between the input and output must have a domain such that the velocity of the wave arrives at the output. The domain in this example will be the travel time required by a shear wave to travel to the length of the model multiplied. A domain this large should capture the wave front and boundary effects.

3.4. Computation Interval

The input file created through Abaqus CAE is used by the Abaqus solver for computation of the model. The solver application is "Standard.exe." Alternatively it is possible to use a DOSBOX command line interface to run the computation. This method uses less memory than the GUI but requires opening the .msg file in the model directory with a text editor to track the computation progress. It is possible to monitor the progress of the analysis through Abaqus CAE by using the monitor results window.
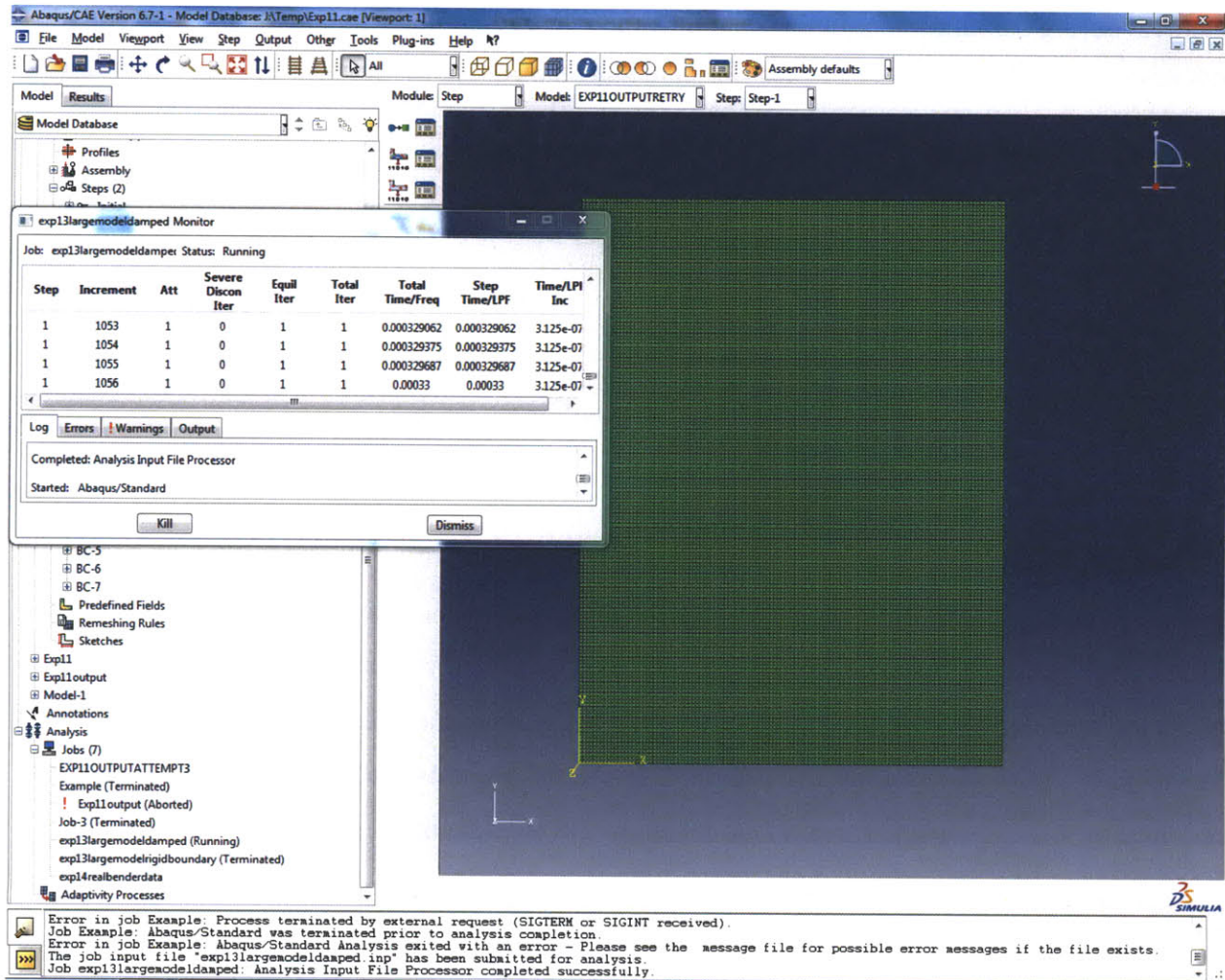
Figure 3.14: An Analysis in Progress.

3.5. Output

At the conclusion of the computation interval Abaqus will write an .OBS file. The OBS file contains information solved through the analysis procedure. The information contained in the OBS file is dependent on the options selected through the field out request. The OBS can contain a complete solution for the entire model or a specific solution for a node set.

It is possible to extract nodal displacements and contact stresses from the example. The values taken through this procedure will serve as the data necessary for processing. Nodal displacements are taken down the centerline, or $\frac{x_1}{2}$ from the lateral boundary. The displacement curves are provided.

Shear Wave Propagation through CL Displacements
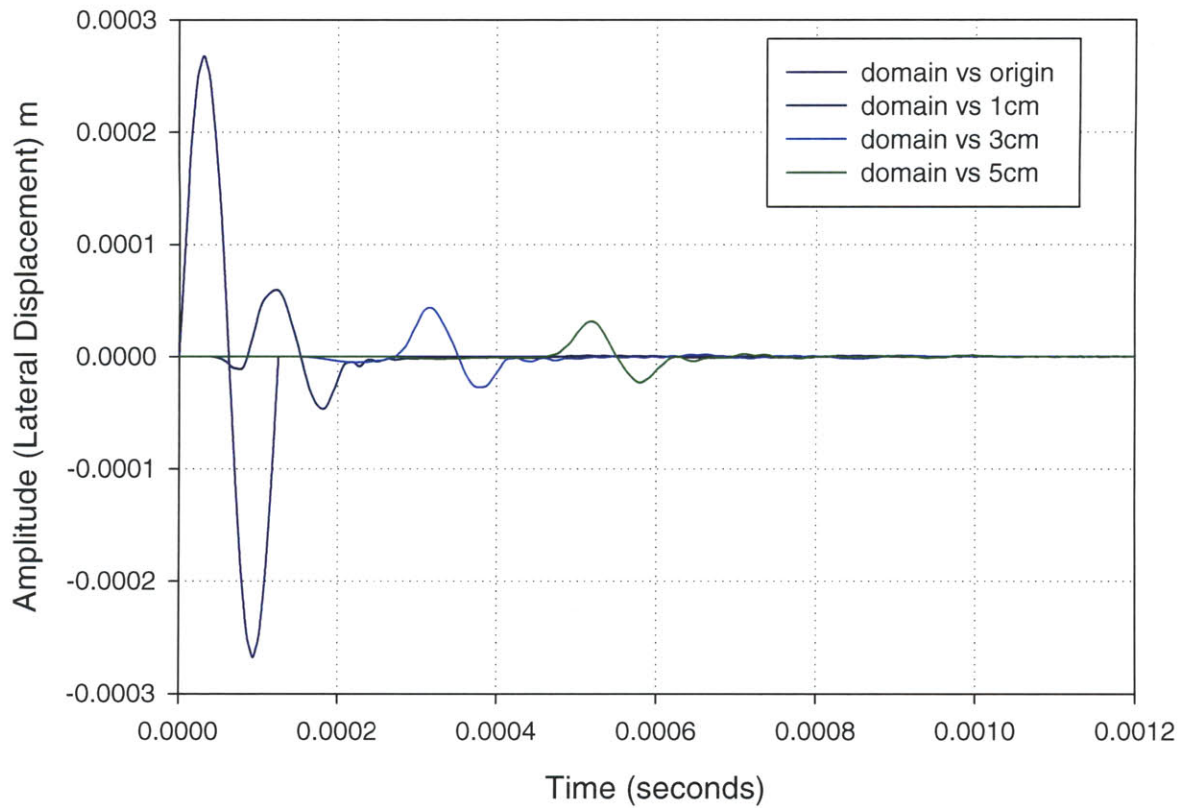
Figure 3.14: Lateral Displacement down centerline.

Figure 3.14 shows the shear wave propagation at the source and depths of 1cm, 3cm, and 5cm. The damped boundary will suppress any reflections from the boundaries. Only a singular pulse is sent through the medium and is represented in the results. The information contained forms the basis for peak to peak wave velocity analysis.
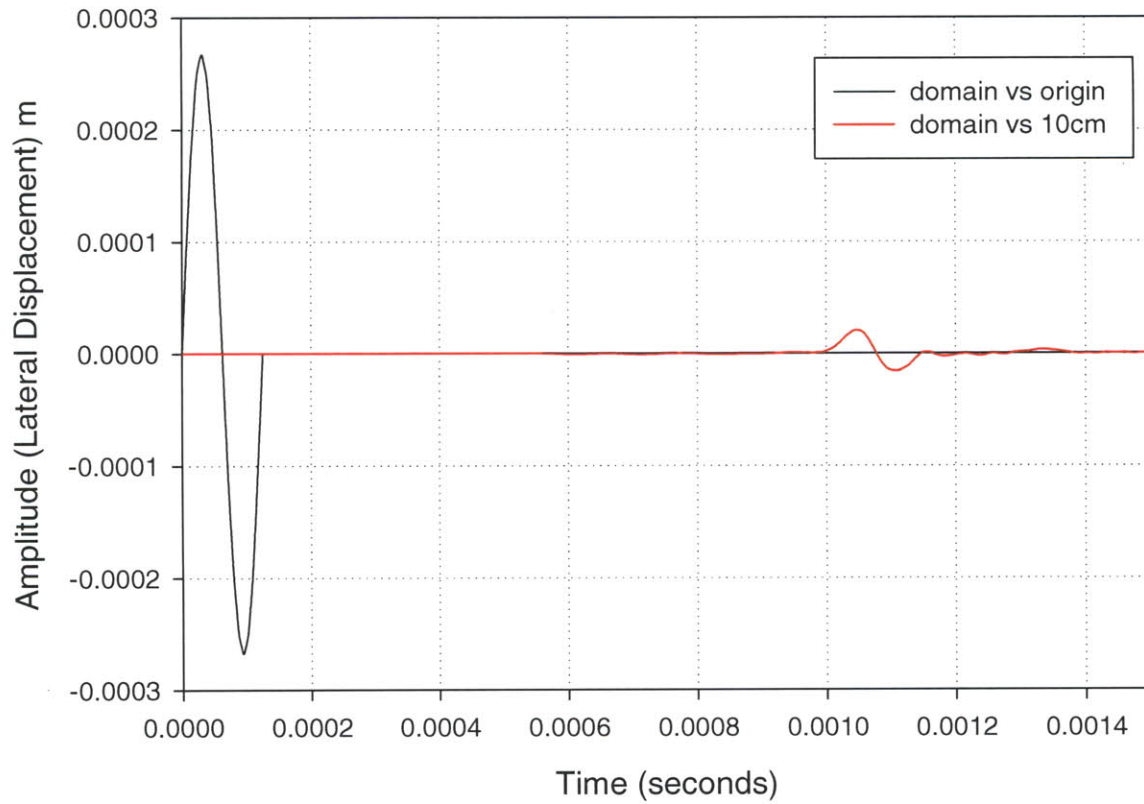
Figure 3.15: Lateral Displacement at centerline Input and Output Spaced at Model Length.

Figure 3.15 shows the displacement curve of a harmonic source at a receiver node at a depth of 10cm down the centerline.

It is possible to calculate the shear strain from the displacement information. Shear strain is given as,

$$\varepsilon s = \frac{\Delta \delta_{\text{L}}}{Verical\ Spacing\ between\ n_1\ n_2} \tag{136}$$

Here the lateral displacement is represented as δ_L. The difference of displacement of node n_1 and n_2 is $\Delta\delta_L$.
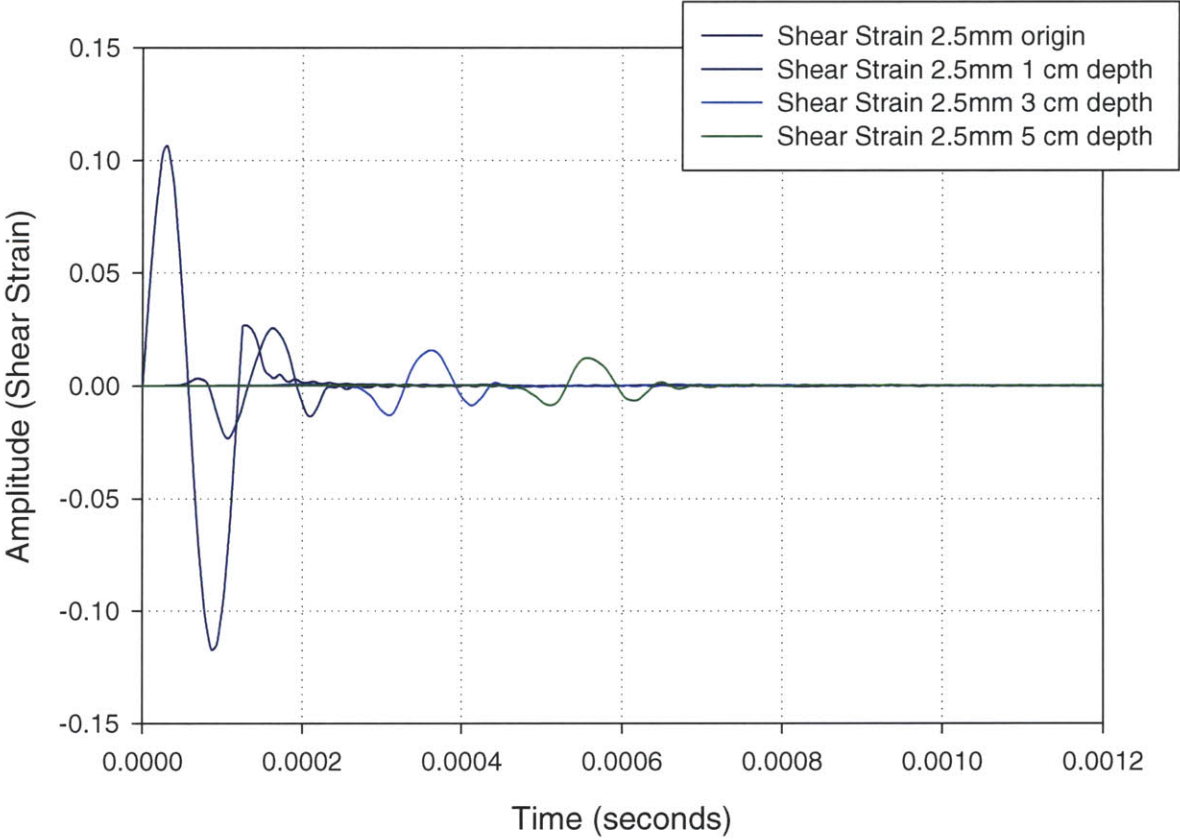
Figure 3.16: Shear Strain calculated down centerline.
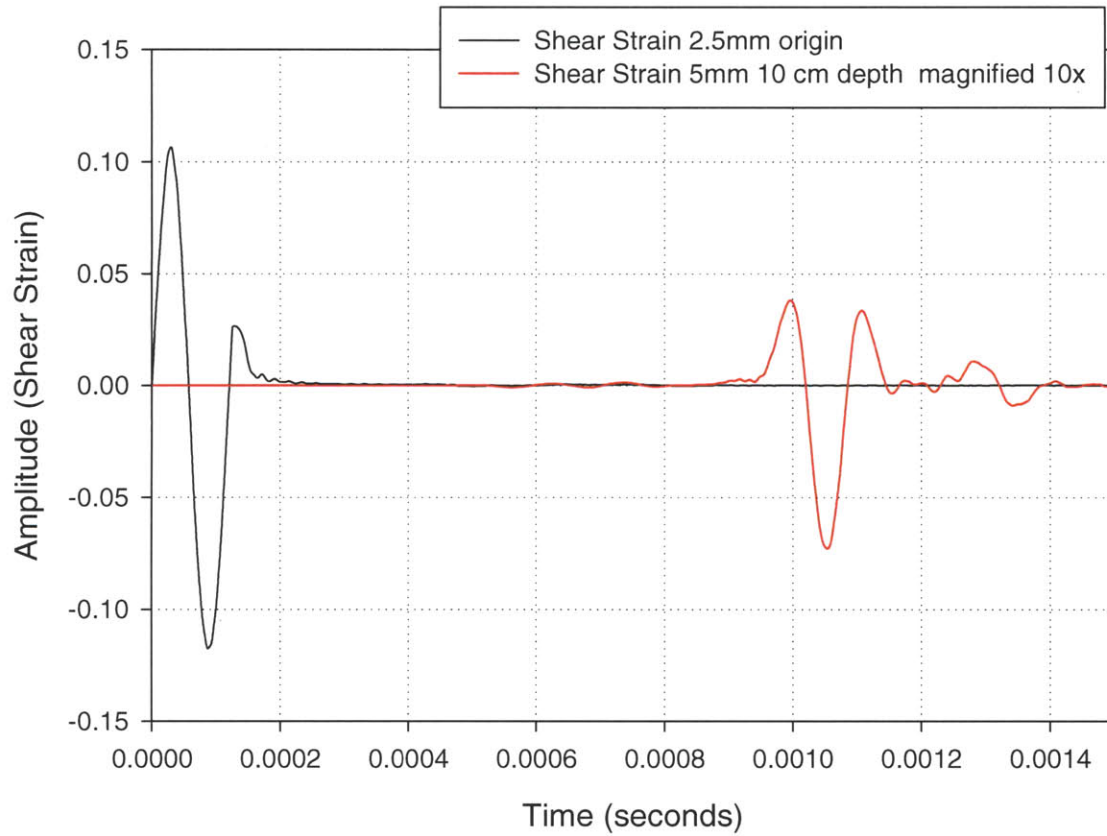
Figure 3.17: Shear Strain down centerline Input and Output Spaced at Model Length. Output Signal Magnified 10x.

Velocity measurements using peak to peak method are attached for both the displacement and shear strain output. A theoretical shear wave velocity was specified in the input analysis. The theorectical shear wave velocity is $100 \frac{m}{s}$. Velocity measurements are provided in Figure 3.18.

Shear Wave Velocity Solved through Peak to Peak Method
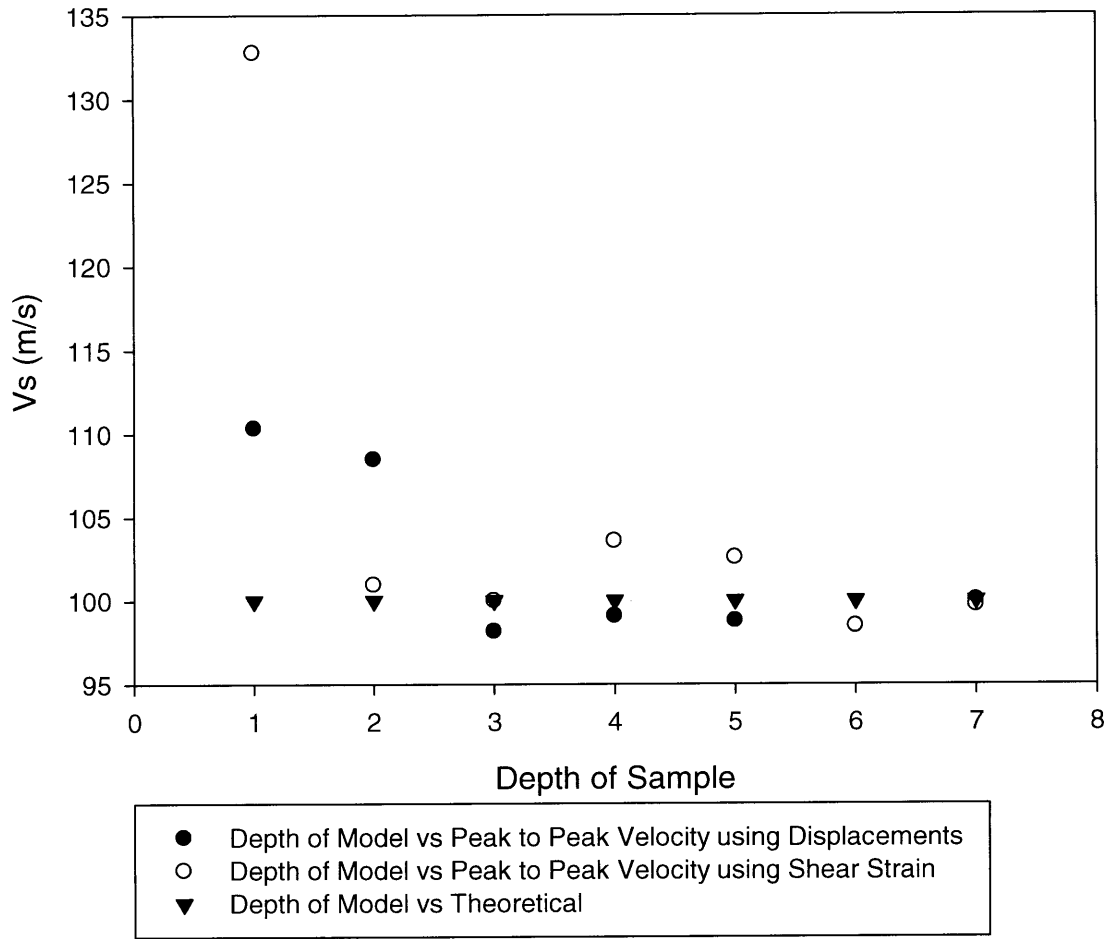
Figure 3.18: Shear Wave velocity measurements. Theoretical Shear Wave Velocity Provided.

4. Meshsize and Integration Time Step Investigation

4.1. Introduction

The accuracy of the numerical analysis is determined through the length of the integration time and mesh resolution (Ju 2007). It is necessary to determine the mesh size and integration time step interval required for dynamic analysis. Standards are reported, such as Su's assertion that Lambda divided by six provides accurate results, and claims should to be verified.

A column model was constructed to determine the effect that mesh resolution has the dynamic numerical analysis. Control values were set so that the all model variables, such as geometry, material definitions, loading and displacement, boundary conditions, and harmonic motion input remained constant. Then a series of comparisons were made that differed in mesh size and integration time. The interdependent variables for the models were the integration time step interval and mesh resolution and the dependant variable was the field output generated at the conclusion of the dynamic analysis.

Numerous mesh resolution and integration time models were assembled using the column model definitions. The field output from the results of the variable mesh size and integration time steps was analyzed using first arrival and and peak to peak velocity measurements.

4.2. Interpretation of Signal

The analysis of wave propagation in an isotropic elastic medium requires the identification of the important characteristics of the body waves, in this model P-wave. These characteristics of the field output that are of interest are P-wavefront velocity and attenuation of the amplitude.

A representative column model was made to describe the important characteristics of a body wave propagation finite element problem. The column model has a defined geometry such that the width $x_1 = 7.5cm$ and a height $z_1 = 10cm$. The material definitions are defined $\rho_m = 2000\frac{kg}{m^3}$ and the Young's Modulus $E = 52\ Mpa$. The material was assumed to be isotropic and elastic.

The model boundaries were imposed at the bottom corners by pins to prevent rigid body motion. The lateral boundary was defined as a damped surface. The dampers simulate an infinite boundary therefore effectively suppressing all incident P and S waves from producing reflections. The dampers are only an approximation of an infinite boundary; the dampers do not provide a prefect condition.

A vertical point displacement was applied on a top surface node located on the centerline. The displacement's amplitude was sinusoidal with one pulse. The frequency of the pulse was 8kHz. The mesh resolution of the model is equal to the shear wavelength divided by 20 or $\lambda_s/20$. The time step increment was set at 312.5 nanosecond per integration iteration. The field output of the analysis is included in Figure 4.1.

The P-wave length is a larger value than the S-wavelength. Setting the standard according to the S-wave length will produce finer mesh resolution ratios. This method can be adapted to P-wave velocity simply by taking the calculated integration time step multiple and dividing it by the ratio of $\frac{Vp}{Vs}$. In the column model this occurs at an integration time step multiple of $\frac{Vp}{Vs}$ or 1.87.

Harmonic motion is a system which undergoes simple sinusoidal motion. A harmonic function experiences a displacement about an equilibrium position between two extreme positions of maximum displacement in a periodic manner. The motion of this system is sinusoidal or can be expressed at the emission node:

$$U_z(t) = A * sin(f * t) = 1m * 10^{-7} * \sin{(8000\,Hz * t)}, \qquad 0 < t \leq .000125\,s$$

$$U_z(t) = 0, \qquad\qquad\qquad\qquad\qquad\qquad t \geq .000125\,s$$

The wave propagation is planar. Mathematically plane waves can be expressed as vertical displacement as a function of time and depth.

$$U(t,z) = A(z) * e^{i(kz-ft)} = A(z)e^{i(80m^{-1}*z-8000Hz*t)}$$

Where the amplitude factor A(z) is attenuated in proportion to source to receiver distance 'z.'

The phase velocity of the wave is equal to the product of the P-wave's frequency in Hertz and wavelength in meters. The phase velocity is equivalent to the P-wave velocity of the wave front for the reason that the P-wave generated is a plane wave. In plane wave propagation there is no frequency dependence of the velocity. The P-wave is not dispersive. The P-wave propagation qualifies as an attenuating planewave.

In an infinite boundary model the P-wave velocity is expressed:

$$V_p = \sqrt{\frac{\lambda + 2G}{\rho_m}} = \sqrt{\frac{E_b}{\rho_m}} = \sqrt{\frac{E(1-\eta)}{\rho_m(1+\eta)(1-2\eta)}}$$

$$V_p = \sqrt{\frac{52 * 10^6 Pa * (1 - .3)}{2000\frac{kg}{m^3} * (1 + .3)(1 - 2 * .3)}} = 187\,\frac{m}{s}$$

This equation is applicable in models such that the lateral motion equals zero at the lateral boundaries. Under this assumption the operative elastic constant becomes$(\lambda + 2G)$ or the Bulk Modulus.

4.2.1. Characterization of the Source

The harmonic source has components that are important in wave propagation. Those characteristics are the maximum positive amplitude, maximum negative amplitude, the

100

asymmetric amplitude, and the frequency. The maximum positive amplitude corresponds to the maximum positive value reached by the source wave. The maximum negative amplitude recorded is equivalent to the vertical displacement of the source wave at phase $\frac{\pi}{2}$. This motion will cause elastic compressive strains, compression of the nodes that compose the mesh, in the model because the convention of the model uses downward displacement as negative integers.
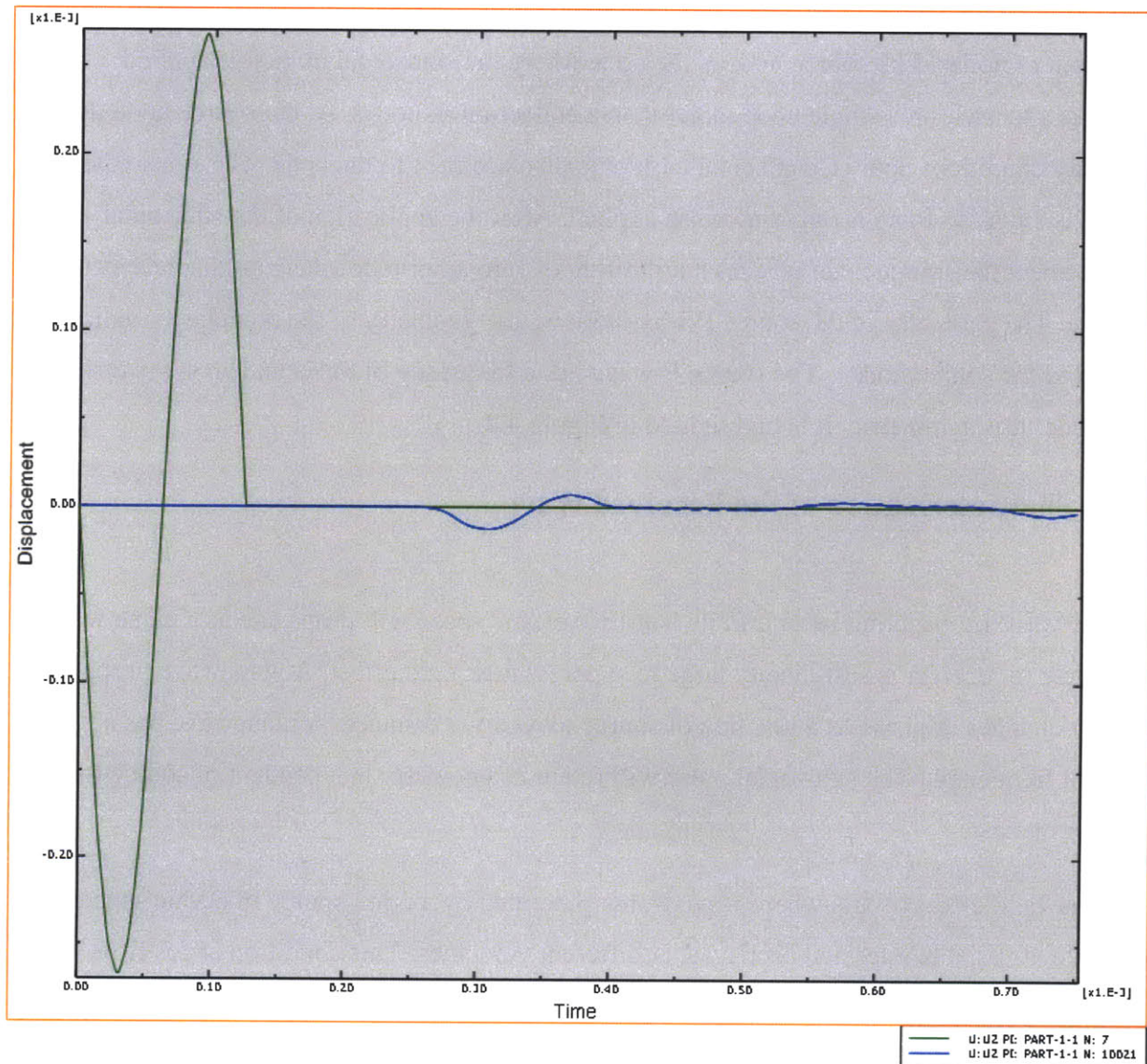

Figure 4.1: Displacement Field Output

The maximum positive amplitude of the source wave is the maximum positive vertical displacement of the wave after a phase of π or 180 $degrees$ after the initial negative amplitude. This phase will cause elastic tensile strains, or extension of the nodes that compose the mesh, because according to the convention of the model tensile displacements are positive.

The displacement output of the source signal has symmetric behavior. The boundary conditions used to define the model in Abaqus allow a defined boundary condition to characterize a node or collection of nodes. The source node is the node where the sinusoidal motion is applied. The source is a located on a single node rather than a collection of nodes. At the source node the boundary conditions apply a sinusoidal harmonic displacement to the node. The sinusoidal motion is singular; there is only one pulse applied. After the application of the sinusoidal displacement the source node reaches equilibrium of zero amplitude where no displacement is possible. The geometry of the source P-wave follows the geometry of the boundary condition applied to the source node. The source P-wave has a frequency of 8kHz and an symmetric amplitude. It is symmetric. It is highlighted in Figure 4.2.

4.2.2. Characterization of the Received Wave

A plane wave propagating in an infinite isotropic elastic space will propagate as a plane wave if the source to receiver is sufficiently large to suppress near field effect. A planewave propagates without changes in phase as a function of source to receiver distance. A planewave has a constant frequency. The sinusoidal pulse will retain its geometry independent of source to receiver distance.

The near field affect occurs where wave fronts generated by a point source in elastic space attenuate at variable rates and propagate at different velocities. This condition arises from the coupling behavior of wave fronts emanating spherically from the source.

In an elastic infinite medium, the harmonic source emanates a P-wave front that is dilatational. The near field affect generates shear wave motion due to compression wave interference. The error from the near field affect can be reduced by increasing the distance from the source to the receiver element. The separation distance is expressed as a ratio of the tip to tip distance and the wavelength of the source, $\frac{L_{tip\ to\ tip}}{\lambda}$. Theoretical work has proven that the near field affect will

cause significant errors in travel time measurements when $\frac{L_{tip\ to\ tip}}{\lambda} < 1$. A ratio between 2 and 10 is recommended.

In the P-wave model the source to receiver distance is 5cm. The tip to tip distance is equivalent to the source to receiver distance in this model. Accordingly, the ratio of tip to tip distance to P-wave length is equal to $\frac{5cm}{2.33cm} = 2.2$, which is greater than 2, and therefore, adequate to suppress the near field affect . The observed output from the Figure 4.2 indicates there is no ambiguous first arrival before the major signal. The absence of a small dip of the vertical and lateral displacement indicates that the near field affect is adequately suppressed.

There are no boundary reflections of P-waves that interfere before the first arrival of the P-wave. The boundaries in this model are attached to dampers which eliminate any possible reflections. The dampers effectively simulate a lateral infinite boundary of the half space. Boundary reflections cannot occur without a boundary change or change in media. The infinite half space medium in this model is isotropic and elastic. All arrivals recorded at the source location corresponds to the wave front traveling from the source to the receiver along a ray path that is parallel to the directional vector of the radius of the source and receiver.

4.2.3. Reflections off the Bottom Boundary

P-wave reflections can occur from the bottom boundary. The bottom boundary does not have dampers applied. When the pwave strikes the bottom boundary it reverses direction and the velocity unit vector becomes negative. The amplitude should remain in compression at phase $\frac{\pi}{2}$ because the bottom boundary is modeled as a rigid surface and pinned at the corners. An incident wave reflecting off of a rigid surface does not alternate its amplitude after the reflection.

The calculated arrival time of the bottom reflection is equal to the distance of the length from the source to the bottom boundary added to the distance between the receiver node and the bottom boundary. The expected domain of the boundary reflection is noted as the number 4 in Figure 4.2.

The calculation becomes.

$$t_{arrival} = \frac{d_{source-bottom\ boundary} + d_{bottom\ boundary-receiver\ node}}{Vp} = \frac{.1m + .05m}{187\frac{m}{s}} = .000802\ seconds$$

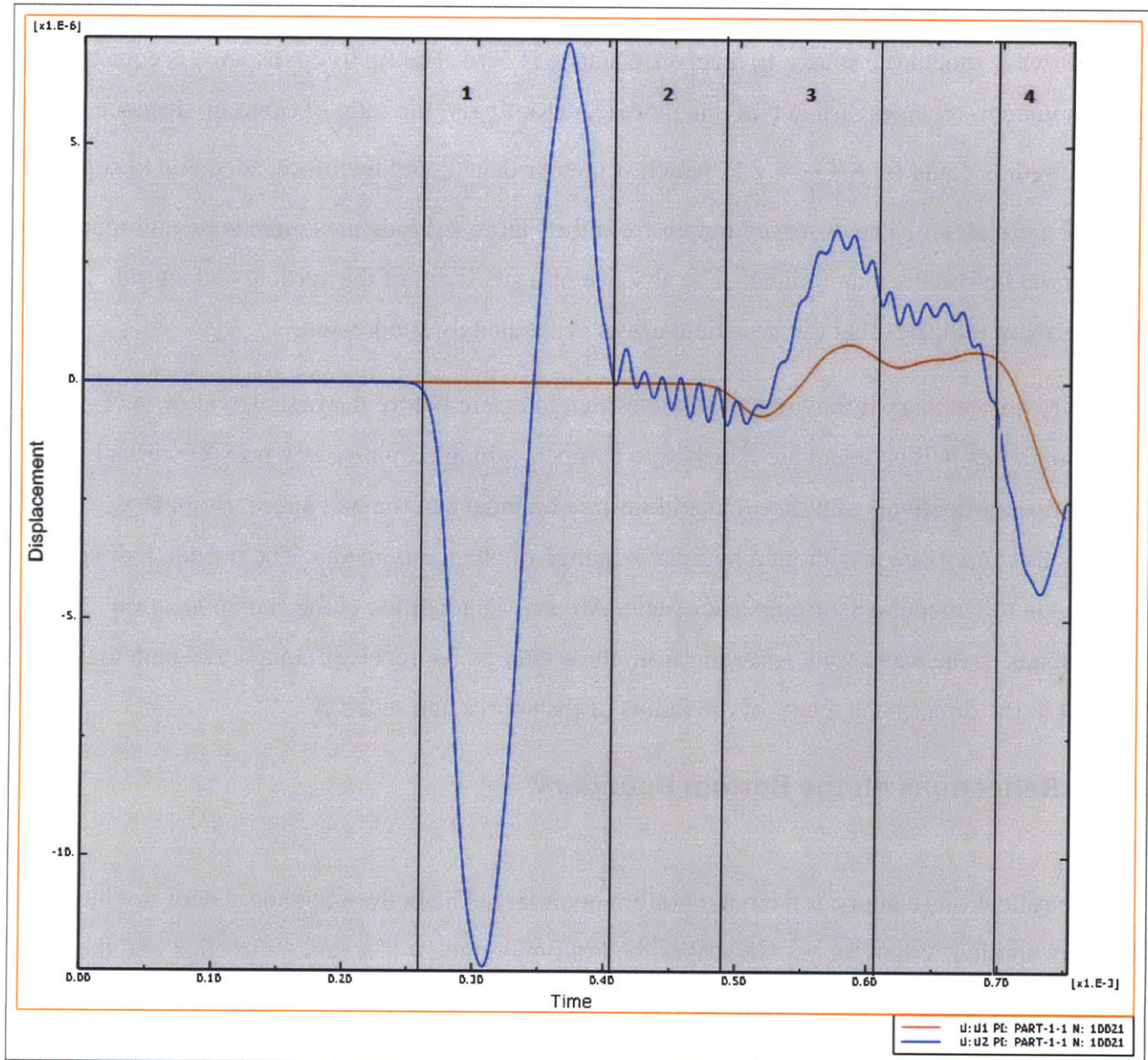
Figure 4.2: Field Output at Receiver Node: Lateral and Vertical Displacements at Source to Receiver Distance = 5cm.

4.2.4. S-wave Arrival

In body wave propagation in a medium where the Poisson's Ratio is greater than zero a vertical point oscillation source will always generate two types of body waves: shear and compression. In a model where the excitation is driven by a vertical point displacement node located at the top surface on the centerline of the mesh. It is expected the S-wave will lag behind the P-wave as a function of the source-receiver distance and the Poisson's ratio of the media.

The S-wave is defined as a longitudinal wave producing displacements orthogonal to its propagation direction. The model used is a two dimensional model, therefore, the orthogonal dimension can only correspond to lateral displacement. The subscript U1 represents the lateral dimension, or 'x', and the subscript U2 represents the vertical direction, or 'z'.

The S-wave can be seen in Figure 4.2. A wave that produces lateral displacements will register a planewave form when the field output records lateral deformation. The orange line in Figure 4.2. represents the lateral displacement; there is an arrival at the predicted travel time of the S-wave.

The frequency of the S-wave will be equal to the source frequency because the body wave is an attenuating planewave. Therefore it is expected that the period of the shear wave should be the reciprocal of the P-wave frequency or the reciprocal of 8kHz or 0.125 milliseconds. According to Figure 4.2., the period of the orange line, the lateral displacement at 5cm, is equal to approximately .125 milliseconds.

The first arrival time of the S-wave can be solved by using the relationships of the known P-wave velocity and the Poisson's Ratio. The calculation is provided. The expected domain of the shear wave is noted as number 3 in Figure 4.2.

$$travel\ time\ of\ S-wave = \frac{.05m}{Vp * \sqrt{\frac{(1-2\eta)}{(2-2\eta)}}} = \frac{.05m}{187\frac{m}{s} * \sqrt{.286}} = \frac{.05m}{100\frac{m}{s}} = 0.5 milliseconds$$

4.2.5. Characterization of the Attenuation

The attenuation analysis of the wave propagation requires measurements of the decaying amplitude. In body waves, P/S waves, this value is defined as the recorded maximum positive displacement magnitude. It is possible to switch convention and use negative amplitude but the phase must be adjusted accordingly to account for the shift. Identical phases of the source and receiver must be used. For instance, if the attenuations of the negative amplitudes are taken then the source and receiver maximum negative amplitude must be negative. This convention is reversed when solving for positive amplitudes.

Alternatively, the difference or differential of the positive and negative phases of the amplitude can be used capture the behavior of the P-wave attenuation. In the Abaqus analysis, it is common to observe waves that do not demonstrate planewave behavior. In non planar behavior, the amplitudes of the positive and negative sine wave lose symmetry as the wave propagation at distances of increasing radii.

The reason for the non planar behavior is that the FEM is only an approximation of an infinite half space and some errors in integration solution distort the true shape of the body wave. Furthermore, the Finite Element method produces a linear solution to a non linear system; this will produce some residual error in the analysis.

4.2.6. Characterization of the Higher Frequency Harmonics ($f \gg 8kHz$)

The higher frequency harmonics after the initial Pwave are correlated to the mesh resolution of the model. Experiments show that the numerical integration of the finite element calculation will always produce some degree of diminutive error in the displacement output. Refining the mesh spacing improves the finite solution and reduces the high frequency harmonic after the plane wave propagates through that point. The displacement field out provided in Figure 4.2. column '2' demonstrates the presence of high frequency harmonics.

The high frequency harmonics demonstrate the principle of the conservation of energy and momentum. The mesh is subjected to a harmonic agitation through a sinusoidal pulse at the initial loading increment, $0 < t \leq .000125$ *seconds*. When the duration of that pulse is finished the energy associated with the pulse and the momentum associated with the velocity of the node vertically adjacent to the source node used for axial strain analysis do not reduce to zero.

106

Furthermore, the nodes at the receiver location do not instantly reach equilibrium after the plane wave P/S waves travel through. Instead there is a degree of remnant motion localized at the node. The motion has an associated momentum and energy that correspond to the velocity of the time derivative of the displacement field. It is theorized that the higher frequency harmonics could be the natural or resonance frequency inherent in the mesh.

The mesh does not have a material damping parameter. Therefore, there is no mechanism to dissipate the energy in the mesh. The Rayleigh damping parameter is zero in this analysis. The modal damping is zero in this analysis. There is no critical damping fraction.

Abaqus implements an alpha damping parameter built into the Implicit Dynamic solver. The alpha damping parameter is an artificial damping variable that grows with the ratio of the time increment to the period of vibration of a model. The alpha damping factor is introduced to keep the integration calculations stable. It is enabled by default in the Dynamic Implicit solver. In the absence of the alpha damping factor the integration solutions have potential for becoming unstable.

The default alpha damping parameter is -0.05, a unit less scalar, set as default in Implicit Dynamic Analysis. The alpha damping parameter of -0.05 introduces just enough artificial damping in the system to allow the automatic time stepping procedure to work smoothly. The alpha damping parameter is enabled for implicit dynamic models.

4.2.7. Travel Time to First Direct Arrival in Output Signal

The first time of arrival method asserts that the travel time between two points in space may be taken as the difference of first direct arrivals at the two points. This computation is achieved through taking the difference between the instantaneous point in time the source signal is sent and the instantaneous start of the major arrival of the receiver signal. In the model the arrival time is the time between the initial non zero amplitude or the source and the beginning of the first arrival signal.

4.2.8. Peak to Peak T

Travel time of the P-wave may be taken as the time between any two characteristic points of the source and receiver wave while ignoring initial weak portions of the received single. The characteristic points in this model are the peaks of the signal and receiver wave.

4.2.9. Axial Strain Calculation

The axial strain scalar field can be calculated from the displacement information. The source and receiver signal can be expressed as an axial strain field rather than vertical displacement field. Axial strain is defined as,

$$\varepsilon_{axial} = \frac{\Delta\delta_L}{Verical\ Spacing\ between\ n_1\ n_2}$$

Here the vertical displacement is represented as δ_L. The difference of displacement of node n_1 and n_2 is $\Delta\delta_L$. The vertical spacing of two vertically adjacent nodes is 0.000625m.
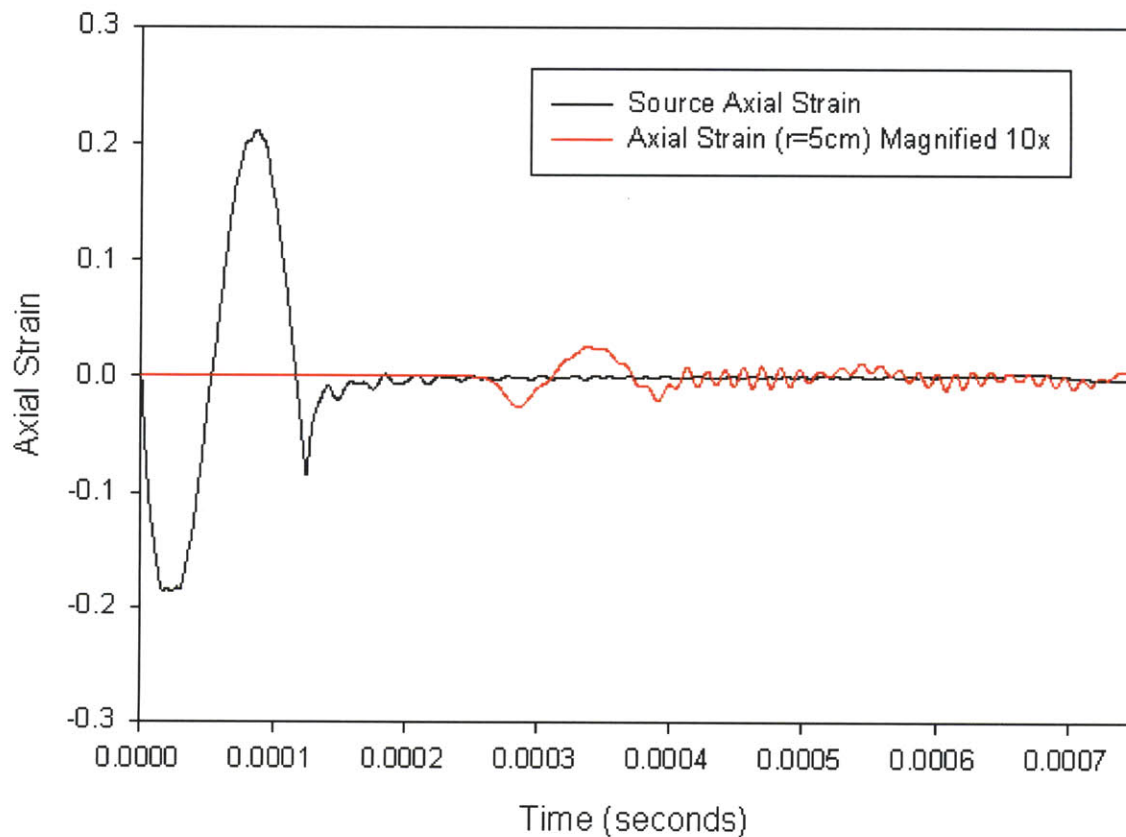
Figure 4.3: Axial Strain Field Output

The strain wave of the source has asymmetric amplitude that oscillates from a global maximum of 0.21 to a global minimum of -0.19. Experiments conducted in the Abaqus implicit dynamic

solver show that the amplitude asymmetry decreases in proportion to the mesh resolution. Accordingly, a fine mesh will approach a symmetric amplitude strain as the vertical nodal spacing approaches zero. The asymmetry is a consequence of the error of using a numerical analysis.
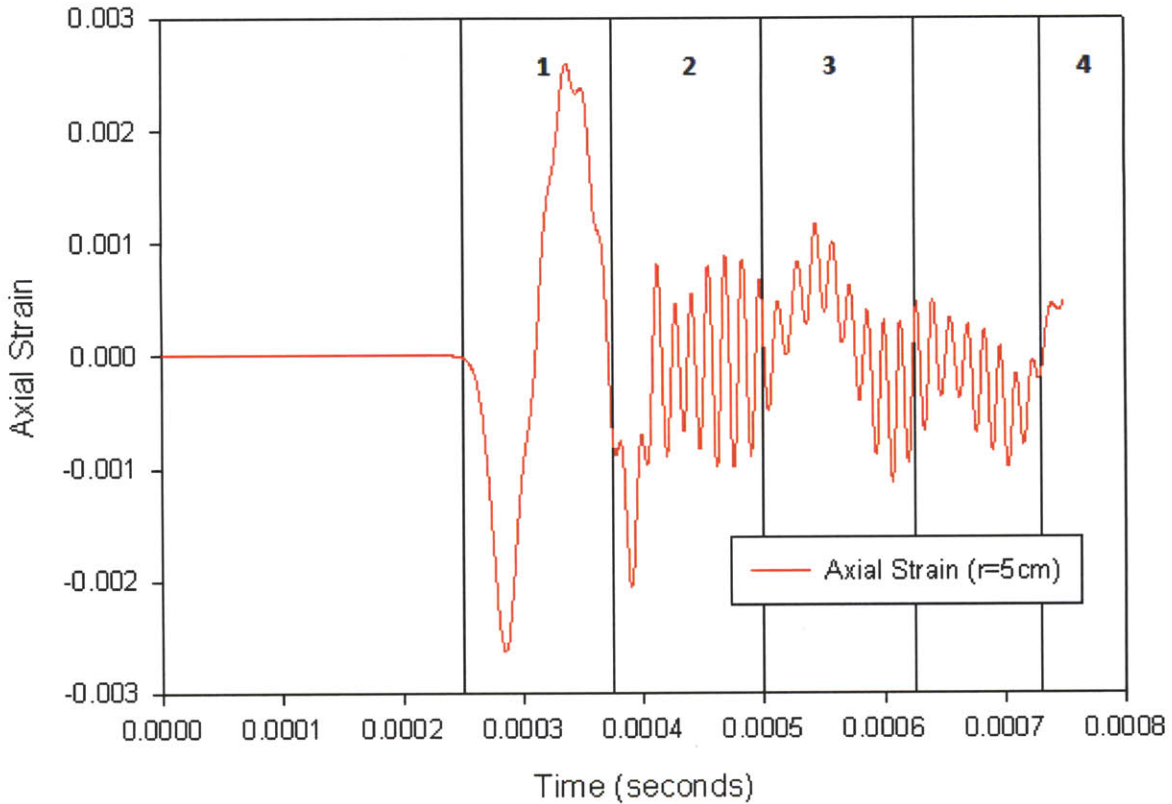
Figure 4.4: Field Output at Receiver Node: Axial Strain

There is a local maximum of the compressive strain recorded after the wavefront completes one wave length. This value is equal to an axial strain of -0.002 at .000395 seconds in Figure 4.4. Experiments indicate that the local maximum corresponds to the axial stress present in the mesh after the source wave completes one wave length.

The higher frequency harmonics are correlated to the mesh resolution. Experiments show that refining the mesh reduces the high frequency harmonic of the axial strain field. The mesh resolution figures provided demonstrate this effect.

The frequency of the received axial strain is equal to the input frequency of 8kHz. The frequency of the axial strain remains constant throughout its propagation; this occurrence agrees with the frequency of the displacement field. Accordingly the wave propagation of the strain field behaves as a planewave.

4.3. Integration Time Variability

The length of the integration time steps for each model was taken as a function of the velocity of the shear wave front and the element length or vertical nodal spacing. The time step duration was varied as a ratio of the integration time step duration and the element length.

$$Integration\ Time\ Step\ Ratio\ = \frac{Integration\ Time\ Step\ (seconds)}{Vertical\ Nodal\ Spacing\ (meters)}$$

The ratio varied from $0.0005\frac{s}{m}$ to $0.01\frac{s}{m}$. The global maximum integration time step tested was 6.25 microseconds the global minimum time step was 312.5 nanoseconds.

A model with a ratio of $0.0005\frac{s}{m}$ has an integration time step duration, t_1, equal to the product of the ratio of $0.0005\frac{s}{m}$ and the vertical nodal spacing of 0.000625m. Moreover, a model with a multiple of $0.01\frac{s}{m}$ has an integration time step duration, t_2, equal to the product of the ratio of $0.01\frac{s}{m}$ and the vertical nodal spacing of 0.000625m .

A table of the selected time step ratios used is provided.

Young's Modulus, E	Calculated	52 Mpa
Shear Modulus, G_{max}	Calculated	16 Mpa
Shear Phase Velocity, V_s	Input	100 m/s
Possion's Ratio, η	Input	0.3
Mass Density, ρ_m	Input	2000 kg/m

Table 4.1. Material Properties

The control variables are known; it is possible to list the independent variables.

Model	Test Number	Vertical Nodal Spacing	$\dfrac{Integration\ Time\ Step}{Vertical\ Nodal\ Spacing}$	Integration Time Step Length (s)
Model 1	1	0.000625m	$0.0005\frac{s}{m}$	3.125E-07
Model 2	2	0.000625m	$0.0014\frac{s}{m}$	8.750E-07
Model 3	3	0.000625m	$0.0023\frac{s}{m}$	1.438E-06
Model 4	4	0.000625m	$0.0032\frac{s}{m}$	2.000E-06
Model 5	5	0.000625m	$0.0041\frac{s}{m}$	2.5625E-06
Model 6	6	0.000625m	$0.005\frac{s}{m}$	3.125E-06
Model 7	7	0.000625m	$0.01\frac{s}{m}$	6.250E-06

Table 4.2. Time Step Ratios

4.4. Displacement Field Output
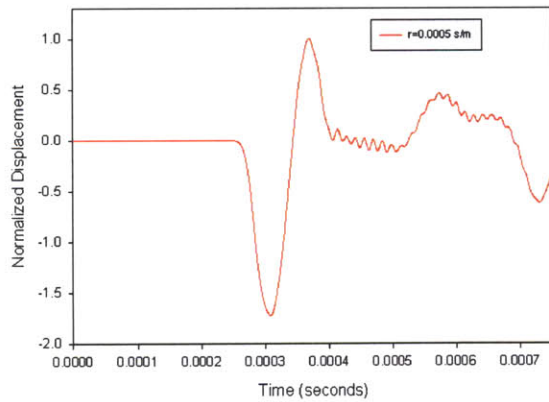
Vertical Displacement r=0.0005 s/m
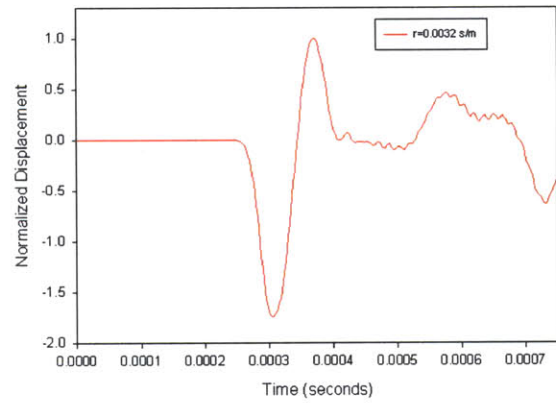
Vertical Displacement r=0.0032 s/m
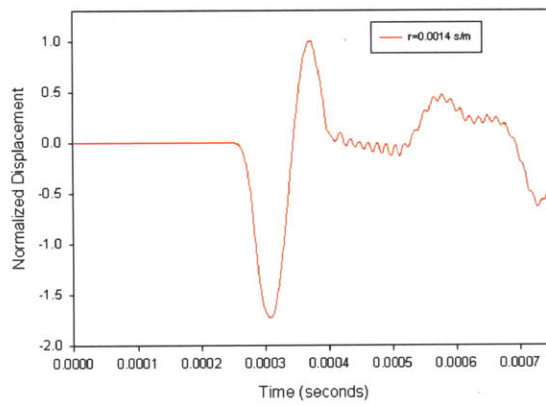
Vertical Displacement r=0.0014 s/m
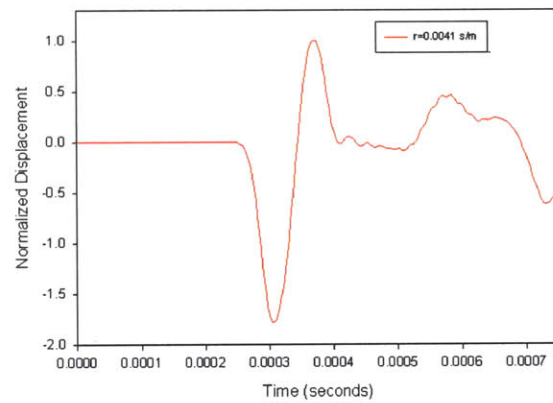
Vertical Displacement r=0.0041 s/m
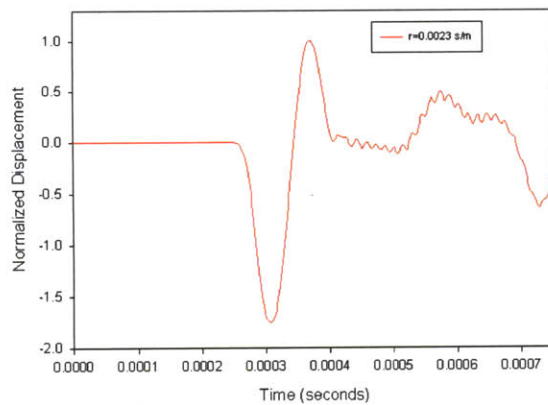
Vertical Displacement r=0.0023 s/m
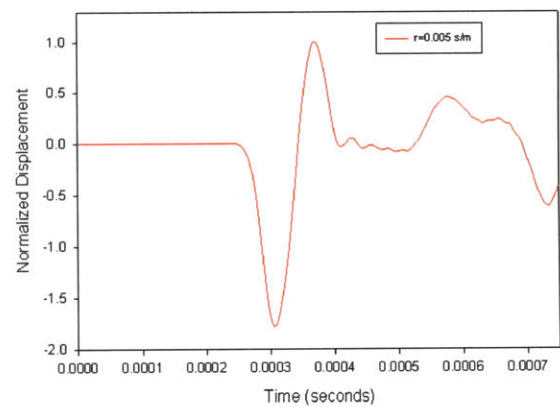
Vertical Displacement r=0.005 s/m

114
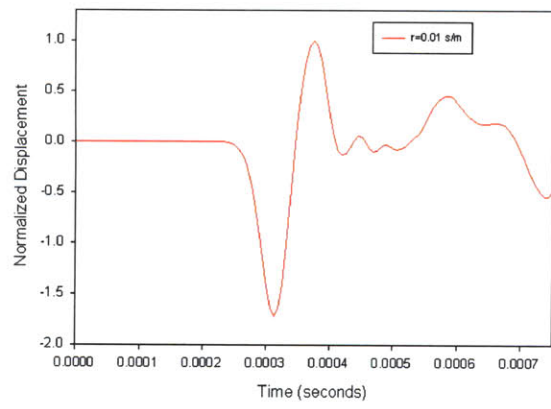
Vertical Displacement r=0.01 s/m

4.5. Axial Strain Field Output
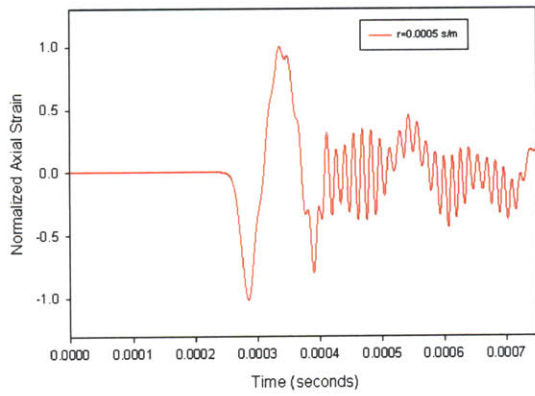
Axial Strain r=0.0005 s/m
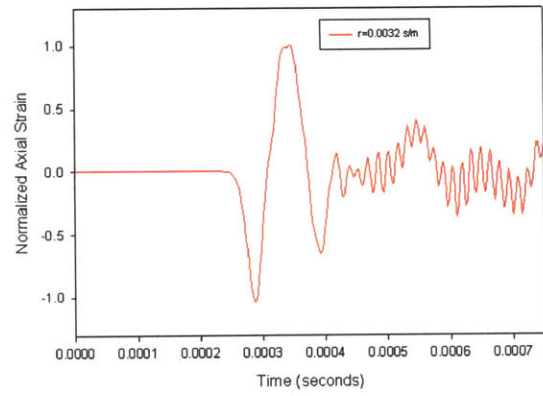
Axial Strain r=0.0032 s/m
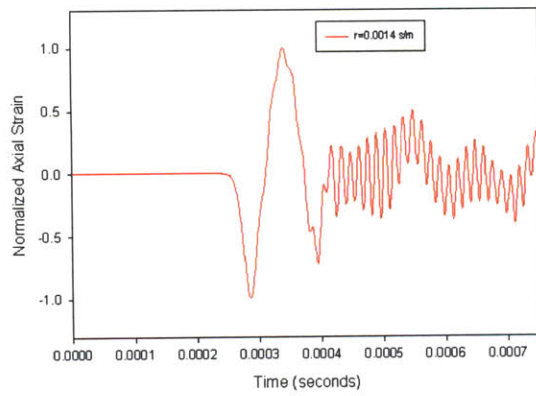
Axial Strain r=0.0014 s/m
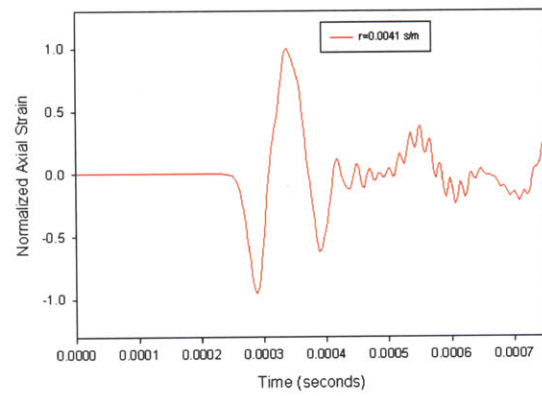
Axial Strain r=0.0041 s/m
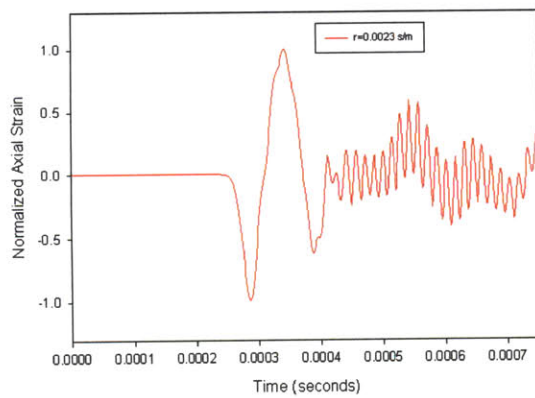
Axial Strain r=0.0023 s/m
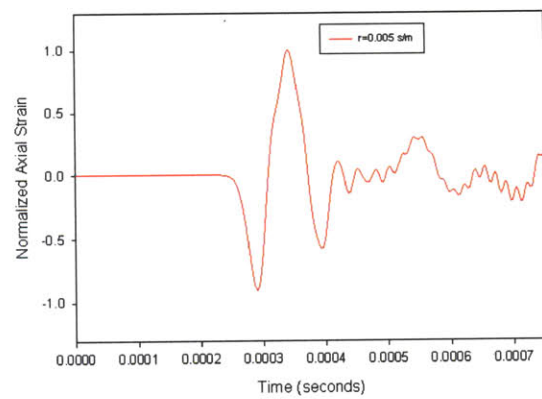
Axial Strain r=0.005 s/m
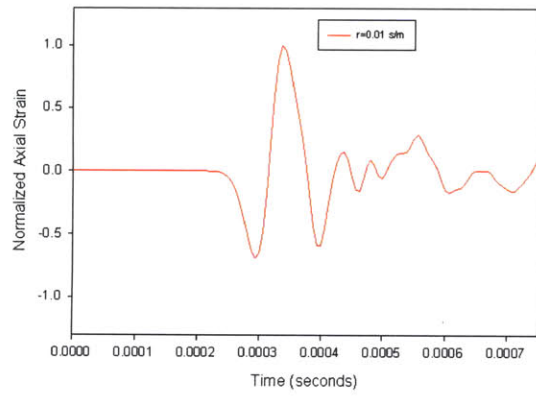
Axial Strain r=0.01 s/m

The symmetry of the waveform appears to degrade at time step ratios larger than 0.0041 s/m. It is recommended to use time step ratios less than 0.0041 s/m

4.6. Velocity measurements of the Displacement Field

The results of the field output test indicate that the travel time of the P-wave remains constant for all ratios tested in the displacement field. Consequently, the first arrival velocity and peak to peak velocity of the displacement and strain output remain constant for all ratios examined.

The travel time of a sinusoidal wave is taken as the time between the two characteristic points of the source and receiver wave front. The source wave front remained constant at the source location; it is the maximum negative amplitude of the signal. Time differentials were measured as the difference of the pulse time recorded at the receiver node receiver and the source.

$$Measured\ Velocity = \frac{dr}{ts_2 - ts_1} = \frac{0.05cm}{.000307s - 0.00003125s} = 181.4\ \frac{m}{s}$$

The first time of arrival method asserts that the travel time between two points in space may be taken as the difference of first direct arrivals at the two points. This computation is achieved by taking the difference between the instantaneous point in time the source signal is sent and the instantaneous start of the major arrival of the receiver signal.

$$Measured\ Velocity = \frac{dr}{ts_2 - ts_1} = \frac{0.05cm}{.0002659s - 0s} = 188\ \frac{m}{s}$$

4.7. Velocity measurements of the Strain Field

The results of the field output test indicate that the travel time of the P-wave remains constant for all ratios tested in the axial strain field. Consequently, the first arrival velocity and peak to peak velocity of the displacement and strain output remain constant for all ratios examined.

$$Measured\ Velocity = \frac{dr}{ts_2 - ts_1} = \frac{0.05cm}{.000289s - 0.000025s} = 189.4\ \frac{m}{s}$$

118

The travel time of a sinusoidal wave is taken as the time between the two characteristic points of the source and receiver wave front. The source wave front remained constant at the source location; it is the maximum negative amplitude of the signal. Time differentials were measured as the difference of the pulse time recorded at the receiver node receiver and the source.

$$Measured\ Velocity = \frac{dr}{ts_2 - ts_1} = \frac{0.05cm}{.000260s - 0s} = 192\ \frac{m}{s}$$

4.8. Time Step Experiment: Decay of higher harmonics

The higher degree harmonics of the displacement field decay as the time step increment increases from 312.5 nanoseconds to 6.25 microseconds. The measured high degree harmonic has a frequency of 62.5kHz of the displacement field. The measured high degree harmonic has a frequency of 66.5kHz of the strain field. The frequency is independent of the time step.

The reduction of the integration time step will linearise the field output of the displacement. Abaqus's plotter uses a linear relationship to interpolate the data points between the integration time step duration. Consequently, the field output will lose resolution at lower timesteps because sinusoidal motion representing the body wave applied in the model is not linear.

At sufficiently large time steps Abaqus cannot capture the high frequency sinusoidal waveform. At large time steps there is observable linearization the field output. Here the higher frequency amplitudes decrease amplitude because Abaqus Standard.exe cannot capture the real waveform. The high frequency component is reduced as the time step ratio increases.

4.9. Mesh Resolution Variability

The mesh resolution of a given model was calculated as a ratio of the S-wave wavelength of the harmonic input wave front to a defined constant. The constant varied from global minimum of 4, which would produce a mesh resolution of $\frac{\lambda_s}{4}$, to a global maximum of 20, mesh resolution of $\frac{\lambda_s}{20}$.

Twenty was used as the global maximum constant because beyond twenty the computation time required for the numerical analysis became too large and impractical for standard methods.

The time step increment ratio was selected as $0.0005\frac{s}{m}$, which is the ratio of the time step increment numerator and the vertical nodal spacing. A time step ratio of $0.0005\frac{s}{m}$ will conserve the arrival signal shape resolution better than high ratios tested. The velocity of the P-wave was determined to be independent of the time step increment ratio. The time step ratio of $0.0005\frac{s}{m}$ produces the finest integration time step resolution.

Model	Mesh Resolution	Vertical Nodal Spacing	$\dfrac{Integration\ Time\ Step}{Vertical\ Nodal\ Spacing}$	Integration Time Step Length (s)
Model 1	$\lambda_s/4$	0.003125m	$0.0005\frac{s}{m}$	1.563E-06
Model 2	$\lambda_s/6$	0.00208m	$0.0005\frac{s}{m}$	1.042E-06
Model 3	$\lambda_s/10$	0.00125m	$0.0005\frac{s}{m}$	6.250E-07
Model 4	$\lambda_s/20$	0.000625m	$0.0005\frac{s}{m}$	3.125E-07

Table 4.3 Mesh Resolutions

4.10. Mesh Resolution: Displacement Field Output: Source / Receiver and Vertical / Lateral Displacement
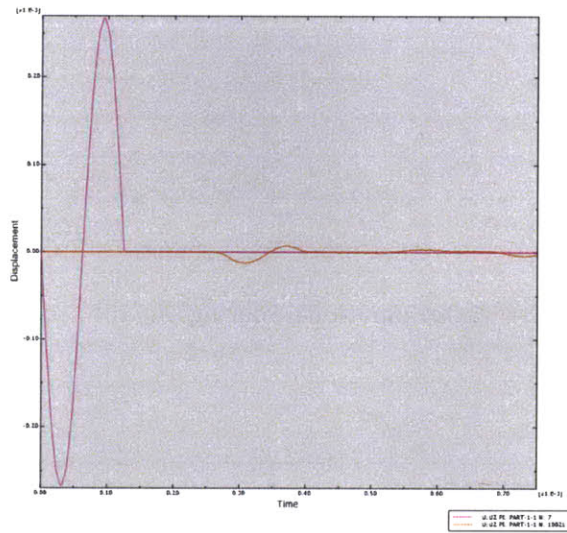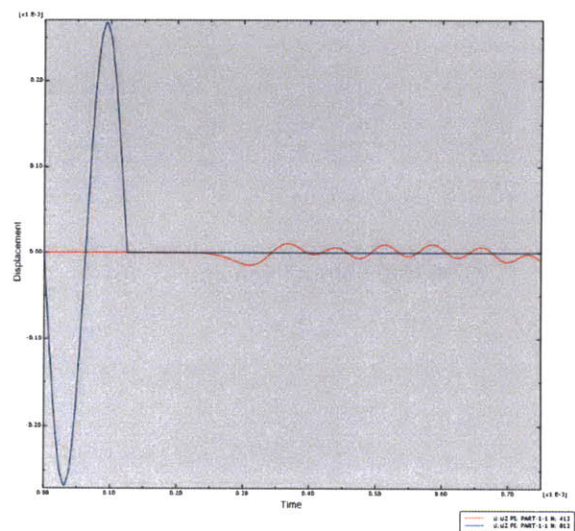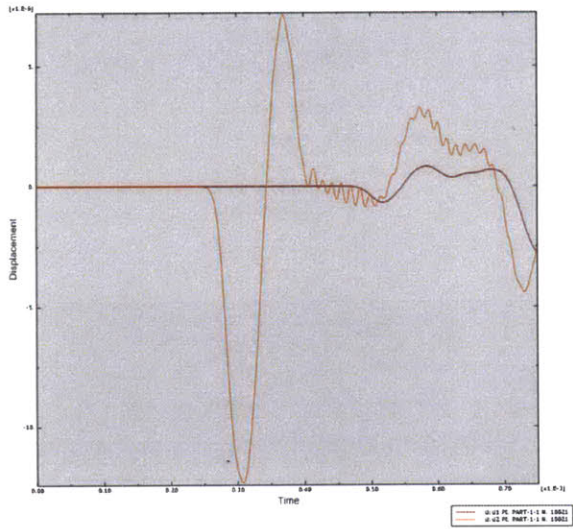

0.000625m Nodal Spacing ($\lambda_s/20$)
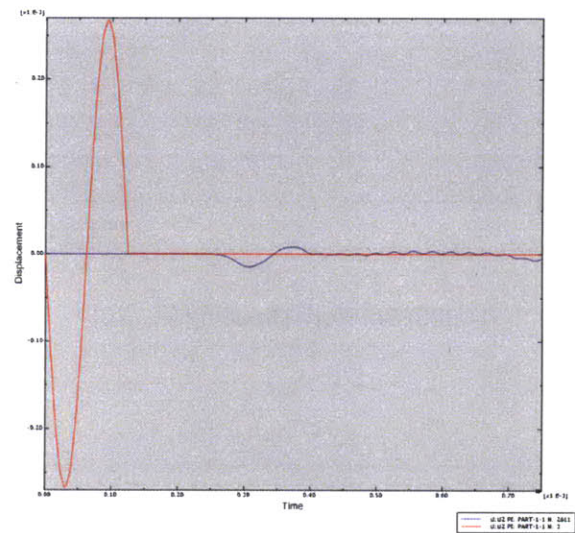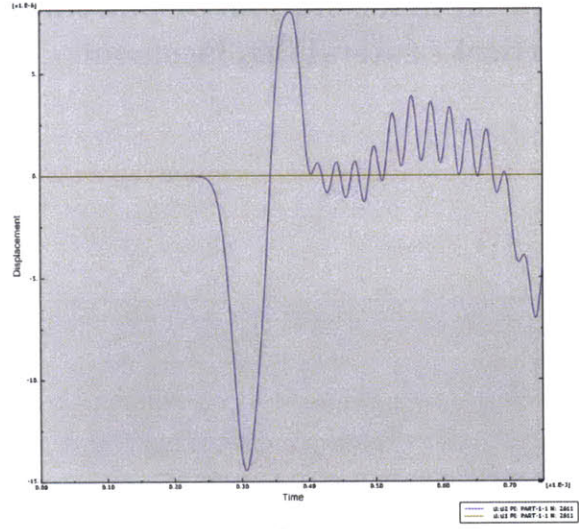

0.00125m Nodal Spacing ($\lambda_s/10$)
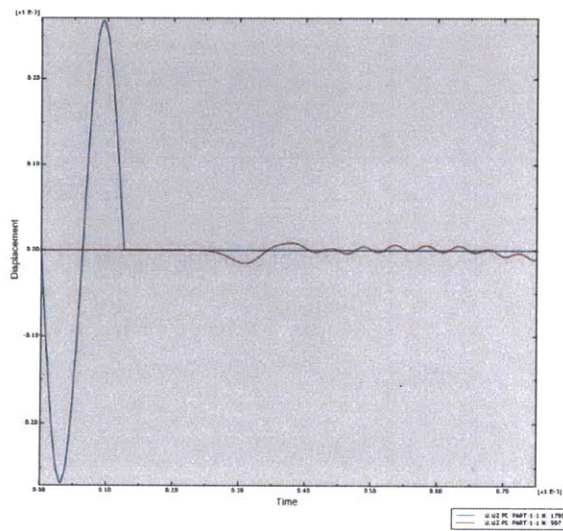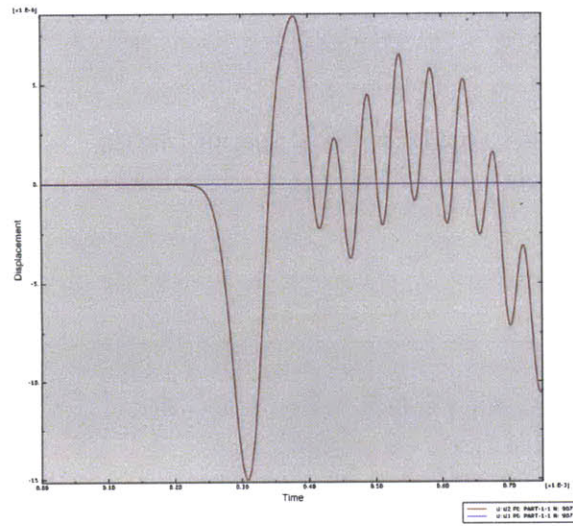

0.00208m Nodal Spacing ($\lambda_s/6$)
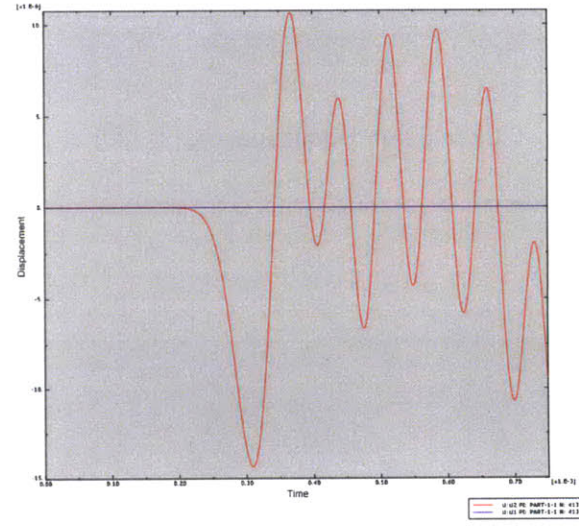

0.003125m Nodal Spacing ($\lambda_s/4$)

0.000625m Nodal Spacing ($\lambda_s/20$)

0.00125m Nodal Spacing ($\lambda_s/10$)

0.00208m Nodal Spacing ($\lambda_s/6$)

0.003125m Nodal Spacing ($\lambda_s/4$)

4.11. Velocity measurements of the Displacement Field

The displacement field was used for P-wave velocity computations. Analysis of the displacement field was conducted using Sigmaplot analysis Data Fit tools. The results of the field output test indicate that the measured velocity using peak to peak method and first arrival method become more accurate as the mesh resolution increases. Consequently, the first arrival velocity and peak to peak velocity of the strain field output enhances as a function of mesh resolution.

The travel time of a sinusoidal wave is taken as the time between the two characteristic points of the source and receiver wave front. The source wave front remained constant at the source location; it is the maximum negative amplitude of the signal. Time differentials were measured as the difference of the pulse time recorded at the receiver node receiver and the source.

$$Measured\ Velocity\ (\lambda_s/20) = \frac{dr}{ts_2 - ts_1} = \frac{0.05m}{0.000305625s - 0.00003125s} = 182.2\ \frac{m}{s}$$

$$Measured\ Velocity\ (\lambda_s/10) = \frac{dr}{ts_2 - ts_1} = \frac{0.05m}{0.000306875s - 0.00003125s} = 181.4\ \frac{m}{s}$$

$$Measured\ Velocity\ (\lambda_s/6) = \frac{dr}{ts_2 - ts_1} = \frac{0.05m}{0.000308432s - 0.00003126s} = 180.4\ \frac{m}{s}$$

$$Measured\ Velocity\ (\lambda_s/4) = \frac{dr}{ts_2 - ts_1} = \frac{0.05m}{0.000309375s - 0.000032302s} = 180.4\ \frac{m}{s}$$

The first time of arrival method asserts that the travel time between two points in space may be taken as the difference of first direct arrivals at the two points. This computation is achieved through taking the difference between the instantaneous point in time the source signal is sent and the instantaneous start of the major arrival of the receiver signal.

$$Measured\ Velocity\ (\lambda_s/20) = \frac{dr}{ts_2 - ts_1} = \frac{0.05m}{0.000268s} = 186.6\ \frac{m}{s}$$

$$Measured\ Velocity\ (\lambda_s/10) = \frac{dr}{ts_2 - ts_1} = \frac{0.05m}{0.000261875s} = 190.9\ \frac{m}{s}$$

$$Measured\ Velocity\ (\lambda_s/6) = \frac{dr}{ts_2 - ts_1} = \frac{0.05m}{0.000253206s} = 197.5\ \frac{m}{s}$$

$$Measured\ Velocity\ (\lambda_s/4) = \frac{dr}{ts_2 - ts_1} = \frac{0.05m}{0.00024375s} = 205.1\ \frac{m}{s}$$

The velocity measurements show two conclusions from the established displacement field data. The decrease of the mesh resolution will overestimate the P-wave velocity using the first arrival method. The decrease of the mesh resolution will underestimate the P-wave velocity.

4.12. Field Output: Analysis of Displacement Field Output.

The models were then calculated using Abaqus solver standard.exe. The field output was extracted as an output database file. Displacement values were calculated from the output database file. Wave velocity measurements were interpreted from the displacement field. Two methods of calculating wave velocity in bender element tests were used: peak to peak and first arrival.

It is evident that the mesh resolution has an observable effect on the field output. Data regression of the velocity measurements show that the mesh resolution has diminishing effect as the mesh resolution exceeds a multiple of twenty. A mesh resolution of lambda divided by six is not adequate for dynamic numerical analysis.

The mesh resolution of λ/20 is the only mesh resolution that records a lateral displacement curve in the model. The lateral displacement field is associated with the shear wave; the shear wave propagating in the 'z' direction will create lateral displacements. The remaining mesh resolutions tested do not record variation of lateral displacement at the receiver node. This is a consequence of the coarse mesh inability to register the propagation of the shear wave.

The velocity measurements suggest that the field output reaches an asymptote when the mesh resolution exceeds a sufficiently large value. At this value the effect of this mesh resolution will not effect on the field output of the numerical analysis. It is evident at the asymptote the rate of change of the field output with respect to the mesh resolution will approach zero. The displacement field out provided demonstrates the increased presence of error high frequency harmonics as mesh resolution decreases.
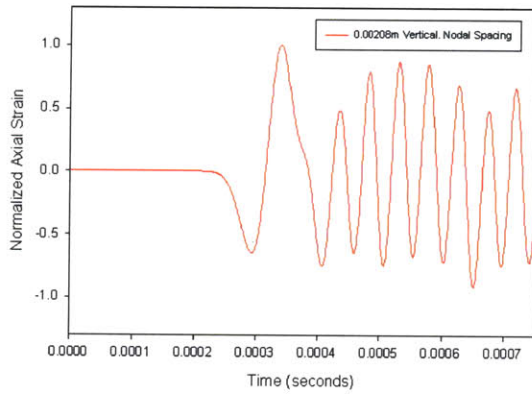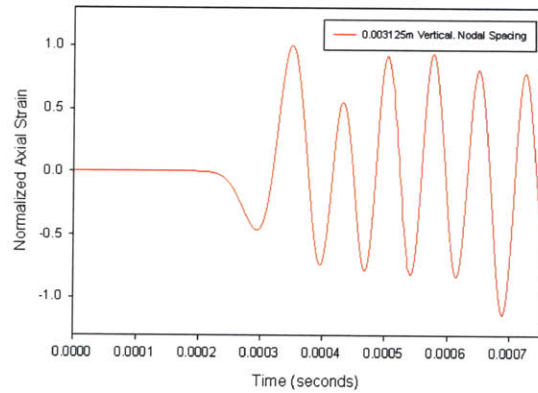
124

4.13. Strain Field Output
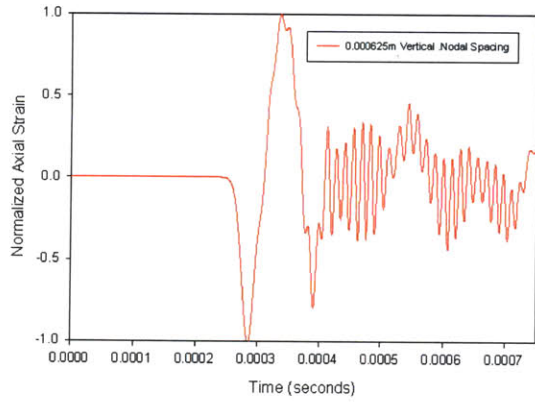
0.000625m Nodal Spacing (λ/20)
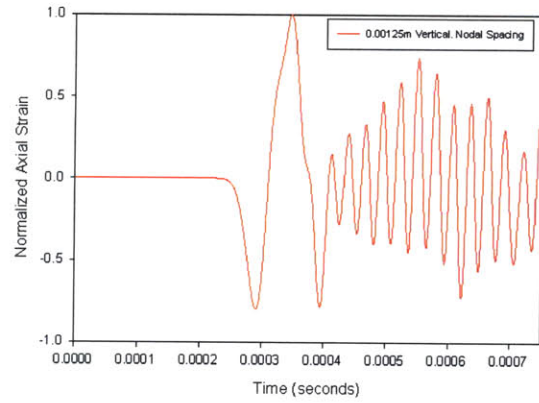
0.00125m Nodal Spacing (λ/10)

0.00208m Nodal Spacing (λ/6)

0.003125m Nodal Spacing (λ/4)

4.14. Velocity measurements of the Strain Field

The axial strain field was used for P-wave velocity computations. Analysis of the axial strain was conducted using Sigmaplot analysis Data Fit tools. The results of the field output test indicate that the measured velocity using peak to peak method and first arrival method become more accurate as the mesh resolution increases. Consequently, the first arrival velocity and peak to peak velocity of the strain field output enhances as a function of mesh resolution.

$$MMeasured\ Velocity\ (\lambda_s/20) = \frac{dr}{ts_2 - ts_1} = \frac{0.05m}{0.000286563s - 0.0000225s} = 189.3\ \frac{m}{s}$$

$$Measured\ Velocity\ (\lambda_s/10) = \frac{dr}{ts_2 - ts_1} = \frac{0.05m}{0.00029125s - 0.00002375s} = 186.9\ \frac{m}{s}$$

$$Measured\ Velocity\ (\lambda_s/6) = \frac{dr}{ts_2 - ts_1} = \frac{0.05m}{0.000293844s - 0.000022924s} = 184.6\ \frac{m}{s}$$

$$Measured\ Velocity\ (\lambda_s/4) = \frac{dr}{ts_2 - ts_1} = \frac{0.05m}{0.00029375s - 0.000025s} = 180.4\ \frac{m}{s}$$

The travel time of a sinusoidal wave is taken as the time between the two characteristic points of the source and receiver wave front. The source wave front remained constant at the source location; it is the maximum negative amplitude of the signal. Time differentials were measured as the difference of the pulse time recorded at the receiver node receiver and the source.

$$Measured\ Velocity\ (\lambda_s/20) = \frac{dr}{ts_2 - ts_1} = \frac{0.05m}{0.000262s} = 190.8\ \frac{m}{s}$$

$$Measured\ Velocity\ (\lambda_s/10) = \frac{dr}{ts_2 - ts_1} = \frac{0.05m}{0.000259375s} = 192.8\ \frac{m}{s}$$

$$Measured\ Velocity\ (\lambda_s/6) = \frac{dr}{ts_2 - ts_1} = \frac{0.05m}{0.000254248s} = 196.6\ \frac{m}{s}$$

$$Measured\ Velocity\ (\lambda_s/4) = \frac{dr}{ts_2 - ts_1} = \frac{0.05m}{0.00025s} = 200.0\ \frac{m}{s}$$

The velocity measurements show two conclusions from the established data of the strain field. The decrease of the mesh resolution will overestimate the P-wave velocity using the first arrival method. The decrease of the mesh resolution will underestimate the P-wave velocity.

4.15. Field Output: Analysis of Strain Field Output.

The models were then calculated using Abaqus solver standard.exe. The displacement field output was extracted as an output database file. Strain scalar values were calculated from the displacement field using the aforementioned method. Wave velocity measurements were interpreted from the strain field. Two methods of calculating wave velocity in bender element tests were used: peak to peak and first arrival.

It is evident that the mesh resolution has an observable effect on the strain field. Data regression of the velocity measurements show that the mesh resolution has diminishing effect as the mesh resolution exceeds a multiple of twenty. A mesh resolution of lambda divided by six is not adequate for dynamic numerical analysis.

Data regression suggests that the field output reaches an asymptote when the mesh resolution exceeds a sufficiently large value. At this value the effect of this mesh resolution will not effect on the field output of the numerical analysis. It is evident at the asymptote the rate of change of the field output with respect to the mesh resolution will approach zero. It is observable through Figure 4.5 and Figure 4.9 that this does occur.

127

5. Results

5.1. Overview

The Results chapter will examine different possible scenarios to model a dynamic analysis with Abaqus FEM analysis. The wave front of both P/S waves will be considered. Love and Rayleigh surface waves will be ignored in this framework. The model will utilize an isotropic elastic medium and a traction/point source perturbation. The field output will be examined with respect to both lateral scalar shear strain and displacement. Additional analysis will be done to solve velocity scalars of the wave front with respect to source receiver distance and attenuation.

5.2. P-Wave Model: Displacement Source

An elastic rod model was constructed in two dimensional space with an uniaxial stress field applied using a prescribed displacement over an emission surface. Lateral motion was unrestrained. A vertical constraint was fixed to the bottom surface of the model to prevent rigid boundary motion. A diagram of the model is provided in Figure 5.51.

The displacement condition is sinusoidal harmonic motion. The parameters of the source vibration are provided in the tabled attached.

Frequency	8000 Hz (rev/sec)
Maximum Displacement	1E-7 m

Table 5.1. Displacement Parameters

The field output of the model captured the uniaxial stress field, displacement field, acceleration field. The axial strain was calculated from the differential vertical displacement of two nodes spaced one element distance apart. The element spacing of the model is 0.000625m or equivalently 0.625mm vertical distance per node. Axial strain was used because of the one dimensional propagation and polarization of the P-wave propagation. Shear strain would be a more suitable strain measurement for the propagation of the shear wave; a shear wave polarization is orthogonal to its propagation.

Data were extracted from selected nodes located along the centerline of the geometry. The vertical spacing of the extraction nodes were one centimeter. Each extraction depth included two

vertically adjacent nodes for the purpose of measuring the axial strain. The nodes were spaced one element length apart. The element length or the vertical spacing of the node is equal to the shear wave length divided by twenty.

The geometry of the rod is sufficiently large to prevent reflections occurring from the bottom boundary. At the source of the harmonic waveform, 0cm, there will be no after effects. The displacement boundary condition oscillates one harmonic period and reaches equilibrium. At equilibrium no vertical displacement is possible.

The maximum depth of extraction was ten centimeters. Accordingly, there are eleven extraction depths at each integer beginning at 0cm and ending at 10cm inclusive.

5.2.1. P-Wave Model: Displacement Field

The vertical displacement of a node is the scalar quantity of displacement with respect to the vertical axis. In a two dimensional model the vertical axis is represented by the subscript 'z' or displacement with respect to the 'z axis'. The vertical displacement of the node was captured with respect to time. The resolution of the time step was fixed at 312.5 nanoseconds, enough to capture fine perturbations of the P-Wave front propagation. Accordingly, there are 3200 independent data points in the field output containing data from each time step.

Figure 5.1. provides the vertical displacement from the displacement model of the extraction nodes.
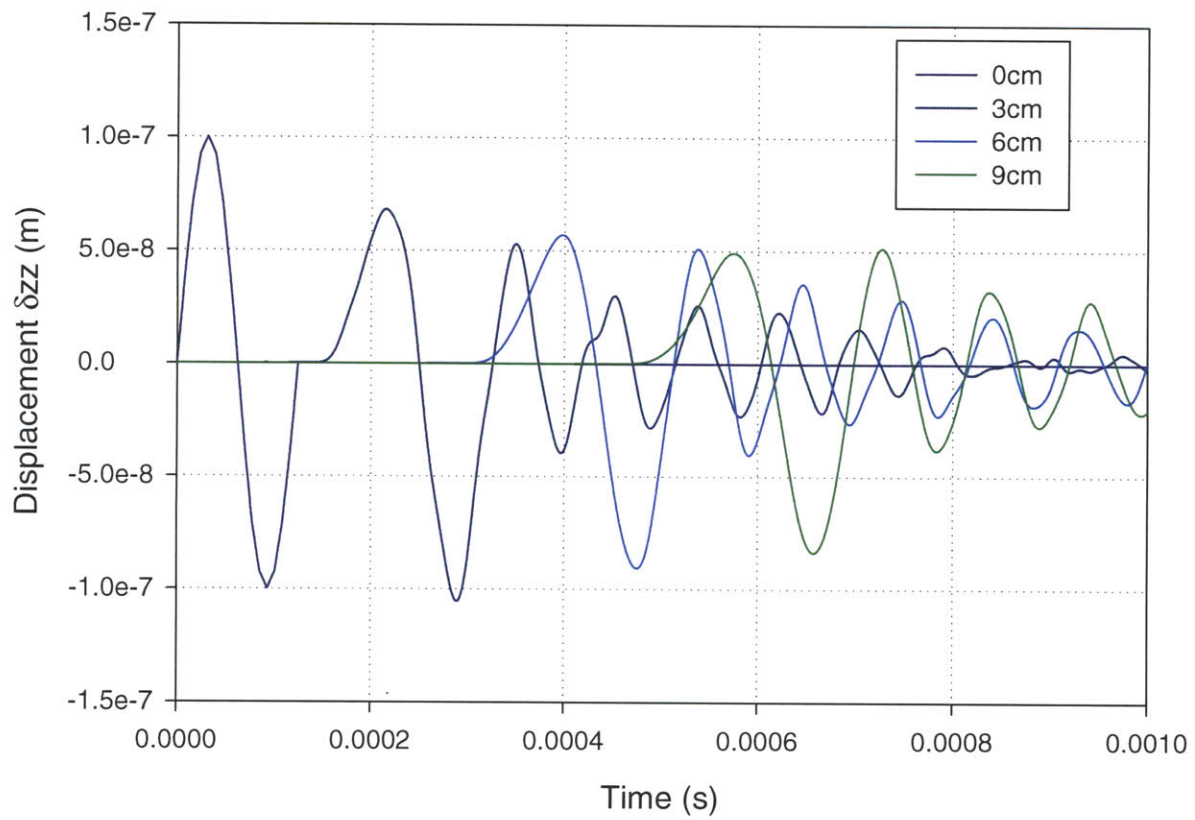
Figure 5.1: The Displacement Field

5.2.2. P-Wave Model: Stress Field

The stress field of the P-Wave propagation can also be computed. According to the Hooke's law the stress field of an elastic solid is directly related to the strain field. This relationship is applicable to seismology where body waves constitute p and s waves arise from stress differentials in media. The stress field is provided for the P-wave displacement model.
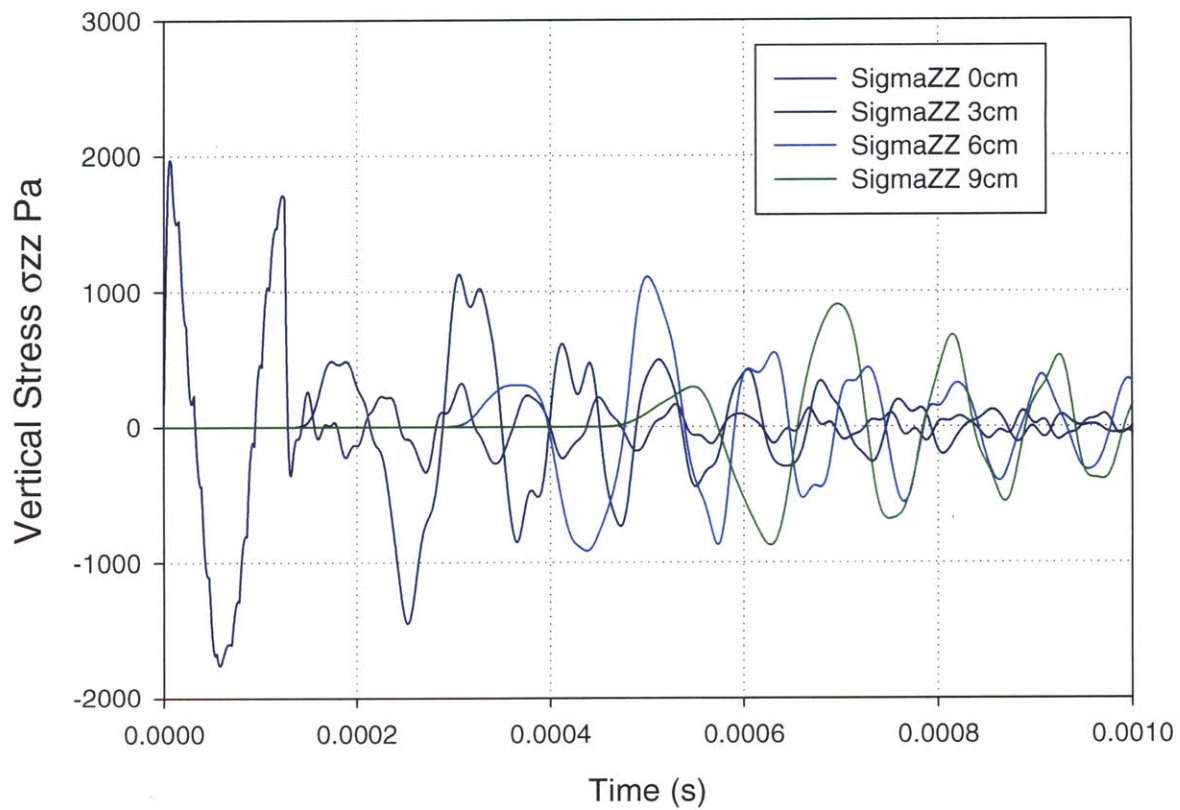
Figure 5.2: The Vertical Stress Field

5.2.3. P-Wave Model: Acceleration Field

According to the wave equation the acceleration of the wave front is equal to the product of the Laplacian of wave front and a constant. The computed acceleration is a scalar quantity with respect to the z axis. The accelerations of the P-Wave are provided.
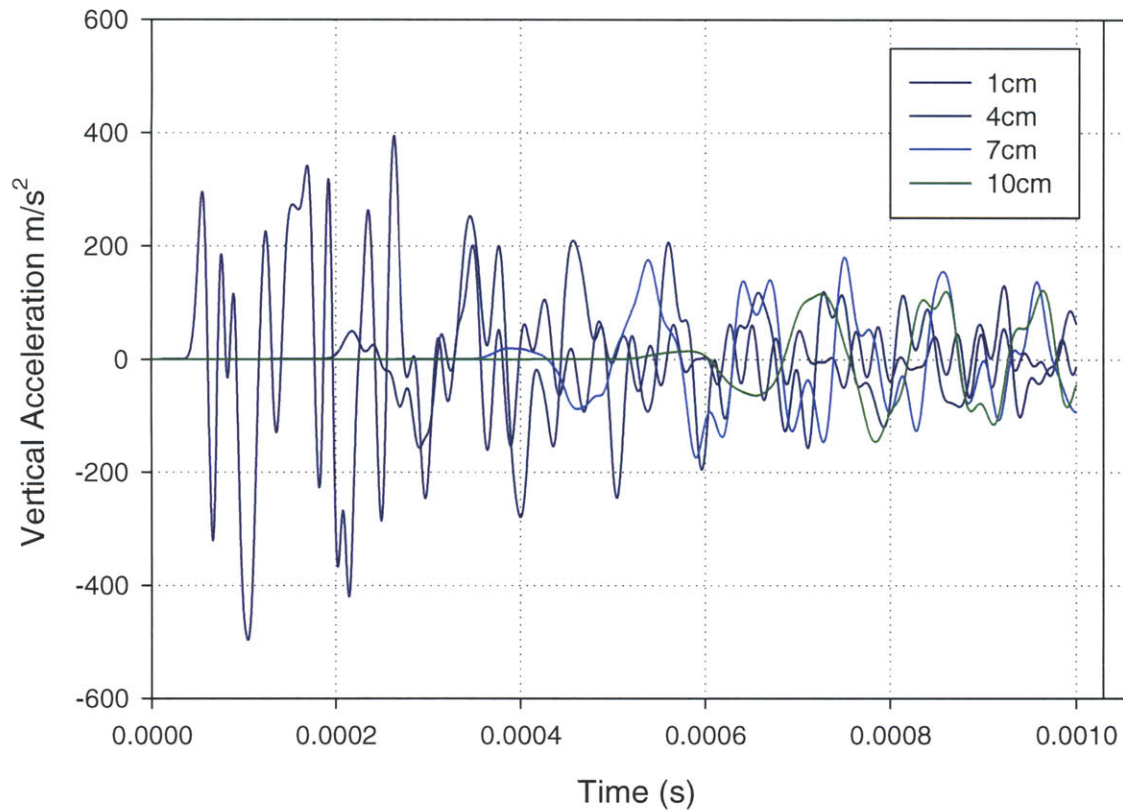
Figure 5.3: The Vertical Acceleration Field

5.2.4. P-Wave Model: Axial Strain Field

The axial strain of the P-Wave front is equal to differential vertical displacement of two nodes spaced one element distance apart. The equation for the axial strain is equal to

$$\varepsilon_{axial} = \frac{\Delta\delta_v}{Verical\ Spacing\ between\ n_1\ n_2}$$

It is possible to record the axial strain using a time domain and integration time step scalar identical to the displacement field.
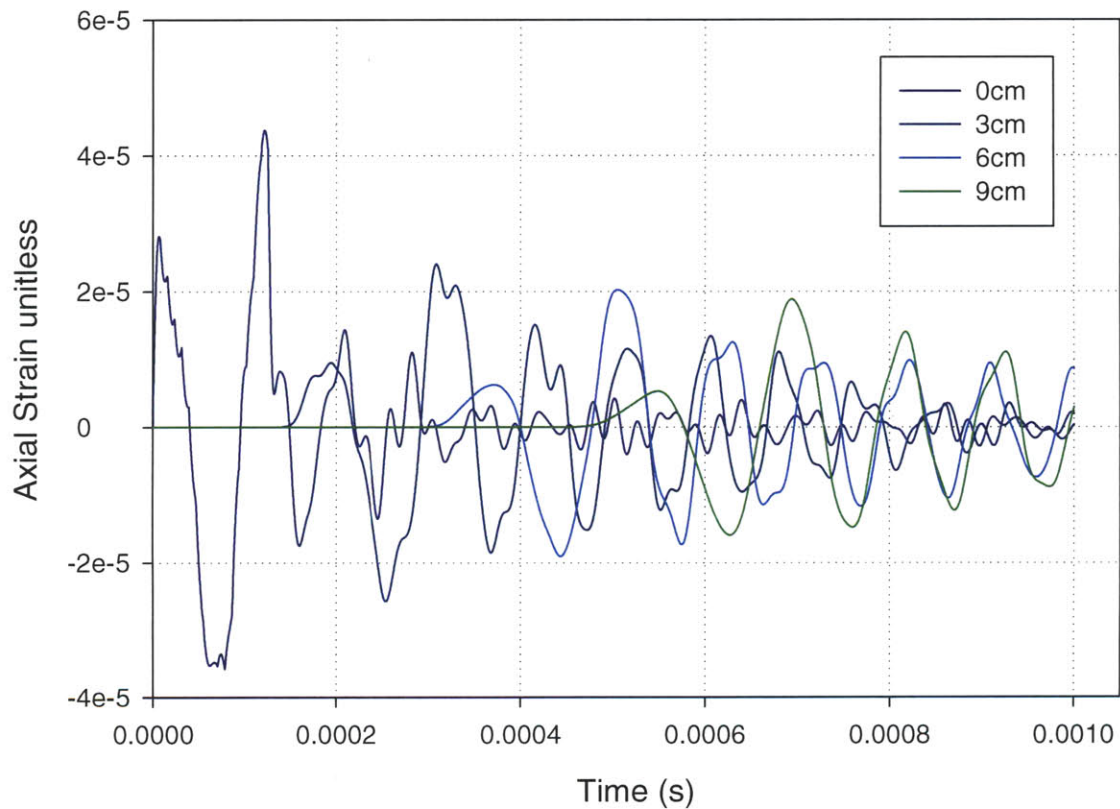
Figure 5.4: The Axial Strain Field

133

5.2.5. P-Wave Model: Attenuation of the Displacement Field

The amplitude of the arrival signal decays as the distance between the source and the arrival signal increases. The maximum amplitude of the wave front is equal to its maximum positive peak or its phase equal to $\frac{\pi}{2}$ of the sinusoidal harmonic motion. The gradual reduction in amplitude as a function of source and receiver distance is provided.
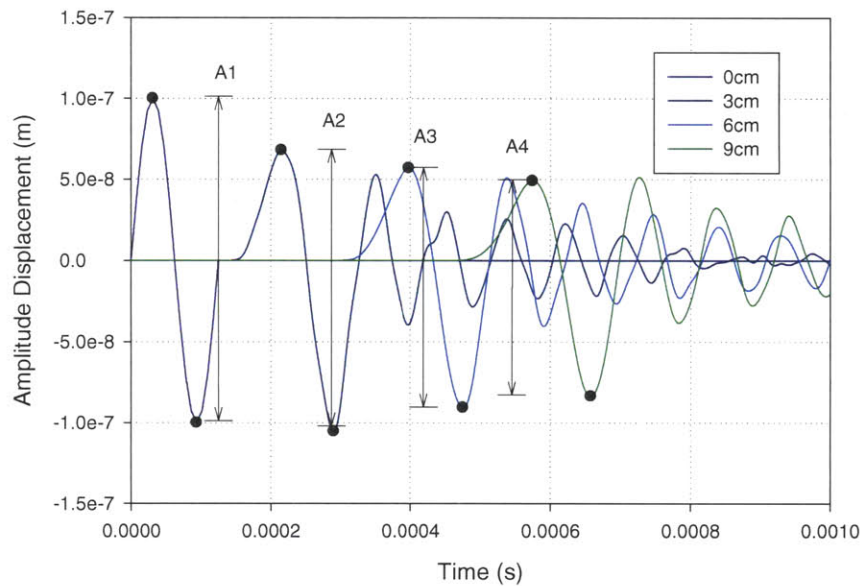
Figure 5.5: Attenuation of the Displacement Field

The points superimposed on the displacement field output represent the amplitude scalars for each P-Wave front corresponding to its unique source/receiver distance. The amplitude scalars were calculated by solving for the differential amplitude of the positive and negative displacements. This calculation is done by taking subtracting the negative phase of the amplitude from the positive phase. Regression analysis was done using the four amplitude scalars representing the maximum positive nodal vertical displacement.

The time scalar of the wavefront is required for attenuation analysis. This calculation was done by using the mean of the time that corresponds with the positive phase and the time that corresponds to the negative phase.

The reduction of the amplitude of the displacement field can be expressed as an inverted polynomial function taking the form, where a_0 and b_0 are numerical constants determined through regression analysis.

$$Amp(r) = a_0 + \frac{b_0}{r}$$

The reduction of the amplitude in the FEM conforms to the observed reduction in amplitude for waves generated by a surface footing. In the case of a surface footing, the decrease in displacement amplitude is proportional to $1/r$.

According to Prakash (1985), for hemispherical p/s wave propagation,

$$Amplitude \propto \frac{1}{r}$$

Regression of the amplitude decay can be done by fitting a first order inverse polynomial function to the data set. This behavior is called Geometric Damping.
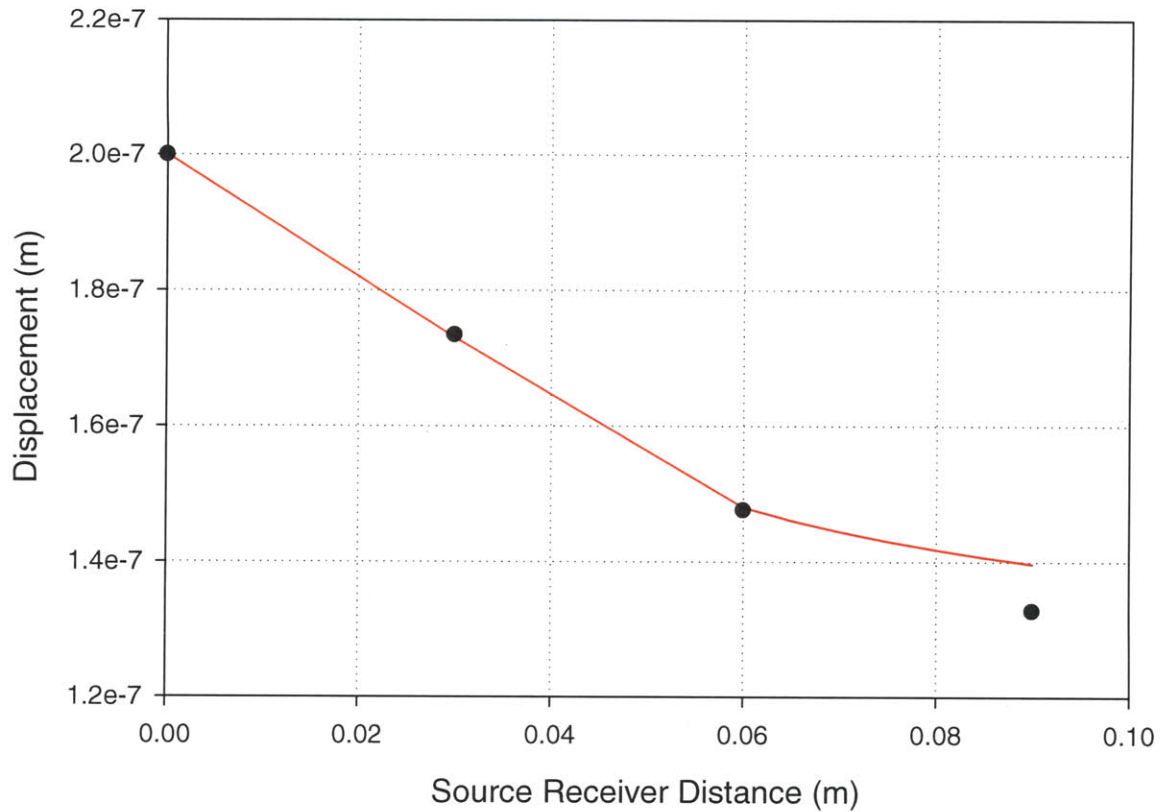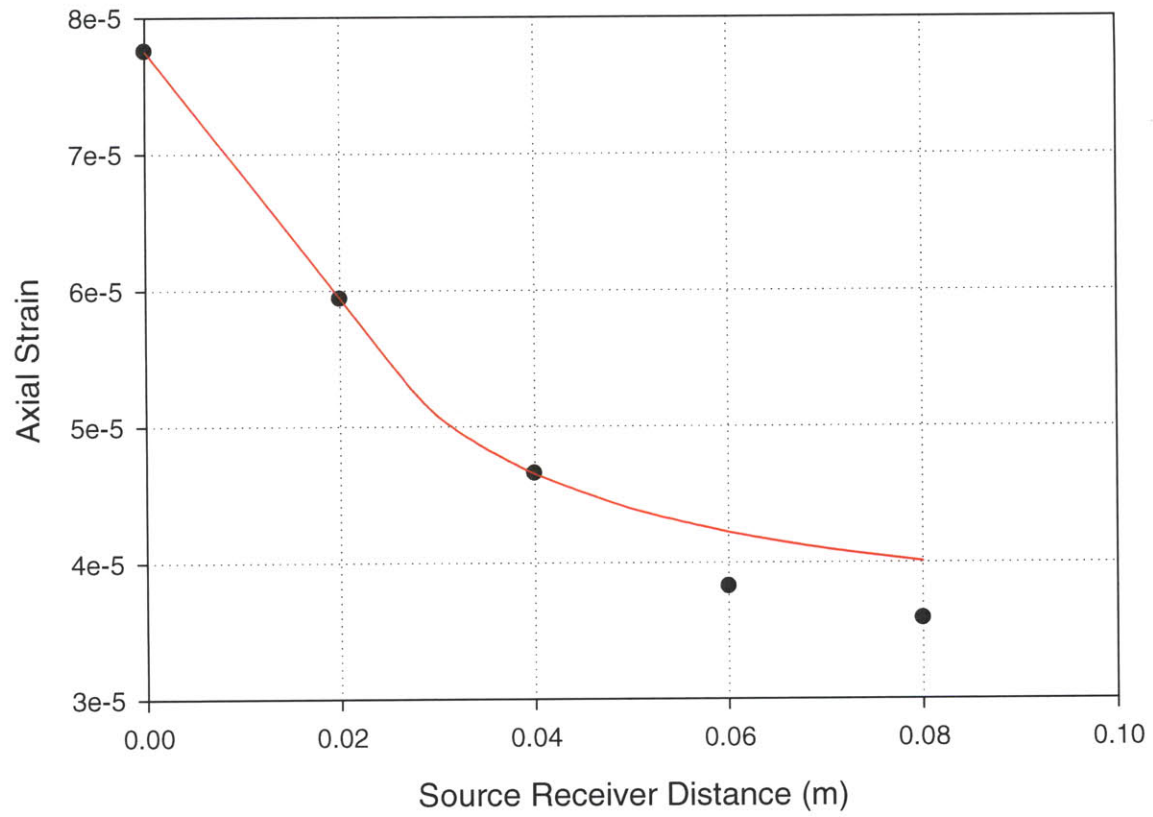
Figure 5.6: Regression of the Attenuation of the Displacement Field

Regression analysis was done on the attenuation of the displacement. The graph shows four arrivals at variable different source/receiver distances in multiples of three centimeters. Each arrival has an associated displacement amplitude and arrival time. The interpolation function is a first order inverse polynomial equation taking the form.

$$Amp(r) = a_0 + \frac{b_0}{r}$$

For the displacement boundary model this equation translates.

$$Amp(r), m = 1.23 * 10^{-7} + \frac{1.5 * 10^{-9}}{r}, \qquad r > .06$$

$$Amp(r), m = 2 * 10^{-7} - 8.3(r), \quad r < .06$$

5.2.6. P-Wave Model: Frequency

The period of the arrival signal changes as the source/distance increases. The arrival frequency of the source signal is calculated by solving the reciprocal of the observed period. The observed period is a variable quantity with respect to the source receiver distance.
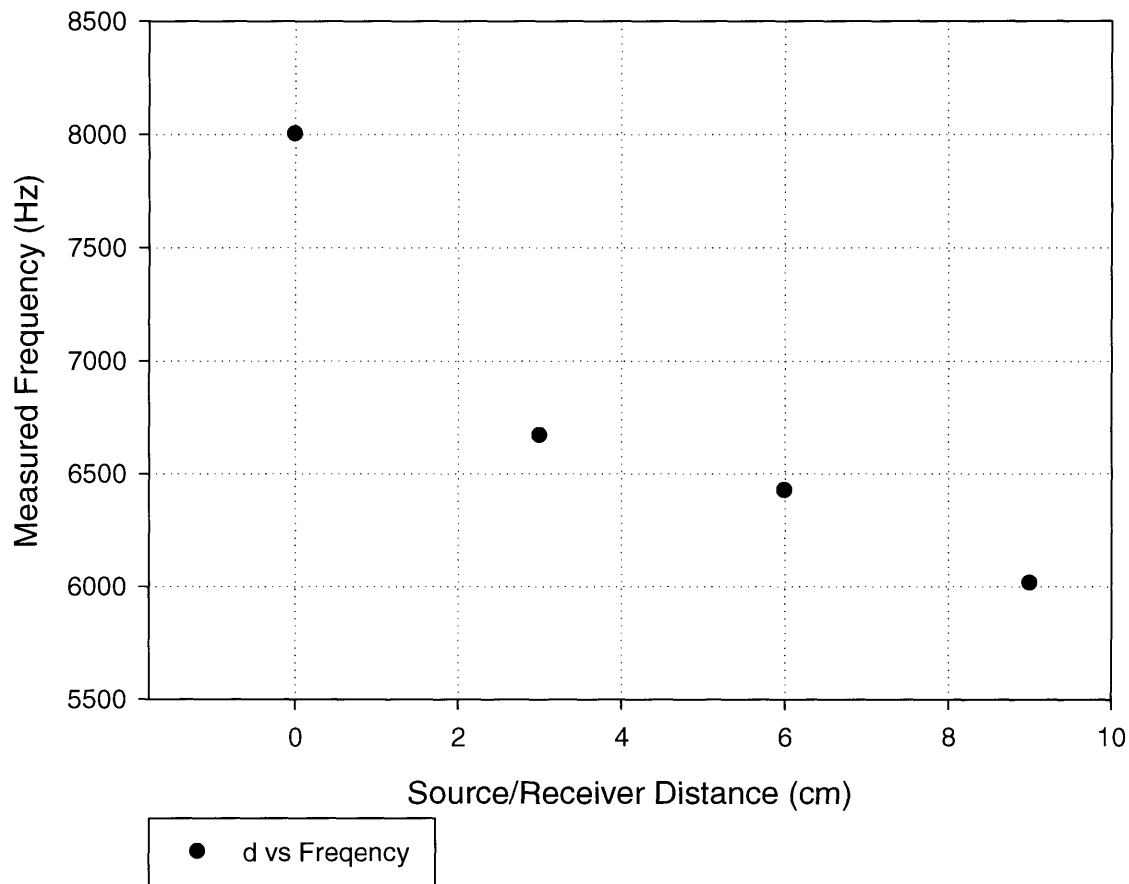
Figure 5.7: Frequency of the Displacement Field

It is observable that the frequency of the displacement field remains varies with respect to depth. The waveform in a free elastic rod model does not exhibits planar behavior.

5.2.7. P-Wave Model: Attenuation of the Axial Strain

The amplitude of the arrival signal decays as the distance between the source and the arrival signal increases. The maximum amplitude of the wave front is equal to its maximum positive peak or its phase equal to $\frac{\pi}{2}$ of the sinusoidal harmonic motion. The gradual reduction in amplitude as a function of source and receiver distance is provided.
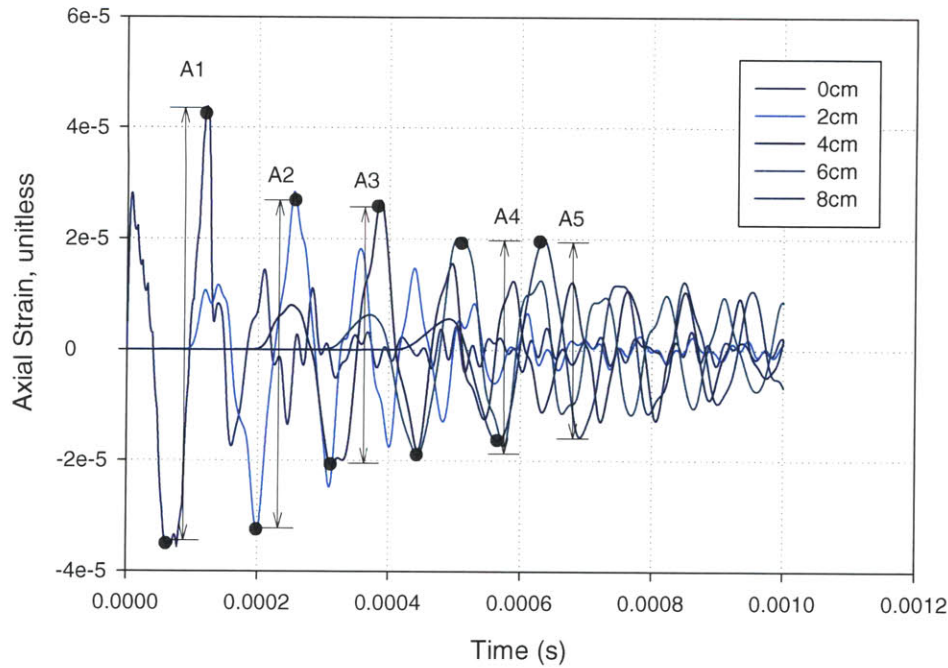
Figure 5.8: Attenuation of the Strain Field

Regression analysis was done on the attenuation of the displacement. The graph shows four arrivals at variable different source/receiver distances in multiples of three centimeters. Each arrival has an associated displacement amplitude and arrival time. The interpolation function is a first order inverse polynomial equation. For the damped infinite boundary model this equation translates.

$$Amp(r), m = 1.82 * 10^{-5} + \frac{1.154 * 10^{-9}}{r}, \qquad r > .03$$

$$Amp(r), m = 7.92 * 10^{-5} - 0.00104(r), \qquad r < .03$$

Figure 5.9: Regression of the Attenuation of the Strain Field

5.2.8. P-Wave Model: Velocity Measurements

Velocity measurements using peak to peak method are attached for the displacement, stress state, acceleration, and axial strain field output. A theoretical shear wave velocity was specified in the input analysis. The theoretical P-wave velocity is $161\ \frac{m}{s}$ Velocity measurements are provided.

5.2.8.1. P-Wave Model: Theoretical Velocity.

The polarization of the P-wave is identical in both the elastic rod traction model and the infinite boundary model. The P-wave front velocity of the elastic rod model and the infinite boundary model is not equivalent.

An infinite boundary model the P-wave velocity is expressed:

$$V_p = \sqrt{\frac{E}{\rho_m}}$$

$$V_p = \sqrt{\frac{52 * 10^6 Pa}{2000\frac{kg}{m^3}}} = 161\ \frac{m}{s}$$

This equation is applicable in elastic rods subject to P-wave agitation in an uniaxial stress state. The Young's modulus is the appropriate modulus in the P-wave velocity subject to an uniaxial and uniform stress state and the rod is allowed to deform laterally. If the conditions are met then the operative elastic constant is the Young's Modulus 'E'.

5.2.9. P-Wave Model: Velocity Measurements Source Receiver Distance

The travel time of a sinusoidal wave is taken as the time between the two characteristic points of the source and receiver wave front. The source wave front remained constant at the source location, 0cm. Time differentials were measured as the time difference of the receiver node receiver and the source. There are ten velocity increments. The measurement begins at 1cm ending at 10cm.
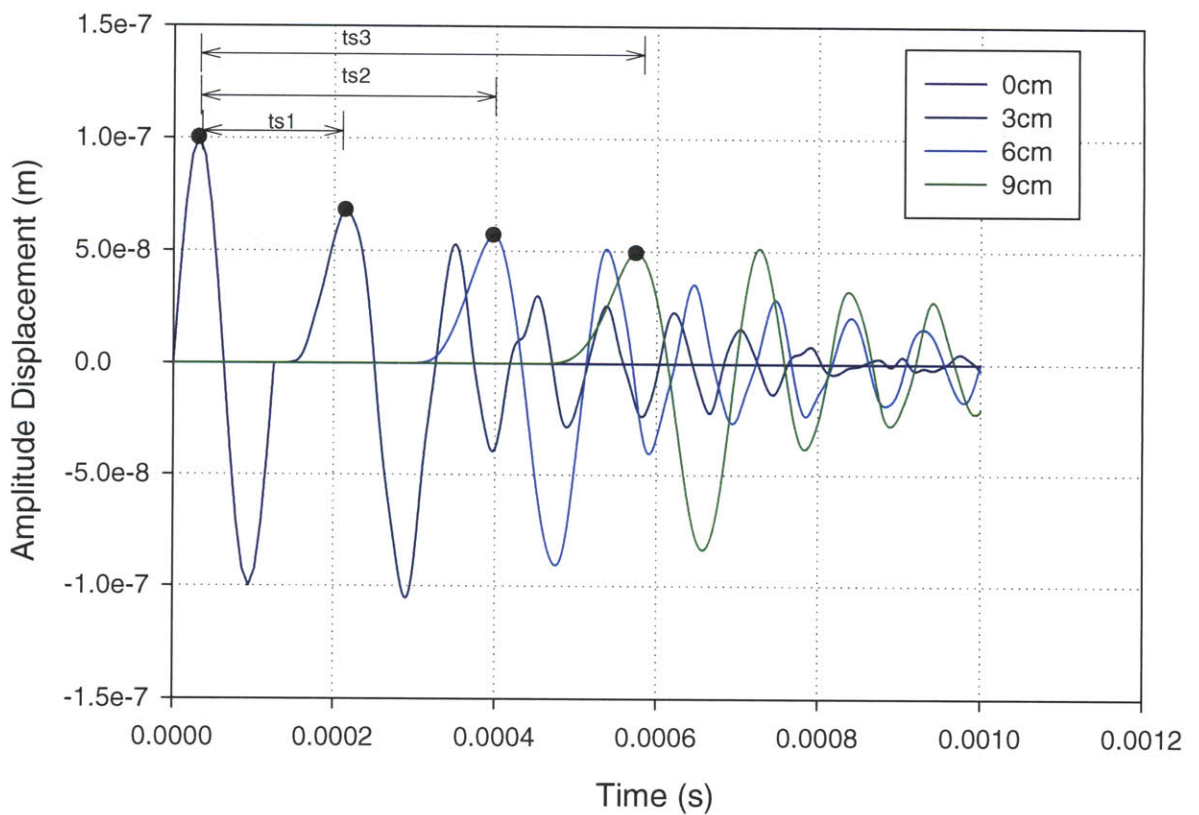
Figure 5.10: Peak to Peak Velocity Calculations

According to this Figure, the peak to peak calculation is represented as the difference between the source wave front and a receiver location at a scalar distance 'r' from the source. This calculation sets the source/receiver distance the independent variable and uses the P-Wave front velocity as the dependent variable.

$$Measured\ Velocity = \frac{dr}{ts_2 - ts_1}$$
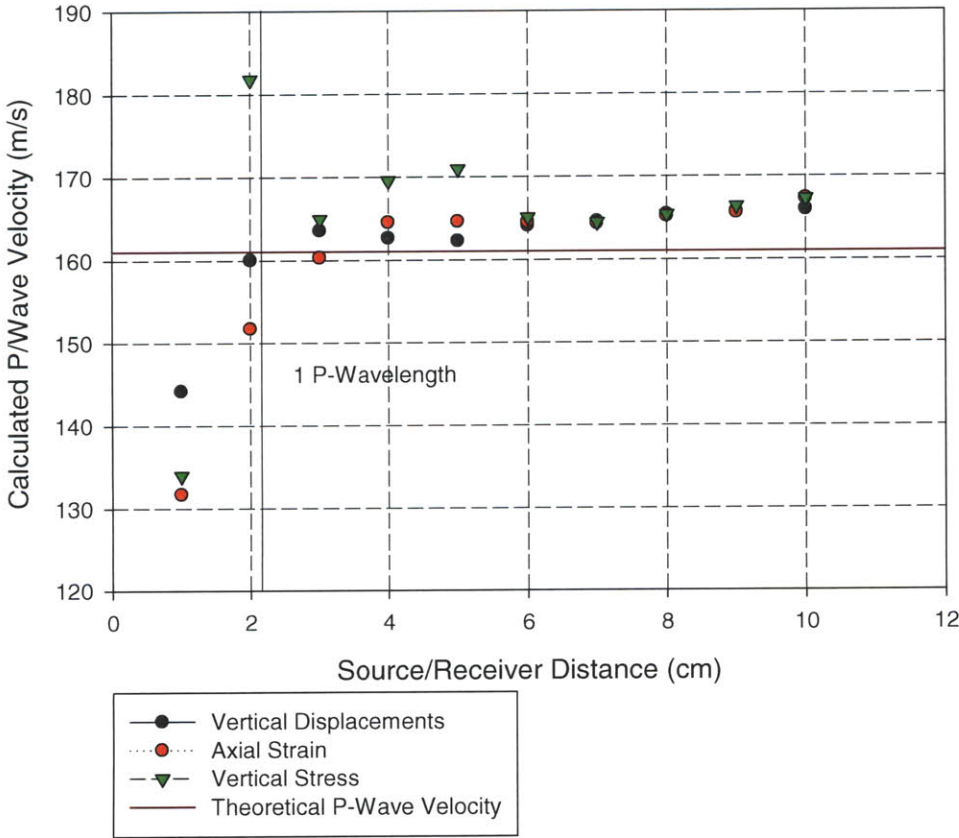
Figure 5.11: Peak to Peak Velocity Results

143

The wavelength of the P-wave is equal to the product of velocity of the P-wavefront and the period of oscillation. This calculation produces:

$$\lambda_p = 161 \frac{m}{s} * .000125s = 2.0125 \text{ cm}$$

It is evident from the velocity measurements that the source receiver peak to peak velocity becomes highly inaccurate when the distance between the source and receiver is less than one P wavelength.

5.2.10. P-Wave Model: Velocity Measurements Variable Travel Distance.

Alternatively the peak to peak calculation can be represented as the difference between two wave fronts propagating down with a source receiver distance r_1 and r_2. The distance delta used for the velocity calculation becomes $r_2 - r_1 = dr$.
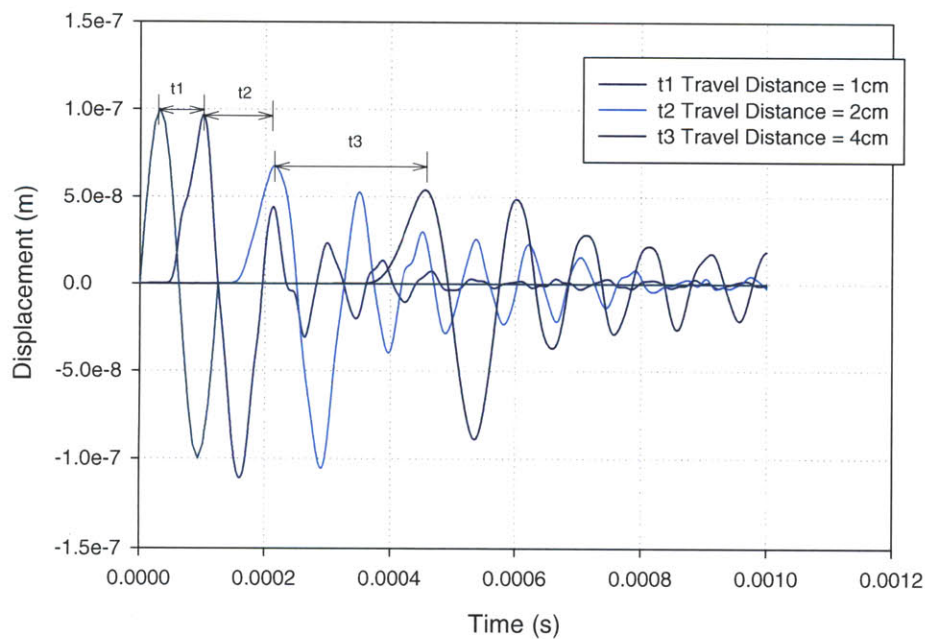
Figure 5.12: Peak to Peak Variable Time Increment Velocity Calculations

The ts time differential values are the independent variable for the velocity calculation. It is possible to compute the velocity of the P-Wave front by taking the source/receiver distance and dividing by the ts time differential.

The time incremented used varied as a function of the source receiver distance. The source receiver distance increments were: 0cm to 1cm, 1cm to 3cm, 3cm to 7cm. This procedure produces source distance increments equal to 1cm, 2cm, and 4cm.

$$Measured\ Velocity = \frac{dr}{ts_n}$$

The methodology produces the following results when computing P-Wave phase velocity.
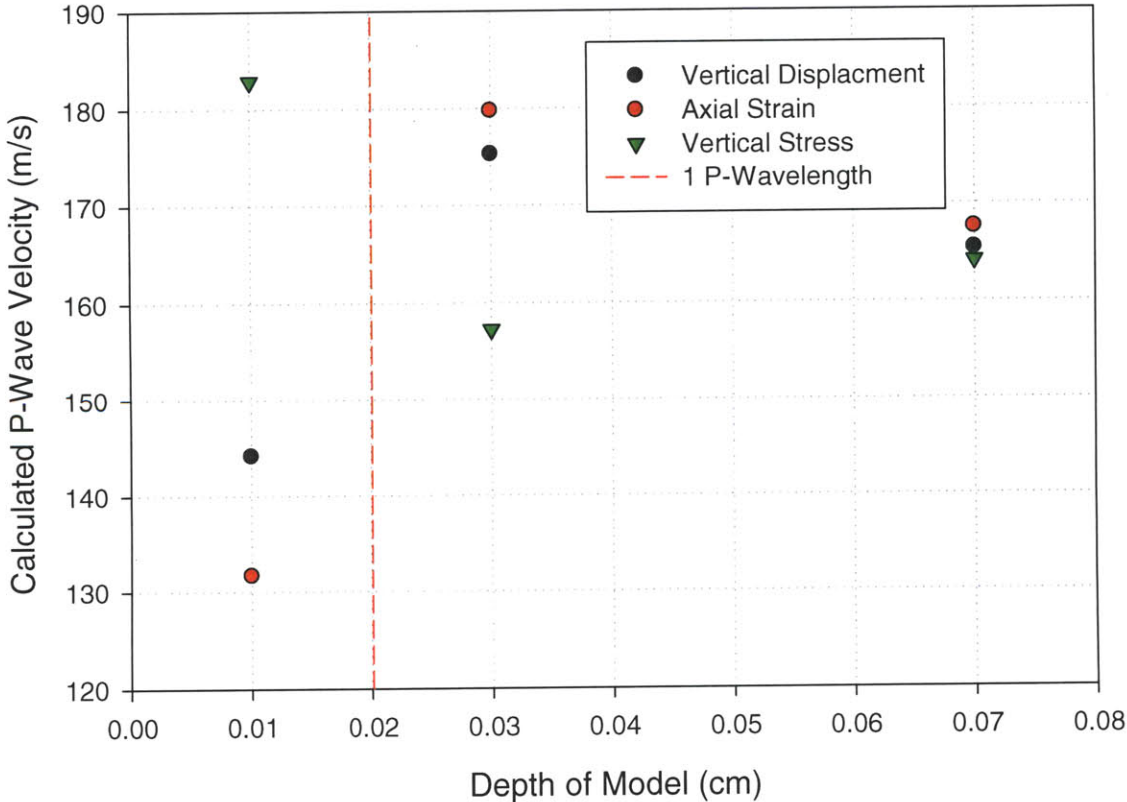
Figure 5.13: Peak to Peak Variable Time Increment Velocity Results

Similar to the Source Peak Velocity measurements, it is evident from the velocity measurements that the source receiver peak to peak velocity becomes highly inaccurate when the distance between the source and receiver is less than one P wavelength.

5.3. P-Wave Traction Model: Applied Force.

An elastic rod model was constructed in two dimensional space. An uniaxial stress field was applied using an applied force traction. Lateral motion was unrestrained. A vertical constraint was fixed to the bottom surface of the model to prevent rigid boundary motion. The displacement condition is sinusoidal harmonic motion. The parameters of the source vibration are provided in the tabled attached.

Frequency	8000 Hz (rev/sec)
Traction	.2 N

Table 5.2 Traction Parameters

Similar to the displacement model, the field output of the model captured the uniaxial stress field, displacement field, acceleration field. The axial strain was calculated from the differential vertical displacement of two nodes spaced one element distance apart.

Data was extracted from selected nodes located at the centerline of the geometry. The vertical spacing of the extraction nodes were one centimeter. Each extraction depth included two nodes for the purpose of solving the axial strain. The maximum depth of extraction was ten centimeters. Accordingly, there are eleven extraction depths at each integer beginning at 0cm and ending at 10cm inclusive.

5.3.1. P-Wave Traction Model: Displacement Field Output

The vertical displacement from the traction model of the extraction nodes is provided.
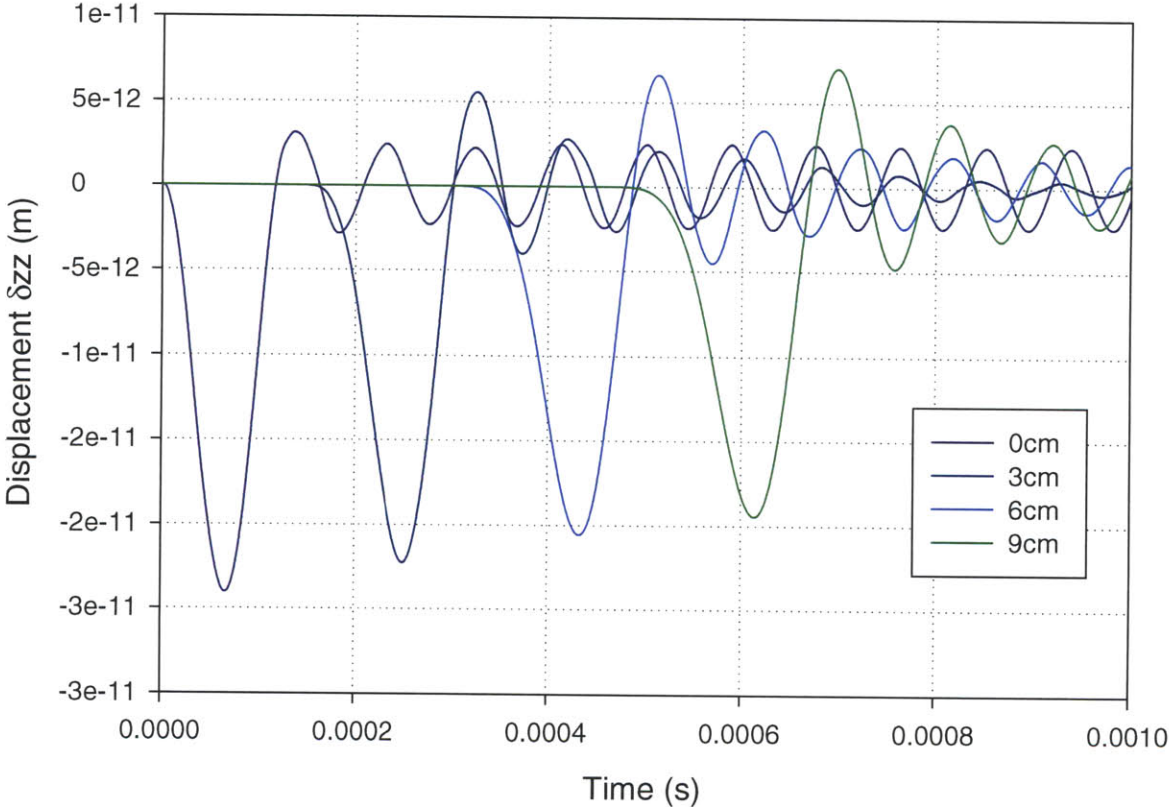
Figure 5.14: The Displacement Field

5.3.2. P-Wave Traction Model: Stress Field

The stress field of the P-Wave propagation can also be computed. This field output may be the most appropriate for computing the velocity of an applied traction model. According to the Hooke's law the stress field of an elastic solid is directly related to the strain field. The stress field is provided.
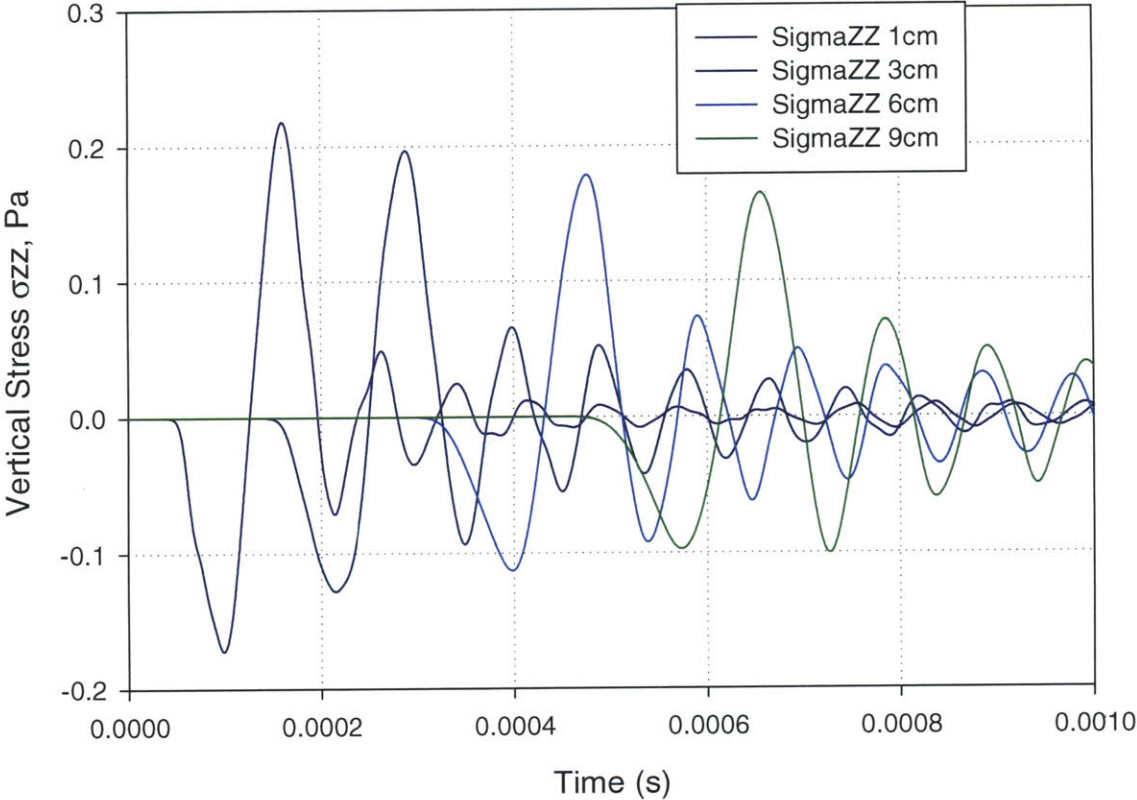
Figure 5.15: The Vertical Stress Field

5.3.4. P-Wave Traction Model: Axial Strain Field

The axial strain of the P-Wave front is equal to differential vertical displacement of two nodes spaced one element distance apart. The equation for the axial strain is equal to

$$\varepsilon_{axial} = \frac{\Delta \delta_v}{Verical\ Spacing\ between\ n_1\ n_2}$$
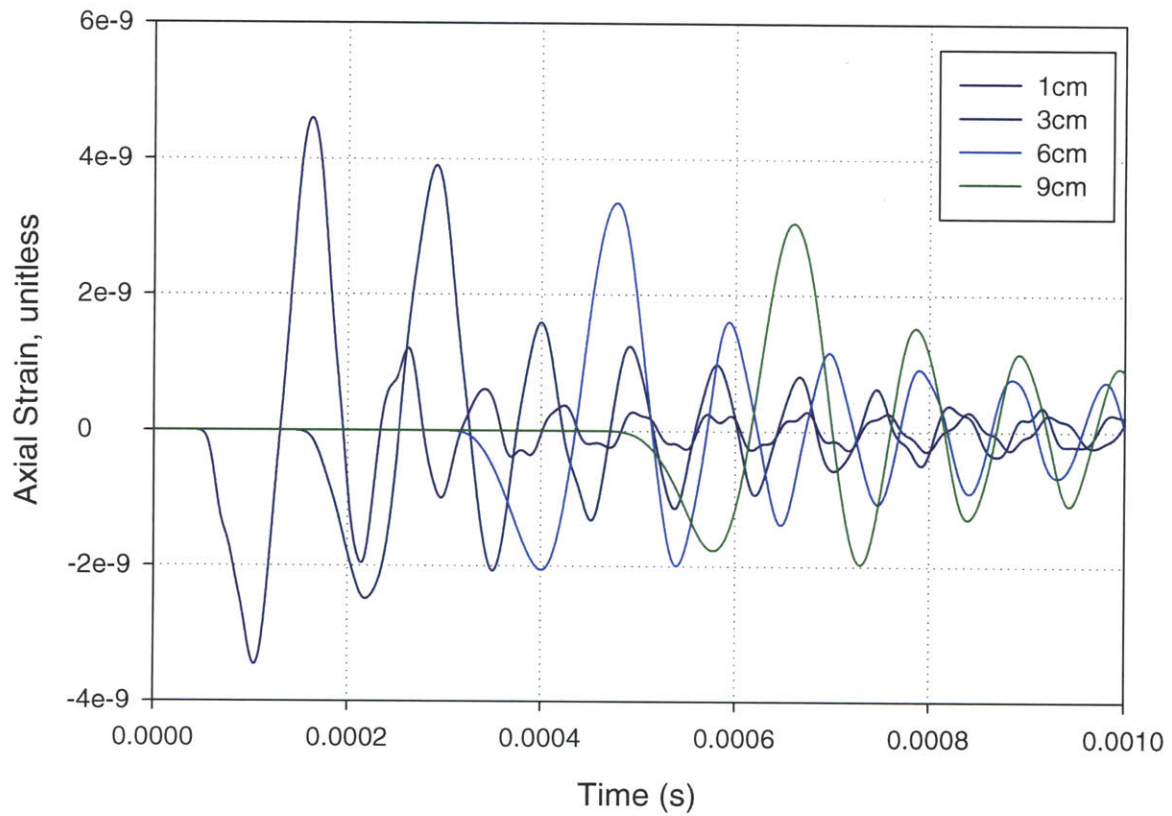
Figure 5.16: The Axial Strain Field

5.3.5. P-Wave Traction Model: Attenuation of the Stress Field

The amplitude of the arrival signal decays as the distance between the source and the arrival signal increases. The maximum amplitude of the P-Wave front is equal to its is maximum positive peak or its phase equal to $\frac{\pi}{2}$ of the sinusoidal harmonic motion. The gradual reduction in amplitude as a function of source and receiver distance is provided.
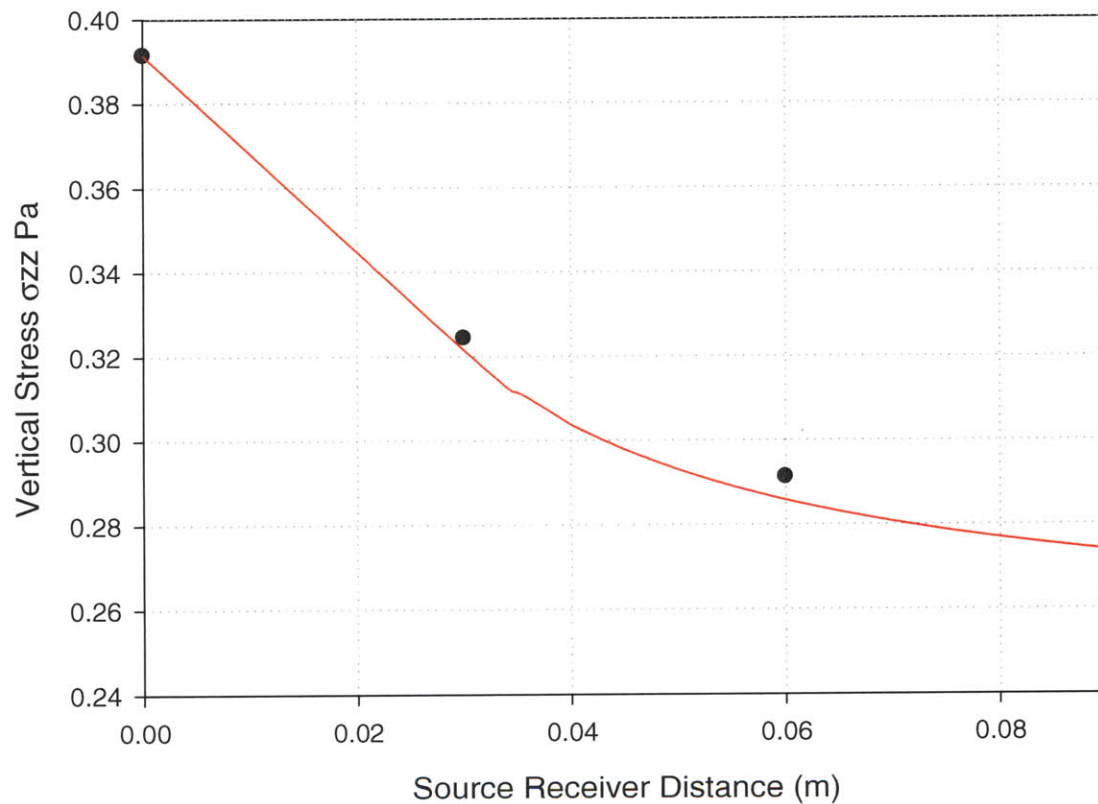
Figure 5.17: Regression of the Attenuation of the Displacement Field

Regression analysis was done on the attenuation of the stress field. The graph shows four arrivals at variable different source/receiver distances in multiples of three centimeters. Each arrival has an associated amplitude and arrival time. The interpolation function is a first order inverse polynomial equation. The reduction of the amplitude of the displacement field can be expressed as a inverted polynomial function where the numerical constants determined through regression analysis.

Accordingly, the regression fit of the interpolation has the following values.

$$Amp(r), Pa = 2.5 * 10^{-1} + \frac{2.15 * 10^{-3}}{r}, \qquad r > 3m$$

$$Amp(r), Pa = ,392 - 2.33(r), \qquad r < 3m$$

5.2.6. P-Wave Traction Model: Frequency

The period of the arrival signal changes as the source/distance increases. The arrival frequency of the source signal is calculated by solving the reciprocal of the observed period. The observed period is a variable quantity with respect to the source receiver distance.

Frequency: PWave Stress Field
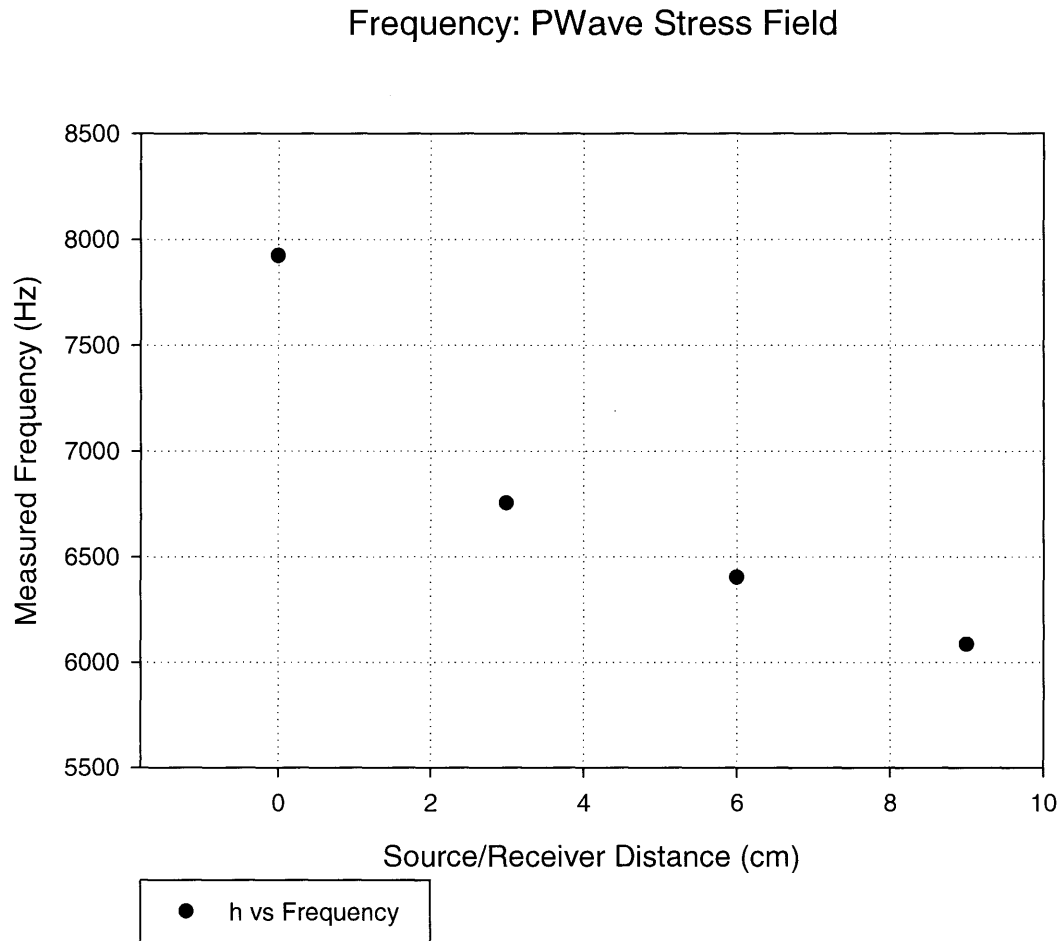
Figure 5.18: Frequency of the Displacement Field

It is observable that the frequency of the displacement field remains varies with respect to depth. The waveform in a free elastic rod model does not exhibits planar behavior.

5.3.7. P-Wave Traction Model: Velocity Measurements

Velocity measurements using peak to peak method are attached for the displacement, stress state, acceleration, and axial strain field output. A theoretical shear wave velocity was specified in the input analysis. The theoretical P-wave velocity is $161\ \frac{m}{s}$ Velocity measurements are provided.

5.3.7.1. P-Wave Traction Model: Theoretical Velocity

The polarization of the P-wave is identical in both the elastic rod traction model and the infinite boundary model. The P-wave front velocity of the elastic rod model and the infinite boundary model is not equivalent.

A infinite boundary model the P-Wave velocity is expressed:

$$V_p = \sqrt{\frac{E}{\rho_m}} = \sqrt{\frac{52*10^6 Pa}{2000\frac{kg}{m^3}}} = 161\ \frac{m}{s}$$

This equation is applicable in elastic rods subject to P-wave agitation in an uniaxial stress state. The Young's modulus is the appropriate modulus in the P-wave velocity subject to an uniaxial and uniform stress state and the rod is allowed to deform laterally. If the conditions are met then the operative elastic constant is E.

5.4.8. P-Wave Traction Model: Velocity Measurements Source Receiver Distance

The travel time of a sinusoidal wave is taken as the time between the two characteristic points of the source and receiver wave front. The source wave front remained constant at the source location, 0cm. Time differentials were measured as the difference of the pulse time recorded at the receiver node receiver and the source.
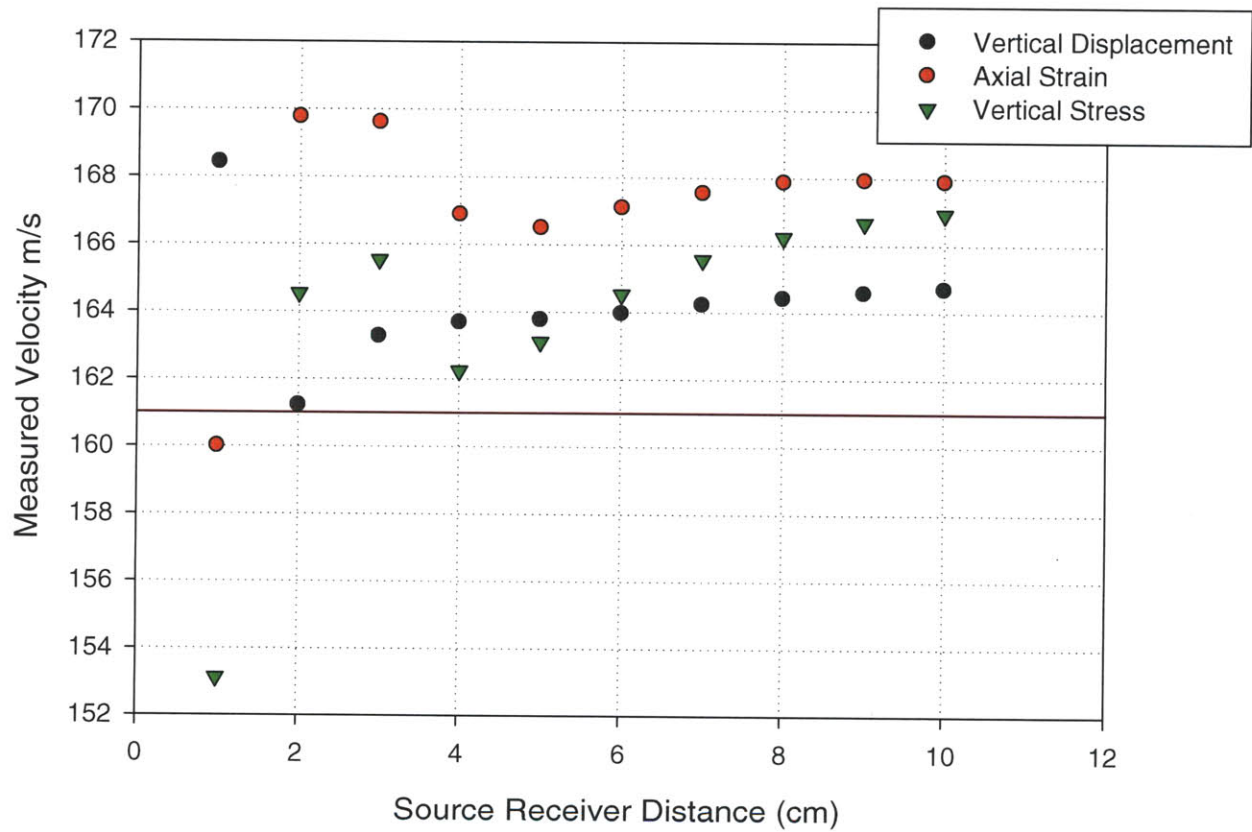
Figure 5.19: Peak to Peak Velocity Results

It is evident from the velocity measurements that the source receiver peak to peak velocity becomes highly inaccurate when the distance between the source and receiver is less than one P wavelength.

5.3.9. P-Wave Traction Model: Velocity Measurements Depth of Model

Similar to the displacement field model, the peak to peak calculation can be represented as the difference between two wave fronts propagating down with a source receiver distance r_1 and r_2. The distance delta used for the velocity calculation becomes $r_2 - r_1 = dr$. The velocity calculation becomes

$$Measured\ Velocity = \frac{dr}{ts_n}.$$

The time incremented used varied as a function of the source receiver distance. The source receiver distance increments were: 0cm to 1cm, 1cm to 3cm, 3cm to 7cm. This procedure produces source distance increments equal to 1cm, 2cm, and 4cm.
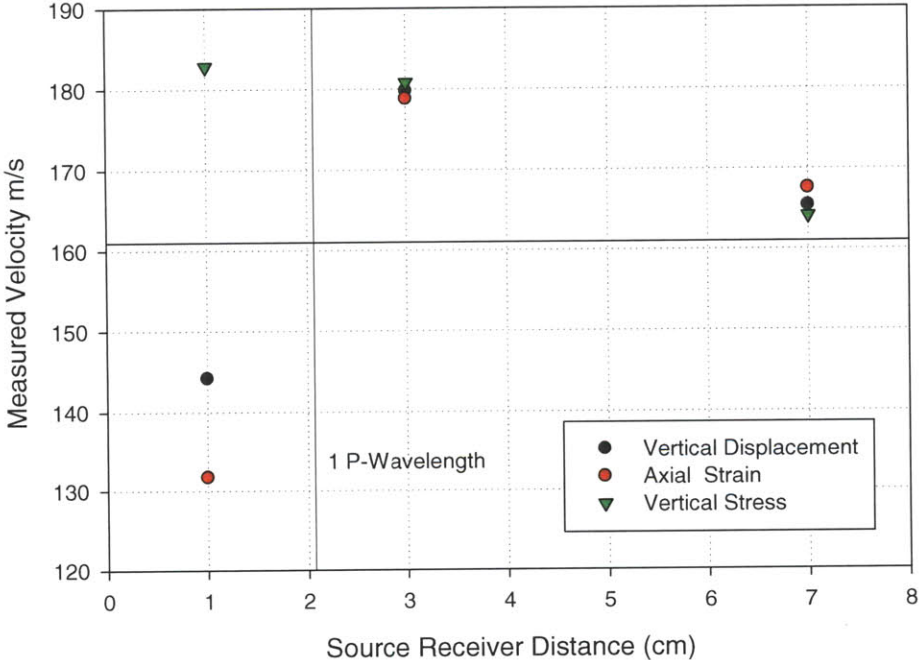
Figure 5.20: Peak to Peak Variable Time Increment Velocity Results

Similar to the Source Peak Velocity measurements, it is evident from the velocity measurements that the source receiver peak to peak velocity becomes highly inaccurate when the distance between the source and receiver is less than one P wavelength.

5.4. P-Wave Infinite Boundary Model: Displacement Point Source

An elastic rod model was constructed in two dimensional space. An uniaxial point displacement was applied using a prescribed displacement over an emission node. Lateral motion was unrestrained. Dampers were applied over the lateral surfaces to simulate an infinite boundary. A vertical constraint was fixed to the bottom surface of the model to prevent rigid boundary motion. A diagram of the model is provided in Figure 5.52.

The displacement condition is sinusoidal harmonic motion. The parameters of the source vibration are provided in the tabled attached.

Frequency	8000 Hz (rev/sec)
Maximum Nodal Displacement	1E-7 m

Table 5.3 Displacement Parameters of Source

The field output down the center of the mode captured the uniaxial stress field, displacement field, acceleration field. The axial strain was calculated from the differential vertical displacement of two nodes spaced one element distance apart.

Data were extracted from selected nodes located at the centerline of the geometry. The vertical spacing of the extraction nodes were one centimeter. Each extraction depth included two nodes for the purpose of solving the axial strain. The maximum depth of extraction was ten centimeters. Accordingly, there are eleven extraction depths at each integer beginning at 0cm and ending at 10cm inclusive.

5.4.1. P-Wave Infinite Boundary Model: Displacement Point Source

The vertical displacement from the displacement model of the extraction nodes is provided.
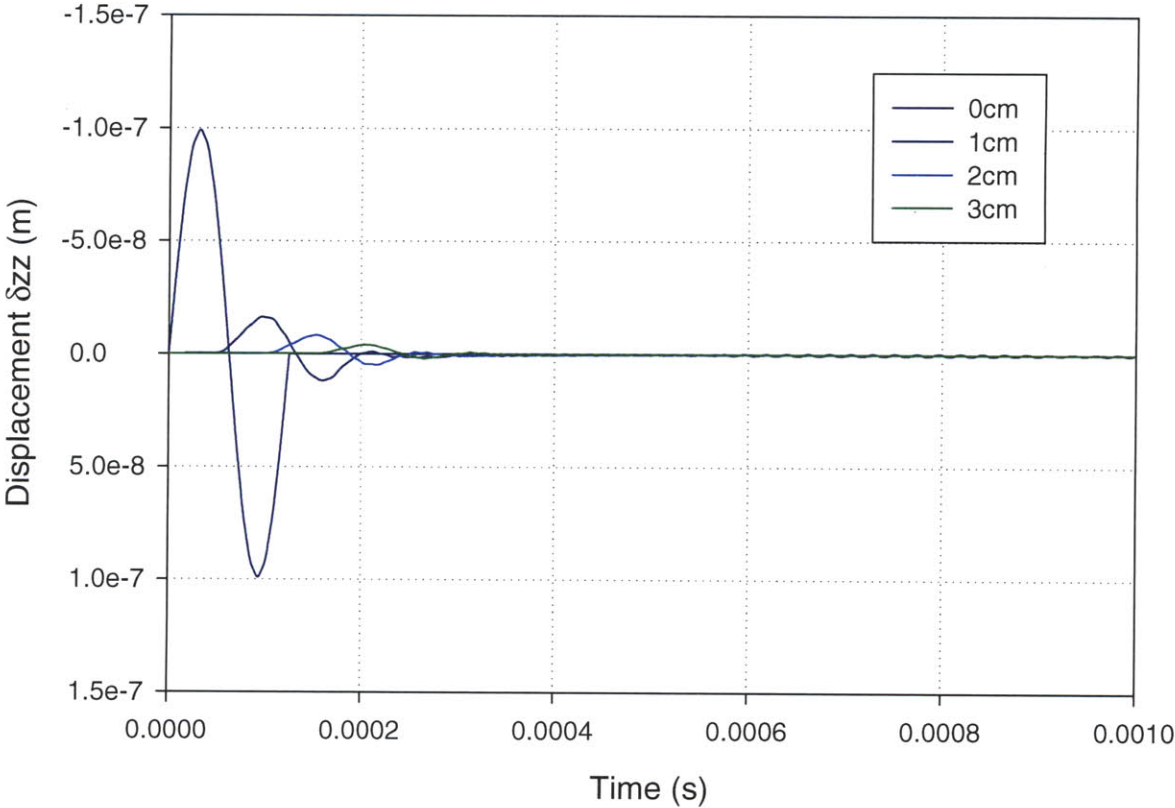
Figure 5.21: The Displacement Field

5.4.2. P-Wave Infinite Boundary Model: Stress Field

The stress field of the P-Wave propagation can also be computed. According to the Hooke's law the stress field of an elastic solid is directly related to the strain field. The stress field is provided.
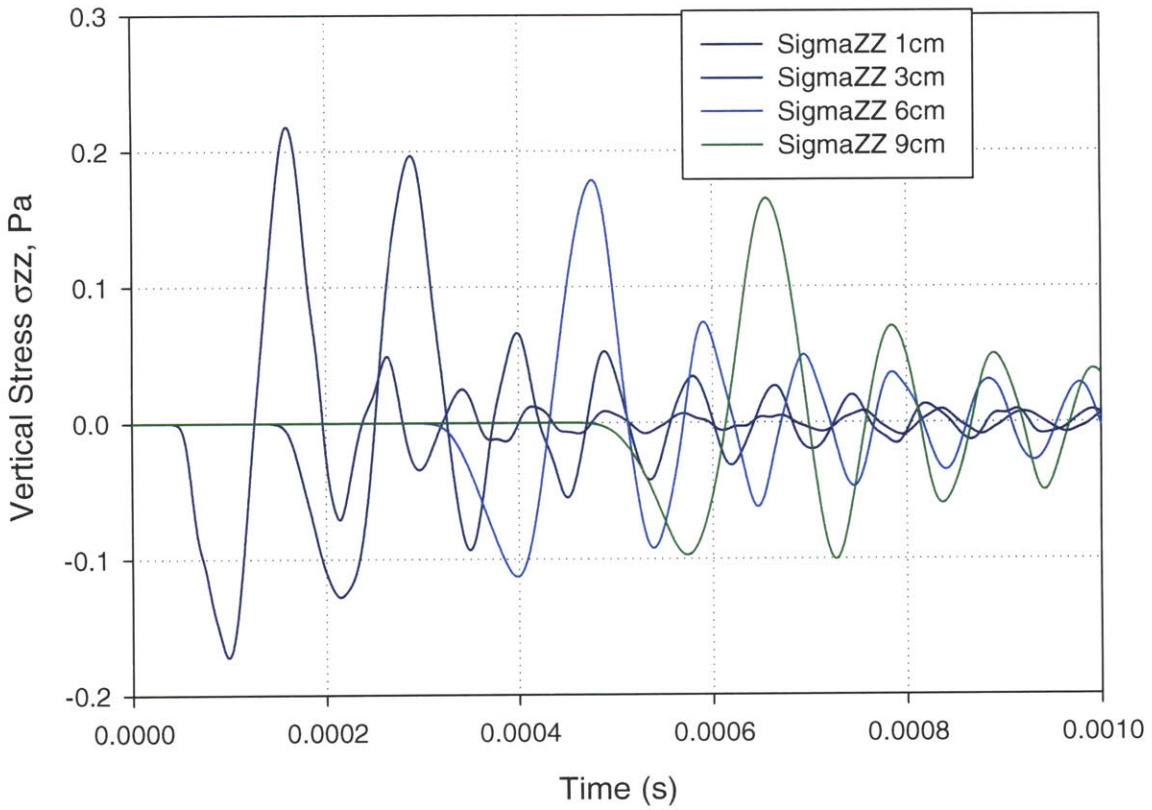
Figure 5.22: The Vertical Stress Field

5.4.4. P-Wave Infinite Boundary Model: Axial Strain Field

The axial strain of the P-Wave front is equal to the differential vertical displacement of two nodes spaced one element distance apart. The equation for the axial strain is equal to

$$\varepsilon_{axial} = \frac{\Delta\delta_v}{Verical\ Spacing\ between\ n_1\ n_2}$$
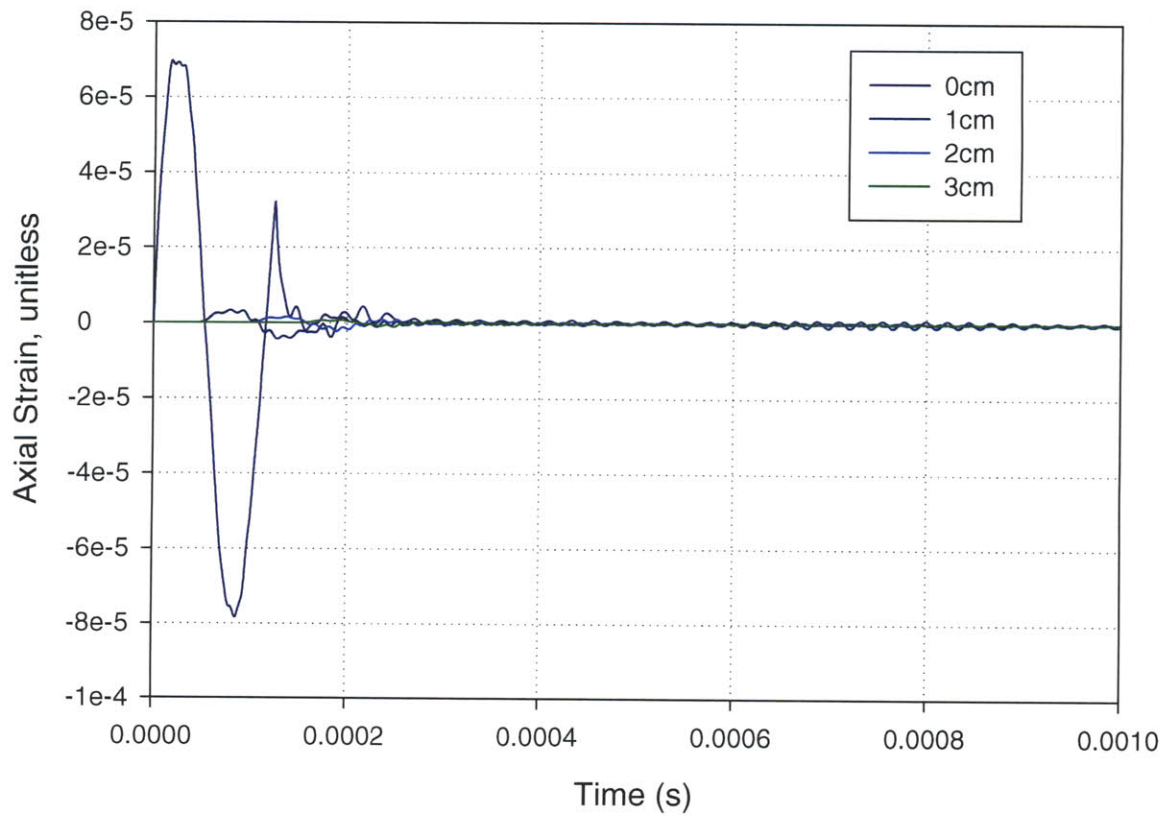
Figure 5.23: The Axial Strain Field

5.4.5. P-Wave Infinite Boundary: Attenuation of the Displacement Field

The amplitude of the arrival signal decays as the distance between the source and the arrival signal increases. The maximum amplitude of the wave front is equal to its maximum positive peak or its phase equal to $\frac{\pi}{2}$ of the sinusoidal harmonic motion. The gradual reduction in amplitude as a function of source and receiver distance is provided.

According to planar wave propagation the positive and negative amplitudes are symmetric. Therefore, it is acceptable to use the positive amplitude at phase $\frac{\pi}{2}$ as the scalar for attenuation analysis rather than taking the difference of the positive and negative amplitudes, as was done with the previous free boundary models examined.
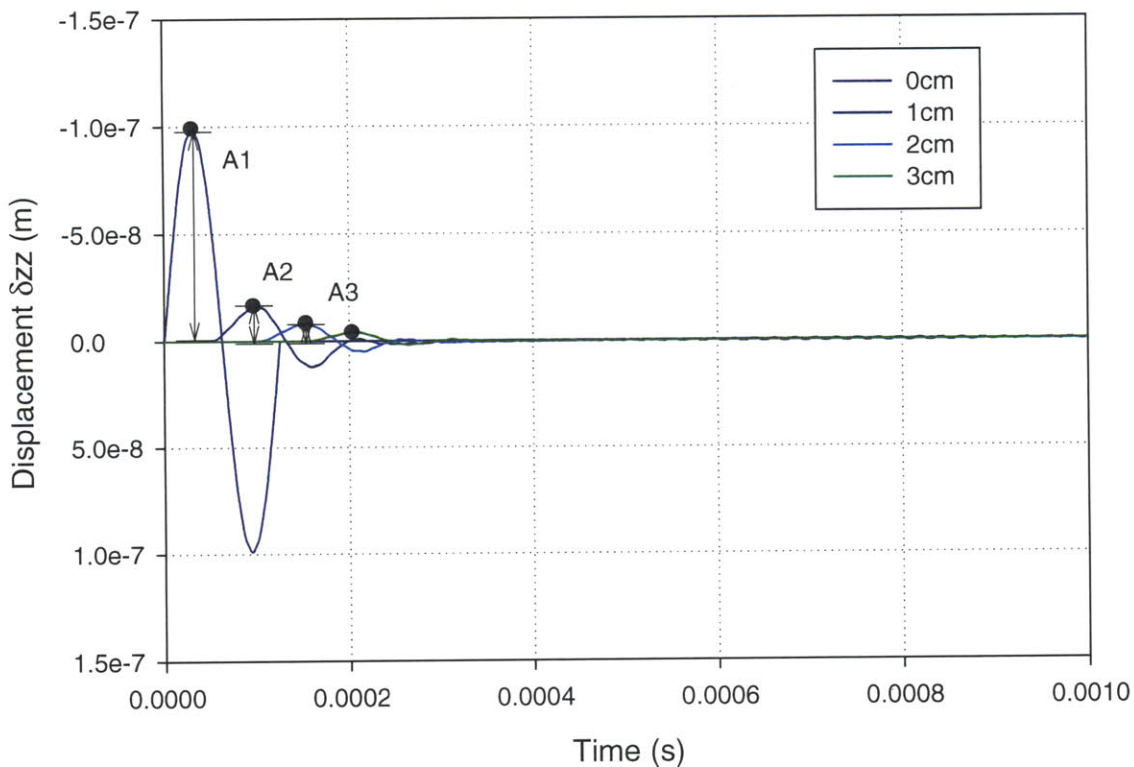
Figure 5.24: Attenuation of the Displacement Field

162
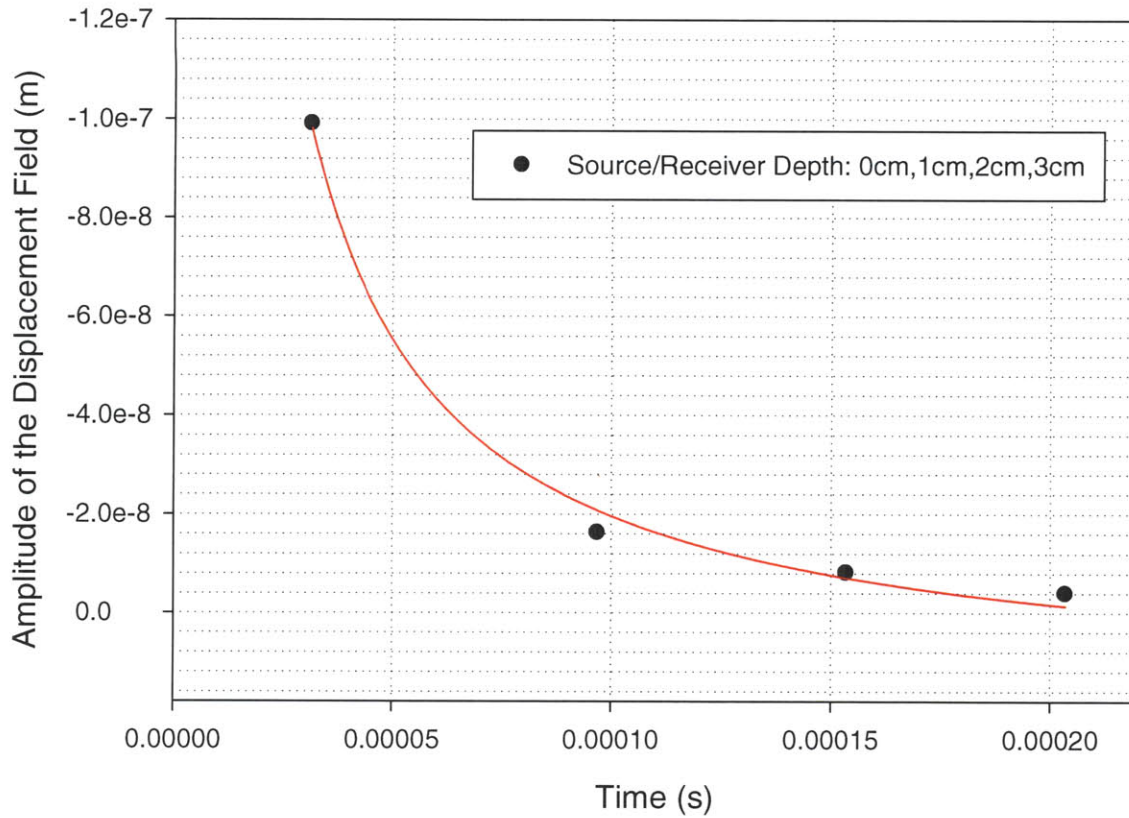
Figure 5.25: Regression of the Attenuation of the Displacement Field

The points superimposed on the displacement field output represent the amplitude scalars for each P-wave front corresponding to its unique distance between the source and receiver. Regression analysis was done using the four amplitude scalars representing the maximum positive nodal vertical displacement.

Similar to the finite rod displacement model, the reduction of the amplitude in the infinite rod model conforms to the observed reduction in amplitude for waves generated by a surface footing. In the case of a surface footing, the decrease in displacement amplitude is proportional to $1/r$.

$$Amplitude \propto \frac{1}{r}$$

The radius of propagation of the wavefront and the wavefront travel time are related:

$$Travel\ Time = \frac{Radius\ of\ Wavefront}{Wavefront\ Velocity}$$

Regression of the amplitude decay can be done by fitting a first order inverse polynomial function to the data set. Geometric Damping will occur in an infinite boundless space such that the wave propagation is hemispherical.

Regression analysis was done on the attenuation of the displacement. The graph shows four arrivals at variable different source/receiver distances in multiples of three centimeters. Each arrival has an associated displacement amplitude and arrival time. The interpolation function is a first order inverse polynomial equation taking the form. In this equation time is the domain. For the damped infinite boundary model this equation is provided.

$$Amp(t) = 1.62 * 10^{-8} + \frac{3.576 * 10^{-12}}{t}, for\ 0 < r < \infty$$

5.2.6. P-Wave Infinite Boundary Model: Frequency

The period of the arrival signal changes as the source/distance increases. The arrival frequency of the source signal is calculated by solving the reciprocal of the observed period in displacement space. The observed period is a variable quantity with respect to the source receiver distance.
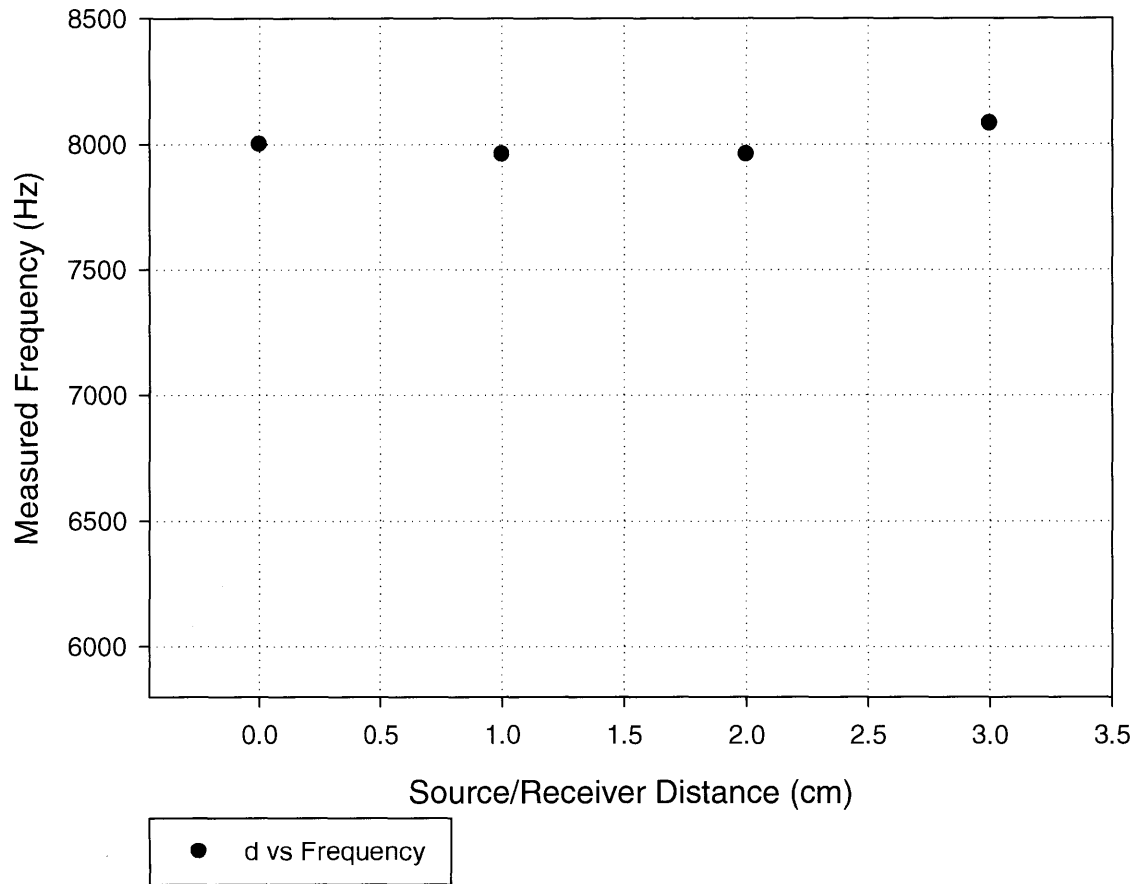
Figure 5.26: Frequency of the Displacement Field

It is observable that the frequency of the displacement field remains constant. Variations of the travel time and the radial distance between the source and receiver do not alter the arrival frequency of the displacement harmonic. The waveform in an infinite boundary exhibits planar behavior.

5.2.7. P-Wave Infinite Boundary Model: Attenuation of the Axial Strain

The amplitude of the arrival signal decays as the distance between the source and the arrival signal increases. The maximum amplitude of the wave front is equal to its maximum positive peak or its phase equal to $\frac{\pi}{2}$ of the sinusoidal harmonic motion. The gradual reduction in amplitude as a function of source and receiver distance is provided.
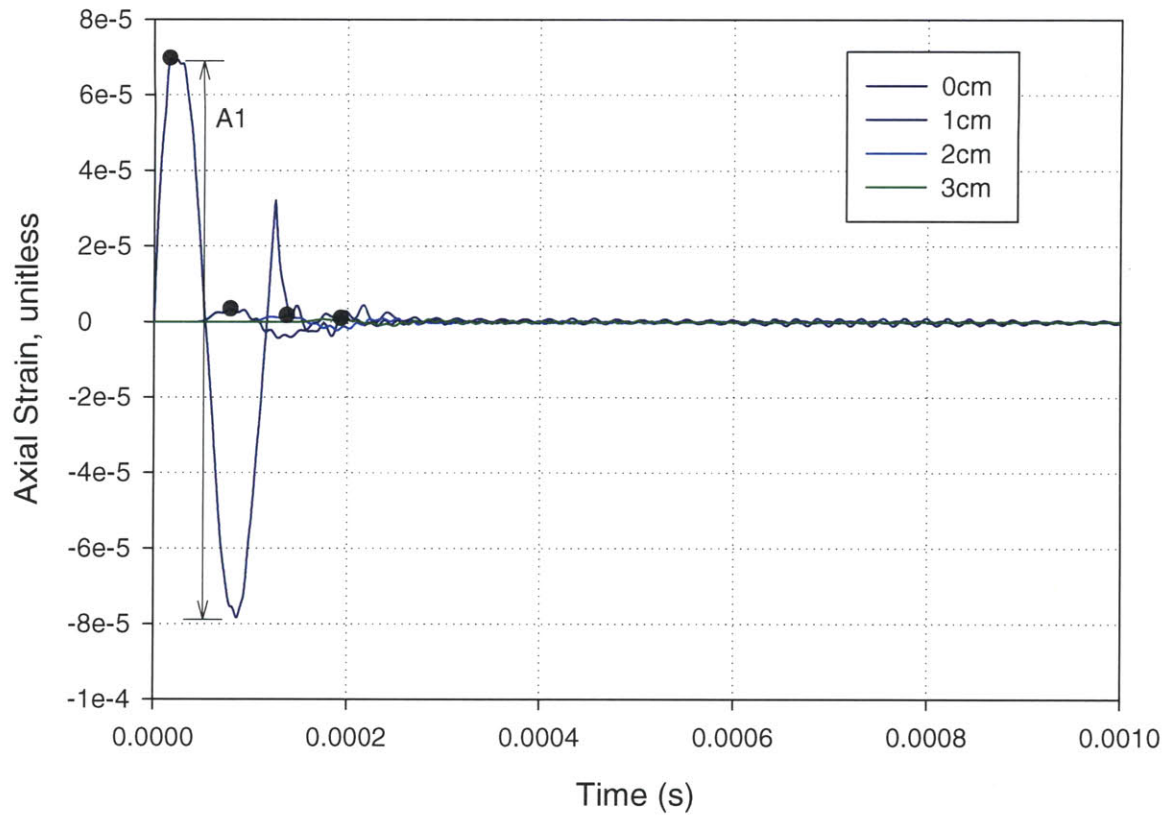
Figure 5.27: Attenuation of the Strain Field
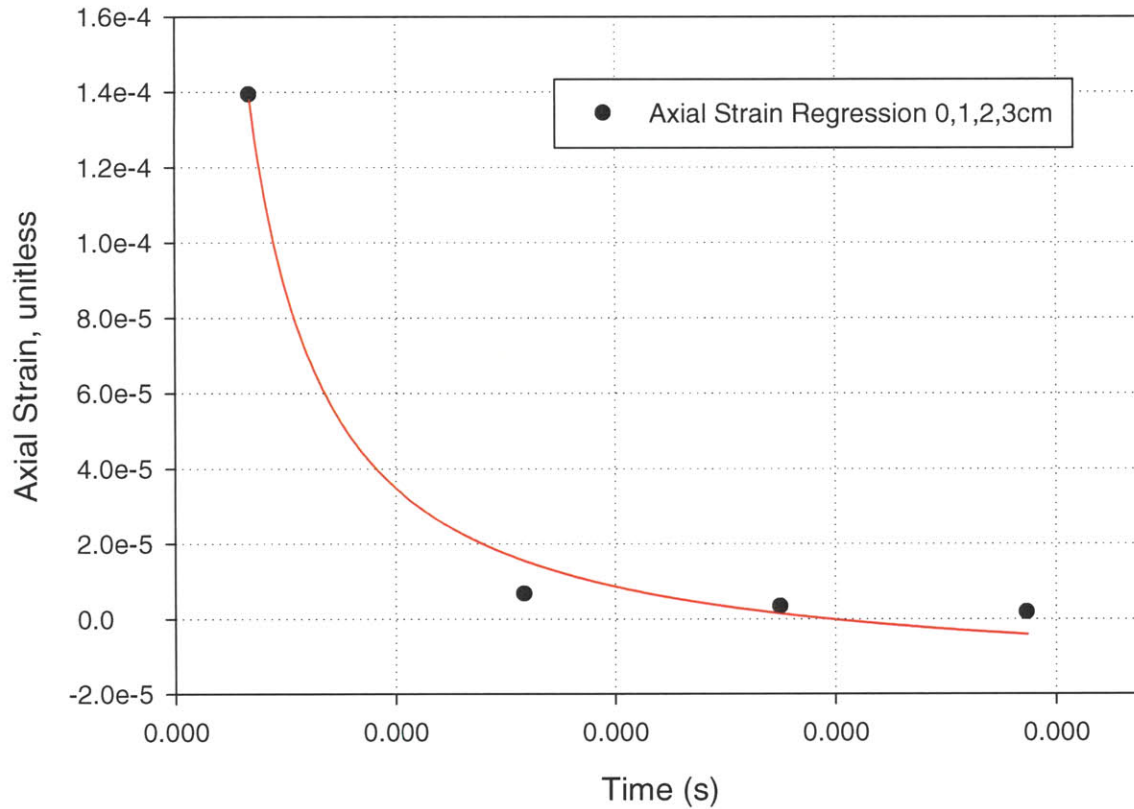
Figure 5.28: Regression of the Attenuation of the Strain Field

Regression analysis was done on the attenuation of the displacement. The graph shows four arrivals at variable different source/receiver distances in multiples of three centimeters. Each arrival has an associated displacement amplitude and arrival time. The interpolation function is a first order inverse polynomial equation taking the form. For the damped infinite boundary model this equation translates.

$$Amp(t), m = -1.77 * 10^{-5} + \frac{-2.63 * 10^{-9}}{t}$$

5.4.8. P-Wave Infinite Boundary Model: Velocity Measurements

Velocity measurements using peak to peak method are attached for the displacement, stress state, acceleration, and axial strain field output. A theoretical shear wave velocity was specified in the input analysis. The theoretical P-wave velocity is $187\,\frac{m}{s}$ Velocity measurements of the P-wavefront are provided.

5.4.8.1. P-Wave Infinite Boundary Model: Theoretical Velocity

The polarization of the P-wave is identical in both the elastic rod traction model and the infinite boundary model. The direction of propagation is radial and the polarization of the displacement, stress, and strain fields are radial.

The P-wavefront velocity of the elastic rod model and the infinite boundary model are not equivalent. In a bound space such that lateral deformations are possible the operative elastic constant is the Young's modulus. If the elastic medium is unbounded or infinite then the Bulk modulus is applicable.

A infinite boundary model the P-wave velocity is expressed:

$$V_p = \sqrt{\frac{\lambda + 2G}{\rho_m}} = \sqrt{\frac{E_b}{\rho_m}} = \sqrt{\frac{E(1-\eta)}{\rho_m(1+\eta)(1-2\eta)}}$$

$$V_p = \sqrt{\frac{52 * 10^6 Pa * (1 - .3)}{2000\frac{kg}{m^3} * (1 + .3)(1 - 2 * .3)}} = 187\,\frac{m}{s}$$

This equation is applicable in models such that the lateral motion equals zero at the lateral boundaries. Under this assumption the operative elastic constant becomes $(\lambda + 2G)$ or the Bulk Modulus.

5.4.9. P-Wave Infinite Boundary Model: Velocity Measurements Source Receiver Distance

The travel time of a sinusoidal wave is taken as the time between the two characteristic points of the source and receiver wave front. The location of the source wave front remained constant at the source: 0cm. Time differentials were measured as the difference of the pulse time recorded at the receiver node receiver and the source.
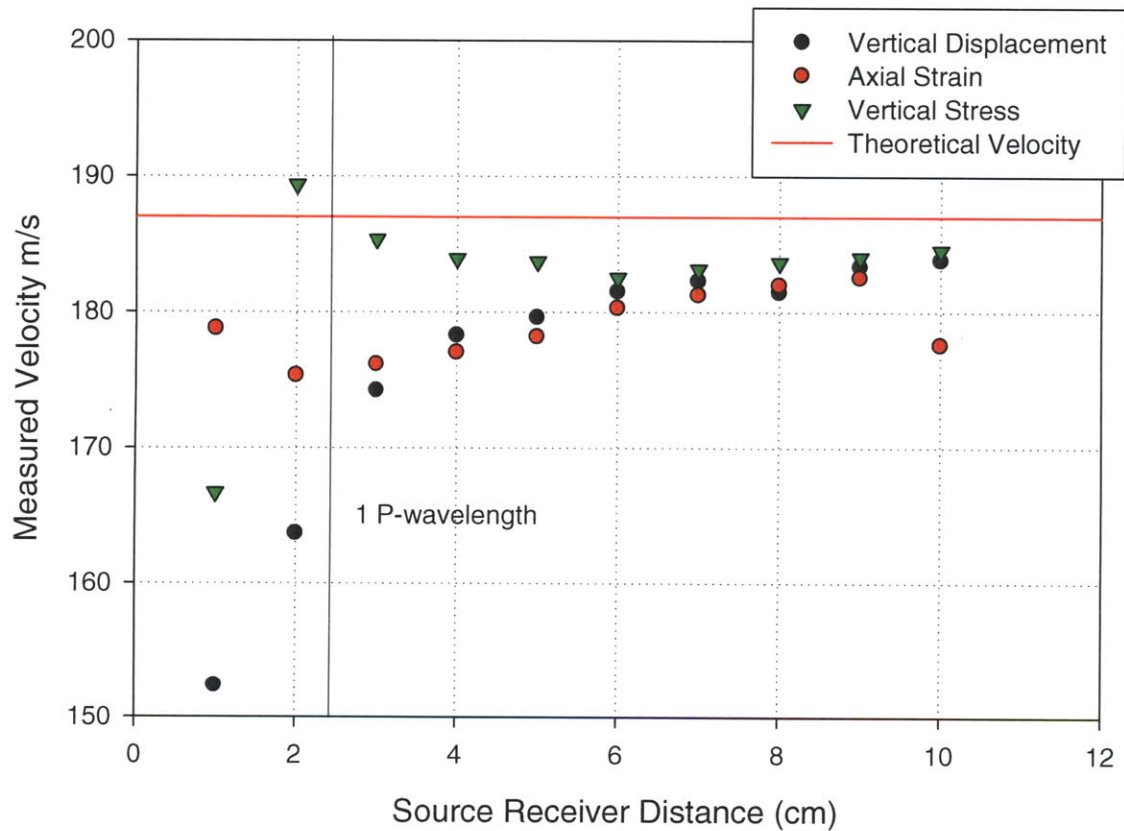
Figure 5.29: Peak to Peak Velocity Results

The wavelength of the P-wave in an infinite half space is equal to the product of velocity of the P-wavefront and the period of oscillation. This calculation produces:

$$\lambda_p = 187\frac{m}{s} * .000125s = 2.23 \text{ cm}$$

It is evident from the velocity measurements that the source receiver peak to peak velocity becomes highly inaccurate when the distance between the source and receiver is less than one P wavelength. After two P-wavelengths between the source and receiver the error becomes asymptotic.

5.4.10. P-Wave Infinite Boundary Model: Velocity Measurements Depth of Model

Alternatively the peak to peak calculation can be represented as the difference between two wave fronts propagating down with a source receiver distance r_1 and r_2 . The distance delta used for the velocity calculation becomes $r_2 - r_1 = dr$. The velocity calculation becomes

$$Measured\ Velocity = \frac{dr}{ts_n}.$$

The velocity of the P-wave front is the dependant variable in this calculation.

Velocity Measurements Peak to Peak
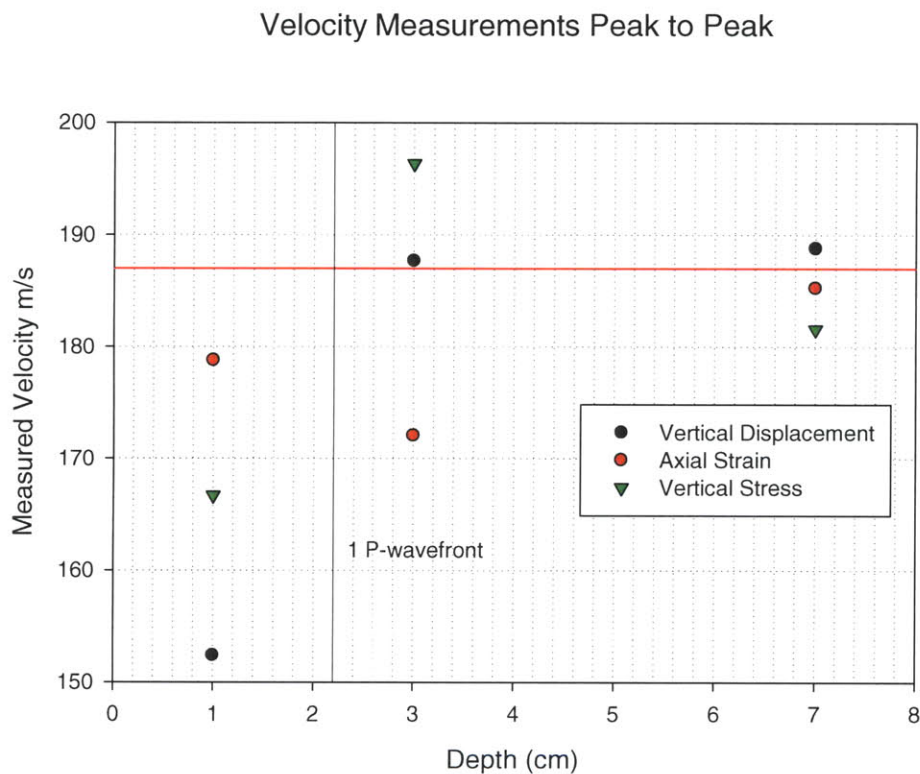
Figure 5.30: Peak to Peak Variable Time Increment Velocity Results

Similar to the Source Peak Velocity measurements, it is evident from the velocity measurements that the source receiver peak to peak velocity becomes highly inaccurate when the distance between the source and receiver is less than one P-wavelength. After two P-wavelengths between the source and receiver the error becomes asymptotic.

5.5. S-wave Damped Boundary Model

An elastic rod model was constructed in two dimensional space with al lateral point displacement applied on the centerline of the top surface. Dampers were applied to the sides of the model to prevent body wave reflections. Vertical and lateral constraint were fixed to the bottom corners of the model to prevent rigid boundary motion. These constraints were modeled as pins.

The displacement condition is sinusoidal harmonic motion. The displacement boundary condition oscillates one harmonic period and reaches equilibrium. At equilibrium no vertical displacement is possible. The parameters of the source vibration are provided in the tabled attached.

Frequency	8000 Hz (rev/sec)
Maximum Displacement	270 micrometers

Table 5.4 Lateral Displacement Parameters of Source

The field output of the model captured the lateral displacement field, and shear strain field. The shear strain was calculated from the differential lateral displacement of two nodes spaced .25mm apart. Shear strain is a more suitable strain measurement for the propagation of the shear wave because a shear wave polarization is orthogonal to its propagation.

Data were extracted from selected nodes located along the centerline of the geometry. The vertical spacing of the extraction nodes were one centimeter. Each extraction depth included two vertically adjacent nodes for the purpose of measuring the shear strain. The nodes were spaced one element length apart. The element length or the vertical spacing of the node is equal to the shear wave length divided by twenty.

The geometry of the rod is sufficiently large to prevent reflections occurring from the bottom boundary. At the source of the harmonic waveform there will be no after effects coming from the bottom boundary.

The maximum depth of extraction was ten centimeters. Accordingly, there are eleven extraction depths at each integer beginning at 0cm and ending at 10cm inclusive.

174

5.5.1. S-wave Infinite Boundary Model: Displacement Field

The lateral displacement of a node is the scalar quantity of dislocation with respect to the vertical axis. In a two dimensional modal the vertical axis is represented by the subscript 'x' in the 'x' axis. The lateral displacement of the node was captured with respect to time. The resolution of the time step was fixed at 312.5 nanoseconds, enough to capture fine perturbations of the S-wave front propagation. Accordingly, there are 3200 independent data points in the field output containing data from each time step. The vertical displacement from the displacement model of the extraction nodes is provided.
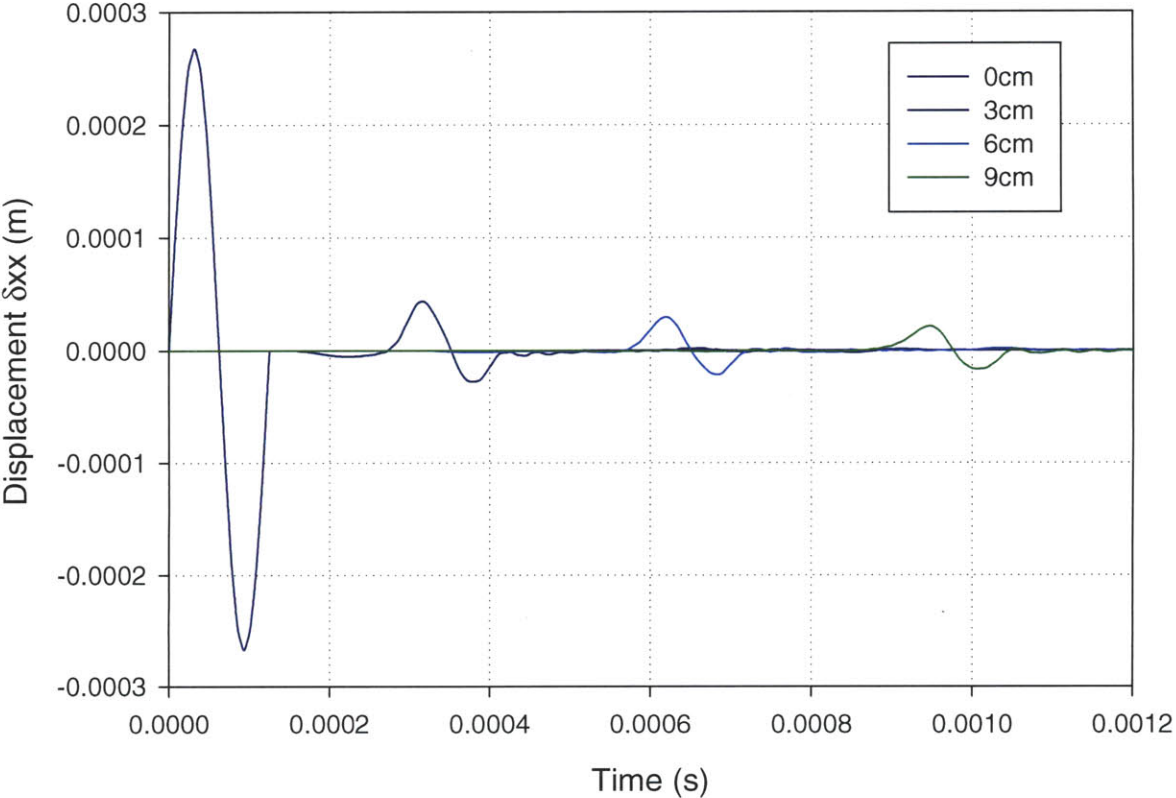
Figure 5.31: The Displacement Field

5.5.2. S-wave Infinite Boundary: Attenuation of the Displacement Field

Regression analysis was done on the attenuation of the stress field. The graph shows four arrivals at variable different source/receiver distances in multiples of three centimeters. Each arrival has an associated amplitude and arrival time. The interpolation function is a first order inverse polynomial equation. Accordingly, the statistical fit of the interpolation has the following values.
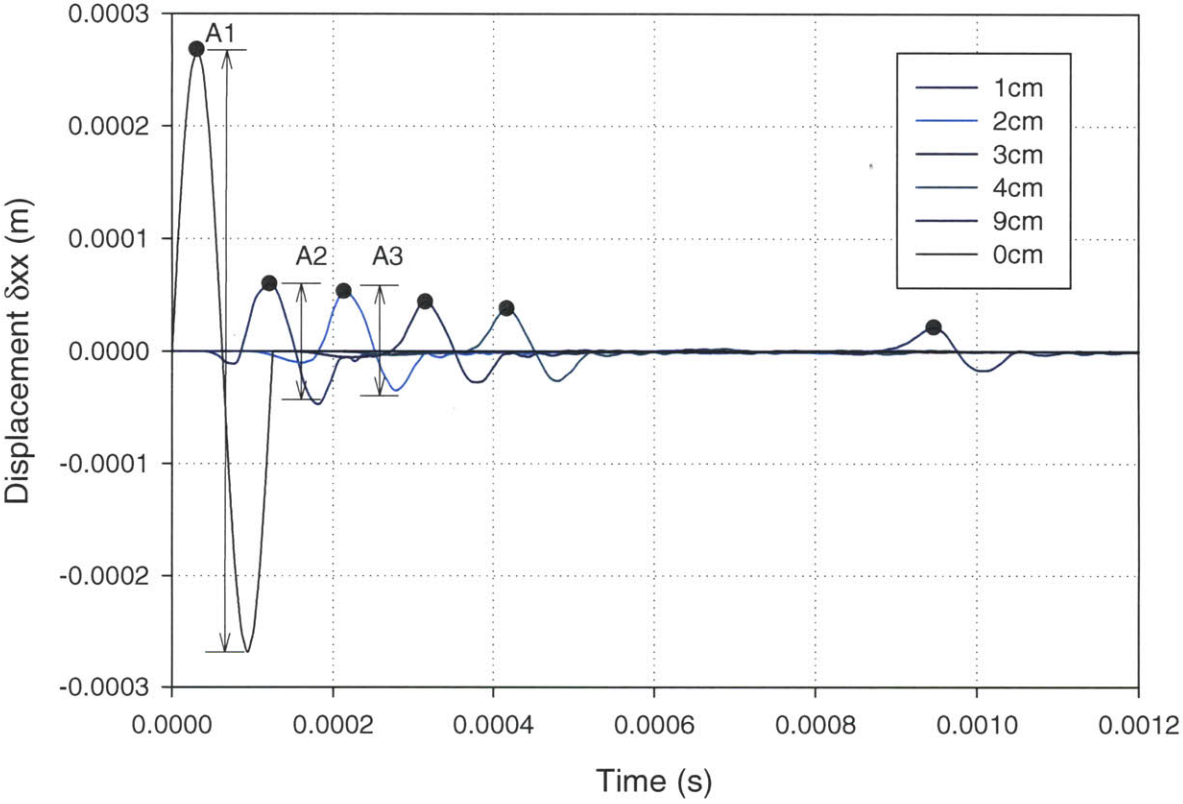
Figure 5.32: Attenuation of the Displacement Field
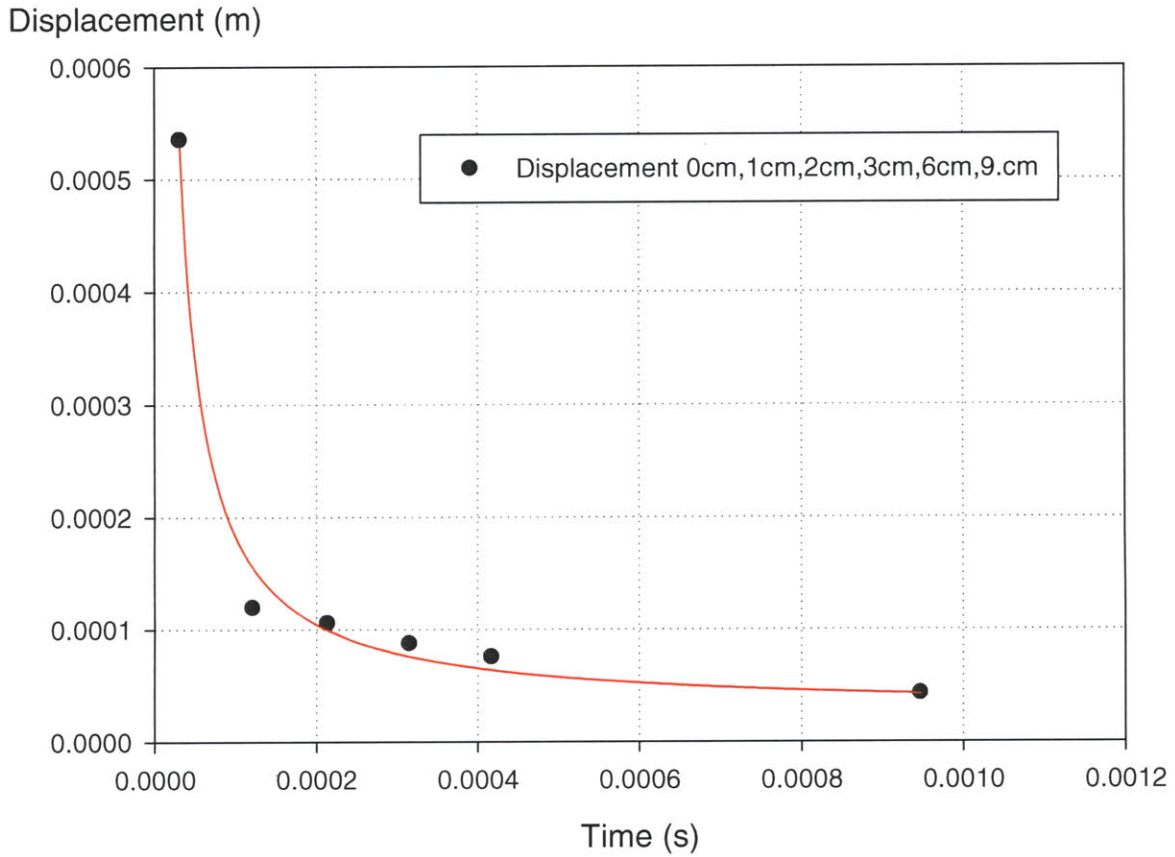
Figure 5.33: Regression of the Attenuation of the Displacement Field

The reduction of the amplitude of the displacement field can be expressed as an inverted polynomial function where the numerical constants determined through regression analysis. Regression analysis of the differential amplitudes produces the regression curve with the equation provided.

$$Amp(t), m = 2.58 * 10^{-5} + \frac{1.57 * 10^{-8}}{t}$$

5.5.3. S-wave Infinite Boundary Model: Frequency

The period of the arrival signal changes as the source/distance increases. The arrival frequency of the source signal is calculated by solving the reciprocal of the observed period. The observed period is a variable quantity with respect to the source receiver distance.
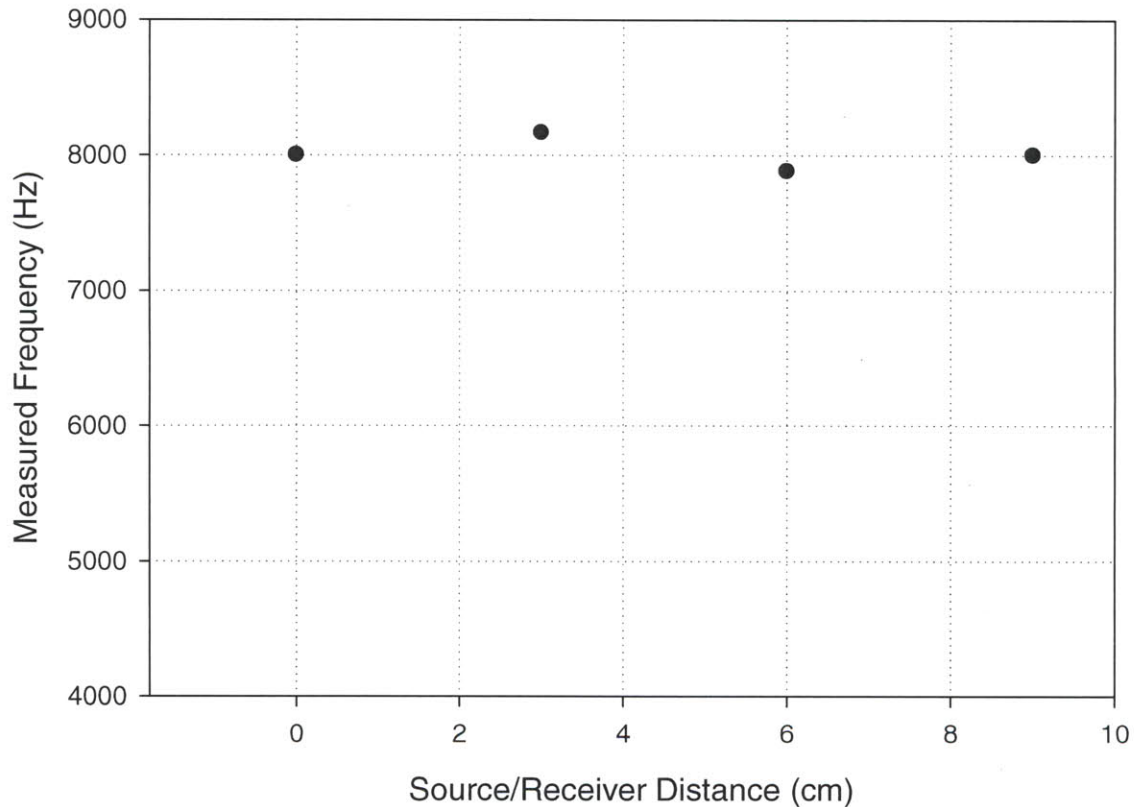
Figure 5.34: Frequency of the Displacement Field

It is observable that the frequency of the displacement field remains constant. Variations of the travel time and the radial distance between the source and receiver do not alter the arrival frequency of the displacement harmonic. The waveform in an infinite boundary exhibits planar behavior.

178

5.5.4. S-wave Infinite Boundary: Attenuation of the Shear Strain Field

Regression analysis was done on the attenuation of the shear strain field. The graph shows four arrivals at variable different source/receiver distances in multiples of three centimeters. Each arrival has an associated amplitude and arrival time. The interpolation function is a first order inverse polynomial equation. Accordingly, the statistical fit of the interpolation has the following values.

Figure 5.35: Attenuation of the Strain Field
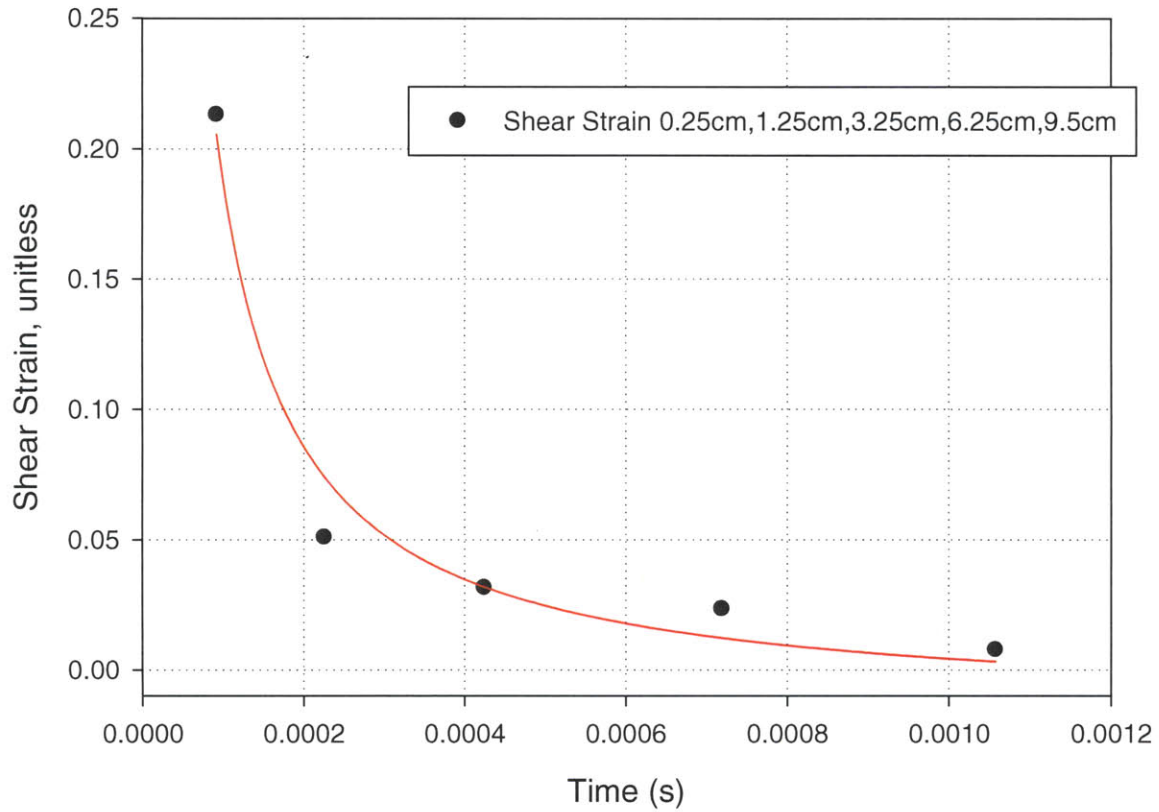
Figure 5.36: Regression of the Attenuation of the Strain Field

The reduction of the amplitude of the displacement field can be expressed as a inverted polynomial function taking the form, where a_0 and b_0 are numerical constants determined through regression analysis.

$$Amp(t), m = -0.0161 + \frac{2.034E - 005}{t}$$

5.5.5. S-wave Infinite Boundary Model: Velocity Measurements Source Receiver Distance.

The travel time of a sinusoidal wave is taken as the time between the two characteristic points of the source and receiver wave front. The source wave front remained constant at the source location, 0cm. Time differentials were measured as the difference of the pulse time recorded at the receiver node receiver and the source.
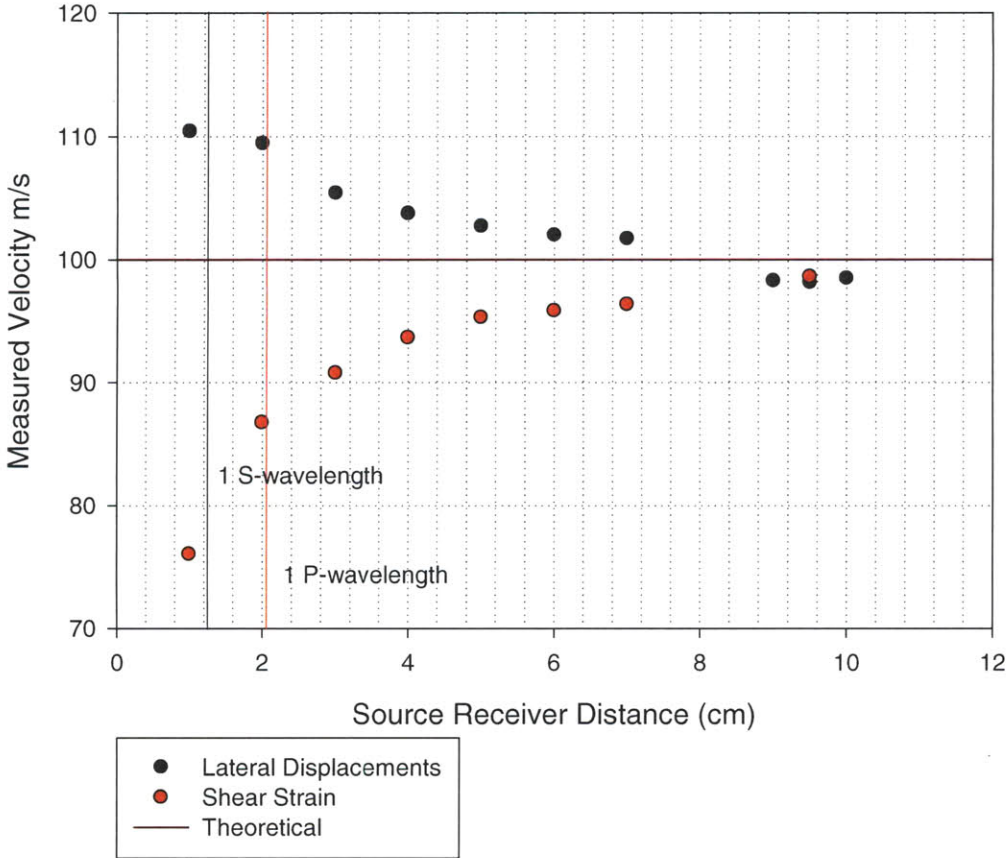
Figure 5.37: Peak to Peak Velocity Results

It is evident from the velocity measurements that the source receiver peak to peak velocity becomes highly inaccurate when the distance between the source and receiver is less than one P wavelength. After two P-wavelengths between the source and receiver the error becomes asymptotic.

5.5.6. S-wave Infinite Boundary Model: Velocity Measurements Depth of Model

Alternatively the peak to peak calculation can be represented as the difference between two wave fronts propagating down with a source receiver distance r_1 and r_2. The distance delta used for the velocity calculation becomes $r_2 - r_1 = dr$. The velocity calculation becomes

$$Measured\ Velocity = \frac{dr}{ts_n}.$$

The time incremented used varied as a function of the source receiver distance. The source receiver distance increments were: 0cm to 1cm, 1cm to 3cm, 3cm to 7cm for the displacement field. The strain field had increments of 0.25cm to 1.25cm, 1.25cm to 3.25cm, 3.25cm to 7.25cm This procedure produces source distance increments equal to 1cm, 2cm, and 4cm.

Figure 5.38: Peak to Peak Variable Time Increment Velocity Calculations
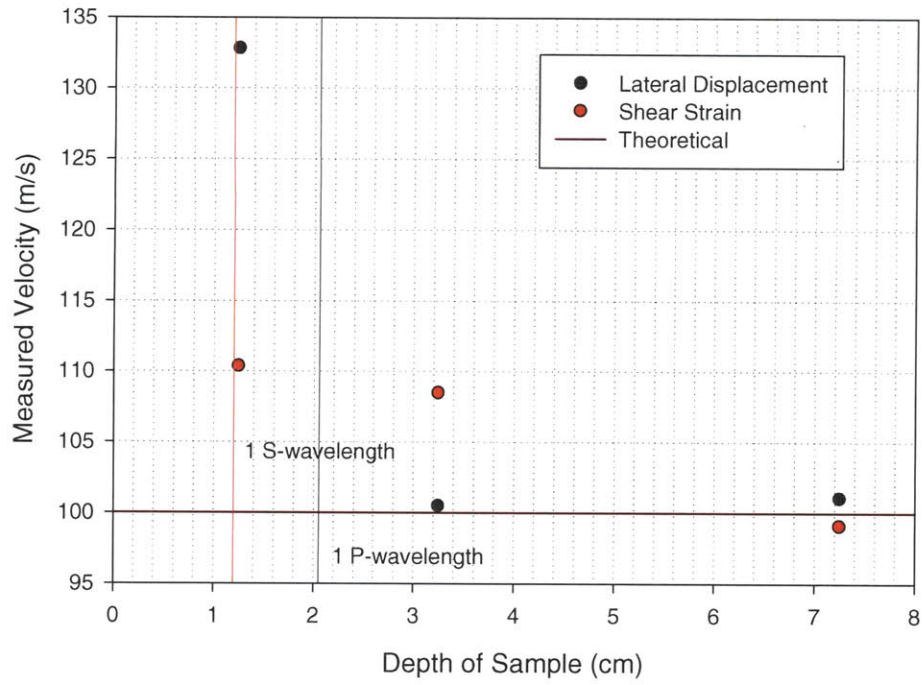
Figure 5.39: Peak to Peak Variable Time Increment Velocity Results

Shear Strain 0cm,3.25cm,6.25cm,9.5cm
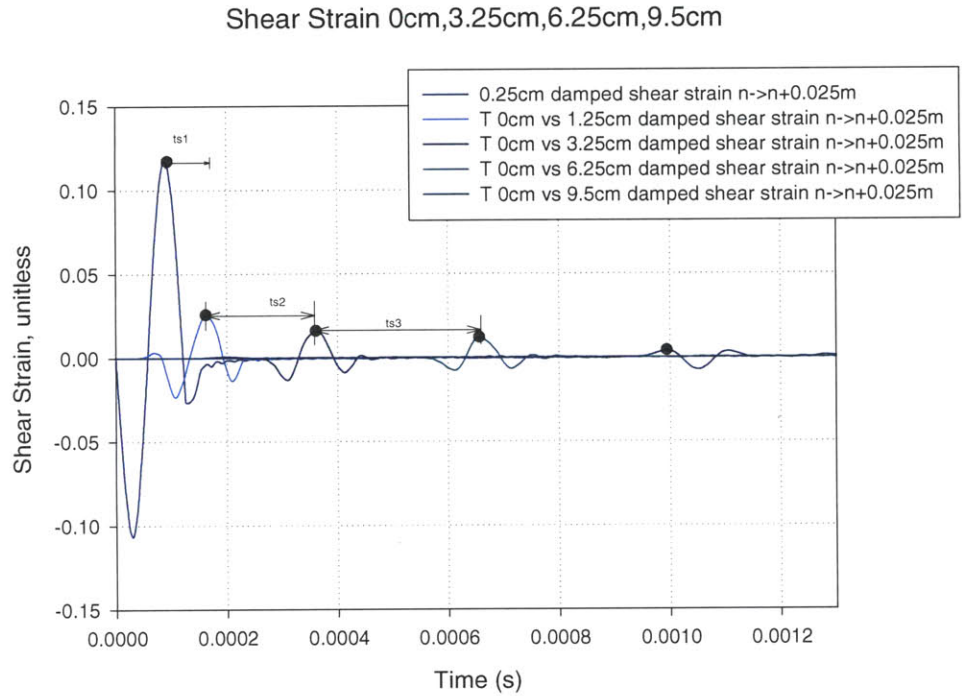
Figure 5.40: Peak to Peak Shear Strain Variable Time Increment Velocity Calculations

Similar to the Source Peak Velocity measurements, it is evident from the velocity measurements that the source receiver peak to peak velocity becomes highly inaccurate when the distance between the source and receiver is less than one P-wavelength. After two P-wavelengths between the source and receiver the error becomes asymptotic.

5.6.0. S-wave Rigid Boundary Model

An elastic rod model was constructed in two dimensional space with al lateral point displacement applied on the centerline of the top surface. Rigid boundaries were applied to the sides of the model to prevent body wave reflections. These boundaries were modeled as rollers. Body wave reflections are possible using rigid boundary conditions. Vertical and lateral constraints were fixed to the bottom corners of the model to prevent rigid boundary motion. These constraints were modeled as pins.

The displacement condition is sinusoidal harmonic motion. The displacement boundary condition oscillates one harmonic period and reaches equilibrium. At equilibrium no vertical displacement is possible. The parameters of the source vibration are provided in the tabled attached.

Frequency	8000 Hz (rev/sec)
Maximum Displacement	270 micrometers

Table 5.5 Lateral Displacement Parameters of Source

The field output of the model captured the displacement field, and strain field. The shear strain was calculated from the differential vertical displacement of two nodes spaced 2.5mm apart. Shear strain is a more suitable strain measurement for the propagation of the shear wave because a shear wave polarization is orthogonal to its propagation.

Data were extracted from selected nodes located along the centerline of the geometry. The vertical spacing of the extraction nodes were one centimeter. Each extraction depth included two vertically adjacent nodes for the purpose of measuring the axial strain. The nodes were spaced 2.5mm apart. The element length or the vertical spacing of the node is equal to the shear wave length divided by twenty.

The geometry of the rod is sufficiently large to prevent reflections occurring from the bottom boundary. At the source of the harmonic waveform there will be no after effects coming from the bottom boundary.

The maximum depth of extraction was ten centimeters. Accordingly, there are eleven extraction depths at each integer beginning at 0cm and ending at 10cm inclusive.

5.6.1. S-wave Rigid Boundary Model: Displacement Field

The lateral displacement of a node is the scalar quantity of dislocation with respect to the vertical axis. In a two dimensional modal the vertical axis is represented by the subscript 'x' in the 'x' axis. The lateral displacement of the node was captured with respect to time. The resolution of the time step was fixed at 312.5 nanoseconds, enough to capture fine perturbations of the S-wave front propagation. Accordingly, there are 3200 independent data points in the field output containing data from each time step. The lateral displacement from the displacement model of the extraction nodes is provided.
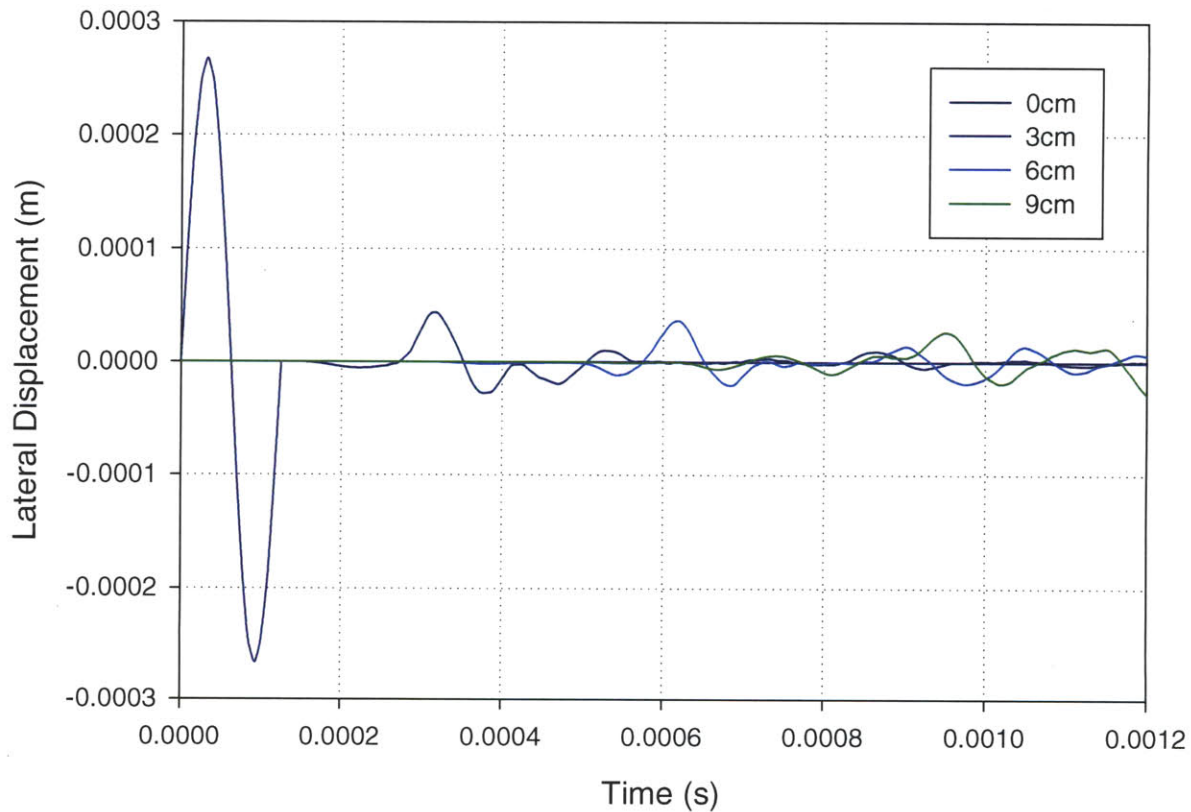
Figure 5.41: The Displacement Field

5.6.2. S-wave Rigid Boundary: Attenuation of the Displacement Field

Regression analysis was done on the attenuation of the stress field. The graph shows four arrivals at variable different source/receiver distances in multiples of three centimeters. Each arrival has an associated amplitude and arrival time. The difference of the positive negative amplitude was taken. This difference is represented in Figure as 'A1'.
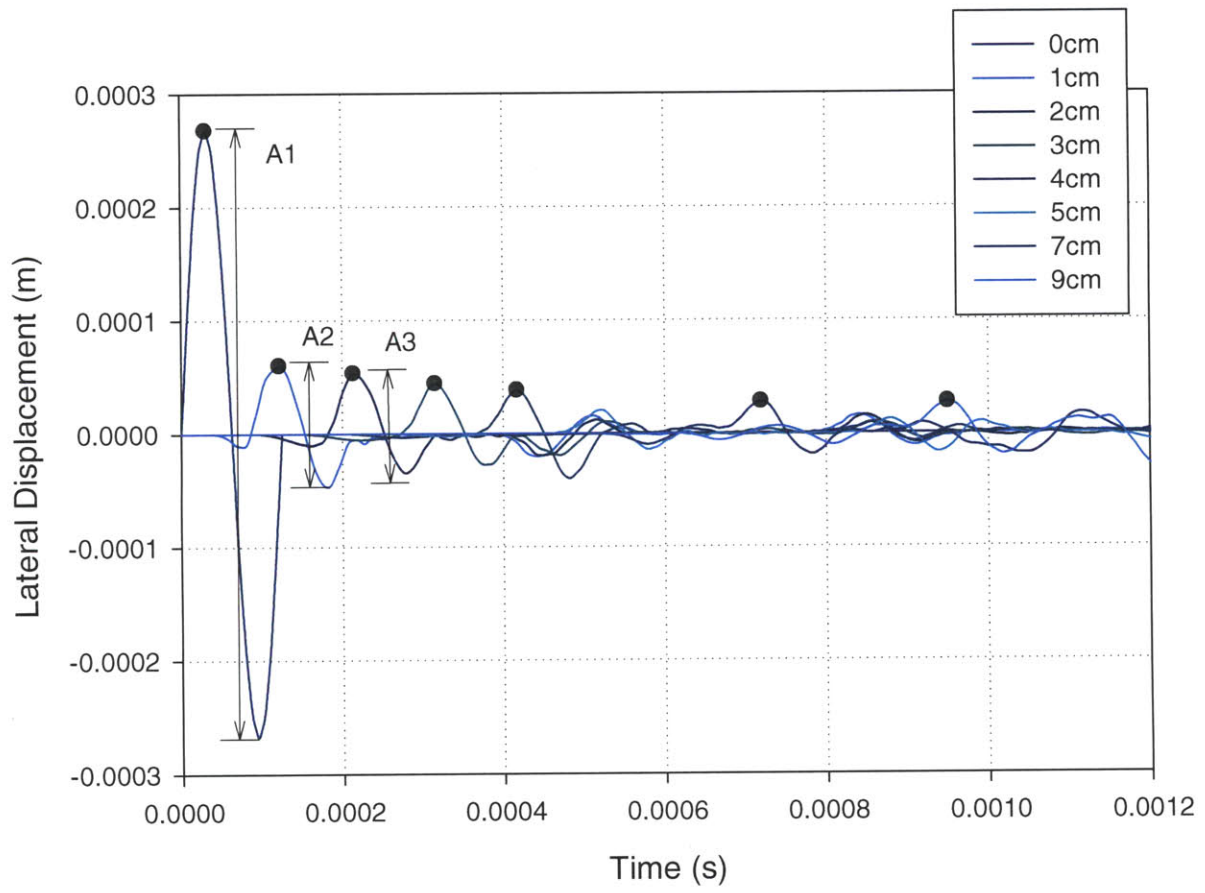
Figure 5.42: Attenuation of the Displacement Field
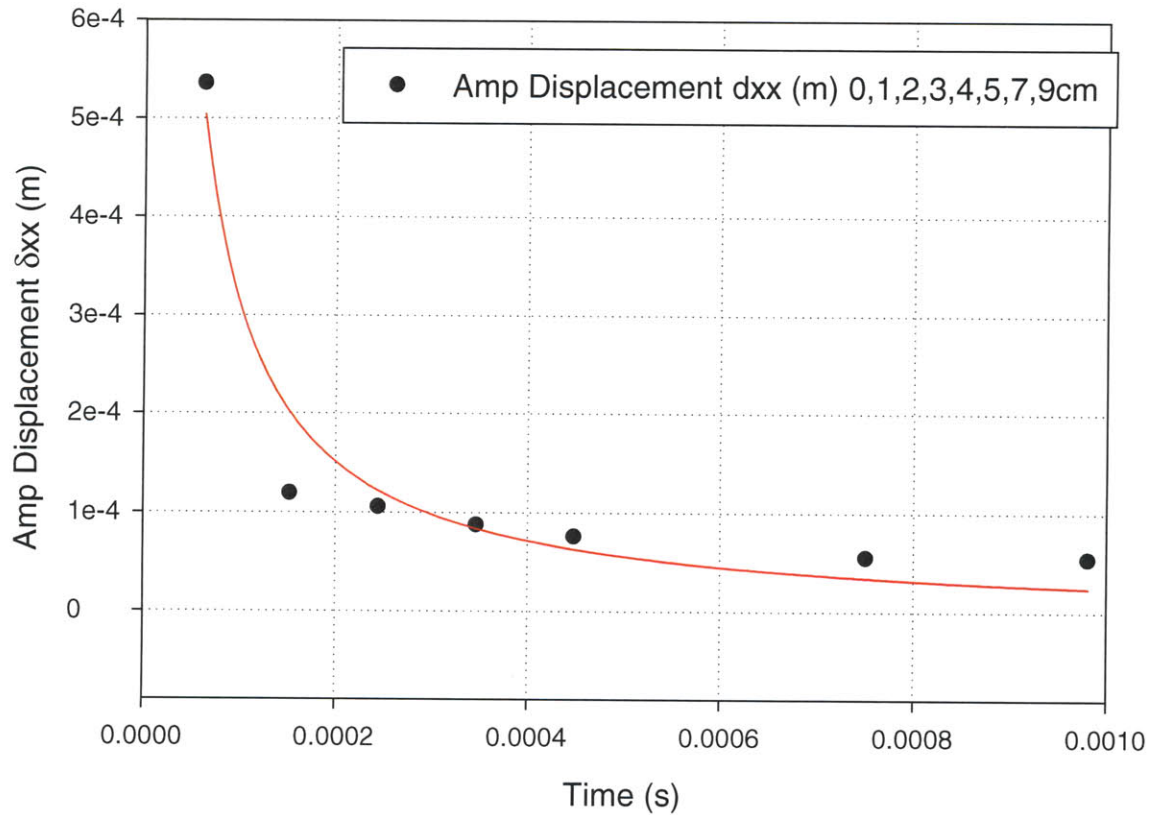
Figure 5.43: Regression of the Attenuation of the Displacement Field

The interpolation function is a first order inverse polynomial equation. Accordingly, the statistical fit of the interpolation has the following values provided in Figure 5.43.

The reduction of the amplitude of the displacement field can be expressed as an inverted polynomial function where the numerical constants determined through regression analysis. Regression analysis of the differential amplitudes produces the regression curve with the equation provided.

$$Amp(t), m = -8.77\text{E} - 6 + \frac{3.202\text{E} - 008}{t}$$

5.6.3. S-wave Model: Frequency

The period of the arrival signal changes as the source/distance increases. The arrival frequency of the source signal is calculated by solving the reciprocal of the observed period. The observed period is a variable quantity with respect to the source receiver distance.
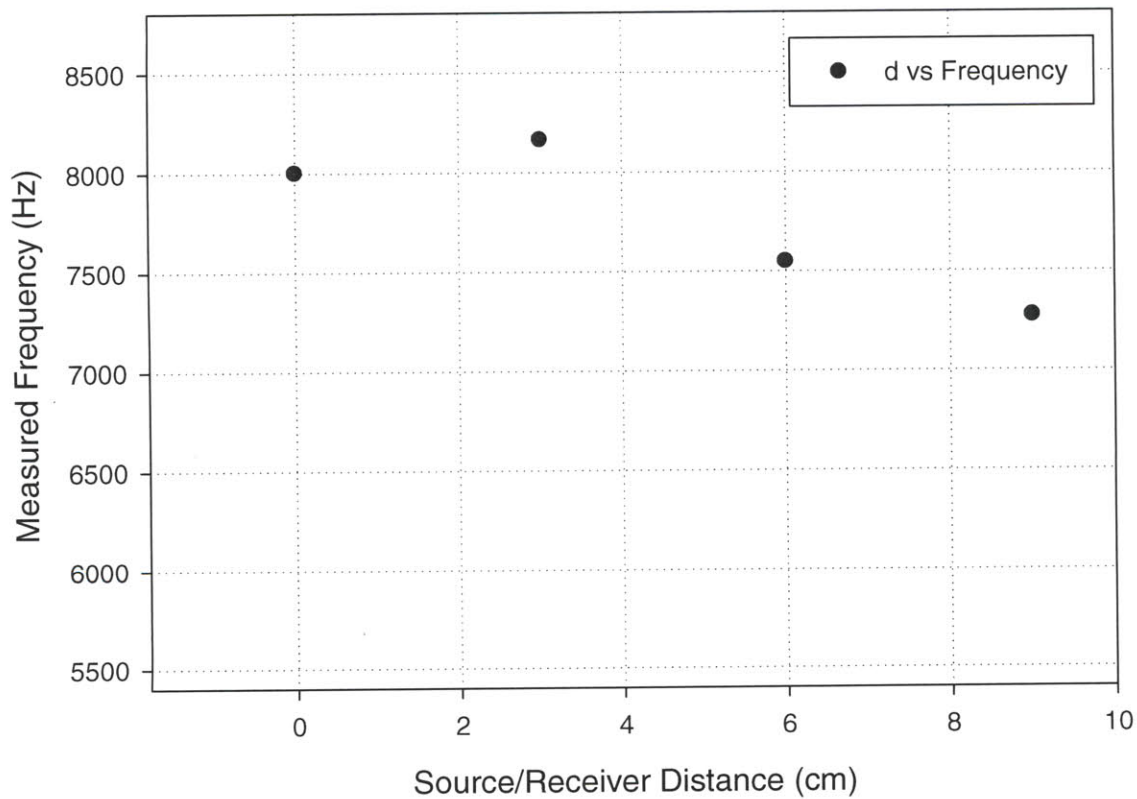
Figure 5.44: Frequency of the Displacement Field

It is observable that the frequency of the displacement field varies with respect to depth. The waveform in a free elastic rod model does not exhibits planar behavior.

5.6.4. S-wave Rigid Boundary: Attenuation of the Shear Strain Field

Regression analysis was done on the attenuation of the shear strain field. The graph shows four arrivals at variable different source/receiver distances in multiples of three centimeters. Each arrival has an associated amplitude and arrival time. The interpolation function is a first order inverse polynomial equation. Accordingly, the statistical fit of the interpolation has the following values.

$$Amp(r), m = -0.0068 + \frac{9.6546E - 006}{r}$$
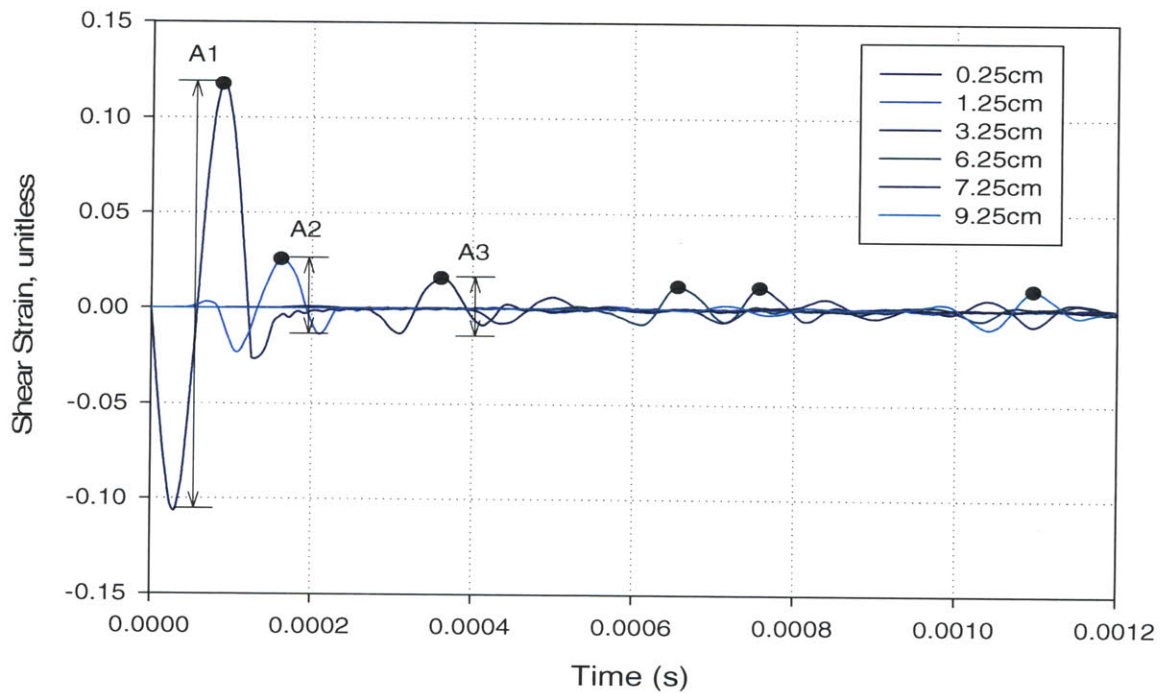
Figure 5.45: Attenuation of the Strain Field
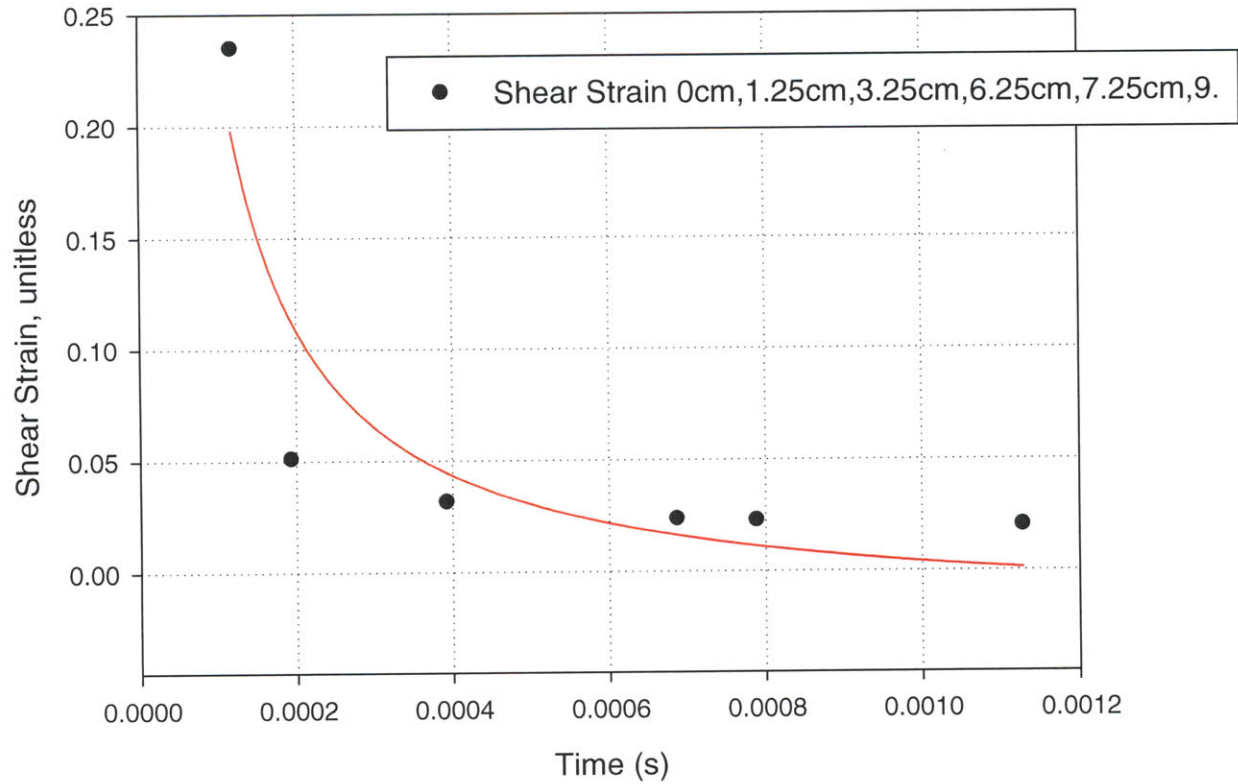
Figure 5.46: Regression of the Attenuation of the Strain Field

The reduction of the amplitude of the displacement field can be expressed as a inverted polynomial function taking the form, where the numerical constants determined through regression analysis.

$$Amp(t), m = -0.022 + \frac{2.611\text{E} - 005}{t}$$

5.6.5. S-wave Rigid Boundary Model: Velocity Measurements Source Receiver Distance

The travel time of a sinusoidal wave is taken as the time between the two characteristic points of the source and receiver wave front.. The source wave front remained constant at the source location, 0cm. Time differentials were measured as the difference of the pulse time recorded at the receiver node receiver and the source.
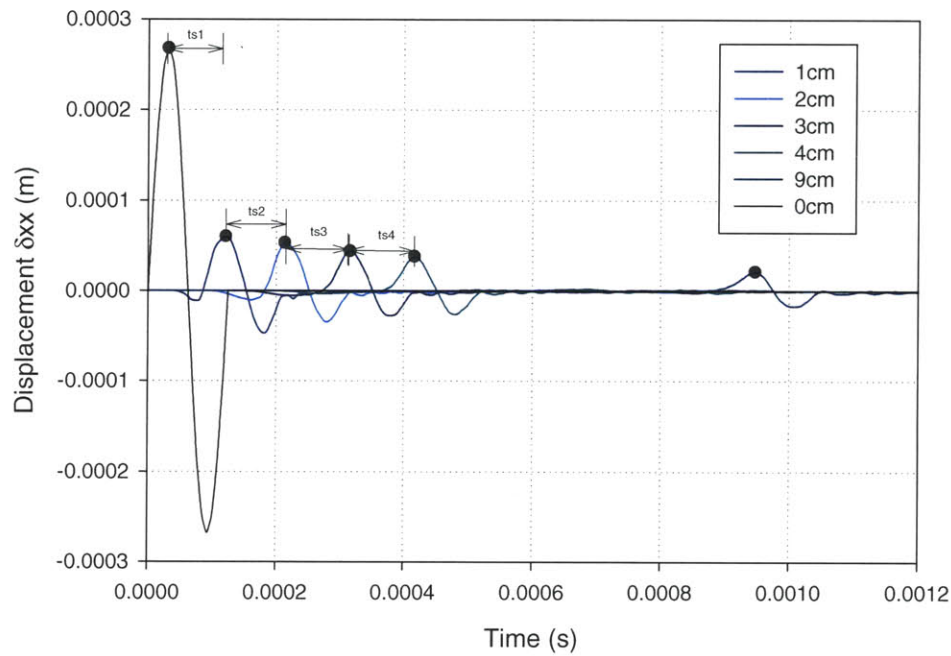
Figure 5.47: Peak to Peak Velocity Calculations
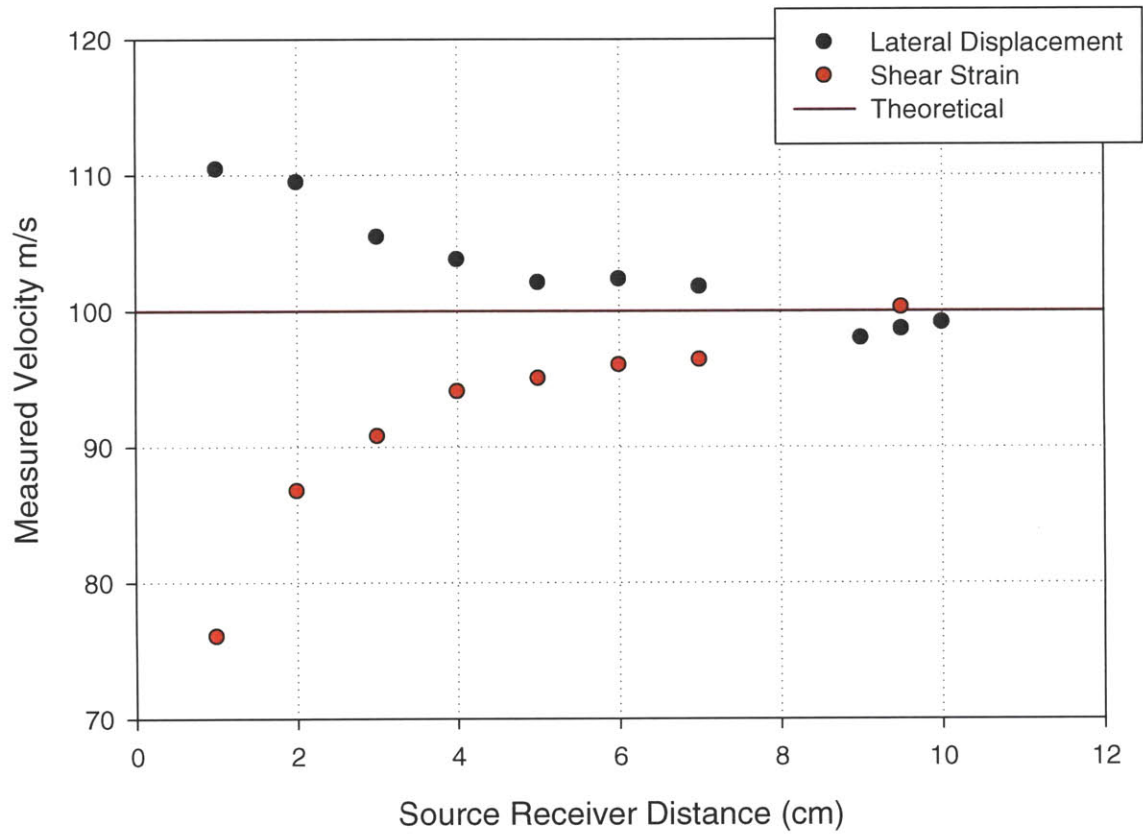
Figure 5.48: Peak to Peak Velocity Results

It is evident from the velocity measurements that the source receiver peak to peak velocity becomes highly inaccurate when the distance between the source and receiver is less than one P wavelength.

5.6.6. S-wave Rigid Boundary Model: Velocity Measurements Depth of Model.

Alternatively the peak to peak calculation can be represented as the difference between two wave fronts propagating down with a source receiver distance r_1 and r_2 . The distance delta used for the velocity calculation becomes $r_2 - r_1 = dr$. The velocity calculation becomes

$$Measured\ Velocity = \frac{dr}{ts_n}.$$

The time incremented used varied as a function of the source receiver distance. The source receiver distance increments were: 0cm to 1cm, 1cm to 3cm, 3cm to 7cm for the displacement field. The strain field had increments of 0.25cm to 1.25cm, 1.25cm to 3.25cm, 3.25cm to 7.25cm This procedure produces source distance increments equal to 1cm, 2cm, and 4cm.

Figure 5.49: Peak to Peak Shear Strain Variable Time Increment Velocity Calculations
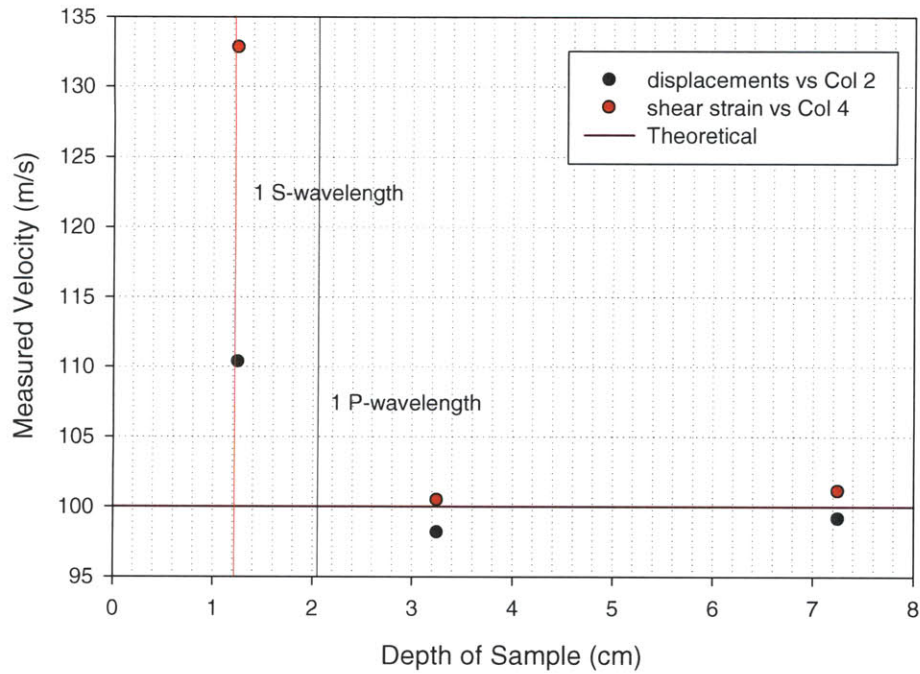
Figure 5.50: Peak to Peak Variable Time Increment Velocity Results

Comparable to the Source Peak Velocity measurements, it is evident from the velocity measurements that the source receiver peak to peak velocity becomes highly inaccurate when the distance between the source and receiver is less than one P-wavelength. After two P-wavelengths between the source and receiver the error becomes asymptotic.

Figure 5.51: Graphical Representation of P-Wave Model Undamped Results
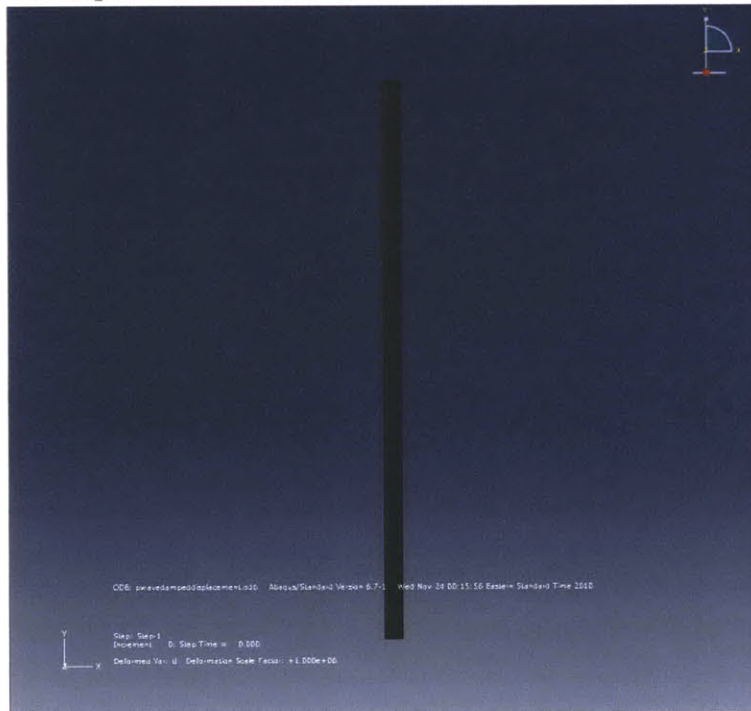
t=0 secs into Analysis. Automatic Scale Factor
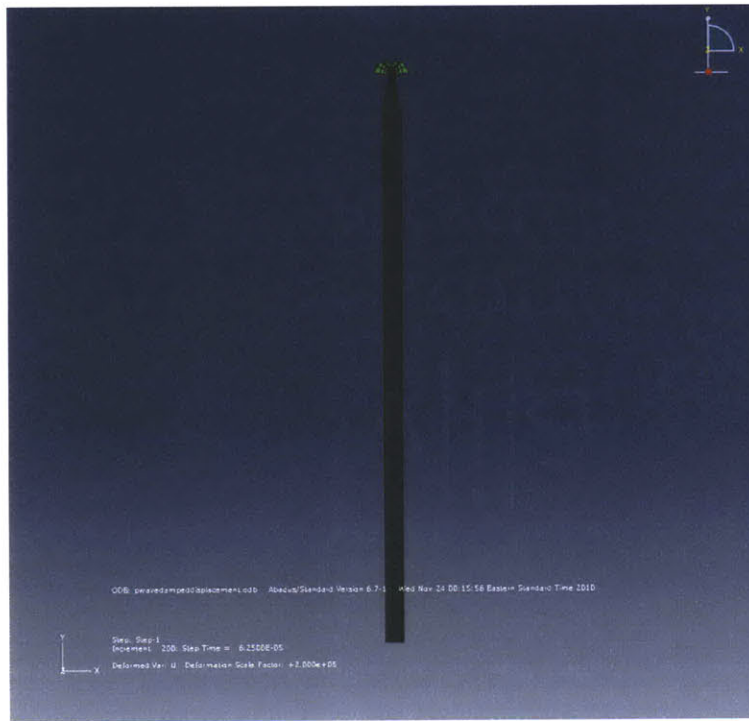
t=6.25E-5 secs into Analysis. Automatic Scale Factor
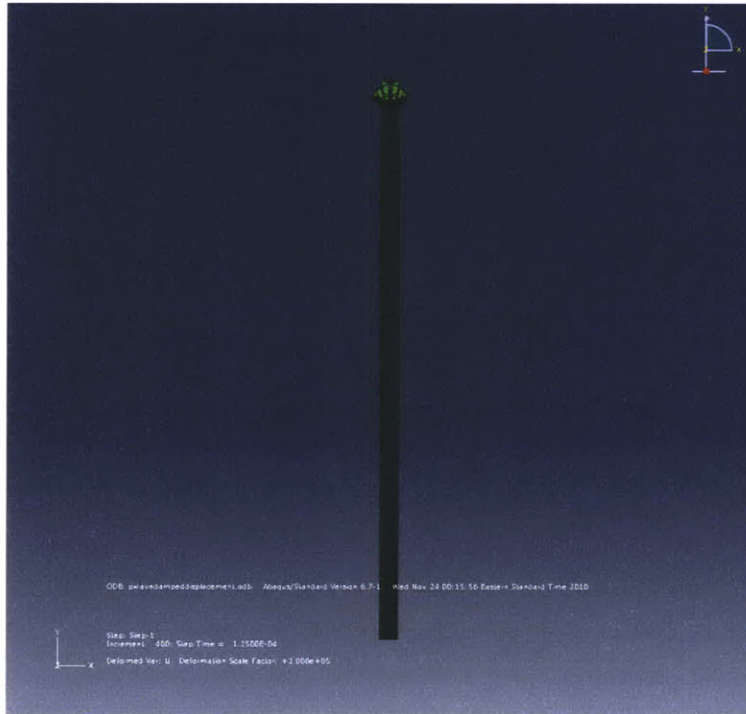
t=1.25E-4 secs into Analysis. Automatic Scale Factor
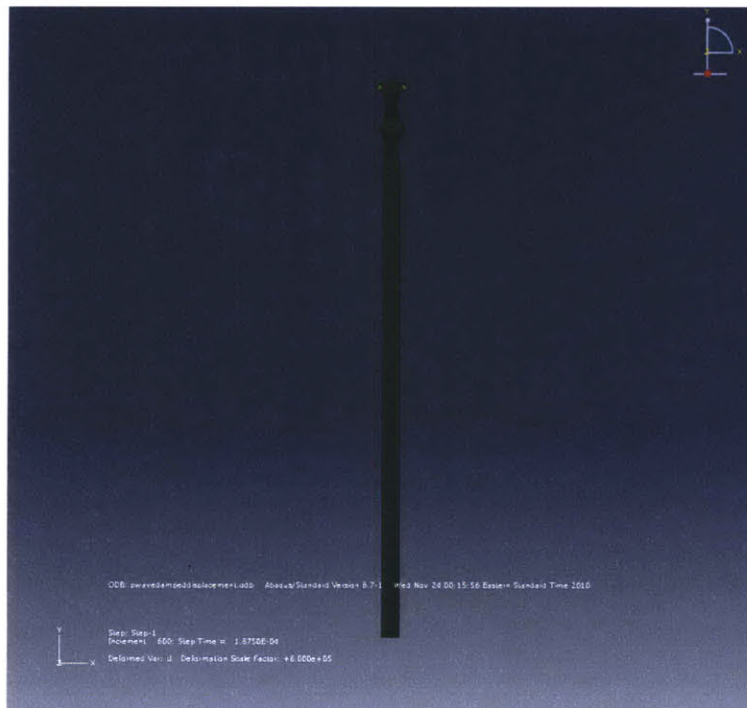
t=1.875E-4 secs into Analysis. Automatic Scale Factor
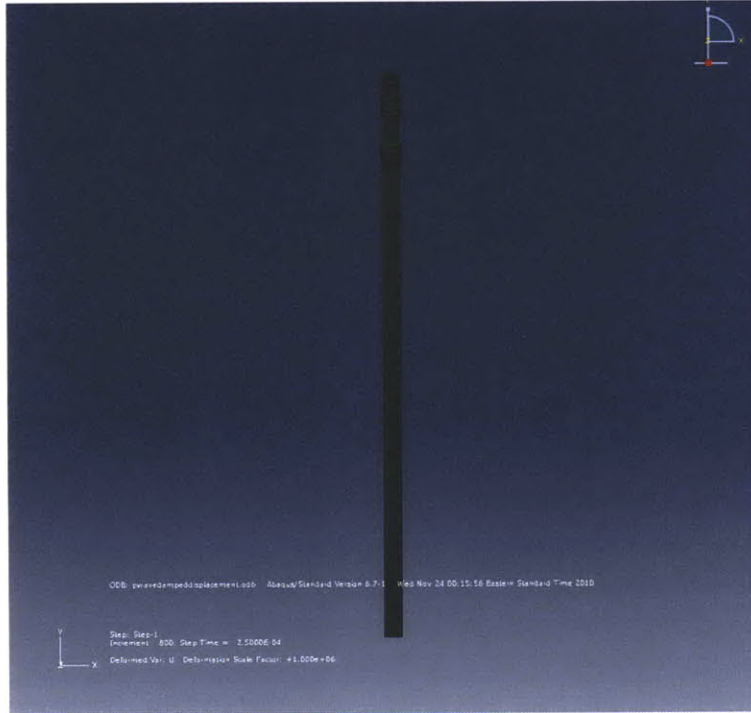
t=2.5E-4 secs into Analysis. Automatic Scale Factor
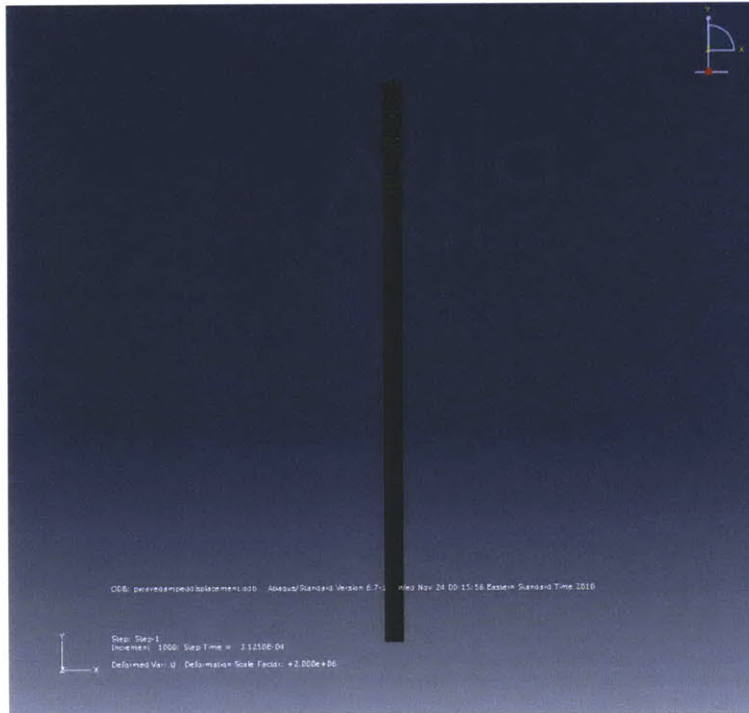
t=3.125E-4 secs into Analysis. Automatic Scale Factor

Figure 5.52: Graphical Representation of P-Wave Model Damped Results
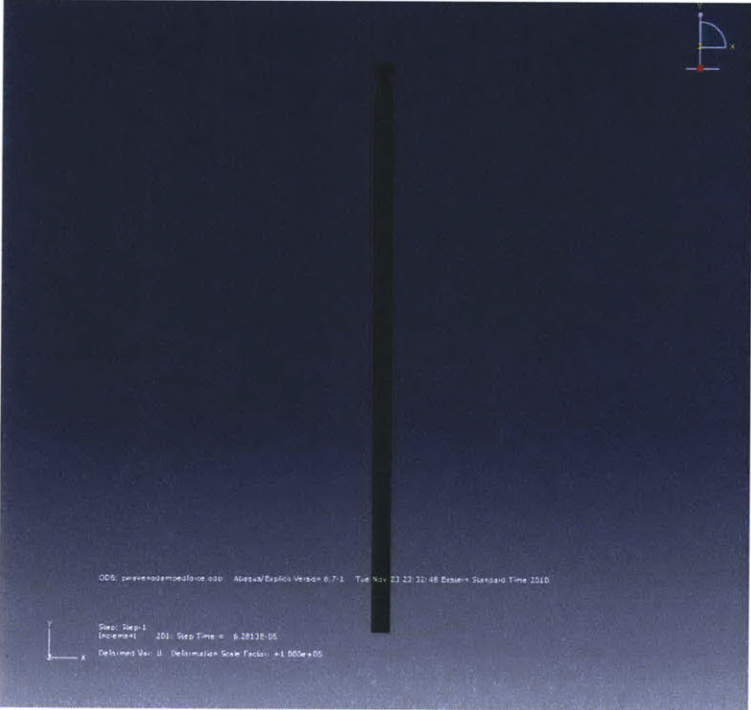
t=0 secs into Analysis. Automatic Scale Factor

t=6.25E-5 secs into Analysis. Automatic Scale Factor
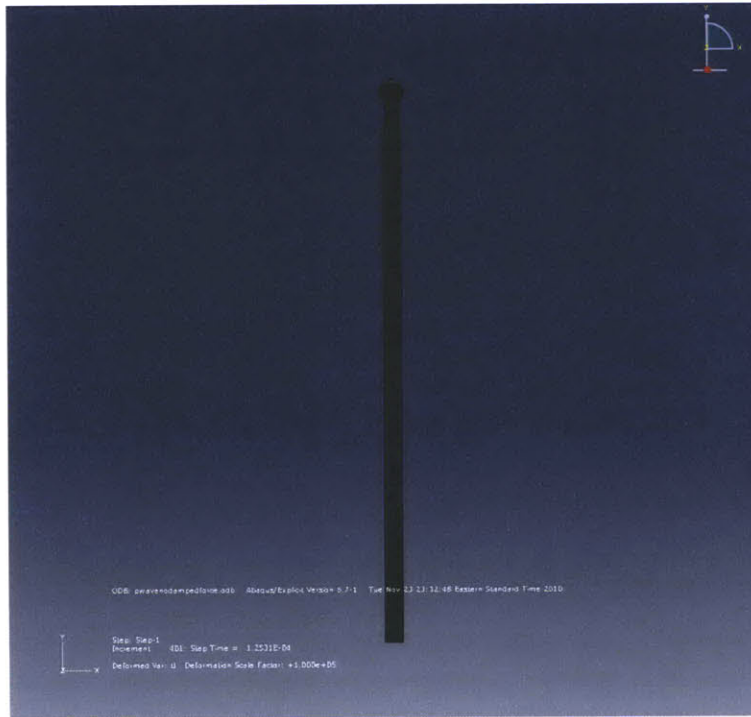
t=1.25E-4 secs into Analysis. Automatic Scale Factor
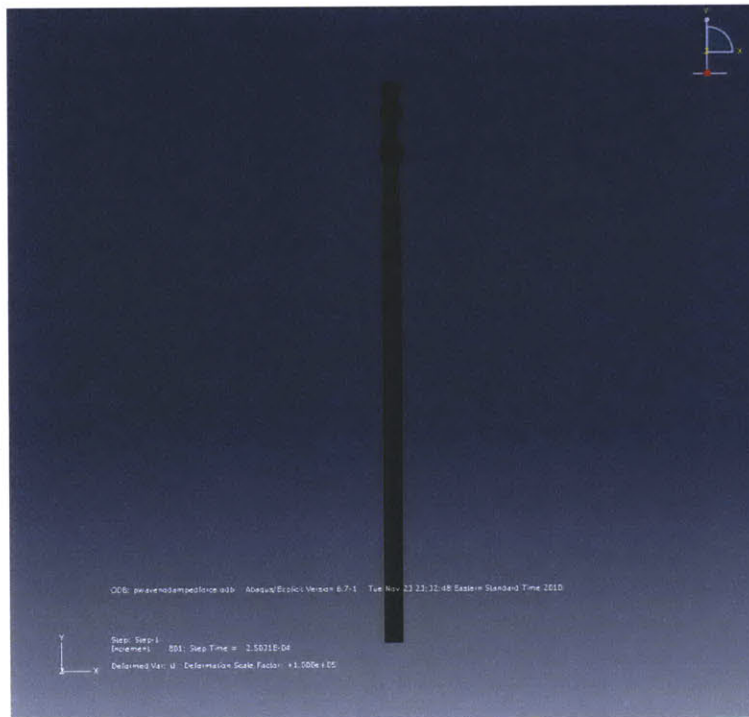
t=1.875E-4 secs into Analysis. Automatic Scale Factor
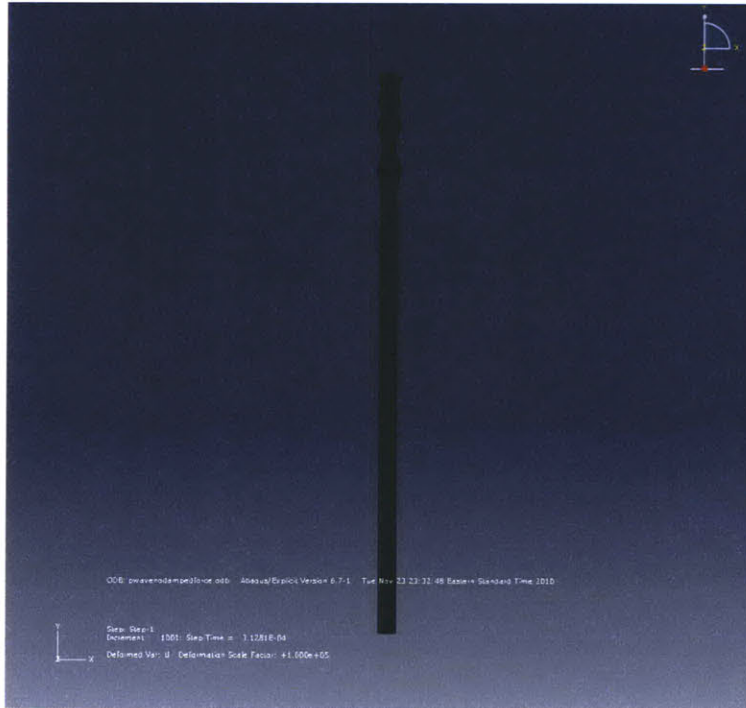
t=2.5E-4 secs into Analysis. Automatic Scale Factor
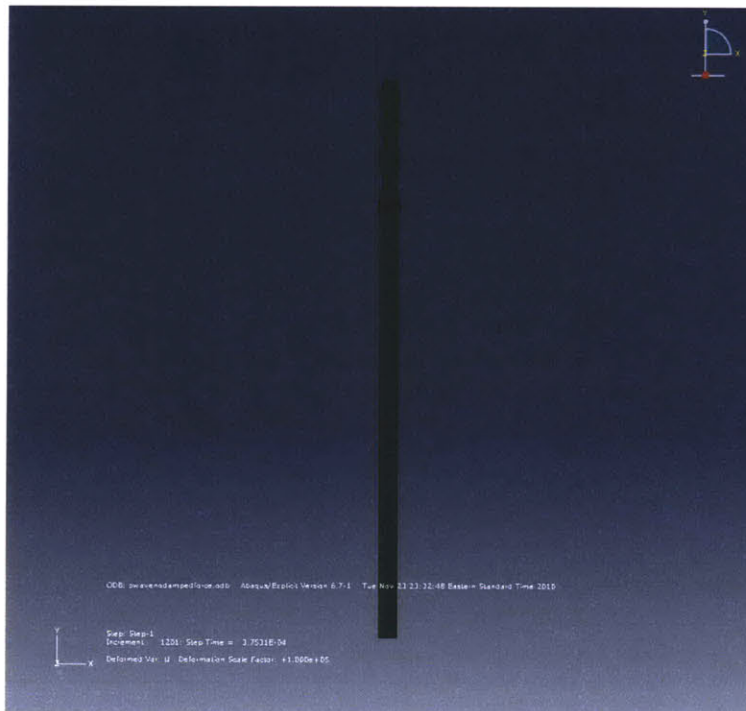
t=3.125E-4 secs into Analysis. Automatic Scale Factor

Figure 5.53: Graphical Representation of S-Wave Model Damped Results
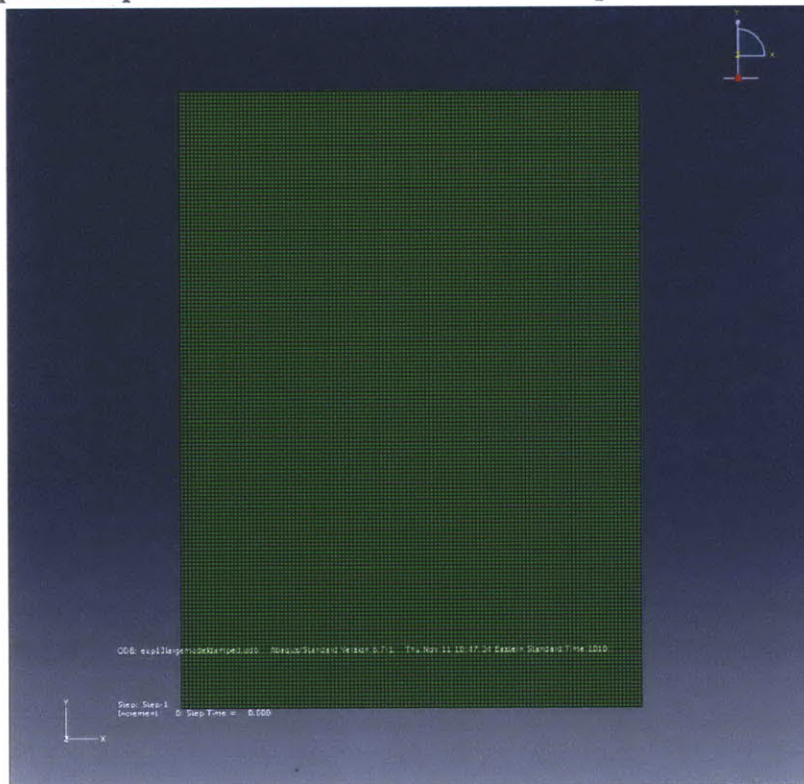
t=0 secs into Analysis. Automatic Scale Factor

t=6.25E-5 secs into Analysis. Automatic Scale Factor

t=1.25E-4 secs into Analysis. Automatic Scale Factor

t=1.875E-4 secs into Analysis. Automatic Scale Factor
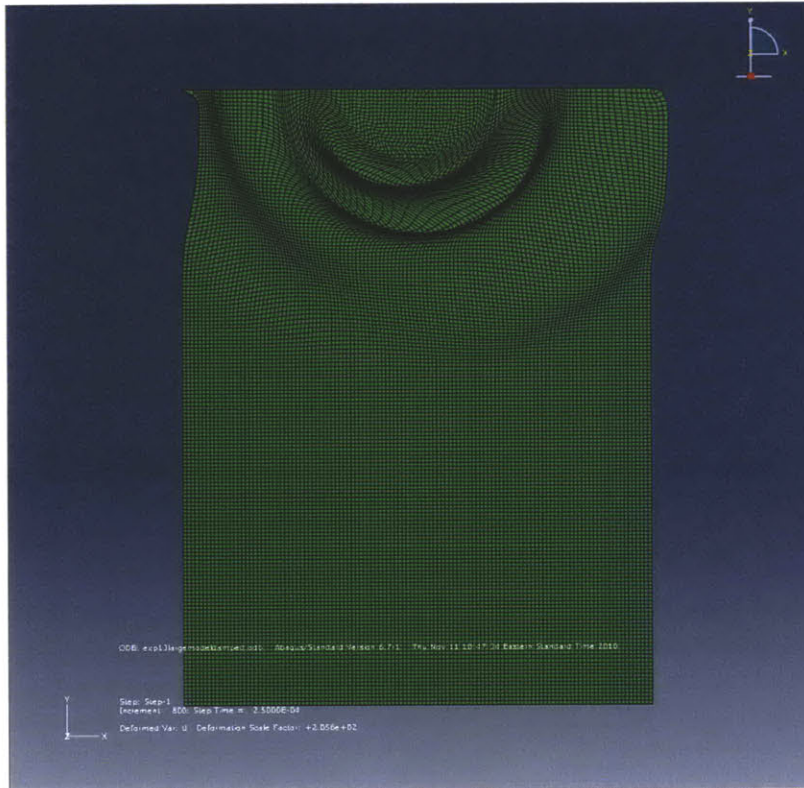
t=2.5E-4 secs into Analysis. Automatic Scale Factor

t=3.125E-4 secs into Analysis. Automatic Scale Factor

t=3.75E-4 secs into Analysis. Automatic Scale Factor

6. Experimental Results

6.1. Overview

The experimental results chapter will investigate two bender element tests on dry Ticino Sand contained in a rigid brass tube. The two tests were reproduced in Abaqus Finite Element program using dynamic implicit analysis. The purpose of the finite element testing was to capture the effect of boundary reflections in a numerical analysis and to make recommendations on measuring the shear velocities using a finite element procedure in a rigid boundary half space.

During body wave propagation it is expected that reflections from incidence P and S-waves reflecting off of the brass sleeve will cause interference at the receiver. Analysis will be done to control for interference from the rigid boundary. The first test will capture the boundary reflections using rollers on the lateral surfaces. The second test will simulate an infinite boundary through the application of dampers applied along the lateral boundary. The dampers effectively suppress all incident reflections from occurring from the lateral boundaries using the cross actual geometry of the real experiment.

Abaqus Implicit Dynamic Analysis was used to model the bender element testing. The wavefront of both P/S waves were considered. Love and Rayleigh surface waves were ignored in the analysis. The models utilized an isotropic elastic medium and a point source perturbation. The field output of the analysis includes lateral scalar shear strain and displacement.

The experimental bender element results require a framework to translate its information gathered from testing to a numerical analysis. A numerical analysis cannot independently determine the Young's modulus of the specimen. A calculation is required from the experimental data to solve for the Young's modulus. A coherent framework is needed to proceed in this section. Therefore, a flowchart was made to provide a method to model the experimental bender element tests.
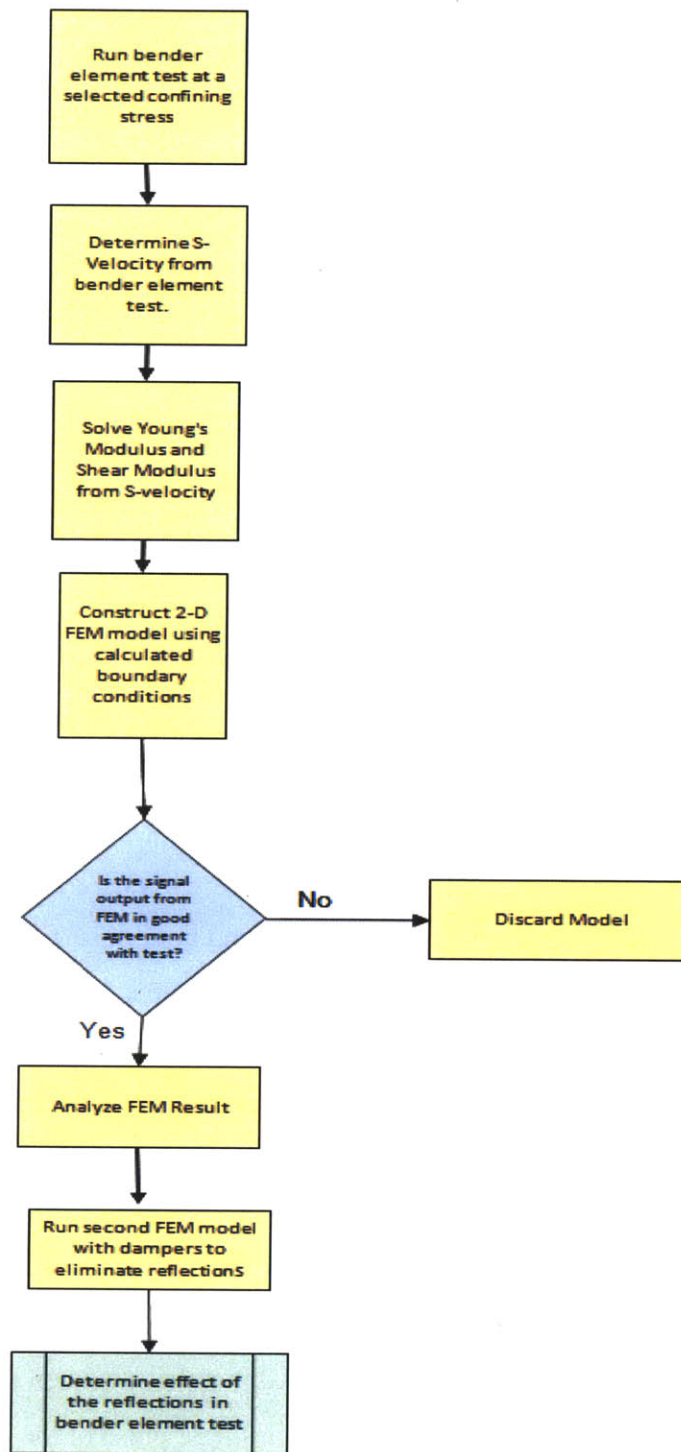
```
┌─────────────────────┐
│   Run bender        │
│   element test at a │
│   selected confining│
│   stress            │
└──────────┬──────────┘
           │
           ▼
┌─────────────────────┐
│   Determine S-      │
│   Velocity from     │
│   bender element    │
│   test.             │
└──────────┬──────────┘
           │
           ▼
┌─────────────────────┐
│   Solve Young's     │
│   Modulus and       │
│   Shear Modulus     │
│   from S-velocity   │
└──────────┬──────────┘
           │
           ▼
┌─────────────────────┐
│   Construct 2-D     │
│   FEM model using   │
│   calculated        │
│   boundary          │
│   conditions        │
└──────────┬──────────┘
           │
           ▼
         ◇ Is the signal          No      ┌──────────────────┐
         ◇ output from   ─────────────────▶│  Discard Model   │
         ◇ FEM in good                     └──────────────────┘
         ◇ agreement
         ◇ with test?
           │
         Yes
           ▼
┌─────────────────────┐
│   Analyze FEM Result│
└──────────┬──────────┘
           │
           ▼
┌─────────────────────┐
│  Run second FEM model│
│  with dampers to    │
│  eliminate reflections│
└──────────┬──────────┘
           │
           ▼
┌─────────────────────┐
│  Determine effect of│
│  the reflections in │
│  bender element test│
└─────────────────────┘
```

Figure 6.1 FEM Modeling Method

Figure 6.1 explains the procedure used to model the bender element tests. The Poisson Ratio and the mass density should be calculated or assumed when the shear modulus is calculated; these properties are essential to model wave propagation. The flowchart presents a framework to model two bender element tests stressed in the consolidometer in Abaqus.

6.2. Introduction: dry Ticino Sand Test 12.1 cm Specimen Height

An experimental bender element test was completed on dry Ticino sand. The specimen height of the sand was 12.1 cm. The effective travel length of the shear wave was defined as the distance between the tips of the elements; the tip to tip distance of the piezoelectric shims was measured to be 9.38 centimeters. The inside diameter of the brass tube, excluding its thickness, was measured equal to 7.5cm. The specimen was subjected to a 43kPa uniaxial confining stress.

The tests were conducted in a consolidometer testing apparatus. The consolidometer applies a 1-D confining stress to the Ticino Sand specimen. The Ticino sand was contained by a hollow brass cylinder. The consolidometer did not apply a stress to the brass boundary tube. Therefore, the brass sleeve does not strain during the testing procedure.

The piezoelectric transducers were mounted on the top and bottom surfaces of the brass sleeve. The top transducer behaves as the source transducer or the source of the body wave. The bottom transducer behaves as the receiver capturing the body wave. The transmitted and received body waves were captured by a digital oscilloscope. A peak to peak velocity calculation was then extracted from the oscilloscope reading.

The transducers were oriented to produce laterally polarized S-waves propagating vertically. The notation of this configuration of the S-wave is S_{VH}, or vertically propagated and horizontally polarized. The S_{VH} wave propagates hemispherically down the specimen from the source transducer to the bottom receiver. The receiver reads a single pulse of the S_{VH} wavefront.

The results are time averaged. The averaging is used to minimize noise and chaotic signal movement. The data acquisition system takes 50 samples of the recorded transducers and time averages the data. A time averaged signal is recommended to produce a stable output signal. The

210

signal was analyzed by 1000 gain. Figure 6.2 shows the source pulse and received signal, the middle frame is the single received pulse, last frame is the average of the received signal or 5o pulses. Figure 6.3 provides an expanded view of the first arrival. The small pulse at the start of the graph ($t < 0.0002\ sec$) is the cross talk of the excitation signal.
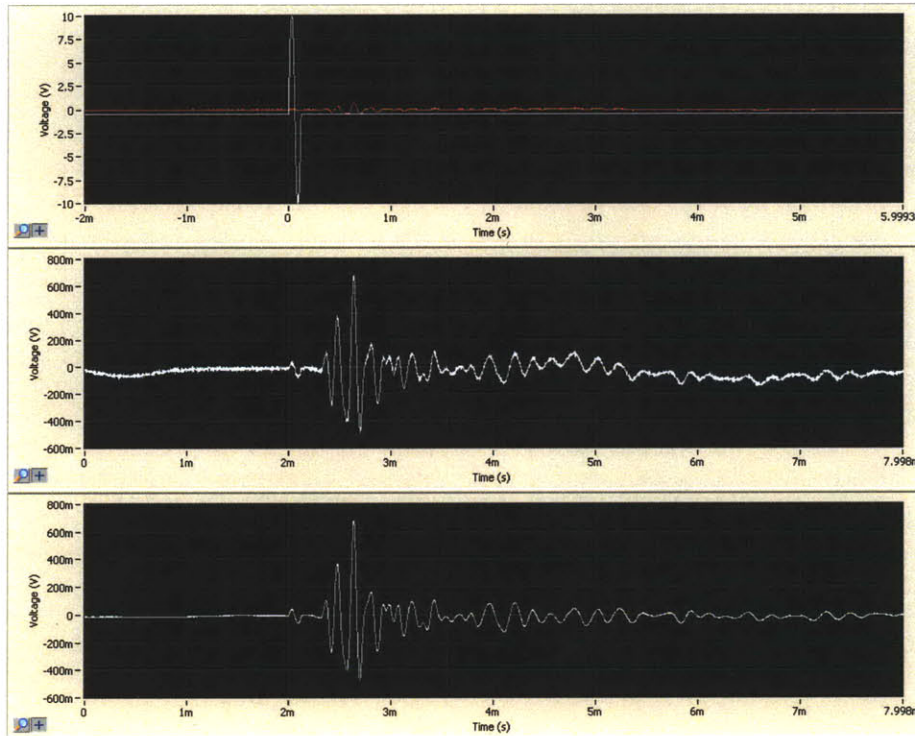
Figure 6.2: Time Averaged Output From Digital Oscilloscope
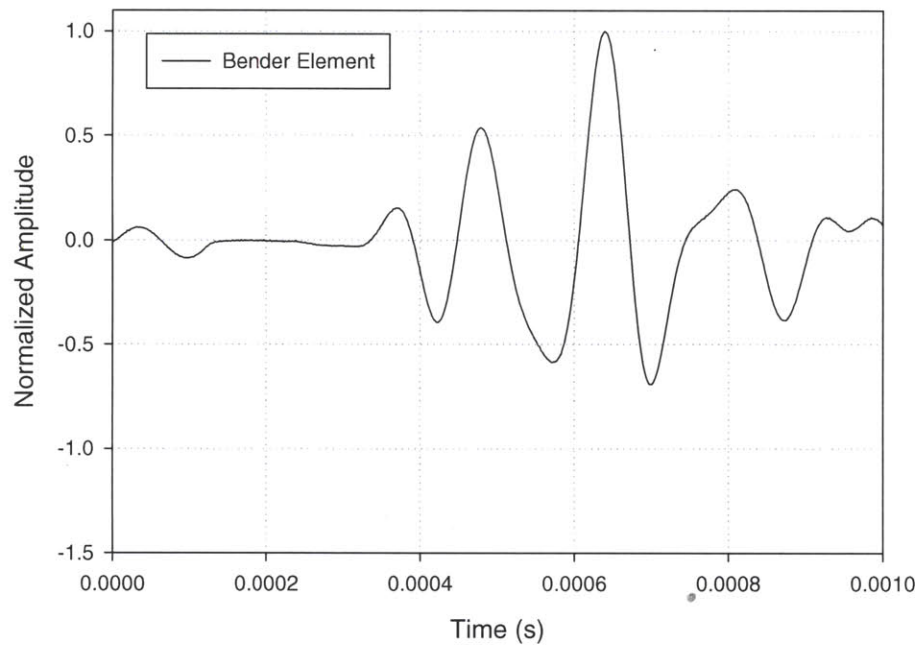
Figure 6.3: Normalized Time Averaged Output

6.3. Velocity Determination

The time averaged output is used as the basis to determine the travel time of the Shear Wave propagating between the source transducer and the receiver transducer. The travel time is defined as the elapsed time between the maximum peak of the source and the maximum peak of the receiver. The distance between the source and receiver is the effective travel length. The determination of the shear velocity is achieved by dividing the tip to tip travel distance by the measured travel time. The peak to peak velocity calculation is provided:

$$Measured\ S - Wave\ Velocity = \frac{dr}{ts_n} = \frac{.0938m}{.000604s} = 155\ \frac{m}{s}.$$

6.4. Calculation of the Shear Modulus, Young's Modulus, and Associated Material Properties

The S-wave velocity can be used to solve for the Young's modulus and the small strain shear modulus of the unsaturated Ticino Sand. It is known that the Shear Modulus has the following relationship.

$$Gmax = \rho * Vs^2 = 1476\,\frac{kg}{m^3} * (155\,\frac{m}{s})^2 = 35.4\,MPa$$

And

$$E = Gmax * 2(1 + v) = 38.7MPa * 2(1 + .3) = 92.2\ MPa$$

The mass density was calculated by massing the Ticino sand in the specimen and dividing it by the volume of the specimen after consolidation. Therefore, the small strain shear modulus and Young's modulus of the unsaturated Ticino sand are known. These values were used as the input material parameters for the Dynamic Implicit Analysis. An assumed of 0.3 Poisson's Ratio is appropriate for Ticino Sand.

A complete table of the material input parameters is provided.

Young's Modulus, E	Calculated	92.2 Mpa
Shear Modulus, G_{max}	Calculated	35.4 Mpa
Shear Phase Velocity, V_s	Calculated	155m/s
Possion's Ratio, η	Assumed	0.3
Mass Density, ρ_m	Measured	1476 kg/m

Table 6.1 Material Properties

214

6.5. Abaqus model of the 12.1 cm Unsaturated Ticino Sand Test

A two dimensional elastic and isotropic model was constructed with rigid boundaries applied to the sides of the model to simulate the effect of the brass sleeve. These boundaries were modeled as rollers. Body wave reflections are possible using rigid boundary conditions. Vertical and lateral constraints were fixed to the bottom corners of the model to prevent rigid boundary motion. These constraints were modeled as pins.

A displacement boundary condition was applied along the center at a depth of one bender element length. The displacement condition is sinusoidal harmonic motion. The displacement boundary condition oscillates one harmonic period and reaches equilibrium. At equilibrium no displacement is possible. The frequency of the source vibration was 8 kHz.

The input displacement of the boundary condition was taken from the piezoelectric specifications. The specifics state that a free displacement condition will create a lateral displacement of 270 micrometers. The lateral displacement is assumed to occur at the free tip of the piezoelectric bender element.

The lateral displacements were extracted from selected nodes located along the centerline of the geometry. The vertical spacing of the extraction nodes were spaced at increments of two centimeters between the source and the receiver. The receiver extraction depth included two vertically adjacent nodes spaced 5.56mm for the purpose of measuring the strain field.

Shear strain is the suitable strain measurement for the propagation of the shear wave because a shear wave polarization is orthogonal to its propagation. The shear strain was calculated from the differential vertical displacement of two nodes spaced 5.56 mm apart. This distance represents the measured distance of one piezoelectric bender element length measured from its free tip to the polyurethane housing.

The mesh resolution exceeds the standard derived from previous experiments. The element length or the vertical spacing of the node used was equal to the shear wave length divided by 32.4. The mesh resolution is finer than the recommended mesh fineness of the shear wavelength divided by twenty. The time increment ratio used was 0.0005 s/m.

6.5.1. Abaqus model of the 12.1 cm Unsaturated Ticino Sand Test Results:

Figures 6.4 and 6.5 show the Abaqus dynamic implicit solution to the bender element test. The displacement field solution and the shear strain solution are superimposed on the actual measured field output of the oscilloscope. The amplitudes of the displacement field, strain field, and voltage are normalized.
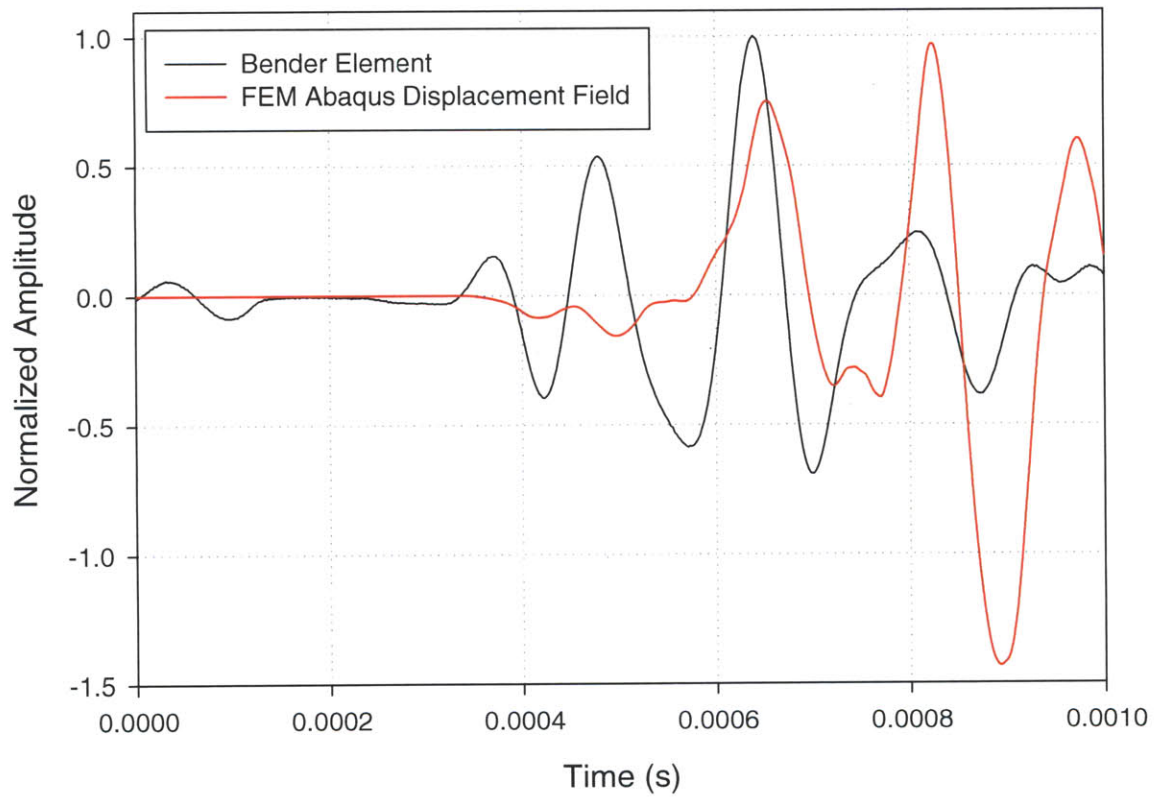
Figure 6.4: Normalized Lateral Displacement and Bender Element
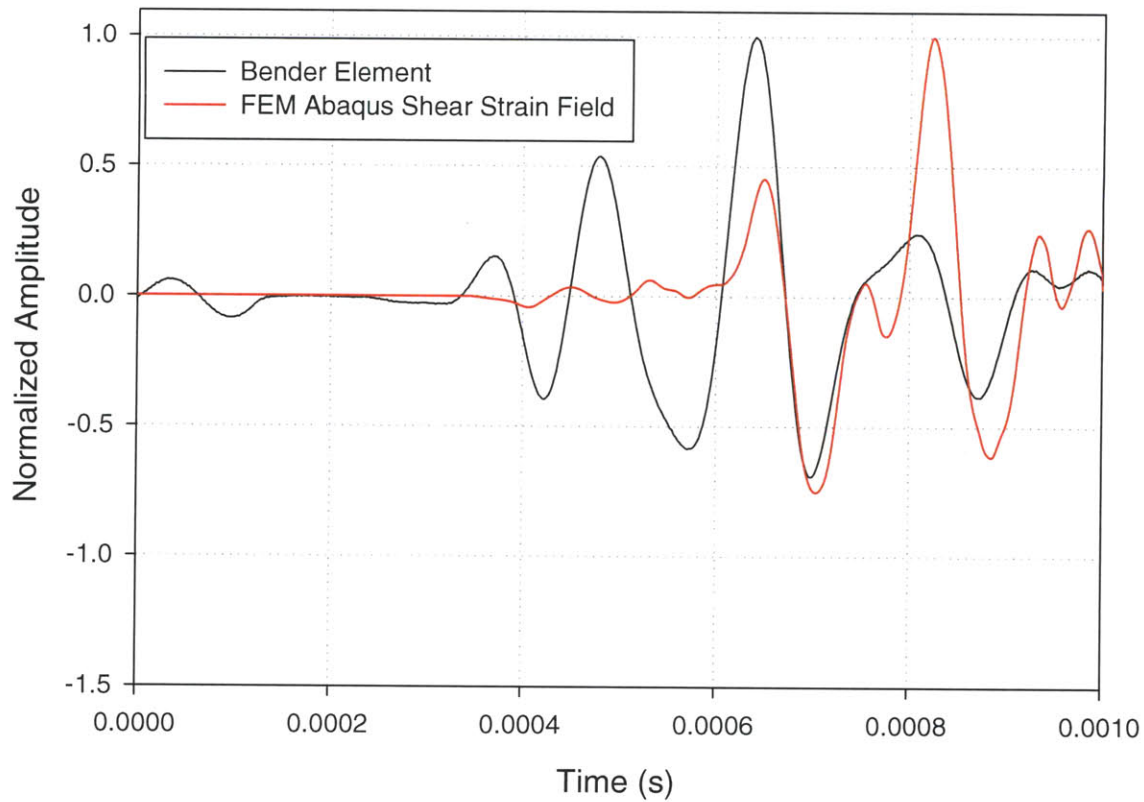
Figure 6.5: Normalized Shear Strain and Bender Element

The normalized displacement and shear field results from the dynamic implicit analysis show similar time-domain amplitude behavior to the oscilloscope data taken from the experimental bender element test. The signal shape from the oscilloscope and the numerical analysis produces a good fit from a domain after .6 ms. Before 0.6 ms noticeable discontinuities are apparent between the numerical analysis and the experimental data of the pre-shear arrival amplitudes. The asymmetric signal output can be explained by the limitations of modeling a three dimensional experimental bender element test using a two dimensional numerical analysis. However, the symmetry of the signals is satisfactory to continue the flowchart analysis.

The travel time of the bender element test shear wavefront and numerical analysis are not equal in Figure 6.4. Instead, there is an observable error. Figure 6.5 shows that the error is minimized in the shear strain field output signal. Moreover, in the damped simulations the error is near zero.

The error can be explained in the displacement field for the rigid model by recognizing that the numerical simulation is only an approximation of the actual wave propagation in the bender element test and not a prefect reproduction. The shear strain field produces a better approximation of the shear wave behavior using Abaqus Implicit Dynamic Analysis than the lateral displacement field.

6.6. Predicted Boundary Reflections

The lateral displacement signal captured by the receiver includes interference from the body wave reflections. The total effect of the body wave reflections represents a superposition of all possible ray paths of the P and S wavefront reflections from the model in a given time domain. The ray paths of the P and S waves can be calculated using simple geometry and the application of Snell's Law.

A wavefront is an imagined surface through all points of equal phase of the body wave. The ray path represents a scalar distance quantity with a defined oriented along the direction of the body wave propagation. The ray path is always normal to the surface of the wavefront. The ray path produces a scalar distance traveled of the wavefront. The travel time of the ray path is solved by taking the product of the distance scalar of the ray path and the velocity of the body plane wave. . In an axial bender element model the body waves travel planar down the specimen propagating radial from the source.

When any body wavefront strikes a boundary a reflected P-wave and a reflected S-wave will emerge. When a ray changes from S to P or from P to S it undergoes a change of velocity. If an incident P waves strikes the boundary then a slower S wave will reflect toward the horizontal. The S-wave is directed toward the horizontal because the ray path has an associated lower angle of reflection. Conversely, if the incident body wave has a velocity less than the reflected body wave, S to P, the, the ray is deflected toward the vertical. In seismology the angle between the incidence ray and the vertical is referred to as the angle of incidence and the angle between the reflected ray and the vertical is referred to as the angle of reflection.

The S-wave travels at a velocity less than the P-wave. The difference of the velocity between the P and S components of the body wave is a function of Poisson's Ratio of the media. The assumed Poisson's Ratio of the Ticino Sand was assumed to be 0.3. The ratio of the P-wave velocity to the S-wave velocity can be expressed:

$$\frac{Vc}{Vs} = \sqrt{\frac{(2 - 2\eta)}{(1 - 2\eta)}} = \sqrt{\frac{(2 - .6)}{(1 - .6)}} = 1.87$$

Therefore it is expected that the P-wavefront will propagate radial from the source at a velocity of 1.87Vs. Therefore it is necessary to compile all the possible ray paths a P-wavefront travels because the P-wave reflections will be captured at the receiver node during the time domain.

6.6.1. Predicted Boundary Reflections P-P

Consider the first scenario that represents an incident P-wave striking the lateral boundary and producing a reflection that arrives at the receiver. The diameter of the model is 0.075m
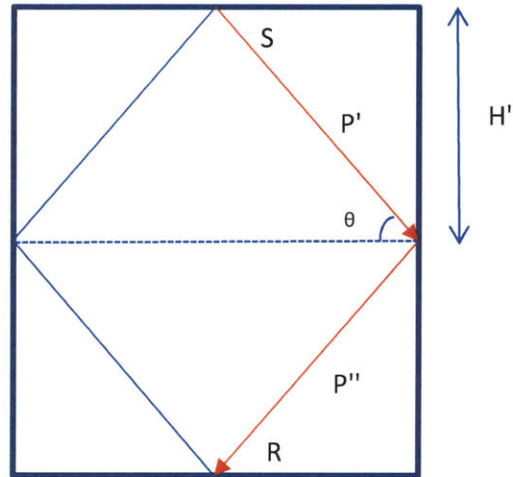
Figure 6.6: P-P Reflection

Here the incident P-wave is represented by P' and the reflected wave P''. Using Snells law:

$$\frac{sin\Theta}{Vp_{incidence}} = \frac{sin\Theta}{Vp_{reflection}}$$

$$Vp_{incidence} = Vp_{reflection} = Vs_{incidence} * 1.87 = 289.85\frac{m}{s}$$

$$H' = \frac{.09388}{2}m = 0.0469m$$

$$\theta = tan^{-1}\left(\frac{0.0469}{0.0375}\right) = 51.3°$$

Therefore,

$$ray\ path\ distance = d_r = 2 * \sqrt{0.0469^2 + 0.0375^2} = 0.120m$$

$$time\ of\ ray\ arrival = \frac{d_r}{Vp} = \frac{0.120m}{289.85\frac{m}{s}} = 0.000414s$$

6.6.2. Predicted Boundary Reflection P-P-P-P

Consider the second scenario that represents an incident P-wave striking the lateral boundary and producing a reflection that arrives at a depth one half to the receiver. The diameter of the model is 0.075m.
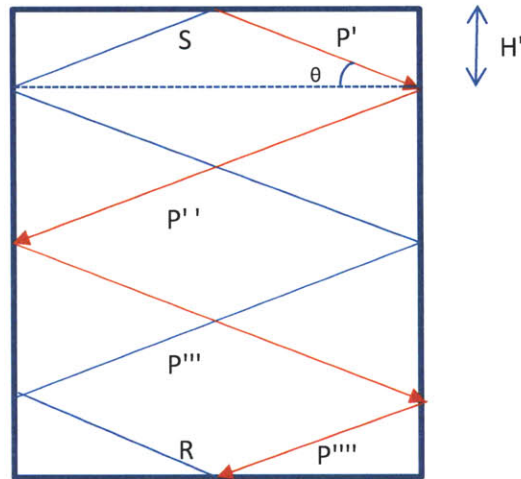
Figure 6.7: P-P-P-P Reflection

Here the incident P-wave is represented by P' and the reflected waves P'', P''', P''''. Using Snells law:

$$\frac{sin\Theta}{Vp_{incidence}} = \frac{sin\Theta}{Vp_{reflection}}$$

$$Vp_{incidence} = Vp_{reflection} = Vs_{incidence} * 1.87 = 289.85 \frac{m}{s}$$

$$H' = \frac{.09388}{6}m = 0.0156m$$

$$\theta = tan^{-1}\left(\frac{0.02345}{0.0375}\right) = 22.6°$$

Therefore,

$$ray\ path\ distance = d_r = 6 * \sqrt{0.02345^2 + 0.0375^2} = 0.244m$$

$$time\ of\ ray\ arrival = \frac{d_r}{Vp} = \frac{0.2659m}{289.85\frac{m}{s}} = 0.000891s$$

6.6.3. Predicted Boundary Reflection P-S

Consider the second scenario that represents an incident P-wave striking the lateral boundary and producing a S-wave reflection. The diameter of the model is 0.075m
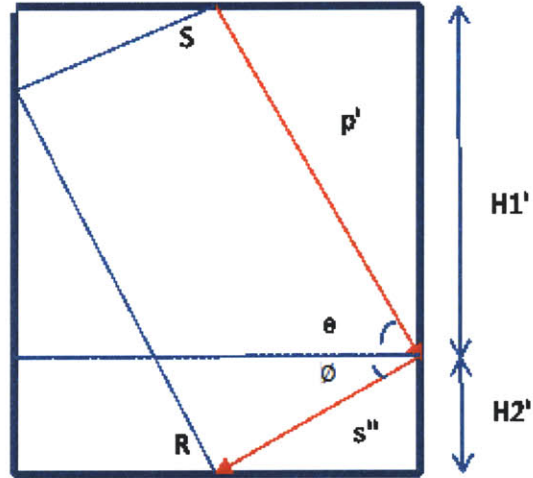
Figure 6.8: P-S Reflection

Here the incident P-wave is represented by P' and the reflected waves S''. Using Snells law:

$$\frac{sin\Theta}{Vp_{incidence}} = \frac{sin\emptyset}{Vs_{reflection}} = \frac{sin\Theta}{289.85\frac{m}{s}} = \frac{sin\emptyset}{155\frac{m}{s}}$$

$$Vp_{incidence} = 1.87 * Vs_{reflection} = 289.85\frac{m}{s}$$

$$H1' + H2' = 0.09388m$$

$$\theta = tan^{-1}\left(\frac{H1'}{0.0375}\right)$$

$$\emptyset = tan^{-1}\left(\frac{H2'}{0.0375}\right)$$

Therefore,

$$\frac{sin\left[tan^{-1}\left(\frac{H1'}{0.0375}\right)\right]}{c} = \frac{sin\left[tan^{-1}\left(\frac{0.09388 - H1'}{0.0375}\right)\right]}{155\frac{m}{s}}$$

$$H1' = 0.074m$$

223

$$H2' = 0.09388 - 0.074 = 0.01988m$$

$$time\ of\ ray\ arrival = \frac{\sqrt{0.074^2 + 0.0375^2}m}{289.85\frac{m}{s}} + \frac{\sqrt{0.01988^2 + 0.0375^2}m}{155\frac{m}{s}}$$

$$time\ of\ ray\ arrival = 0.000286s + 0.000274s = 0.000560s$$

6.6.4. Predicted Boundary Reflections Critical Angle Reflection, CR

When an S-wave reflects on a rigid boundary there is a theoretical incident angle that makes the sin of the angle of reflection for the wave equal to 1. This is known as the critical angle. The critical angle can be found from Snell's law by putting in an angle of 90° for the angle of the reflected P-wave.

The interface of the boundary must be capable of supporting a P-wave to traverse. The prescribed boundary only lateral constraints were applied on the boundary however the interface was free to move vertically. It is possible that a dilatational P-wave front can travel along the boundary interface. Therefore, it is possible that a critical angle arrival is received at the receiver.
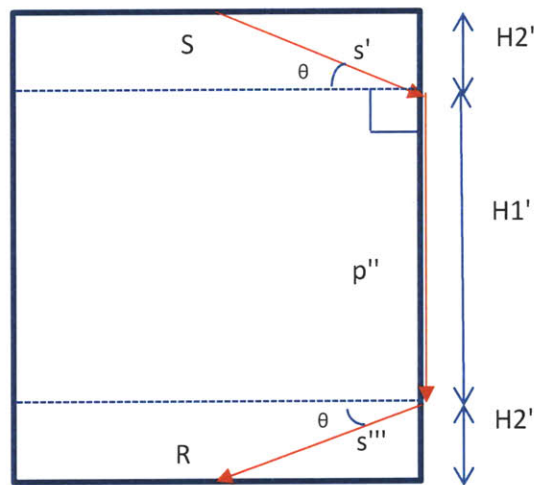
Figure 6.9: Critical Angle Reflection

$$\frac{sin\Theta}{Vs_{incidence}} = \frac{sin90}{Vp_{reflection}}$$

$$sin\Theta = \frac{Vs_{incidence}}{Vp_{reflection}} = \frac{155\frac{m}{s}}{289.85\frac{m}{s}}$$

A P-wave can never create a critical S-wave because the sin of any angle can never be greater than unity.

$$\Theta = sin^{-1}\left[\frac{155\frac{m}{s}}{289.85\frac{m}{s}}\right] = 32.3°$$

$H1' = 0.0938m - 2 * 0.0375m * tan(32.3°) = 0.0465m$

Therefore,

$$time\ of\ ray\ arrival = \frac{2\sqrt{0.024^2 + 0.0375^2}\,m}{155\frac{m}{s}} + \frac{0.0465m}{289.85\frac{m}{s}} = 0.000448s$$

6.6.5. Predicted Boundary Reflections P'

The geometry of the rod allows reflections occurring from the bottom boundary. Consider a scenario that represents an incident P-wave reflecting off the bottom boundary and striking the receiver. It is possible that a P-wave can produce lateral deformation from the Poisson effect. The material properties of the mesh require lateral deformations when vertically deformed. The diameter of the model is 0.075m.
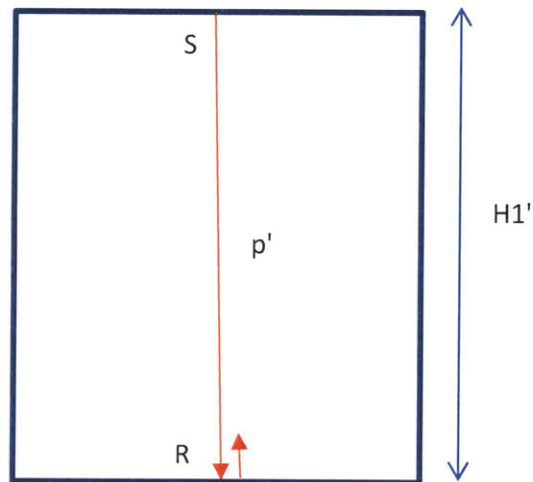
Figure 6.10: P' Reflection

Here the incident P-wave is represented by P' and the reflected wave P''. Using Snells law:

$$\frac{sin\Theta}{Vp_{incidence}} = \frac{sin\Theta}{Vp_{reflection}}$$

$$Vp_{incidence} = Vp_{reflection} = Vs_{incidence} * 1.87 = 289.85 \frac{m}{s}$$

$$H1' = \frac{.09388}{1} m = .09388m$$

$$\theta = 0°$$

Therefore,

$$ray\ path\ distance = .09388m + 0.00556m = .0994m$$

$$time\ of\ ray\ arrival = \frac{d_r}{Vp} = \frac{0.994m}{289.85\frac{m}{s}} = 0.00034s$$

6.6.6. Predicted Boundary Reflections Conclusions

The arrival times calculated using Snell's law in a rigid half space produces accurate predictions of the boundary reflection travel times. The travel time calculations for each mode of reflection are functions of the velocities of the body waves, the ratio of the radius of the model, and the distance between the source and receiver. It is possible to calculate expected reflection takes using the ray path travel distance in a confided uniaxial model.
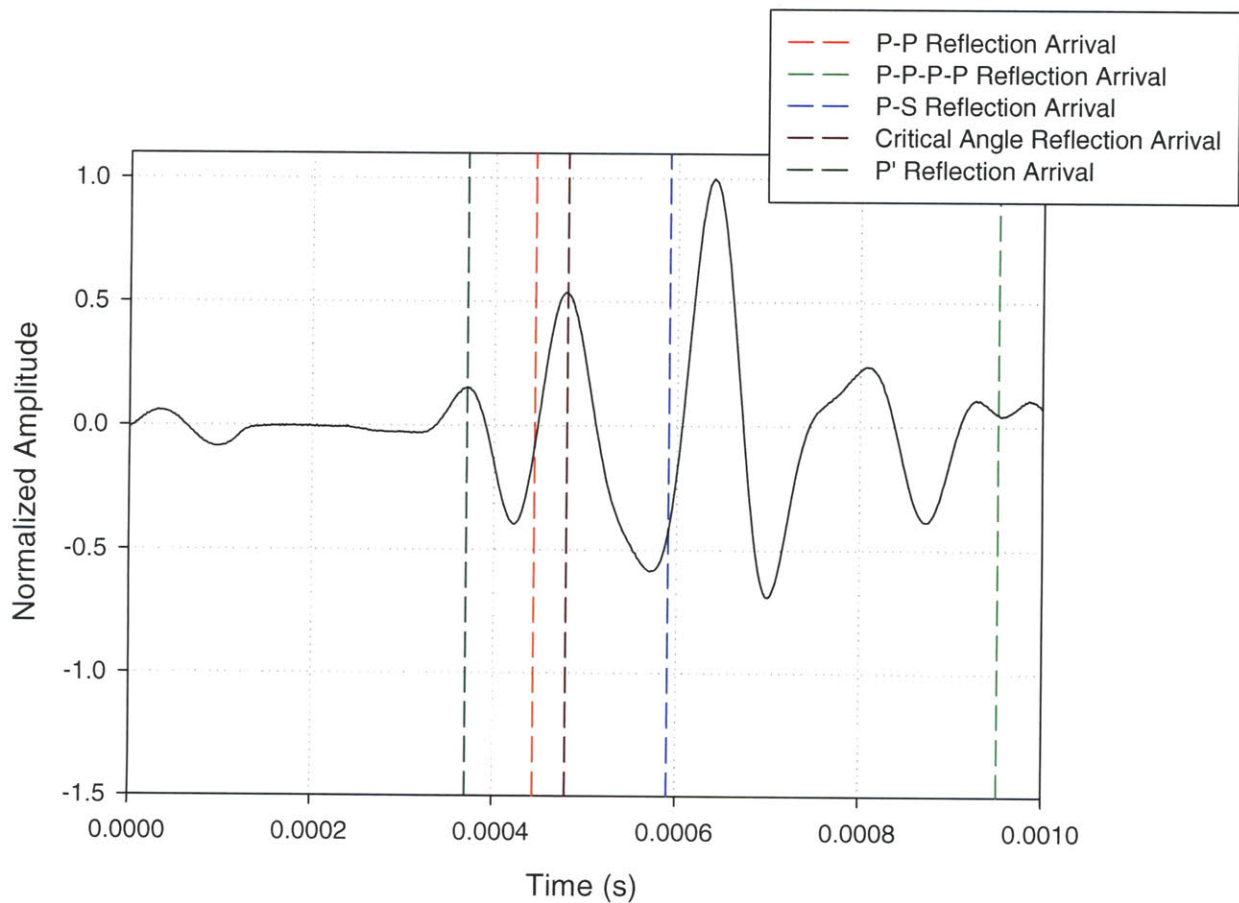
Figure 6.11: Reflection Conclusions

There is an overlap of arrival times produced from the calculated reflections during the interval of periodicity of the harmonic. The output signal captured by the digital oscilloscope is the superposition of all the possible reflections arriving at the source within a given time domain. The interference of the bodywave forms may be constructive, whereby the amplitude of the

reflected wave increases amplitude for the interference, or destructive whereby the observed amplitude is decreased or suppressed.

6. 7. Predicted Boundary Reflections Velocity Measurements

Peak to peak velocity measurements were taken on the field output and strain output of the rigid boundary model to investigate the relationship of the model rigid geometry to the measured shear velocity.
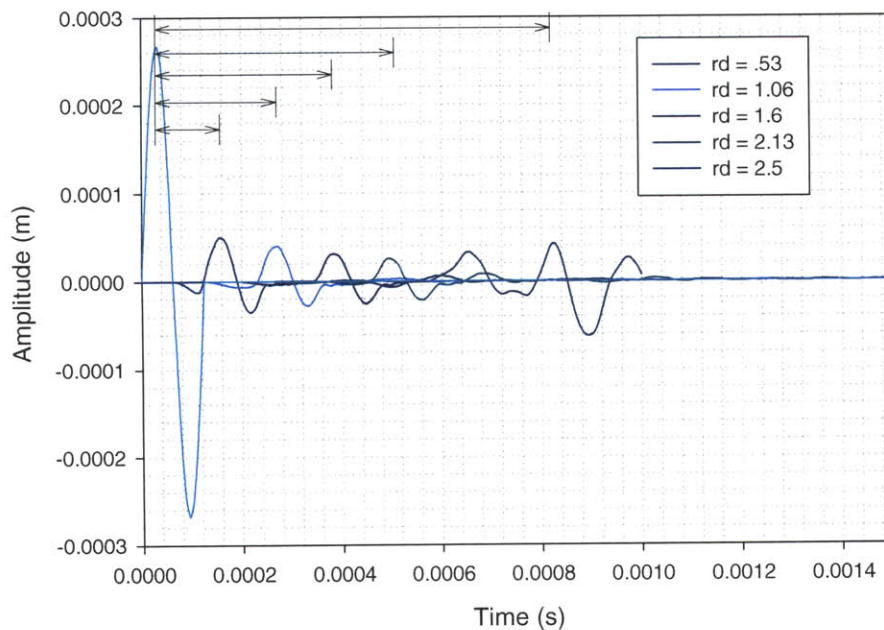
Figure 6.12: Travel Times; Various Rd

The superposition boundary reflection rays contribute to the shape of the observed displacement field and strain field. It is expected that the reflection rays may distort the true location of the shear wave front at the receiver when taking a velocity measurement. For this reason, the domain is expressed as a ratio of the distance between the source and receiver, d, and the radius of model, r. The radius is defined as the distance from the source harmonic to the rigid boundary in an axisymmetric space. This is called the geometric ratio.

The geometric ratio, rd, can be expressed

$$r_d = \frac{d}{r}$$
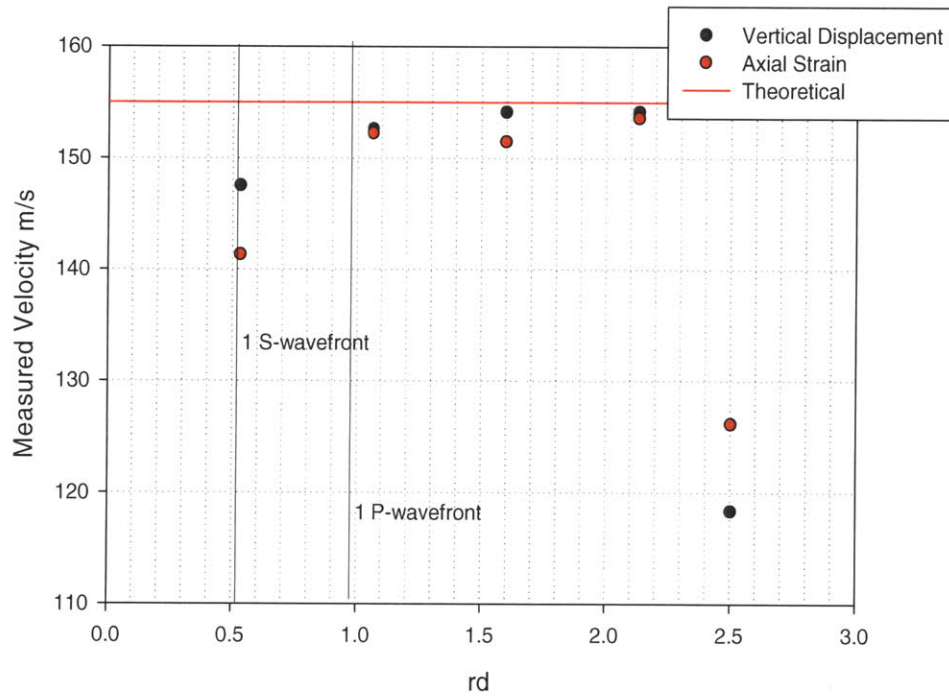
Figure 6.13: Velocity Conclusions

The sudden reduction in velocity at rd 2.5 contradicts a fundamental property of plane wave propagation; that the propagation velocity remains constant. In models simulating an infinite half space the observed peak to peak velocity was planar beyond one P-wavelength. Therefore, the jump of the measured peak to peak velocity must be a consequence of the rigid boundary. The amplitude of the reflected waveform exceeds the amplitude of the actual S-wave and therefore the travel time calculation becomes a function of the reflected waveform at a geometric ratio of

2.5. At a geometric ratio of 2.5 the measured velocity corresponds to the measured velocity of a reflected waveform and not the actual S-wave.
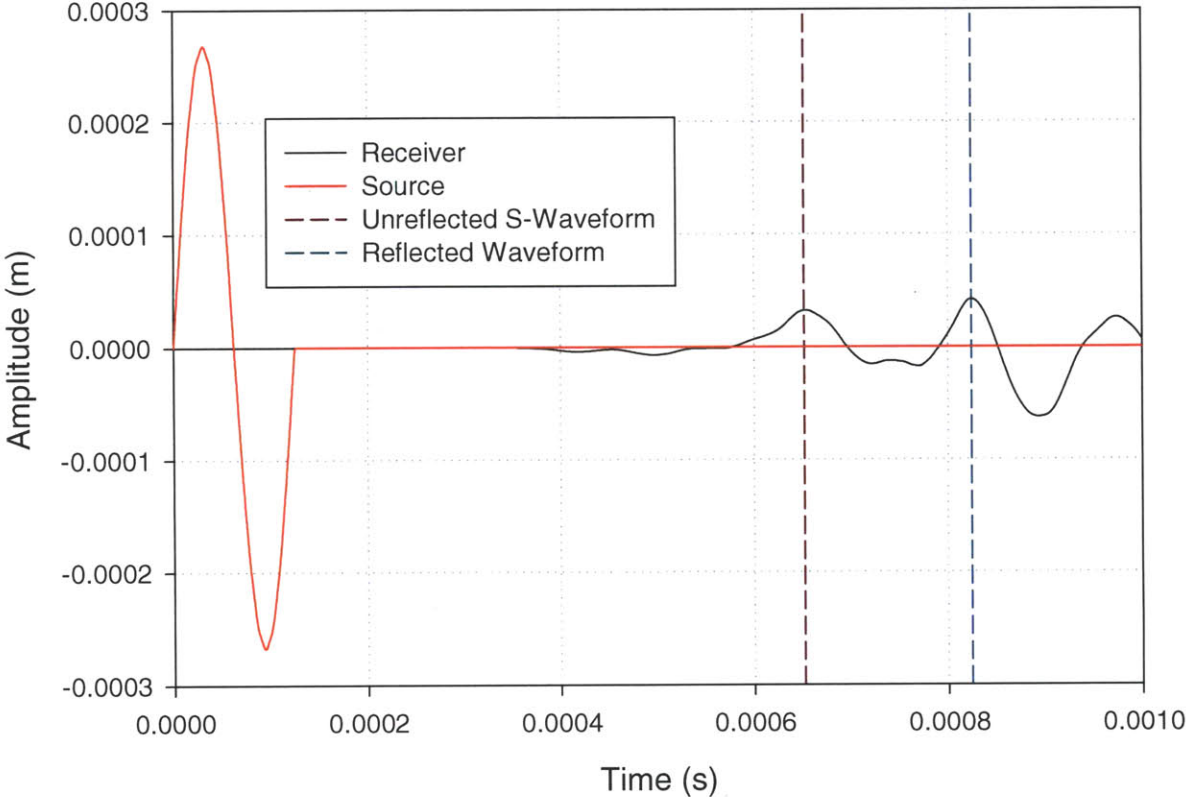
Figure 6.14: Travel Time: Rd = 2.5

Figure 6.14 demonstrates that there is a clear distortion of the measured peak to peak velocity as the model ratio, rd, approaches 2.5. Therefore, it is recommended in a rigid boundary simulation to have the source receiver distance less than a rd of 2.5. Furthermore, to avoid the near field affect a source receiver distance greater than 2 S-wave lengths for a shear wave velocity bender test.

6.8. Abaqus model of the 12.1 cm Unsaturated Ticino Sand Infinite Half-Space

A two dimensional elastic and isotropic model was constructed with identical material properties and geometry as the rigid boundary model. Dampers were applied to the lateral boundaries of the

model to eliminate the effect of reflections the of brass sleeve in the field output. The dampers represent fictitious forces applied at the lateral boundary to simulate an infinite continuum of elements.

The geometry of the rod allows reflections occurring from the bottom boundary. Vertical and lateral constraints were fixed to the bottom corners of the model to prevent rigid boundary motion. These constraints were modeled as pins.

A displacement boundary condition was applied along the center at a depth of one bender element length. The displacement condition is sinusoidal harmonic motion. The displacement boundary condition oscillates one harmonic period and reaches equilibrium. At equilibrium no displacement is possible. The frequency of the source vibration was 8 kHz.

The input displacement of the boundary condition was taken from the piezoelectric specifications. The specifics state that a free displacement condition will create a lateral displacement of 270 micrometers. The lateral displacement is assumed to occur at the free tip of the piezoelectric bender element.

The lateral displacements were extracted from selected nodes located along the centerline of the geometry. The vertical spacing of the extraction nodes were spaced at increments of two centimeters between the source and the receiver. The receiver extraction depth included two vertically adjacent nodes spaced 5.56mm for the purpose of measuring the strain field.

Shear strain is the suitable strain measurement for the propagation of the shear wave because a shear wave polarization is orthogonal to its propagation. The shear strain was calculated from the differential vertical displacement of two nodes spaced 5.56 mm apart. This distance represents the measured distance of one piezoelectric bender element length measured from its free tip to the polyurethane housing.

The mesh resolution exceeds the standard derived from previous experiments. The element length or the vertical spacing of the node used was equal to the shear wave length divided by 32.4. The mesh resolution is finer than the recommended mesh fineness of the shear wavelength divided by twenty. The time increment ratio used was 0.0005 s/m.

Figure 6.15: Normalized Damped Lateral Displacement and Bender Element
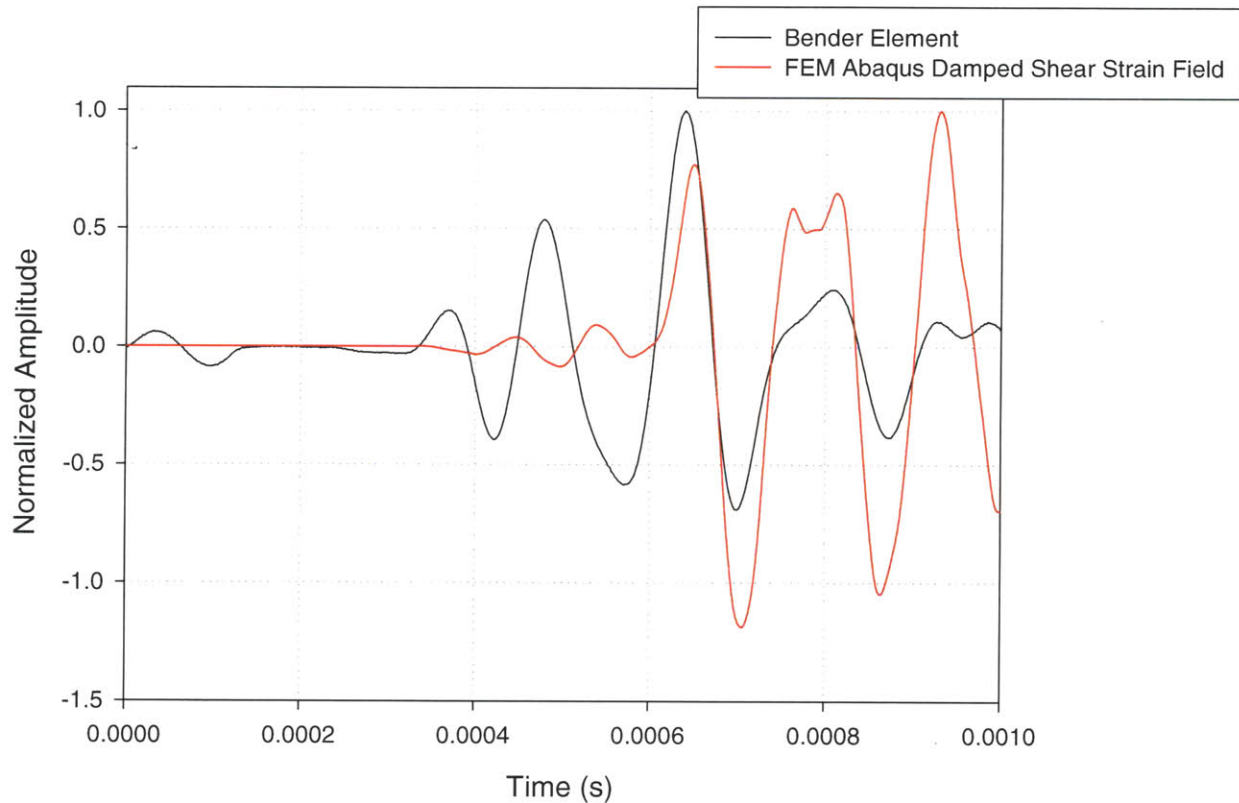
Figure 6.16: Normalized Damped Shear Strain and Bender Element

The damped Abaqus Implicit Dynamic simulation produces a better representation of the bender element signal shape than the rigid boundary model. Specifically, the normalized amplitude of the positive and negative phases of the shear arrival are better conserved than the undamped model. The rigid boundary model had noticeable asymmetric behavior in the arrival amplitudes, while the damped model conserves symmetric with the bender element test. It is recommended to use a damped model to analyze the true shear wave front in a bender element test.

The normalized displacement and shear field results from the dynamic implicit analysis show similar time-domain amplitude behavior to the oscilloscope data after 0.6 ms. The prearrival shear reflections are effectively damped in this model therefore, they are suppressed in the strain and displacement fields. After 0.6 ms, the bender element amplitude field and the numerical analysis have similar signal shapes. The damped displacement field is a better representative of the bender element oscilloscope data than the damped shear strain field.

Figure 6.17 Results: Received Signal of Bender Element Testing in Unsaturated Ticino Sand Specimens and FEM Experimental Model.

Unsaturated Ticino Sand 0.0125m Received Experimental Signal

Unsaturated Ticino Sand 0.0297m Received Experimental Signal
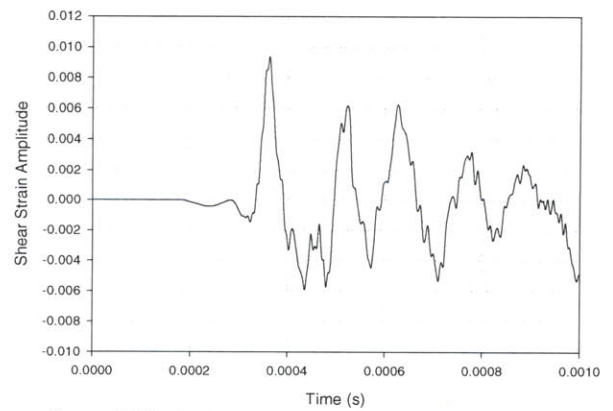

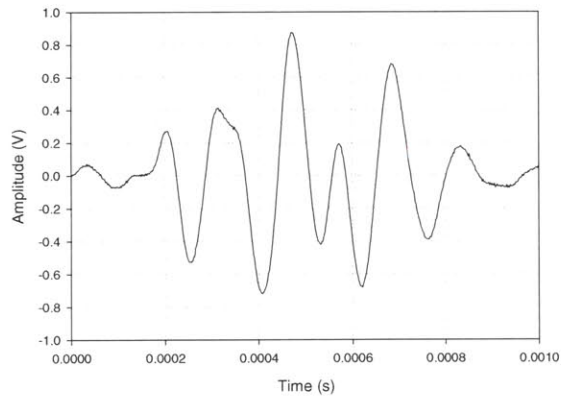Unsaturated Ticino Sand 0.0125m FEM Analysis Prediction using Lateral Displacements

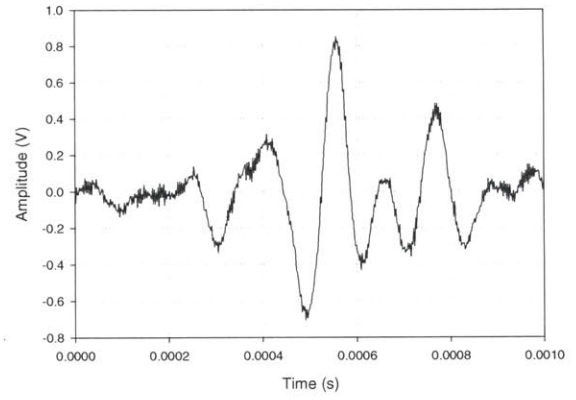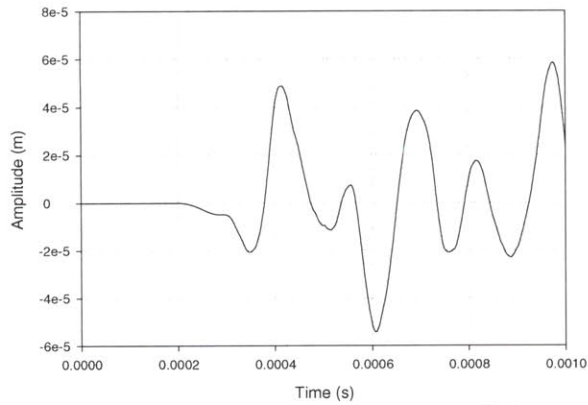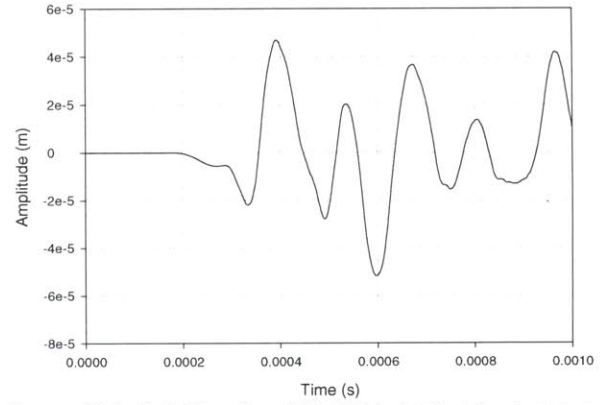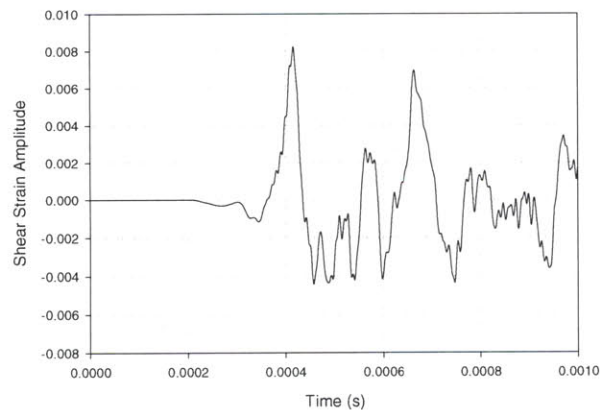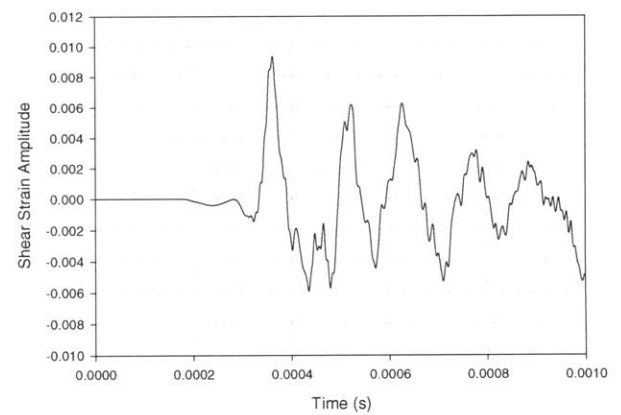Unsaturated Ticino Sand 0.0297m FEM Analysis Prediction using Lateral Displacements

Unsaturated Ticino Sand 0.0125m FEM Analysis Prediction using Shear Strain

Unsaturated Ticino Sand 0.0297m FEM Analysis Prediction using Shear Strain

236
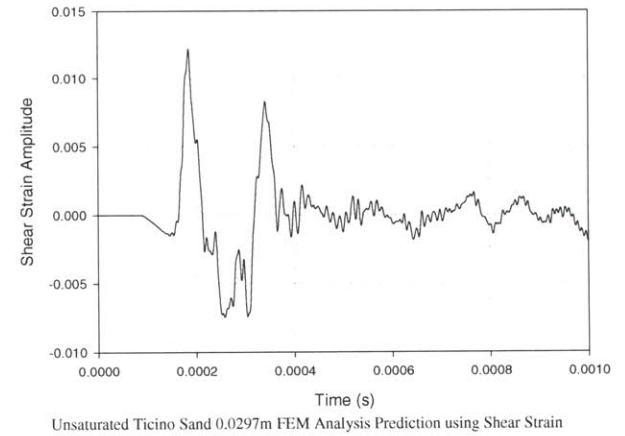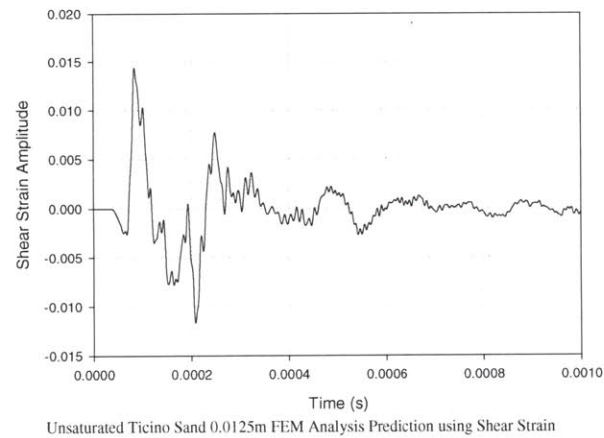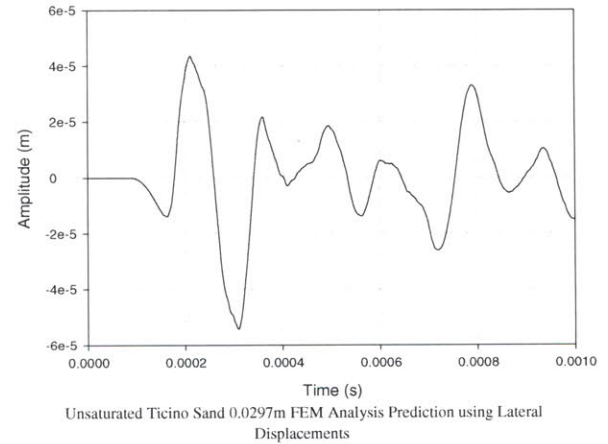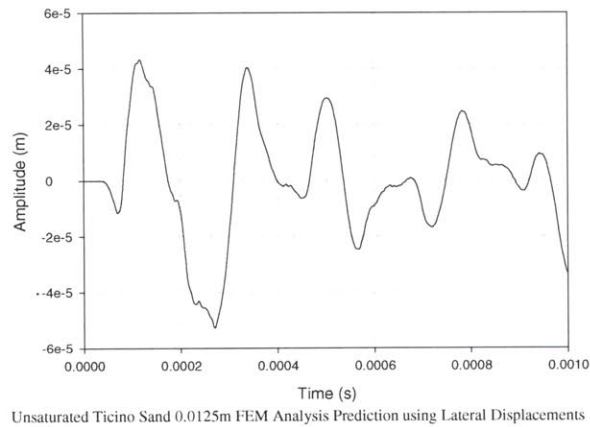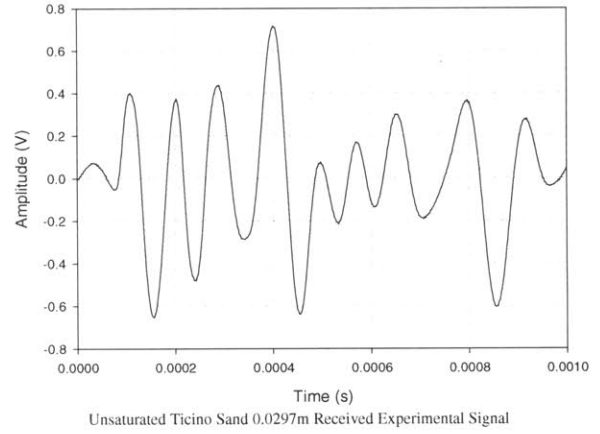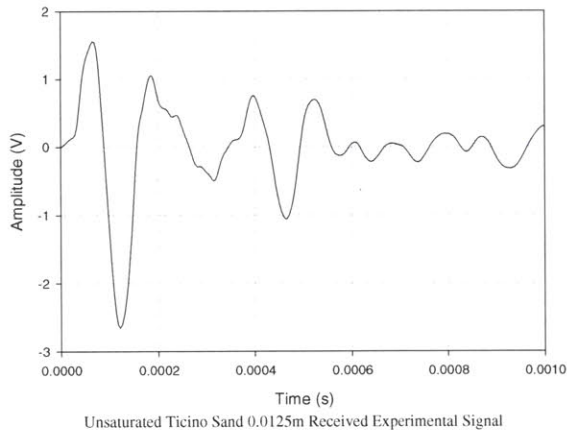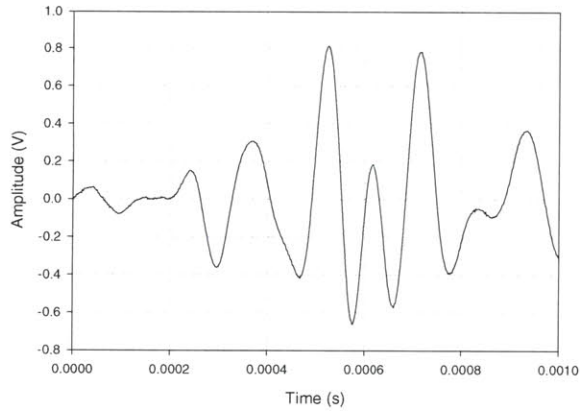
Unsaturated Ticino Sand 0.074m Received Experimental Signal

Unsaturated Ticino Sand 0.06m Received Experimental Signal
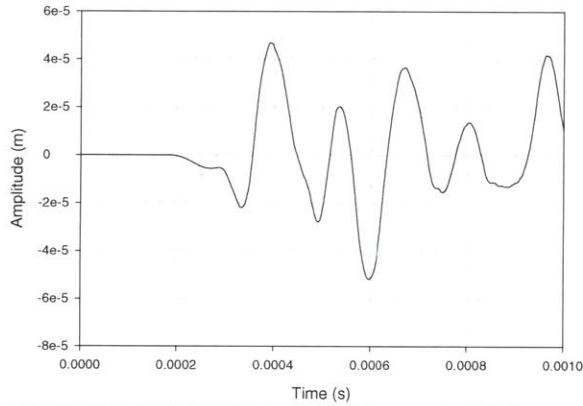
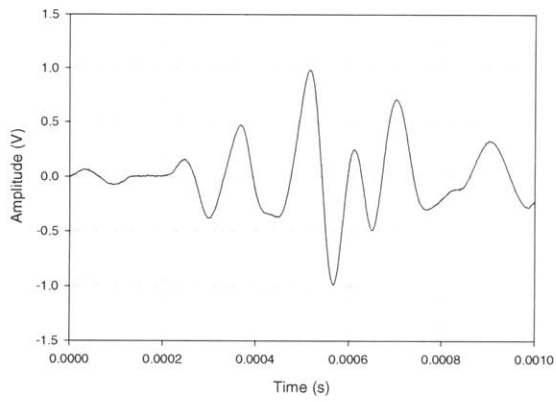Unsaturated Ticino Sand 0.074m FEM Analysis Prediction using Lateral Displacements
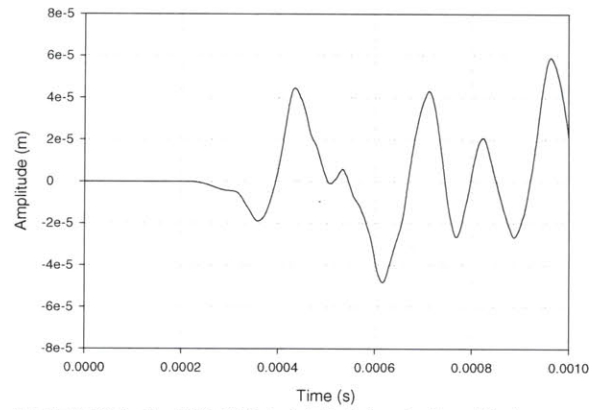
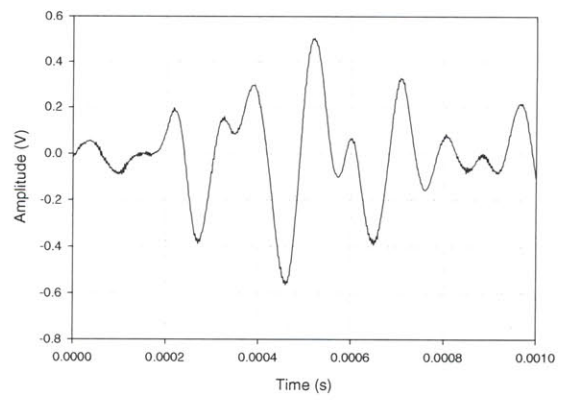Unsaturated Ticino Sand 0.06m FEM Analysis Prediction using Lateral Displacements
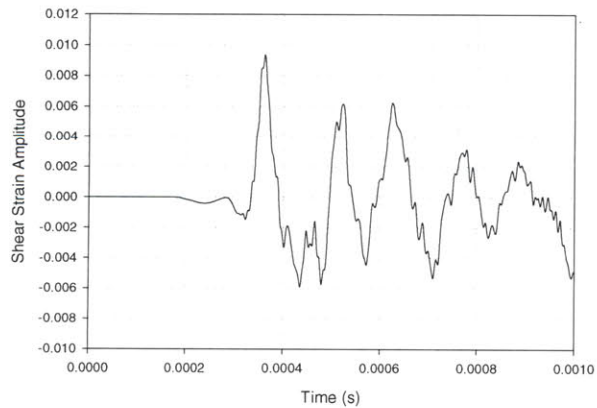
Unsaturated Ticino Sand 0.074m FEM Analysis Prediction using Shear Strain
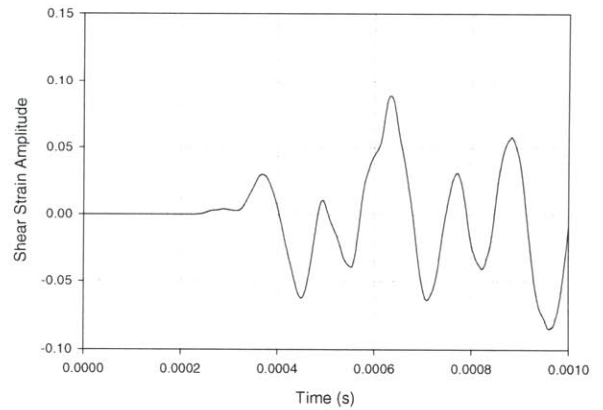
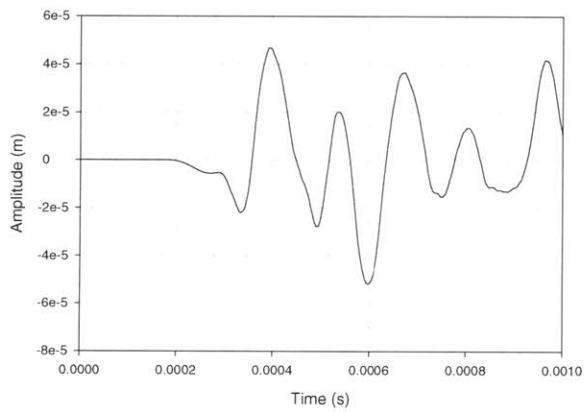Unsaturated Ticino Sand 0.06m FEM Analysis Prediction using Shear Strain
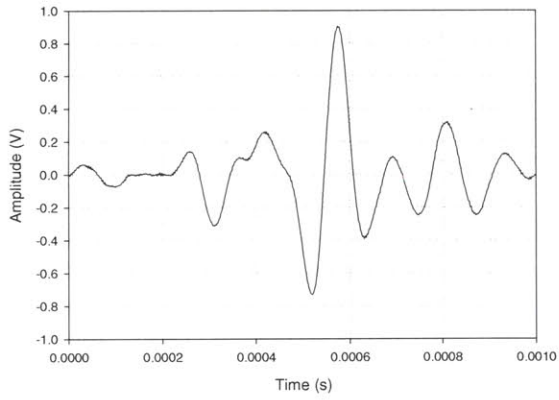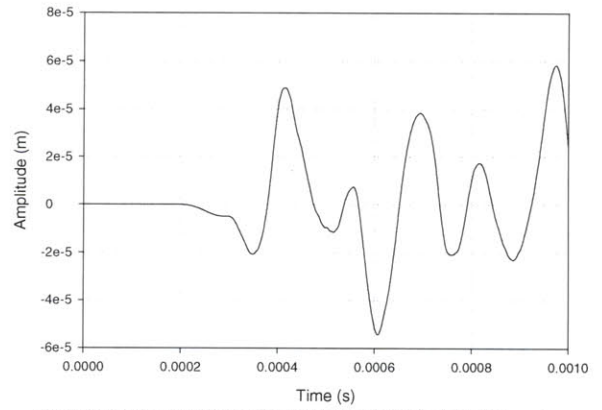
Unsaturated Ticino Sand w/ Paper Sleeve 0.0737m Received Experimental Signal
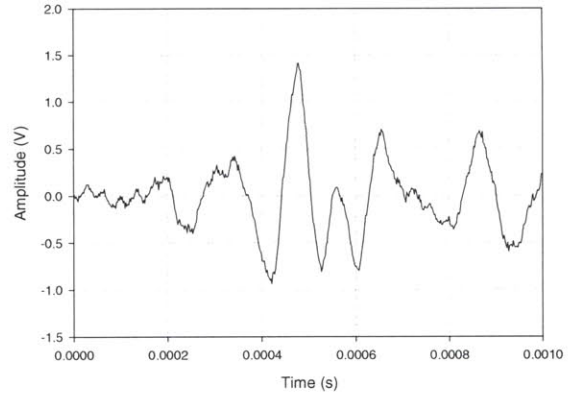
Unsaturated Ticino Sand w/ Paper Sleeve 0.059m Received Experimental Signal
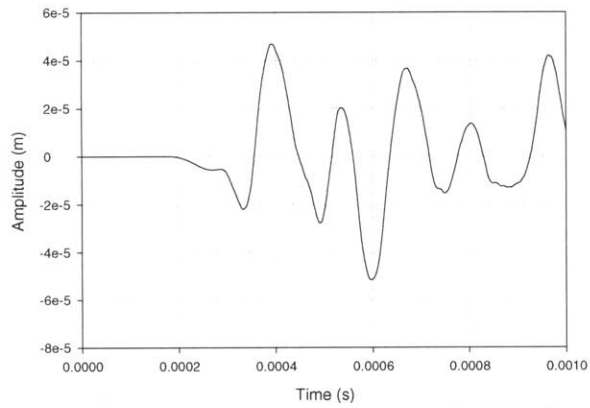
Unsaturated Ticino Sand w/ Paper Sleeve 0.0737m FEM Analysis Prediction using Lateral Displacements
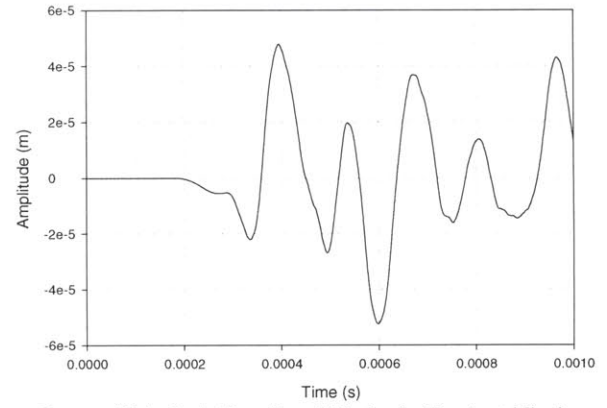
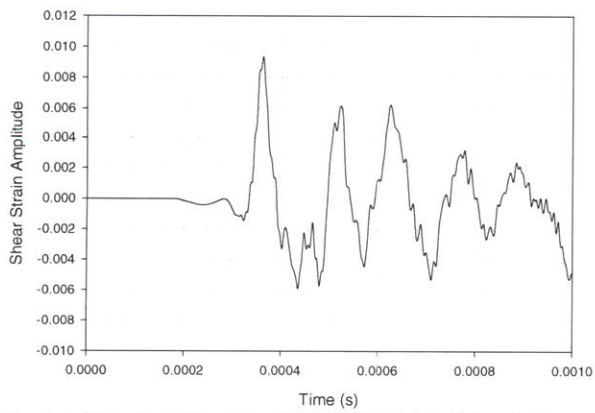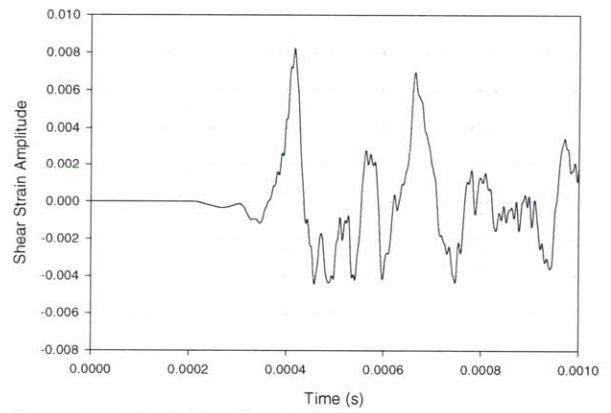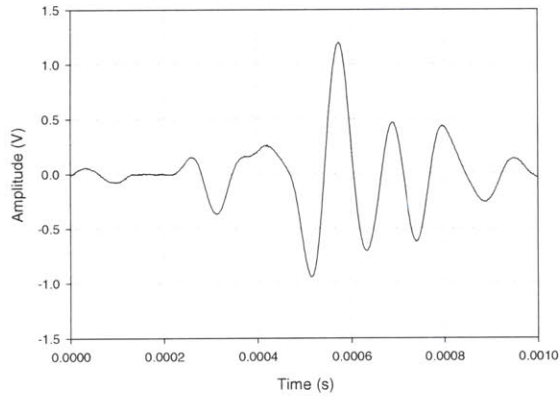
Unsaturated Ticino Sand w/ Paper Sleeve 0.059m Received Experimental Signal
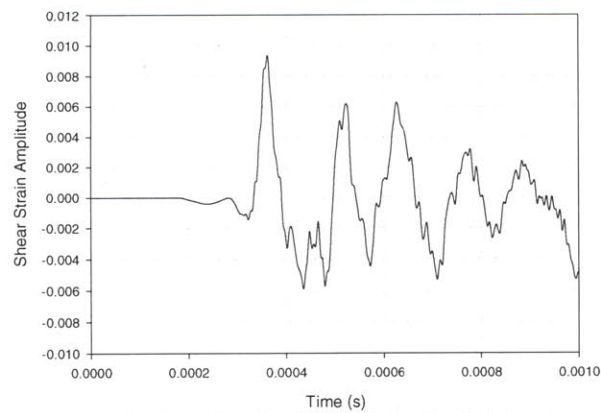
Unsaturated Ticino Sand w/ Paper Sleeve 0.0737m FEM Analysis Prediction using Shear Strain
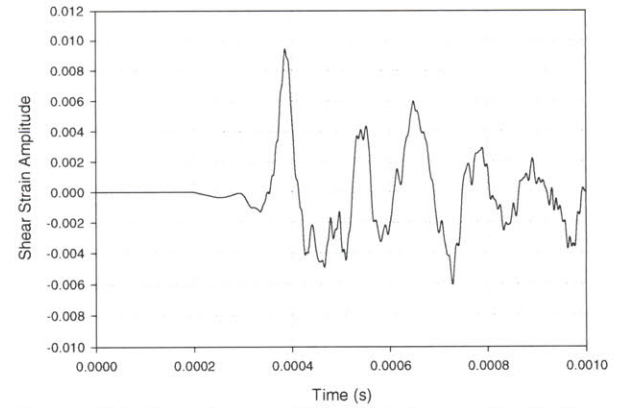
Unsaturated Ticino Sand w/ Paper Sleeve 0.059m FEM Analysis Prediction using Shear Strain

238
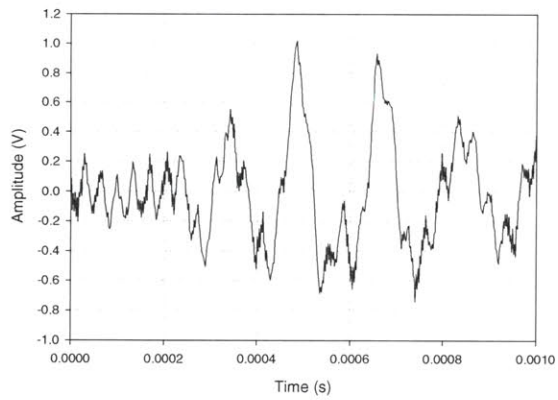
Unsaturated Ticino Sand 0.066m Received Experimental Signal
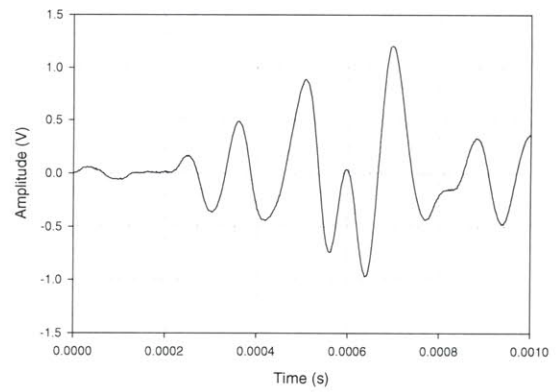
Unsaturated Ticino Sand 0.074m Received Experimental Signal

Unsaturated Ticino Sand 0.066m FEM Analysis Prediction using Lateral Displacements

Unsaturated Ticino Sand 0.074m FEM Analysis Prediction using Lateral Displacements

Unsaturated Ticino Sand 0.066m FEM Analysis Prediction using Shear Strain

Unsaturated Ticino Sand 0.074m FEM Analysis Prediction using Shear Strain

239
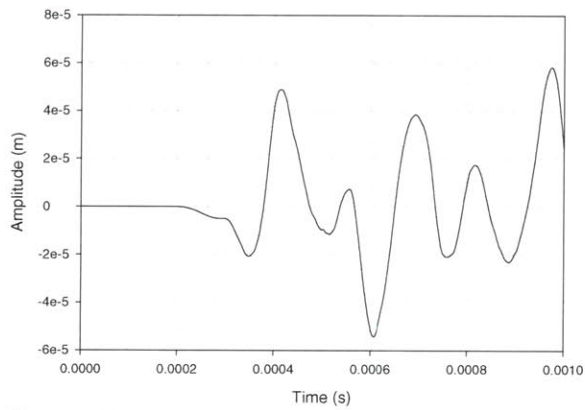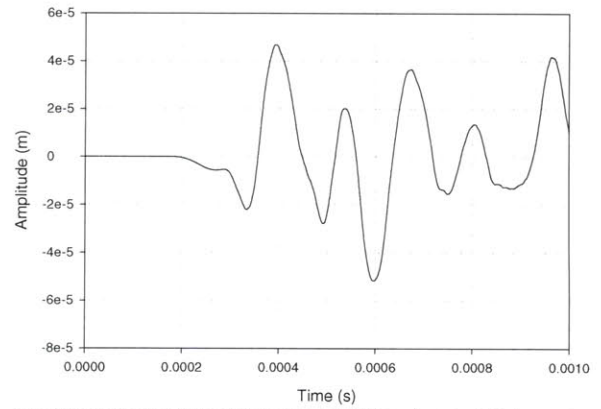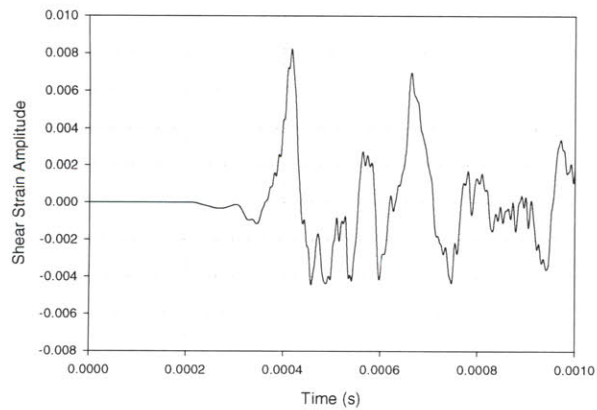
Unsaturated Ticino Sand 0.067m Received Experimental Signal

Unsaturated Ticino Sand w/ Paper Sleeve 0.076m Received Experimental Signal

Unsaturated Ticino Sand 0.067m FEM Analysis Prediction using Lateral Displacements

Unsaturated Ticino Sand w/ Paper Sleeve 0.076m FEM Analysis Prediction using Lateral Displacements
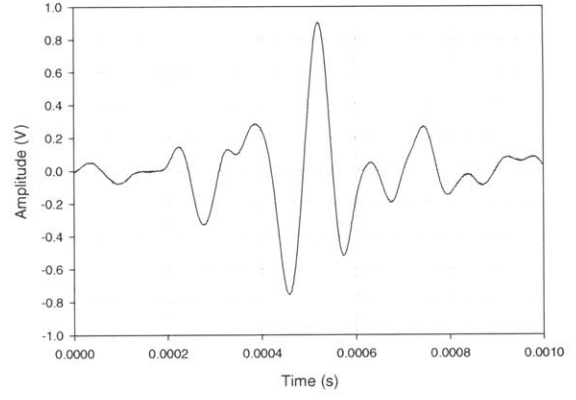

Unsaturated Ticino Sand 0.067m FEM Analysis Prediction using Shear Strain

Unsaturated Ticino Sand w/ Paper Sleeve 0.076m FEM Analysis Prediction using Shear Strain

240

Unsaturated Ticino Sand w/ Paper Sleeve 0.074m Received Experimental Signal

Unsaturated Ticino Sand w/ Paper Sleeve 0.067m Received Experimental Signal

Unsaturated Ticino Sand w/ Paper Sleeve 0.074m FEM Analysis Prediction using Lateral Displacements

Unsaturated Ticino Sand w/ Paper Sleeve 0.067m FEM Analysis Prediction using Lateral Displacements

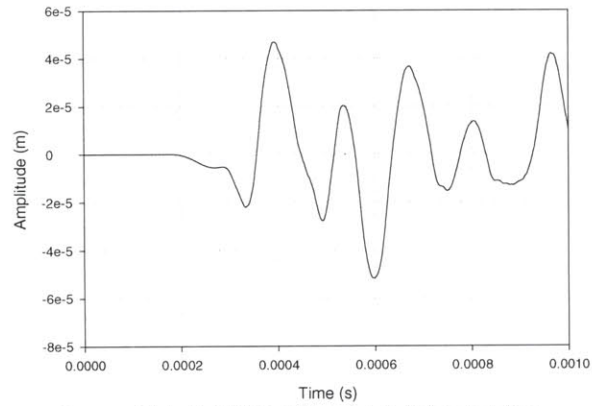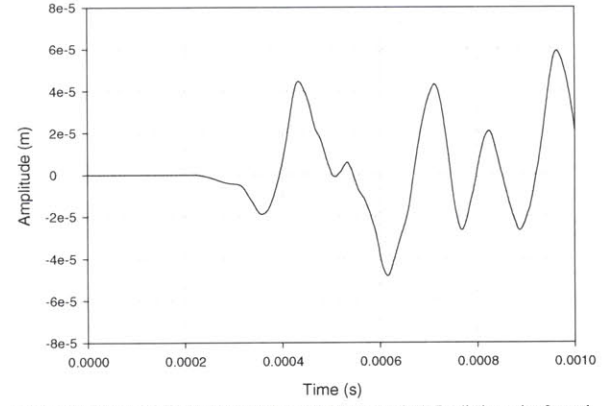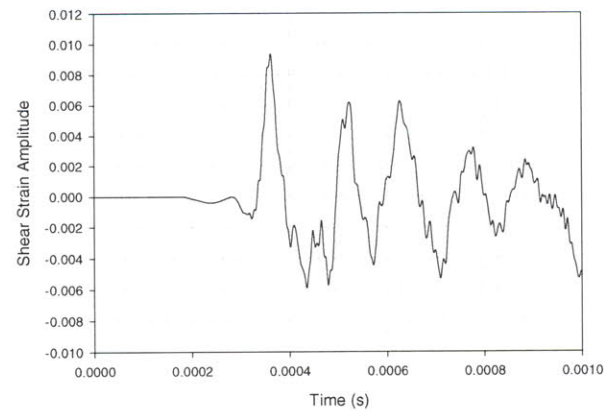Unsaturated Ticino Sand w/ Paper Sleeve 0.074m FEM Analysis Prediction using Shear Strain

Unsaturated Ticino Sand w/ Paper Sleeve 0.067m FEM Analysis Prediction using Shear Strain

241

Unsaturated Ticino Sand 0.0739m Received Experimental Signal

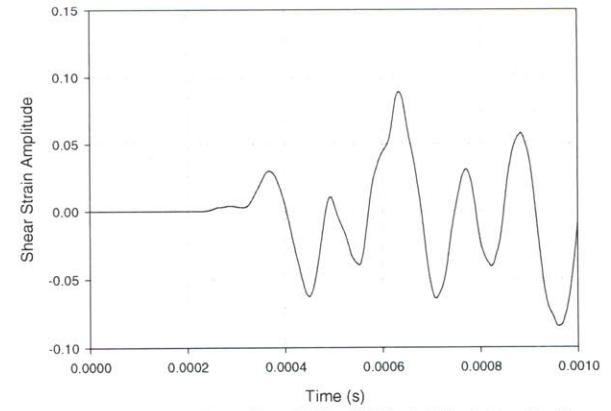Unsaturated Ticino Sand w/ Paper Sleeve 0.070m Received Experimental Signal

Unsaturated Ticino Sand 0.0739m FEM Analysis Prediction using Lateral Displacements
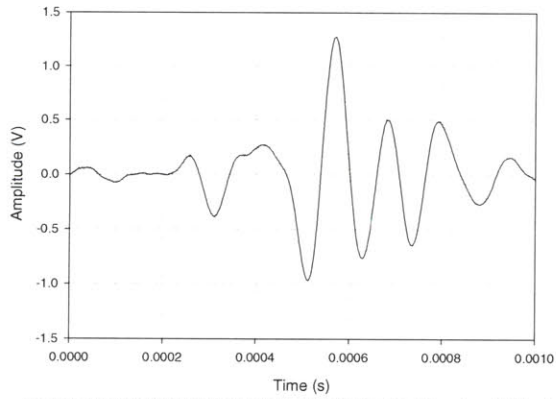

Unsaturated Ticino Sand w/ Paper Sleeve 0.070m FEM Analysis Prediction using Lateral Displacements
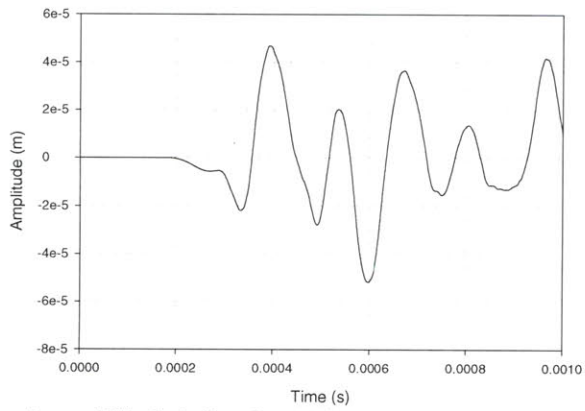

Unsaturated Ticino Sand 0.0739m FEM Analysis Prediction using Shear Strain
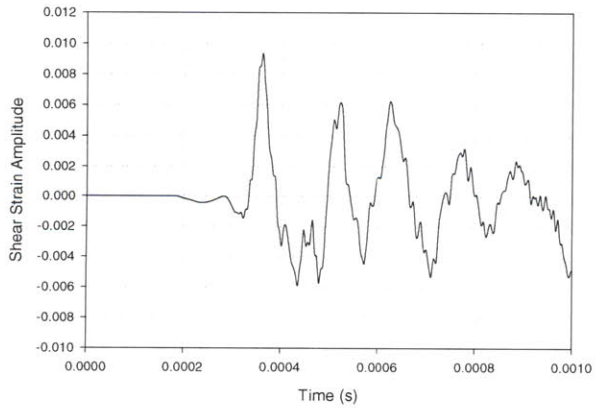

Unsaturated Ticino Sand w/ Paper Sleeve 0.070m FEM Analysis Prediction using Shear Strain

Unsaturated Ticino Sand w/ Paper Sleeve 0.0739m Received Experimental Signal
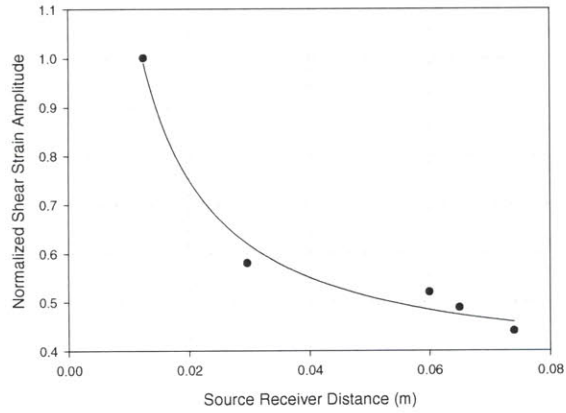

Unsaturated Ticino Sand w/ Paper Sleeve 0.0739m FEM Analysis Prediction using
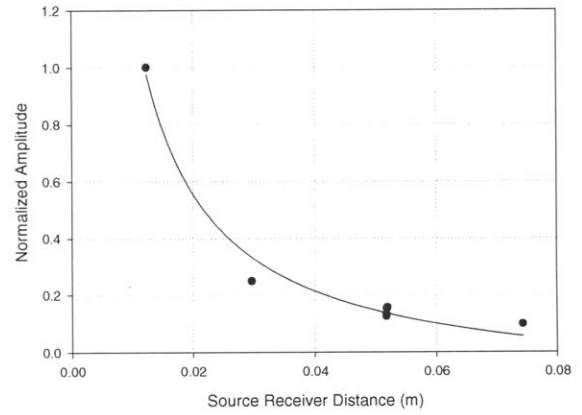Lateral Displacements

Unsaturated Ticino Sand w/ Paper Sleeve 0.0739m FEM Analysis Prediction using Shear
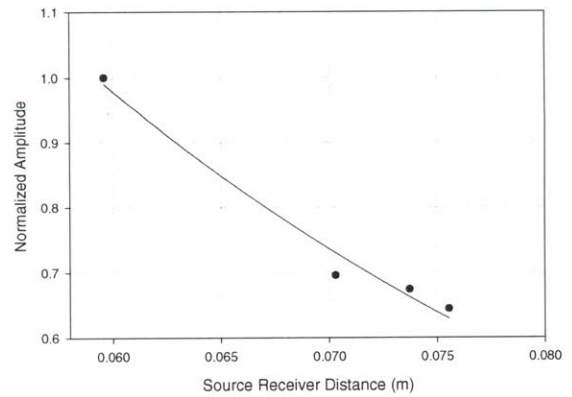Strain

Figure 6.18: Results: Attenuations of Bender Element Testing in Unsaturated Ticino Sand Specimens and FEM Experimental Model.

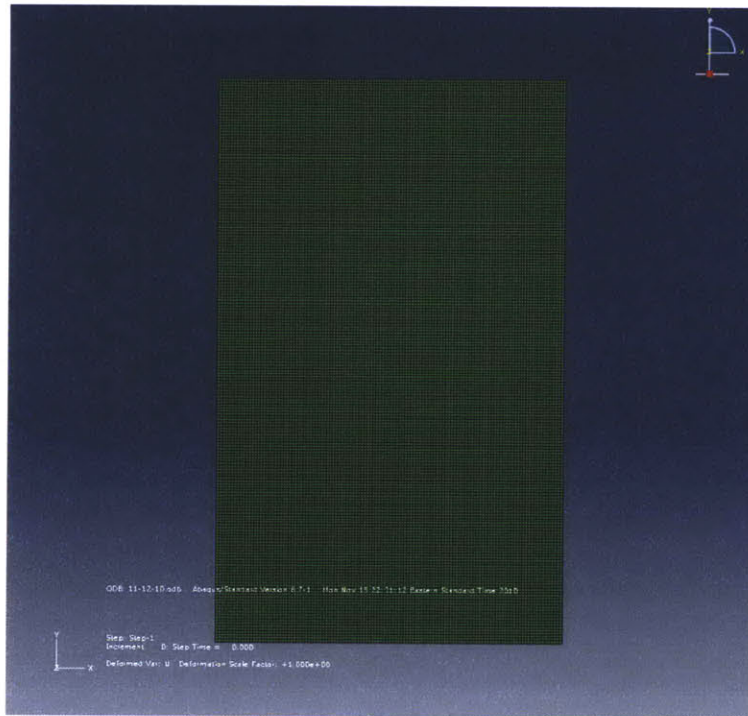FEM Predicted Shear Strain Attenuation of Ticino Sand

Experimental Attenuation of Ticino Sand using the Bender Element Technique

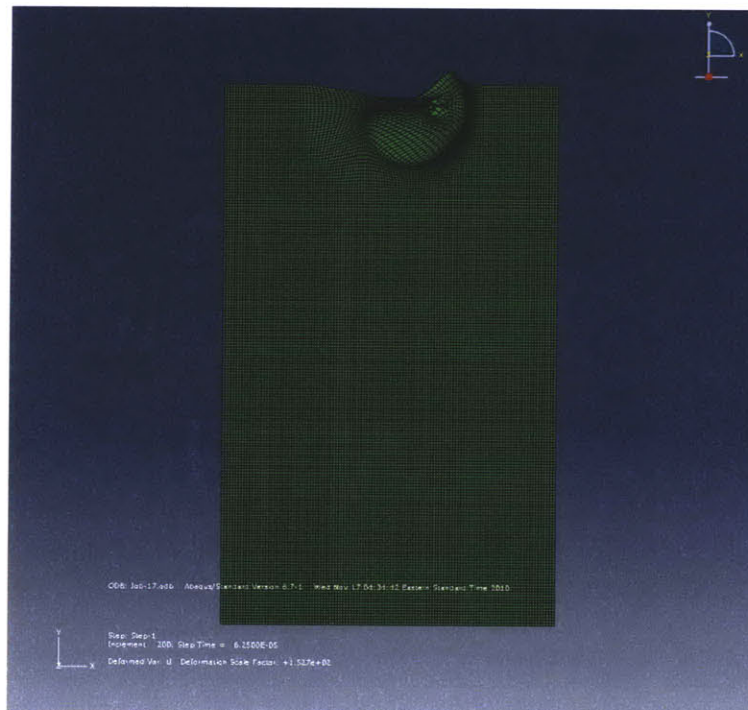Experimental Attenuation of Ticino Sand using the Bender Element Technique with paper inserts

Figure 6.19: Graphical Representation of Unsaturated Ticino Sand Model Damped Lateral Boundary

t=0 secs into Analysis. Automatic Scale Factor

t=6.25E-5 secs into Analysis. Automatic Scale Factor

t=1.25E-4 secs into Analysis. Automatic Scale Factor

t=1.875E-4 secs into Analysis. Automatic Scale Factor

t=2.5E-4 secs into Analysis. Automatic Scale Factor

t=3.125E-4 secs into Analysis. Automatic Scale Factor

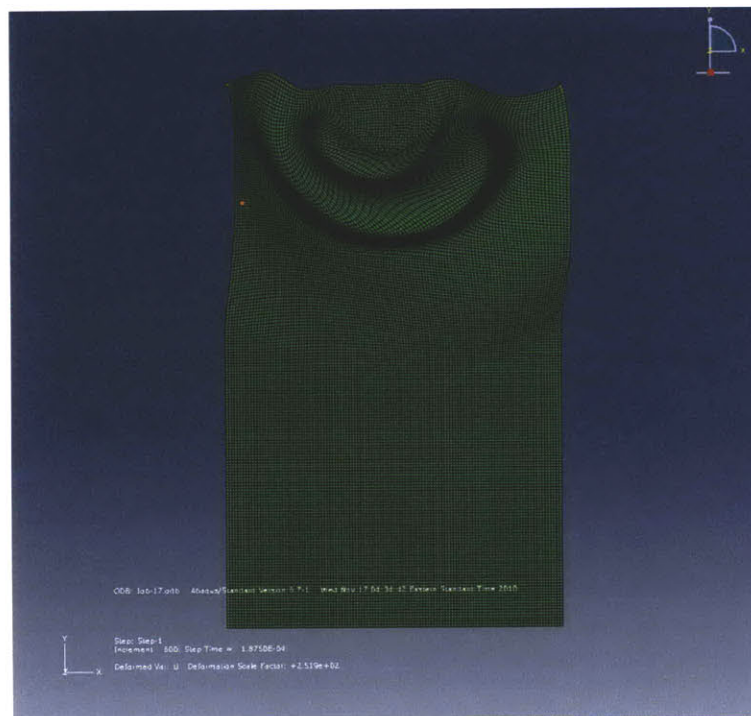**Figure 6.20: Graphical Representation of Dry Ticino Sand Model Rigid Lateral Boundary**

t=0 secs into Analysis. Automatic Scale Factor

t=6.25E-5 secs into Analysis. Automatic Scale Factor

t=1.25E-4 secs into Analysis. Automatic Scale Factor

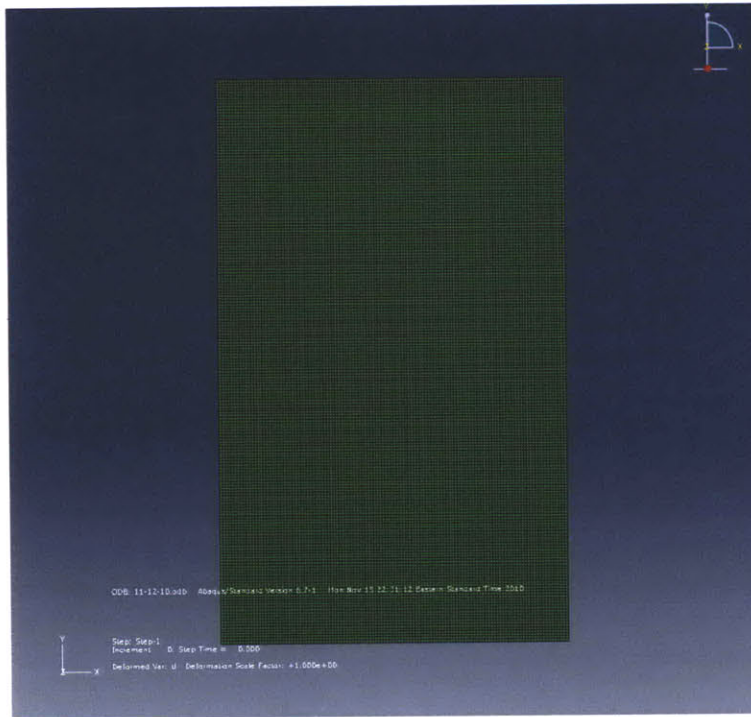t=1.875E-4 secs into Analysis. Automatic Scale Factor
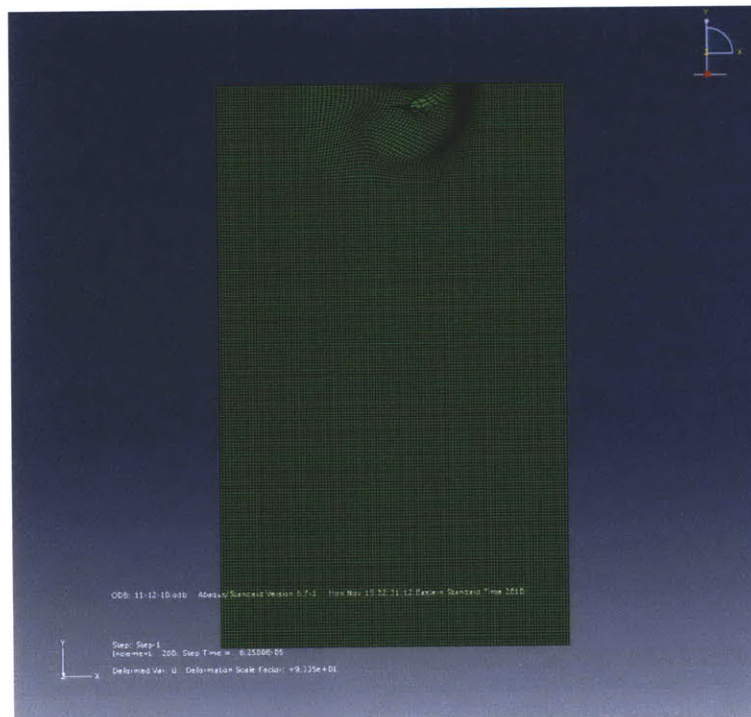
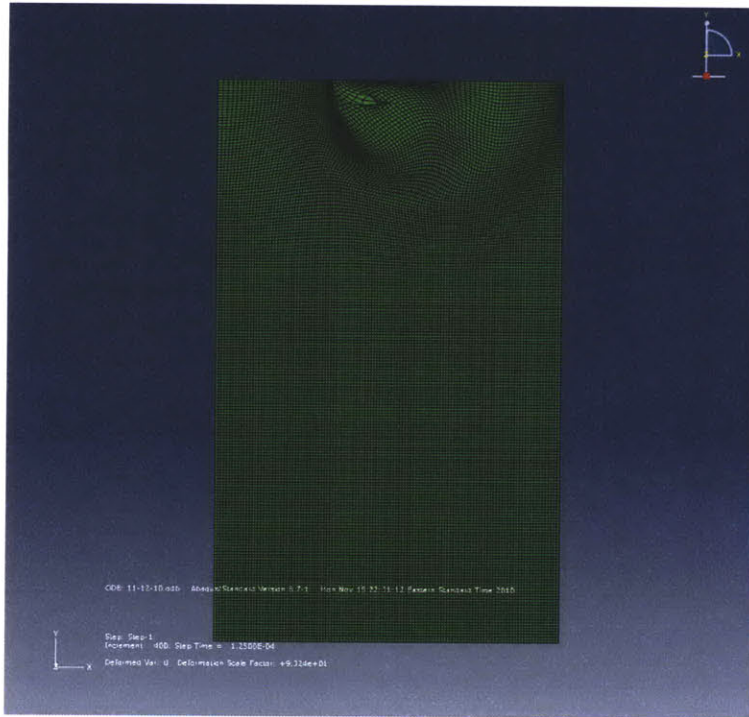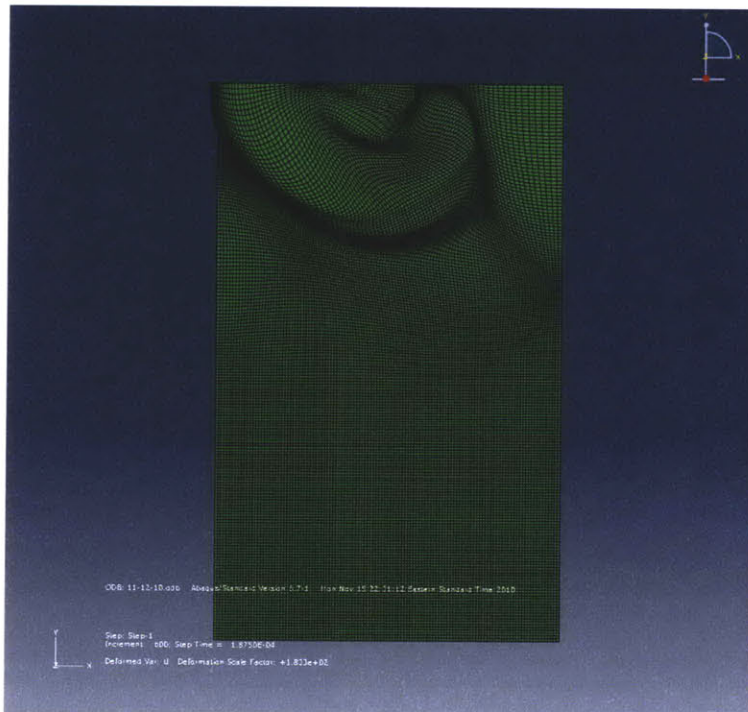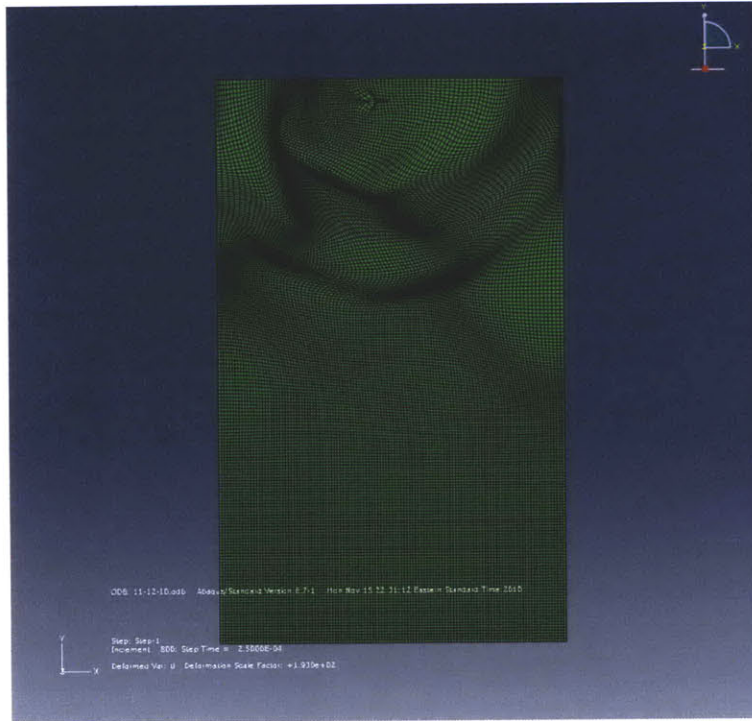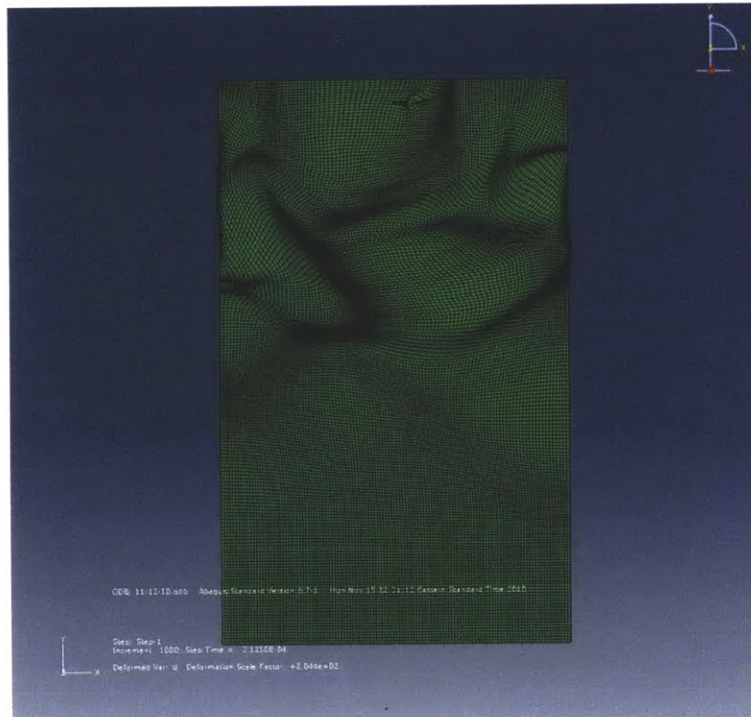t=2.5E-4 secs into Analysis. Automatic Scale Factor

t=3.125E-4 secs into Analysis. Automatic Scale Factor

Chapter 7:

7.1. Summary and Conclusions

This thesis focuses on four main points: 1. Explaining the construction of a representative bender element test in 2-D plane strain space using Abaqus Implicit Dynamic procedures 2. Investigating the ideal mesh resolution and time step configuration of a 2-D plane strain model 3. Reproducing simple wave propagation models using rigid boundaries and dampers 4. Reproducing bender element testing in a consolidometer using dry Ticino Sand.

7.2. Conclusions:

Bender element testing is an attractive testing method for geotechnical engineers because it gives engineering properties of the soil in a non-destructive test. It is advantageous to reproduce a bender element test using the finite element method, which acts as a supplementary check of the bender element test. The finite element method analysis can support the conclusions made regarding the calculation of the velocity and subsequently the material properties derived from such velocity interpretations. Moreover, a finite element test can provide insight into the oscilloscope data, particularly in making predictions about the occurrence of body wave reflections. After investigating the finite element method using Abaqus the following conclusions were reached:

1. The shear strain field output is recommended when modeling the oscilloscope S-wavefront. An axial strain field output is recommended when modeling the oscilloscope P-wavefront.

2. A mesh resolution of twenty elements per shear wavelength is recommended to preserve the wavefront symmetry. A time step ratio, the ratio of the integration time step duration

and the element length, of 0.0005 is recommended to capture the fine time perturbations of the signal.

3. The Implicit Dynamic analysis can produce phase velocities in an infinite half space that conform to the velocities predicted using the engineering properties of the media when the source to receiver distance exceeds 1-P wavelength. The error associated with the peak to peak velocity calculation is approximately five percent.

4. The Implicit Dynamic analysis predicts inaccurate velocities when the source to receiver distance is less than 1-P wavelength.

5. A source to receiver distance of greater than 2 S-wavelengths is recommended to achieve the minimize error in the peak to peak velocity calculation.

6. When the geometric ratio, the ratio of the distance between the source and receiver and the radius of the model, is less than 2.5 Abaqus predicts the largest amplitude of the receiver signal will be the unreflected body wave. When the geometric ratio is greater than 2.5 largest amplitude of the receiver signal may be a reflected body wave not the unreflected wavefront.

7. The addition of Dampers along the boundaries can effectively simulate an infinite boundary.

References

Erlingsson S., Bodare A. (1992). "Vertical S waves in Soil Stratum Over Halfspace" Soil Dynamics and Earthquake Engineering. pp 427-434

Kausel E., Manolis G. (2000). "Wave Motion in Earthquake Engineeing" WIT Press Jan 2000. Wu. Tien Hsing. 1972. "Soil Dynamics" Allyn and Bacon Press Jan 1971.

Prakash. S. (1983). "Soil Dynamics" MchGraw-Hill Press. Feb 1983

Richart F.E., Hall Jr. J. R., Woods R.D. (1970) "Vibrations of Soils and Foundations" Prentice-Hall Press Oct 1970

Conte Enrico, Cosentini R. M., Troncone Antonello. (2009). "Shear and Dilational Wave Velocities for Unsaturated Soils" Soil Dynamics and Earthquake Engineering, Vol. 29, Issue 6, pp 946-952

Fioravante V, Capoferri (2001). "On the Use of Multi-Directional Piezoelectric Transducers in Triaxial Testing" Geotechnical Testing Journal, Vol. 24, Issue 3, pp 243-255.

Erlingsson S., Bodare A. (1992). "Vertical S waves in Soil Stratum Over Halfspace" Soil Dynamics and Earthquake Engineering. pp 427-434

Joviĉiĉ V, Coop MR. (1998). "The Measurement of Stiffness Anisotropy in Clays with Bender Element Tests in the Triaxial Apparatus" Geotechnical Testing Journal, Vol. 21, Issue 1, pp 3-10.

Ni, S. H. (1987). "Dynamic Properties of Sand Under True Triaxial Stress States from Resonant Column and Torsion Shear Tests," Ph.D. thesis, The University of Texas in Austin.

Qiu, Tong, Fox J. Patrick. (2008). "Effective Soil Density for Propagation of Small Strain Shear Waves in Saturated Soil". Journal of Geotechnical and Geoenvironmental Engineering, ASCE, December, 1815-1819.

Shibuya S, Hwang SC, Mitachi T. (1997). "Elastic shear modulus of soft clays from shear wave velocity measurement" Geotechnique, Vol. 47, Issue 3, pp 593-601.

Stokoe, K. H., II, Hwang, S. K., Lee, J. N. K., and Andrus, R.D. (1995). "Effects of Various Parameters on the Stiffness and Damping of Soils at Small to Medium Strains," Proceedings of I

International Symposium On Prefailure Deformation Characteristics of Geomaterials, IS -
Hokkaido, Shibuya, Mitachi, and Miura, Eds., Balkema, Vol. 2, pp.785–816.

Viggiani, G., Atkinson, J.H., (1997) " Interpretation of Bender Element Tests" *Geotechnique 47*,
No. 4, pp 873-877, 1997

Deniz, R. (2008). "Bender elements and bending disks for measurement of shear and
compressional wave velocities in large sand specimens" Master's Thesis, Northeastern
University, Boston, MA

Santagata, M.C., Germaine J.T., and Ladd, C.C. (1999), "Factors Affecting the Initial Stiffness
of Cohesive Soils," of Geotechnical and Geoenvironmental Engineering, Vol. 131, No. 4, April
2005, pp. 430-441.

Abaqus Analysis Manual. Simulink Software Inc. Abaqus 6.71. MIT subscription service.
Accessed 11-12-2010

Arulanthan, Boulander, and Riemer (1998) "Analysis of Bender Element Tests" Geotechnical
Testing Journal. Vol 21 No 2 1998 pp 120-131.

Assimaki, Dominic "Topography Effects in the 1999 Athens Earthquake: Engineering Issues in
Seismology" PhD. Thesis. Massachusetts Institute of Technology 2004. Print.

Ju Shen-Haw, Ni Sheng-Huoo (2007) "Determining Rayleigh Damping Parameters of Soils for
Finite Element Analysis" International Journal for Numerical and Analytical Methods in
Geomechanics. Vol 31. pp 1239-1255

Piezo Systems, Inc. "Introduction to Piezoelectric Transducers." *Piezo Systems: Piezoceramic,
PZT, Piezoelectric Transducers* . Web. 07 Jan. 2011. <http://www.piezo.com/>.

Kolsky. H. (1953). "Stress Waves in Solids" Oxford University Press. Published 1953.

Kausel E. (2005) "Waves Propagation Modes: From Simple Systems to Layered Soils"
International Centre For Mechancial Sciences, Udine, Italy, 2005.

Van Der Hilst, Robert. *12.501 Essentials of Geophysics, Fall 2004*. (Massachusetts Institute
of Technology: MIT OpenCourseWare), http://ocw.mit.edu (Accessed 13 Jan, 2011). License:
Creative Commons BY-NC-SA

Mei, Chiang, Rodolfo R. Rosales, and Triantaphyllos Akylas. *2.062J Wave Propagation, Fall
2006*. (Massachusetts Institute of Technology: MIT OpenCourseWare), http://ocw.mit.edu
(Accessed 13 Jan, 2011). License: Creative Commons BY-NC-SA

Ladd, C.C., Foot, R., Ishihara, K., Poulos, H.G. and Schlosser F. (1977) "Stress-deformation and strength characteristics," Proc. 9th ICSMFE, Vol. 2, State-of-the-Art-Paper, pp. 421-494.

Lee JS, Santamarina JC. (2005). "Bender elements: performance and signal interpretation". Journal of Geotechnical and Geoenvironmental Engineering, ASCE 2005;131(9) pp. 1063-1070

Kumar J, Madhusudhan BN. (2010). "Effect of relative density and confining pressure on Poisson Ratio from bender and extender elements tests". Geotechnique, Vol. 60, Issue 7. pp. 561 –567